The pathophysiology and functionality of metabolic microRNAs in Type 2 Diabetes Mellitus.

By

Leslie Roteta Sedgeman

Dissertation

Submitted to the Faculty of the

Graduate School of Vanderbilt University

in partial fulfillment of the requirements

for the degree of

DOCTOR OF PHILOSOPHY

in

Molecular Physiology and Biophysics

December 15, 2018

Nashville, Tennessee

Approved:

Alyssa Hasty, Ph.D.

David A. Jacobson, Ph.D.

Christopher V. Wright, D.Phil.

John M. Stafford, M.D, Ph.D.

Manuel Ascano Jr., Ph.D.

ACKNOWLEDGEMENTS

First, I would like to thank the wonderful members of the Vickers lab for making the last years in the lab challenging, entertaining and for always keeping me on my toes. Carrie, I am so happy to have shared this journey both in the lab and in grad school with you. Although we are so different, I have grown so much from working with you and having you as my colleague and friend. Dani, thank you always being my supporter, no matter how tough grad school got, you always encouraged me with a smile. You have become my dear friend and I treasure all the life experiences we have shared in the last 5 years. To Ryan, thank you being in my 30-foot lab radius - that decision to sit in 306 4 years ago shaped my experience more than I could have imagined. I have learned so much from you, about specific techniques, but also about being a scientist. Thank you being patient with me, encouraging and supporting me, challenging me to think outside the box and helping me build my science network. To Wanying, thank you first and foremost for everything you do to keep the lab running. Your wit and work ethic are contagious and you never cease to amaze with all of your knowledge both in and outside the lab. To Marisol, thank you for your endless amount of biostatistics and coding knowledge and all of your help and patience with sequencing analysis, graphs and biostats questions. I am certain the graphs in my papers and presentations would have been much more boring without you. To all the other current and past members of the lab, Cindy Toth, Rob Taylor, Stuart Landstreet, Linh Truc-Trahn, Evan Chadhuri, Meaghan Kuzmic, Dani Contreras and all the summer and visiting students, thank you for all of your help in the lab.

None of this would have been possible without Kasey – thank you for taking me into your lab as one of your first students and for teaching me to be a better scientist. I am enormously grateful for all of the independence you gave me in the lab, letting me drive projects in new directions and test out my own hypotheses. Thank you for your support, guidance, and all of the opportunities you have given me as a grad student to develop my own science community. Your

enormous positivity, even in times of struggle, challenged me to be a better scientist, writer and presenter and helped me get to where I am today.

I would also like to thank my committee for their endless support and commitment to my training. I am so grateful that each of you dedicated your time during my committee meetings, department presentations, and one-on-one meetings giving me feedback, challenging me to think about data in a new way and overcoming technical challenges. To everyone in the MPB department, thank you for creating such a wonderful environment for training. Especially to Karen Gieg, thank you for always having an answer to every little question I ever had. To Roger Colbran and Richard O'Brien, thank you for your leadership of the department the last few years and your commitment to training. I am so grateful for all of our interactions the last 6 years and all of your encouragement and advice as I navigated the peer-review process this past year.

Next, I want to thank all of my friends that have made Nashville home for the last 6 years. Dani, Monika, Denise, Heather, Lauren, Michelle, Darwin – thank you always being a source of stress relief, helping me stay balanced and just sharing time outside the lab. To my family, thank you for supporting me through all of these years of school. Mom, thank you for all of the sacrifices you made to make my education possible. Thank you for supporting me the last few years with visits to Nashville, endless encouragement and lots of love. Papi, gracias for todo tu amor de lejos. Pauline and Eileen, I am so lucky to have the best sisters in the world. You both make me laugh every time I talk to or see you. Your positive energy and grace are contagious and I am so gratefully to have you as my cheerleaders. To my new family, the Sedgemans, thank you for welcoming me into your family and for all of your support. Lastly, to my biggest supporter, Carl, thank you for absolutely everything. You have stood by me every step of the way, and seeing you at the end of each day made every challenge a little bit easier. I cannot imagine having gone through grad school without you.

As they say, it takes a village. To everyone that has helped me along the way, THANK YOU!

ACKNOWLEDGEMENTS OF SUPPORT

This work was supported by the American Heart Association 15PRE25090205 (LRS), 14CSA20660001 (KCV); and the National Institutes of Health T32HL007411 (LRS), 5R25GM062459-10 (LRS), P01HL116263 (MFL), R01HL128996 (KCV) DK20593 (KCV), and K22HL113039 (KCV). Mouse islet isolations were performed by the Islet Procurement & Analysis Core which is supported by the Vanderbilt Diabetes Research and Training Center (P60 DK020593). Insulin measurements were performed by the Vanderbilt Hormone and Analytical Services Core which is supported by NIH grants: DK059637 (MMPC) and DK020593 (DRTC). Flow Cytometry experiments were performed in the VMC Flow Cytometry Shared Resource. The VUMC Flow Cytometry Shared Resource is supported by the Vanderbilt Ingram Cancer Center (P30 CA68485) and the Vanderbilt Digestive Disease Research Center (DK058404).

TABLE OF CONTENTS

ABBREVIATIONS

4SU	4-thiouridine
4TU	4-thiouracil
ABCA1	ATP-binding cassette A1
ABCG1	ATP-binding cassette G1
ACOX	acyl-CoA oxidase
Ago	Argonaute
ApoA-I	apolipoprotein A-I
ApoA-II	apolipoprotein A-II
ApoA-IV	apolipoprotein A-IV
ApoB	apolipoprotein B
ApoC-I	apolipoprotein C-I
ApoC-II	apolipoprotein C-II
ATP	adenosine triphosphate
BA	bile acids
BAS	bile acid sequestrant
BKS	C57BL/KsJ
BW	body weight
$[Ca^{2+}]_i$	intracellular calcium concentration
cAMP	cyclic adenosine monophosphate
cDNA	complementary DNA
C-peptide	connecting peptide
CAR	constitutive androstane receptor
CI	confidence intervals
cf	cell-free

Colesevelam	colesevelam HCL
Cre	Cre recombinase
CREB	cAMP response-element binding protein
Ct	threshold cycle
CTGF	connective tissue growth factor
CYP7A1	cholesterol 7-α-hydroxylase
DIA	diazoxide
DIO	diet-induced obesity
DGCR8	DiGeorge syndrome critical region 8
DGUC	density gradient ultracentrifugration
DNA	deoxyribose nucleic acid
DMSO	dimethyl sulfoxide
DPP4	dipeptidyl peptidase 4
EGFR	epidermal growth factor receptor
EGP	endogenous glucose production
ER	endoplasmic reticulum
ERα	estrogen receptor α
ERK	extracellular signal–regulated kinase
Ex-4	exendin-4
FBS	fetal bovine serum
FBXW7	F-box and WD repeat domain containing 7
FDA	Federal Drug Administration
FOXO	forkhead protein family
FXR	farnesoid X receptor
G6P	glucose-6-phosphate
G6Pase	glucose-6-phophatase

GABA	gamma aminobutyric acid
GAPDH	glyceraldehyde 3-phosphate dehydrogenase
GC-MS	gas chromatography-mass spectrometry
Gck	glucokinase
GIP	gastric inhibitory peptide
GIPR	gastric inhibitory peptide receptor
GK	Goto-Kakizaki
GLUT1	glucose transporter 1, encoded by *SLC2A1*
GLUT2	glucose transporter 1, encoded by *SLC2A2*
GLUT3	glucose transporter 1, encoded by *SLC2A3*
GLP-1	glucagon-like-peptide 1
GLP1R	glucagon-like peptide 1 receptor
GPCR	G-protein coupled receptor
GR	glucocorticoid receptor
GSIS	glucose-stimulated insulin secretion
GW182	glycine-tryptophan protein of 182KDa
HA	hemaglutinin
HbA1c	hemoglobin A1c
HBSS	Hank’s buffered salt solution
HCAEC	human coronary aortic endothelial cells
HDL	high-density lipoproteins
HDL-C	HDL cholesterol
HEK293	human embryonic kidney 293
HFD	high fat diet
HMGCR	3-hydroxy-3-methylglutaryl-coA reductase
HOMA-β	homeostatic model assessment of β cell function

HOMA-IR	homeostatic model assessment of insulin resistance
HRP	horseradish peroxidase
IACUC	Institutional Animal Care and Use Committee
IBMX	3-isobutyl-1-methylxanthine
ICAM1	intercellular adhesion molecule-1
INSIG2	insulin induced gene 2
INSR	insulin receptor
i.p.	intraperitoneally
IP	immunoprecipitation
IRB	Institutional Review Board
IRS	insulin receptor substrate
JAK2	Janus kinase 2
K_{ATP}	ATP-sensitive potassium channel
KCl	potassium chloride
KO	knockout
LDL	low-density lipoproteins
LDL-C	low-density lipoprotein cholesterol
LDLR	low-density lipoprotein receptor
LNA	locked nucleic acids
LPDS	lipoprotein deficient serum
LXR	liver-X-receptor
MAP3K8	mitogen-Activated Protein Kinase Kinase Kinase
MβCD	methyl-β-cyclodextran
Med1	mediator complex subunit 1
miR	microRNA
miRNA	microRNA

mRNA	messenger RNA
Mtpn	myotrophin
MV	microvesicles
MVB	multivesicular bodies
NAFLD	non alcoholic fatty liver disease
nHDL	native HDL
NHP	non-human primate
NeuroD	neuronal differentiation 1
Ngn3	Neurogenin-3
nSMase2	neutral sphingomyelinase 2
nt	nucleotides
OCT1	organic cation transporter 1
ORF	open reading frame
PABPC	polyadenylate-binding protein
PAR-CLIP	photoactivatable ribonucleoside-enhanced crosslinking and IP
PBS	phosphate buffered saline
PCK	phosphoenolpyruvate carboxykinase 1
PDK4	pyruvate dehydrogenase kinase 4
PKA	protein kinase A
PKC	protein kinase C
PPAR	peroxisome proliferator-activated receptor
Pol II	polymerase II
pre-miR	precursor miRNA
pri-miR	primary miRNA
pri-miR-375	primary transcript of miR-375
Ran-GTP	Ras-related nuclear protein-guanosine triphosphate

RCT	reverse cholesterol transport
RIA	radioimmunoassay
RIPA	radioimmunoprecipitation assay
RISC	RNA induced silencing complex
RNA	ribonucleic acid
RPM	reads per million total reads
RQV	relative quantitative value
RRP	readily releasable pool
RT-PCR	real-time polymerase chain reaction
RXR	retinoid-X-receptor
SCAP	SREBP cleavage-activating protein
SEC	size exclusion chromatography
SEM	standard error of the mean
SDS-PAGE	sodium dodecyl sulfate-polyacrylamide gel electrophoresis
SID-1	systemic RNA interference deficient-1
SIDT1	SID-1 transmembrane family member 1
SIDT2	SID-1 transmembrane family member 2
siRNA	silencing RNA
SNARE	soluble N-ethylmaleimide-sensitive factor attachment protein receptor
SQLE	squalene epoxidase
SR-BI	scavenger receptor BI
SRE	sterol response element
SREBP-1a	sterol response element binding protein 1a, encoded by *SREBF1*
SREBP-1c	sterol response element binding protein 1c, encoded by *SREBF1*
SREBP-2	sterol response element binding protein 2, encoded by *SREBF2*
sRNA	small RNA

STAT3	signal transducer and activator of transcription 3
STZ	Streptozotocin
SUR	sulfonylurea receptor
T1D	Type 1 Diabetes
T2D	Type 2 Diabetes
T->C	thymidine to cytidine
TGR5	bile acid receptor
Trans-PARCLIP	Transfer-photoactivatable ribonucleoside-enhanced crosslinking and IP
U6	U6 spliceosomal RNA
UMP	uridine monophosphate
UPRT	uracil phosphoribosyltransferase
UTR	untranslated region
Veh	vehicle
VGCC	voltage-gated Ca^{2+} channels
VLDL	very low-density lipoprotein
WAT	white adipose tissue
WT	wildtype C57B6/J
ZDF	Zucker Diabetic Fatty

LIST OF TABLES

LIST OF FIGURES

CHAPTER I

INTRODUCTION

Diabetes Mellitus

More than 30 million people in the United States (9.4% of the population) and 420 million people worldwide have diabetes, and the numbers are expected to rise, with a projected global prevalence of 640 million by 2040(1). Diabetes is characterized by chronic hyperglycemia (fasting blood glucose levels >126 mg/dL or >6.5% glycated hemoglobin A1c (HbA1c)). If uncorrected, hyperglycemia can cause diabetic ketoacidosis, retinopathy, peripheral neuropathies, and an increased risk for cardiovascular and kidney disease. Furthermore, hyperglycemia can result in kidney disease, blindness and limb amputation - long-term consequences that impact quality of life. Additionally, it is estimated that in 2012, diabetes caused 3.7 million deaths from diabetes alone and/or associated co-morbidities such as cardiovascular diseases, chronic kidney disease and tuberculosis (Global Report on Diabetes – World Health Organization). There is a pressing need to define the physiological and pathophysiological mechanisms that characterize diabetes to develop better tools to diagnose and treat patients with this disease. Work presented in this dissertation provides key insights into extracellular RNAs and their role in diabetes and advances our understanding of the molecular mechanisms of a drug, colesevelam, used in treatment of diabetes. Therefore, the next two sections will focus on the two main forms of diabetes: type 1 and type 2 diabetes (T1D and T2D).

Type 1 Diabetes

T1D accounts for the minority of the total diabetes burden in the population, although it accounts for the majority of diabetes cases in the younger age groups. T1D is an autoimmune disease characterized by insulin deficiency due to β cell loss(2). The etiology of T1D is not

completely understood, although both genetic and environmental factors are thought to contribute(3). The last stage in disease development is T-cell mediated destruction of β cells in response to autoantibodies against insulin and numerous other antigens in the insulin granule(2, 3). The process of β cell destruction often takes place during a prolonged period of time over which patients are asymptomatic and euglycemic, but test positive for autoantibodies(4). By the time of onset of clinical symptoms, 80-95% of β cell mass has been destroyed(5). Currently, there is no cure for T1D, and patients depend on lifelong insulin injections, although novel medical devices such as insulin pumps, and artificial pancreas are in development. Despite this, patients still suffer both micro- and macro-vascular complications from this disease(2). For this reason, there is a great need to develop biomarkers to accurately predict disease and monitor β cell death.

Although T1D is not the focus of the work presented in this dissertation, in Chapter IV, I investigated changes in a plasma and high-density lipoprotein (HDL) ribonucleic acids (RNA), specifically the microRNA (miRNA, miR), miR-375-3p in a rodent model of β cell destruction using the pharmacological agent, streptozotocin (STZ). STZ is a cytotoxic compound that contains a glucose moiety that directs the chemical to the pancreatic β cells(6). T1D can be induced in mice using a single high dose, or repeated low doses. Importantly, STZ is rapidly cleared through the liver and kidney(6), allowing investigation of the effects of β cell loss and hyperglycemia in this model, without additional cytotoxic effects. In Chapter IV, I present my findings using this model, and discuss the literature on plasma miR-375-3p changes in both rodent models and patients with T1D.

Type 2 Diabetes

Much of the work presented in this dissertation aims to further understand the molecular mechanisms that underlie T2D and its treatments. T2D is the most common cause of diabetes and accounts for about 90-95% of all cases. T2D is a complex heterogeneous disease caused by impairments in insulin sensitivity and β cell dysfunction (Figure 1-1) (7, 8). Briefly, the β cells in

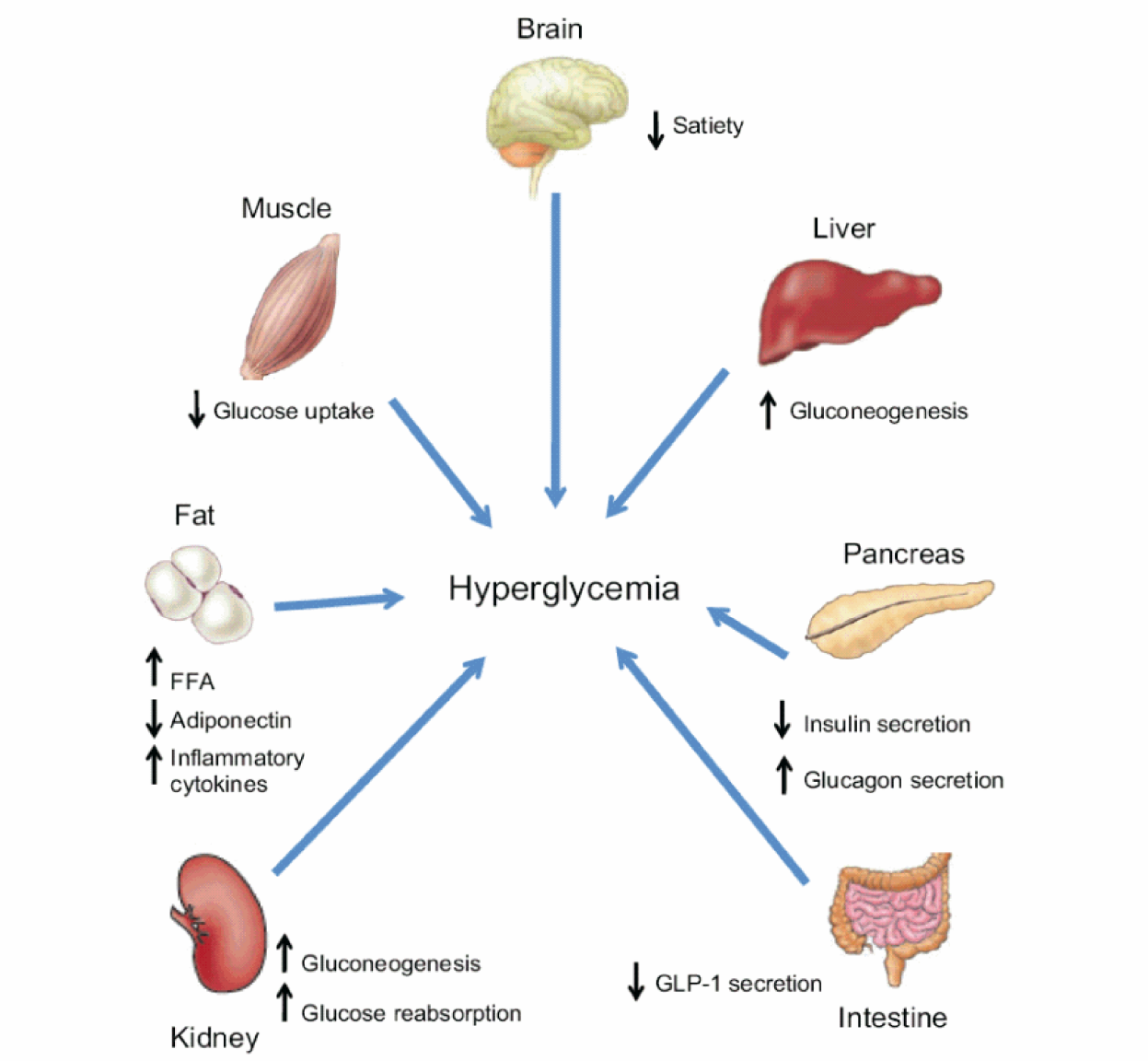

Figure 1-1. Multiorgan dysfunction in T2D. From Cornell, S. Ther Clin Risk Manag. 2015 Apr 16;11:621-32.

the islets of Langerhans in the pancreas synthesize insulin, a polypeptide hormone. Insulin is stored in granules and released once triggered by the elevation of blood glucose. Insulin exhibits a multitude of effects in many tissues, with liver, muscle and adipose tissue being the most important target organs for insulin action. Insulin is the principal hormone that regulates the uptake of blood glucose into most cells, including adipocytes and skeletal muscle. Insulin is also the major signal for converting glucose to glycogen for storage in the liver and for inhibiting the production of glucose in the liver during non-fasting conditions.

Key metabolic tissues, such as muscle, adipose tissue, and liver, normally are sensitive to insulin. However, insulin resistance in these tissues is a key contributor of T2D and studies have shown that insulin resistance occurs years before any evidence of glucose intolerance or β cell failure(9). At the cellular level, insulin resistance can manifest as mitochondrial oxidative dysfunction, endoplasmic reticulum stress, oxidative stress or impaired insulin signaling(9). Insulin resistance, along with obesity, elevated triglycerides, low high-density lipoprotein (HDL) and elevated blood pressure are componenets of the metabolic syndrome, which is a risk factor for T2D(10).

Obesity is one of the major risk factors for T2D and epidemiological studies have consistently shown that T2D results from an interaction between genetic predisposition and lifestyle factors including obesity, cigarette smoking, lack of physical activity and excess caloric intake(11, 12). Despite the importance of lifestyle modifications in the treatment of T2D, most patients cannot escape the value of pharmacotherapy to achieve target blood glucose concentrations(13). All Federal Drug Administration (FDA)-approved therapies for treating hyperglycemia in T2D lower HbA1c levels, mainly by two key mechanisms: improving insulin production/secretion from β cells or improving insulin sensitivity in muscle, adipose tissue and/or liver (Figure 1-2). Two of the most common classes of T2D drugs are biguanides and sulfonylureas. A review of the most common T2D drug classes is provided next as pharmacological agents that alter insulin secretion from the β cell were used in Chapter III to

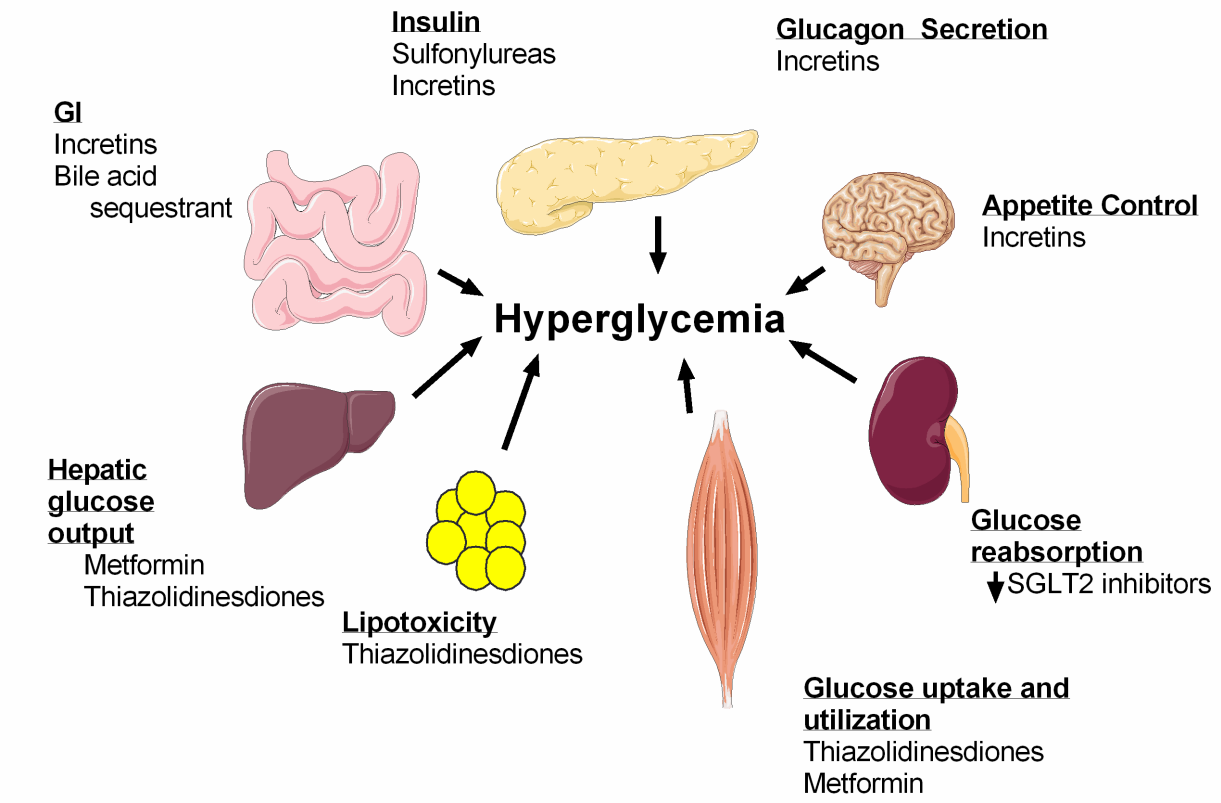

Figure 1-2. Tissue sites and mechanisms of T2D pharmacotherapies. Adapted from Evans JL, Balkan B, Chuang E, et al. Oral and Injectable (Non-insulin) Pharmacological Agents for Type 2 Diabetes. [Updated 2016 Jul 20]. In: De Groot LJ, Chrousos G, Dungan K, et al., editors. Endotext [Internet]. South Dartmouth (MA): MDText.com, Inc.; 2000-.

uncover the mechanisms of HDL-miRNA export, and Chapter IV presents work aimed at identifying the molecular mechanisms of the bile acid sequestrant (BAS), colesevelam.

Therapies for T2D

Metformin, a biguanide derivative first introduced in the 1950s, is a potent antiglycemic agent and the first-line therapy based on its efficacy, safety, and reasonable cost(1). While the mechanism of action of metformin remained elusive for many years, recent evidence has emerged that metformin preferentially acts in the hepatocyte, due to the expression of the organic cation transporter 1 (OCT1), which facilitates the cellular uptake of metformin(14). As such, a growing body of evidence suggests that metformin's primary function is to inhibit hepatic gluconeogenesis, by two key mechanisms: inhibiting gluconeogenic enzyme activity or reduction of gluconeogenic subtrates(15, 16). Additionally, metformin has been proposed to exert its beneficial metabolic actions in part through the modulation of the incretin axis, by increasing circulating levels of glucogon-like peptide 1 (GLP-1), which promote insulin secretion(17, 18), and by improving insulin-stimulated glucose uptake(19).

The second most prescribed drug for T2D is glipizide, which belongs to the sulfonylurea drug class. Sulfonylureas stimulate insulin secretion from pancreatic β cells, by a non-glucose dependent mechanism. Importantly, due to the role of sulfonylureas in promoting insulin secretion, they are only effective when residual pancreatic β cells are present. Additionally, a key side effect of sulfonylureas is hypoglycemia, as insulin secretion can occur in the absence of high glucose, particularly with long-acting sulfonylureas, in elderly patients, or after exercise or a missed meal(20). Sulfonylureas work by binding with high affinity the sulfonylurea receptor (SUR) subunit of the adenosine triphosphate (ATP)-sensitive potassium channel (K_{ATP}), and inducing channel closure. Inhibition of the K_{ATP} channels by glucose or sulfonylureas causes depolarization of the β cell plasma membrane and induces the secretion of insulin-containing granules. The K_{ATP} channel is composed of two subunits, Kir6.x (Kir6.1 and Kir6.2) and SUR (SUR1, SUR2A,

SUR2B) subunits. While the K_{ATP} channel is present in numerous tissues, the subunit composition is tissue specific. In the β cell the K_{ATP} channel is composed of the SUR1 and Kir6.2 subunits, whereas in heart and skeletal muscle Kir6.2 is found in association with SUR2A and with SUR2B in brain and smooth muscle(21, 22). This tissue specificity of the SUR subunits is important pharmacologically because some sulfonylureas (tolbutamide, glipizide and gliclazide) block SUR1 specifically, whereas others (glimepiride, repaglinide and meglitine) block both SUR1 and SUR2 subunits(21, 23). Because sulfonylureas target the insulin insufficiency of T2D, they are often used in combination with metformin or other drug classes that improve insulin sensitivity(1).

Incretin-based therapies represent another key class of antidiabetic drugs, which also target insulin insufficiency. Unlike sulfonylureas which stimulate glucose independent insulin secretion, incretin-based therapies enhance glucose-stimulated insulin secretion (GSIS). This class of therapies is made up of glucagon-like peptide 1 receptor (GLP1R) agonists and dipeptidyl peptidase 4 (DPP4) inhibitors. GLP-1 is an incretin hormone secreted by intestinal L cells, that exerts its effects by binding to the GLP1R expressed on the plasma membrane of the β cell(24). GLP-1 improves GSIS, stimulates insulin gene expression, and acts as a β cell mitogen to promote proliferation and survival(25). However, its clinical utility is limited due to its rapid clearance by DPP4 (GLP-1 half-life 1.5-2.1 minutes)(26). Therefore GLP-1 analogues that are resistant to enzymatic degradation by DPP4 have been developed as therapies; in contrast to endogenous GLP-1, synthetic GLP1R agonists, such as liraglutide, have plasma half-lives of up to 13h (liraglutide)(27). DPP4 inhibitors increase the levels of endogenous GLP-1 by inhibiting the DPP4 enzyme(24). An exciting feature of GLP1R agonists is that they have the potential to delay or reverse T2D disease progression by promoting β cell proliferation and insulin biogenesis, and suppressing β cell apoptosis. Similarly, a recent meta-analysis reported that DPP4 inhibitors also have the capacity to improve β cell function, suggesting that incretin-based therapies have the potential to reverse disease progression and perhaps decrease disease burden(24, 28).

Improving β cell function, however, is not the only pharmacologic strategy; some additional T2D drug therapies have emerged from the cardiovascular field and alter lipid metabolism. One such class is bile acid sequestrants (BAS), which have been used as lipid-lowering therapies for decades. BAS bind to bile acids (BA) in the intestine which prevents their reabsorption and promotes BA excretion in the feces. Normally, 95% of BAs are reabsorbed by the intestine and transported back to the liver via enterohepatic circulation(29). Hepatic cholesterol 7-α-hydroxylase (*CYP7A1*) is the first and key enzyme in the conversion of cholesterol to BAs which are then secreted into the bile to facilitate absorption of lipids and lipid-soluble vitamins in the intestine(29). However, in response to BA depletion, hepatic CYP7A1 is upregulated to increase BA synthesis. Consequently, BA synthesis from cholesterol in the liver depletes the cellular cholesterol pools and promotes *de novo* cholesterol synthesis via activation of sterol response element binding protein 2 (SREBP2) activity and transcription of its target genes, including the low-density lipoprotein receptor (LDLR) to restore cellular cholesterol levels. The upregulation of LDLR removes cholesterol from the circulation for use in BA synthesis, resulting in reductions in circulating low-density lipoproteins (LDL)(30, 31). Hence, the use of BAS as lipid-lowering agents, where BAS have been reported to decrease LDL cholesterol (LDL-C) levels by 15% and total plasma cholesterol levels by 10%(32).

More recently, in 2008, the FDA approved colesevelam HCl (colesevelam), a second-generation BAS as a therapy for T2D, based on three seminal clinical studies (33-35). Despite the potential for colesevelam as both a lipid-lowering and antidiabetic agent, the use of BAS in the treatment of T2D is not commonplace, mainly due to the moderate to mild glucose-lowering effects requiring combination therapy, and the gastrointestinal side effects such as constipation due to decreased BA flux in the intestine(36). Additionally, at present a clear mechanistic understanding of how colesevelam and other BAS lower glucose does not exist. Colesevelam is not absorbed in the intestine, therefore the therapeutic effects derived from this drug are likely mediated by changes in BA signaling or other indirect effects, i.e. gut incretins and alterations in

cholesterol synthesis. In fact, it is likely that BAS exert their effect on multiple metabolic tissues through numerous signaling cascades. The most studied mechanism for colesevelam's glucose lowering properties have been gut incretins. For example, colesevelam has been reported to increase GLP-1 secretion from intestinal L-cells via a mechanism requiring the G-protein coupled BA receptor (TGR5)(37, 38). Additionally, Beysen *et al*. have reported that in humans, colesevelam treatment increases plasma levels of gut-derived incretins that promote insulin secretion, e.g. GLP-1 and gastric inhibitory peptide (GIP)(39). Similarly, Shang *et al*. have reported the same increase in GLP-1 and GIP in a diet induced rodent model of T2D(40). However, these effects are only modest, and while it is likely that incretins contribute to improvements in glycemic control with colesevelam, there are likely other mechanisms at play as well. Furthermore, in humans Beysen *et al*. have reported effects of colesevelam on gluconeogenesis and glycogenolysis, the process of glycogen breakdown to glucose (39), whereas in mice, Potthoff *et al*. found that colesevelam improves hepatic glucose metabolism and suppress glycogenolysis (37, 41). Due to these differing hypotheses presented for colesevelam's effect on glucose regulation, this presented a unique opportunity to investigate whether miRNAs contribute to colesevelam's mechanism of action by regulating gene networks through miRNA changes. Studies investigating the functional role of miR-182 in colesevelam's mechanism of glucose control are presented in Chapter V.

Mouse Models in T2D Research

Rodents are the most commonly used animal model of T2D in biomedical research. Although different animal models have different characteristics, each mimics a specific set of genetic, endocrine, metabolic and morphologic phenotypes that occurs in human T2D. While there are numerous rodent models of obesity, metabolic syndrome and T2D, the following section focuses on the rodent models used in this dissertation, including *db/db* mice and ZDF rats and other commonly used rodent models.

The two main categories of T2D rodent models are diet-induced obese (DIO) and spontaneous or genetically derived diabetic animals. Obesity is the main risk factor for T2D development in humans, and similar to humans, obese mice are prone to developing insulin resistance. As such, some strains of mice develop T2D-like phenotypes when fed a high fat diet (HFD). When WT mice (C57BL/6J) are fed a standard chow diet, these animals are lean and do not exhibit metabolic abnormalities, however, when fed a HFD, particularly males, develop obesity, glucose intolerance, moderate insulin resistance and elevated blood glucose levels, but they do not develop diabetes(42).

Two common mouse models of obesity and diabetes arose from spontaneous mutations at the Jackson Labs, the *ob/ob* mouse and the *db/db* mouse. *Ob/ob* and *db/db* mice represent the earliest mouse models of T2D, and continue to be the most widely used mouse models today(43). *ob/ob* are deficient in leptin, whereas, *db/db* mice have mutations in the leptin receptor, and both models result in hyperphagia and development of an obese phenotype (43). Leptin is a hormone produced by the adipocyte and taken up by the brain to regulate food intake and energy expenditure(43). The *ob/ob* mutation is caused by a single autosomal recessive mutation encoding a premature stop codon in the leptin gene on chromosome 6, rendering a biologically inactive protein(43, 44). These mice are obese by 4 weeks of age, and have β cell hyperplasia, reduced energy expenditure and obesity(45). Phenotypes in the *ob/ob* mouse vary by genetic background: on the C57BL/6J background, *ob/ob* mice have transient hyperglycemia, whereas on the C57BL/KsJ (BKS) background, mice develop severe hyperglycemia and β cell failure(45). *Db/db* mice harbor a deleterious point mutation in the leptin receptor gene(46, 47), resulting in abnormal splicing and production of an abnormal gene product(43). *Db/db* mice, are similar to *ob/ob* mice in that both models are obese, display hyperinsulinemia, and hyperglycemia(45). On a C57BL/6J background, *db/db* mice develop insulin resistance, but on the BKS background, mice are severely diabetic(45). Male *db/db* BKS mice have elevated fasting glucose levels as early as 8 weeks and insulin and connecting peptide (C-peptide) levels peak at 10 weeks(45). β cell mass

similarly expands from 6 weeks to 10 weeks, when it reaches its peak, and begins to decrease gradually(48). In Chapter V, we used *db/db* BKS mice to study hepatic miRNA changes in response to colesevelam to test whether they contributed to the anti-diabetic effects of colesevelam.

Another animal model of T2D is the Zucker Diabetic Fatty (ZDF) rat, which exhibits leptin receptor deficiency. Not unlike human forms of obesity, this model of obesity also displays insulin resistance(49). Male rats are obese and have hyperinsulinemia by 8 weeks of age, and subsequently develop hyperglycemia in response to β cell loss(50). In Chapters IV & V, we use ZDF rats as models of T2D to measure miRNA changes on HDL and to study the effect of hepatic miRNAs in response to colesevelam. Another commonly used rat model of T2D is the Goto-Kakizaki (GK) rat, a non-obese Wistar rat with chronic hyperglycemia. These rats display high glucose levels during a glucose tolerance and have abnormalities in islet morphology and hormone secretion(49).

The studies presented in this dissertation focused on commonly used models of T2D that would allow us to profile miRNA changes in response to T2D and to study the role of colesevelam. For Chapter IV, we chose to profile miRNA changes in plasma and HDL in ZDF rats and db/db mice and to validate these changes in a cohort of human subjects consisting of healthy and T2D patients. For the studies presented in Chapter V, we used ZDF rats and db/db mice to investigate the glucose lowering effects of colesevelam. While the preliminary work was performed in ZDF rats, additional work using pharmacological miRNA inhibitors were performed in the *db/db* mouse model to expand the findings beyond one rodent model.

Physiological and Molecular Regulation of Glucose

Pancreatic Islets

The islets of Langerhans are critical organs in T2D for their role in hormone secretion. While the molecular mechanisms of insulin secretion are well understood, the full islet secretome is not well defined. Work in this dissertation aimed to investigate whether islets secrete miRNAs and to study the cellular processes that regulate this. Therefore, an introduction to the cells of the pancreatic islet and the molecular mechanisms that regulate insulin secretion are provided next.

The islets of Langerhans form the endocrine part of the pancreas, account for 2% of the total mass of the pancreas. It has been estimated that a human pancreas contains between 3.2 and 14.8 million islets(51). The islets are enclosed by a dense network of capillaries and surrounded by a thin collagen capsule that separates the endocrine islets from the exocrine pancreas(52). In the mouse, around 60% of islet cells are β cells (insulin-producing), 30% are α cells (glucagon-producing) and the remaining 10% of cells are δ cells (somatostatin-producing), γ or PP cells (pancreatic polypeptide-producing), and ε cells (ghrelin-producing)(51). In a coordinated way, these cells sense changes in nutrient levels in plasma and respond by secreting a mixture of islet hormones into the portal blood.

β cells are the most studied cell type in the islet and the main focus of studies performed in Chapter III, therefore, I will next describe in detail β-cell biology and the molecular mechanisms of insulin secretion. β-cells make and secrete insulin in response to elevated glucose concentrations. Insulin is the only hormone capable of lowering blood glucose levels and is essential for cellular nutrient uptake and survival, through its action on peripheral tissues, such as liver, skeletal muscle and adipose tissue(52).

Insulin is transcribed as proinsulin and proteolytically processed to the active 51-aminoacid peptide, insulin. Proinsulin, is split into three parts, an A and B chain, and C chain that connects the previous two. In the biologically active insulin molecule, the A and B chains remain

connected by two disulfide bonds, and the C chain is cleaved. The C chain is also known as C-peptide and is released with insulin in 1:1 molar ratio(52). Because the half-life of C-peptide is longer than insulin *in vivo(53)*, it is often used in research as a surrogate for insulin secretion. Insulin is packaged in secretory granules in complex with zinc, forming insulin-zinc hexamers(52). It is estimated that approximately 10^{12} secretory granules are released from β-cells each day(52). Insulin granules are released both constitutively and in response to elevated levels of glucose and other nutrients, with the latter accounting for the majority of insulin release(54). Due to this unique property of insulin, defects in the regulated release of insulin result in severe metabolic dysfunctions associated with T2D.

GSIS is a tightly controlled process. Insufficient insulin release and the accompanying hyperglycemia are hallmarks of both T1D and T2D, whereas over secretion of insulin results in hypoglycemia, limiting glucose fuel for the brain which can lead to a coma. For this reason, insulin secretion occurs in response to a glucose stimulus. In response to elevations in glucose, both human and rodent β cells trigger a series of cellular processes that culminate in biphasic secretion of insulin (Figure 1-3). Upon elevation in plasma, glucose enters the β cell through glucose transporters on the plasma membrane and is phosphorylated to glucose-6-phosphate (G6P) by glucokinase (GCK) (55). Glucose is metabolized to pyruvate and passes into the mitochondria where via the Krebs cycle it results in the generation of ATP (55). ATP is the endogenous ligand of the K_{ATP} channel, and similar to the action of sulfonylureas discussed above, ATP-dependent closure of the K_{ATP} channel results in plasma membrane depolarization and initiation of the β cell electrical activity(55). In response to this depolarization, calcium ions (Ca^{2+}) enter the cell through voltage-gated Ca^{2+} channels (VGCC), resulting in a rise in intracellular Ca^{2+} levels ($[Ca^{2+}]_i$) and stimulating pulsatile release of insulin(54). Elevated $[Ca^{2+}]_I$ facilitates the fusion of insulin to the plasma membrane in a soluble N-ethylmaleimide-sensitive factor attachment protein receptor (SNARE)-dependent process(55).

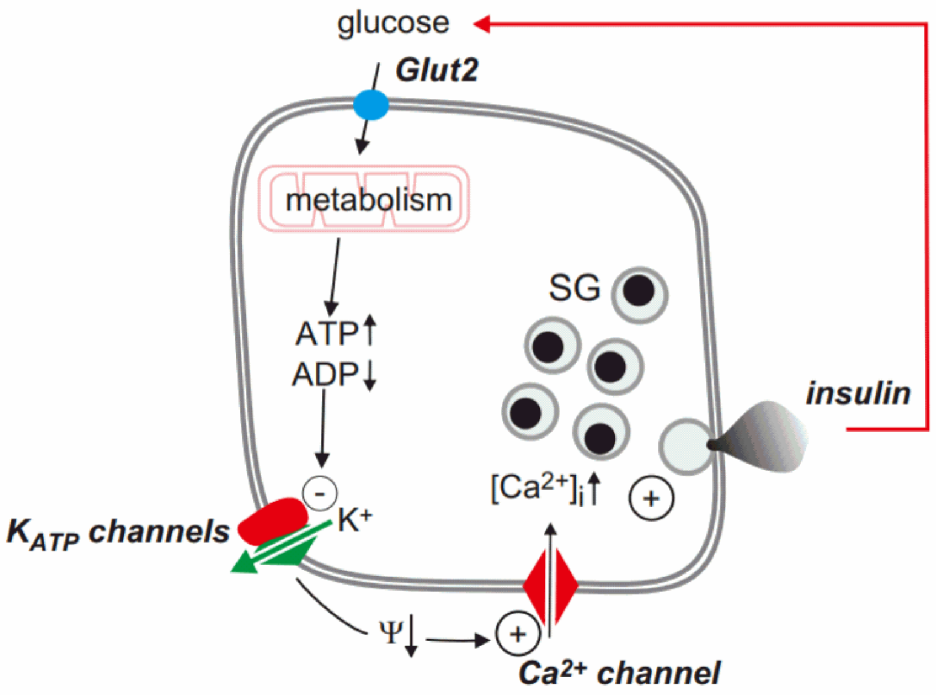

Figure 1-3. Mechanisms of insulin secretion in the β cell. From Rorsman, P & Ashcroft, FM. Physiol Rev. 2018 Jan 1;98(1):117-214

The biphasic secretion of insulin involves the first phase peaking with 5-6 minutes post glucose challenge, and the second phase, a gradual release of insulin, lasting for an additional 30 minutes(55). The first phase of insulin secretion releases granules that are pre-docked at the plasma membrane from what is referred to as the readily releasable pool (RRP)(56). In mice, it is estimated that each β-cell contains approximately 13,000 insulin granules(57). RRPs only make up a small amount of the insulin granules in the cell and only a few of these are released during the first phase. To support this biphasic release, concurrently with first phase insulin secretion, additional insulin granules are mobilized and trafficked to the plasma membrane to support second phase insulin secretion. Granule mobilization is thought to be an ATP-dependent process, and the microtubule kinesin has been implicated in the transport of insulin-containing granules towards SNARE sites to replenish the RRP(56, 57) . The distinction between first and second phase insulin secretion is also important for disease, as the selective loss of first phase insulin secretion is an early feature of T2D(57).

Beyond glucose, numerous other nutrients, drugs, neurotransmitters and hormones can modulate GSIS, however only glucose and sulfonylureas can initiate the electrical signals needed for insulin secretion on their own. Many other nutrients are capable of amplifying or potentiating insulin secretion, but cannot do so on their own. These include most amino acids, fatty acids, neurotransmitters and hormones, including the incretins GLP-1 and GIP(54). In response to a meal, amino acids are elevated in the plasma membrane which help to potentiate GSIS(58). Acetocholine and a number of other hormones augment insulin secretion through G-protein coupled receptor (GPCR) signaling through the phosphoinositide pathway and activation of protein kinase C (PKC). GLP-1 is a gut hormone secreted by enteroendocrine L-cells. GLP-1 acts by activation of the GLP1R which results in activation of adenyl cyclase and a rise in cyclic adenosine monophosphate (cAMP)(54, 59). In the presence of glucose, GLP-1 potentiates insulin secretion by increasing action potential firings and it has been shown to also increase the number of insulin granules that are released(54, 57). GIP is released from the enteroendocrine K-cells,

and is thought to exert many of its effects on insulin secretion through a similar mechanism as GLP-1, although mediated through the GIP receptor (GIPR), rather than GLP1R. Unlike GLP1R, GIPR is downregulated in response to hyperglycemia(60) and the stimulatory effect of GIP is reduced in T2D(61). Nevertheless, these amplifying pathways are important regulators of insulin secretion and as discussed above, GLP1R agonists and agents that prevent the degradation of GLP-1 (DDP-4 inhibitors) are important pharmacological agents in the treatment of T2D in the clinic.

The second most abundant cell type in the islet is the α cells. α cells secrete glucagon, a 29-amino acid peptide derived from the proglucagon gene through proteolytic cleavage. Proglucagon is also the precursor for GLP-1, GLP-2, and glicentin, synthesized and secreted from enteroendocrine cells(62, 63). Glucagon is considered to be the counter hormone to insulin, and concerted regulation of insulin and glucagon secretion is critical for regulation of blood glucose. The main function of glucagon is the prevention of hypoglycemia, through action of glucagon in the liver to promote gluconeogenesis(51) (discussed below). Glucagon action is also impaired in T2D; as first described by Unger and colleagues, in T2D, suppression of glucagon in high glucose is impaired resulting in increased gluconeogenesis, under conditions when this process is normally suppressed(64, 65). While α cells are much less studied than β cells, recent findings have suggested that α cells have the potential to transdifferentiate to β cells in response to gamma aminobutyric acid (GABA), although the effect of this process on islet architecture and function is not fully understood(51, 66).

α and β cells are more abundant and better studied than the other islet-cell types, δ, PP and ε cells(52). δ cells secrete somatostatin, a potent insulin and glucagon blockers. PP cells secrete the hormone pancreatic polypeptide, and ε cells secrete ghrelin, a hormone first isolated from the rat stomach. δ, PP and εcells constitute 5-10%, <1% and 1% respectively(52). While the research presented in this dissertation focuses on β cells, some experiments were performed

using human and mouse islets and it is important to understand that primary islets are also made up of non-β cells.

Most of the knowledge gained about islets and islet cell function has been garnered from rodent studies, and there are key differences between human and rodent islets that warrant consideration. Architecturally, rodent islets contain a core of β cells surrounded by a layer of non-β cells with a width of one to three cells deep, termed a mantle-core arrangement (Figure 1-4A) (67). Human islets, on the other hand, display a more complex arrangement, with a scattered distribution of cells which has led investigators to disagree about whether the arrangement of cell types in human islets is random or not (Figure 1-4B) (68, 69). In opposition to the hypothesis of random cell arrangement is the finding that non-β-cells are adjacent to blood vessels that penetrate and branch within the islet(67, 70-72). This issue of islet morphology is important because it appears to have functional importance in rodents. In a number of rodent models in which insulin secretion is decreased, islet morphology is also altered(70, 73, 74). Nevertheless, beyond the controversial human islet architecture, it is clear that there is far more variability in human islets than in rodent islets, in terms of composition, size and morphology(67).

Another key difference between human and mouse islets is the differences in glucose transporters in the β cell. The predominant glucose transporter in mice is glucose transporter 2 (Glut2, encoded by *Slc2a2)*, whereas in humans, glucose transporter 1 (GLUT1, encoded by *SLC2A1*) and glucose transporter 3 (GLUT 3, encoded by *SLC2A3*) predominate(75). This difference is important due to the different transport capacities between these transporters (K_m values: GLUT1 6mM, GLUT2 11mM, GLUT3 1mM). As such, GSIS is detected at glucose concentrations as low 3mM in humans, much lower than the stimulatory concentration in mice, 6mM(54, 75). These differences are important considerations when comparing human and rodent phenotypes and are critical to keep in mind when translating findings in rodent islets to human islets.

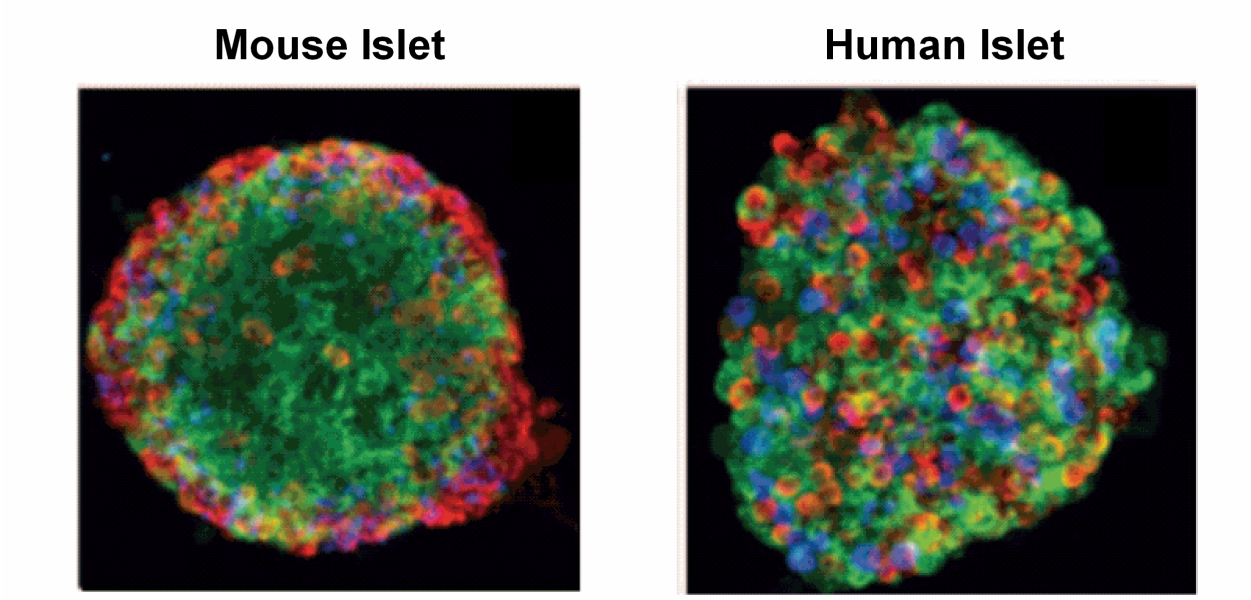

Figure 1-4. Differences in islet architecture between mouse and human. β cells, green; α cells, red; δ cells, blue. From Brissova, M. et. al. J Histochem Cytochem. 2005 Sep;53(9):1087-97.

Liver

The liver plays a major role in the regulation of glucose control by regulating both glucose and glycogen production and breakdown. The main cell type in the liver is the hepatocyte, accounting for ~80% of liver cells(76). In both humans and rodents, blood glucose enters the hepatocyte through GLUT2 and is phosphorylated by GCK to G6P(76). G6P is unable to be transported by glucose transporters and is retained in the hepatocyte. In most mammalian tissues, including the liver postprandially, catabolism of G6P to pyruvate for ATP generation occurs through glycolysis(77). Under conditions of abundant carbohydrates, the liver can also produce glycogen, a storage form of glucose, through a process known as glycogenesis (Figure 1-5A) (77). Excess carbohydrates can also be converted into fatty acids through lipogenesis which are then incorporated into very-low-density lipoproteins (VLDL) for transport to and storage in white adipose tissue (WAT) (77). Conversely, under conditions of fasting, the liver also plays a key role in generating glucose to maintain euglycemia and supply the brain, red blood cells and skeletal muscle with glucose. Normally, during an overnight fast, glycogen is converted to glucose through glycogenolysis (Figure 1-5B) (77). However, during prolonged fasting, gluconeogenesis generates glucose from other fuel sources such as lactate from muscle, or red blood cells, or glycerol from lipolysis in WAT(77). Through multiple biochemical reactions, glycogen or pyruvate are converted back to G6P. Dephosphorylation of G6P is the rate-limiting step of both gluconeogenesis and glycogenolysis, and G6P is dephosphorylated by glucose-6-phosphatase (G6Pase)(76).

These metabolic processes in the liver are regulated by various hormones. During fasting and exercise, glucagon is the primary regulator of endogenous glucose production (EGP), the process of glucose generation and release into circulation by either gluconeogenesis or glycogenolysis(78). Glucagon promotes EGP mainly through glycogenolysis, and minimally through gluconeogenesis(78). In the acute setting, glucagon stimulates EGP by promoting the phosphorylation of the protein kinase A (PKA) and inhibition of pyruvate kinase, leading to

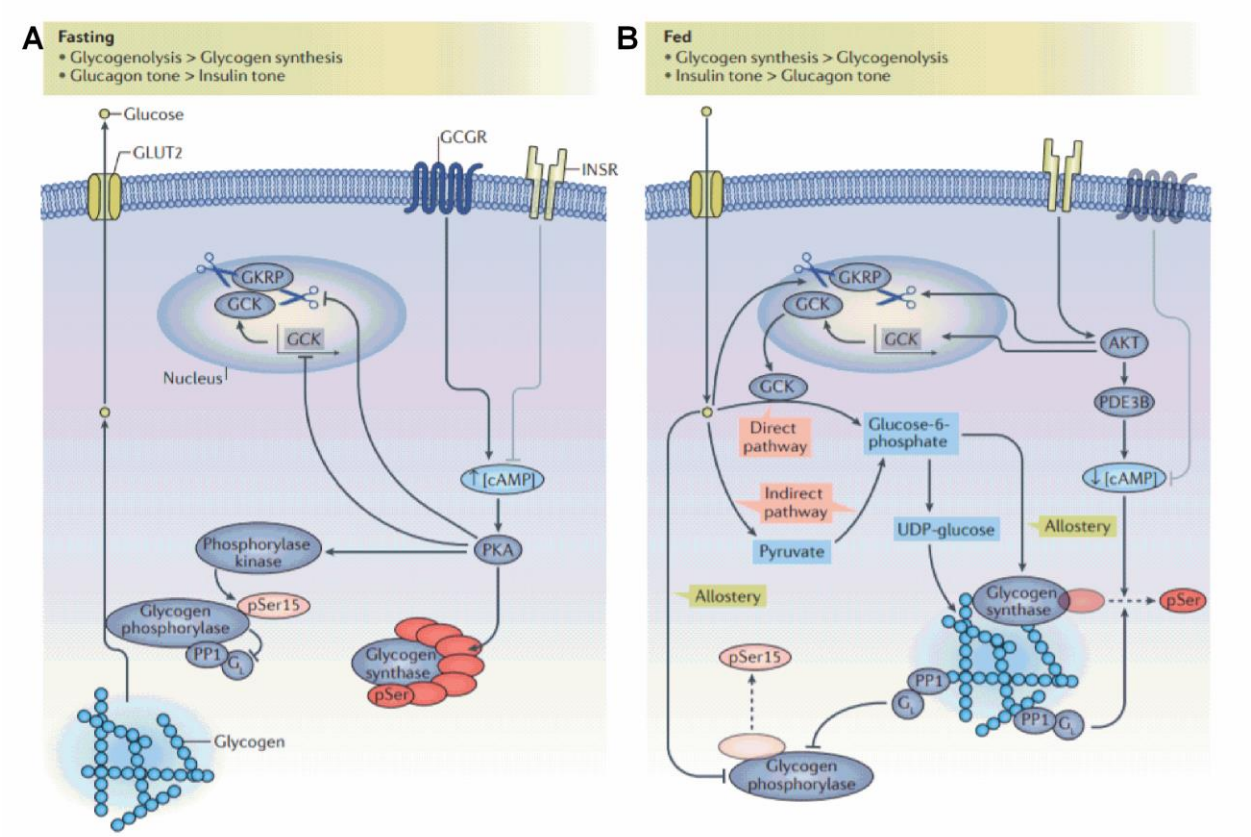

Figure 1-5. Hepatic control of glucose and glycogen during fasting and feeding. From Petersen, MC, Vatner, DF & Shulman, GI. Nature Reviews Endocrinology volume 13, pages 572–587 (2017).

inactivation of Gck and overall switch to inhibit glucose uptake (Figure 1-5) (78, 79). Glucagon signaling also has effects on transcriptional activators of EGP, mainly through the transcription factors cAMP response element-binding protein (CREB), and the forkhead protein family (FOXO)(80). CREB and FOXO1 are active during fasting in response to glucagon signaling to promote the transcription of key gluconeogenic genes, *G6PASE* and phosphoenolpyruvate carboxykinase 1 (*PCK1*)(80). In this way, glucagon simultaneously inhibits hepatic glucose uptake and storage and stimulates EGP to maintain euglycemia.

Conversely, postprandially, a rise in both circulating glucose and insulin suppresses gluconeogenesis and glycogenolysis, and promotes glucose uptake. Insulin exerts its actions on the insulin receptor (INSR) on the plasma membrane, leading to the activation of the INSR tyrosine kinase, that in turn catalyses the phosphorylation of a number of substrates, including the insulin receptor substrate (IRS), resulting in Akt phosphorylation and activation (Figure 1-5B) (81). While the action of insulin in the skeletal muscle and WAT is critical for increasing glucose uptake, in the liver, the main action for insulin signaling is suppression of EGP, mainly through deactivation of FOXO proteins to inhibit EGP. Insulin also suppresses glucagon secretion from the α cell to aid in suppression of EGP(82).

Insulin signaling is critical for normal regulation of glucose, but in response to excess nutrients, excess lipid accumulation and increased inflammation that can occur in obesity, insulin resistance develops(83). In individuals with insulin resistance, basal levels of EGP are increased, and insulin suppression of EGP during the fed state is impaired(79). Hepatic insulin resistance also leads to the accumulation of triglycerides, which are a hallmark of non alcoholic fatty liver disease (NAFLD)(79). Since insulin resistance is also a component of T2D, drugs that are used to improve hepatic insulin sensitivity, such as metformin, have widespread clinical use.

Colesevelam, a BAS, is a drug approved to treat hypercholesterolemia, and hyperglycemia, but its glucose-lowering mechanisms are not fully understood. While many of the effects of colesevelam have been attributed to improvements in β cell function, some studies have

also shown hepatic effects(41). In humans, colesevelam reduced both fasting and post prandial glucose levels, and resulted in a reduction in glycogenolysis(39, 84). In rodents, Potthoff *et al*. reported an increase in glycogenolysis with colesevelam(37), whereas Meissner *et al*. reported increased metabolic clearance rate, without any effects on EGP(85). However, this effect is likely independent of improvements in insulin sensitivity as three clinical studies reported no change in the homeostatic model assessment of insulin resistance (HOMA-IR) with colesevelam(33, 39, 86), and two additional studies found no improvements in peripheral or hepatic insulin resistance using the clamp method(87, 88). Therefore, in Chapter V, I examined whether a hepatic miRNA, miR-182-5p, that was upregulated with colesevelam could mediate some of the effects of colesevelam on glucose control. I found that loss of miR-182-5p partially reversed the glucose lowering effects of colesevelam(89), however, further studies will be required to elucidate which metabolic pathways in the liver are altered by miR-182-5p.

Lipoproteins

Work presented in this dissertation focuses on extracellular RNAs that are part of the pancreatic β cell secretome. As discussed in detail later in this introduction, RNAs are carried outside the cell by numerous carriers, including lipoproteins. While the RNA-carrying properties of lipoproteins are novel, research into lipoproteins and their role in cardiovascular disease has spanned many decades, and some of the key findings are discussed next.

Lipoproteins are complex particles composed of proteins that aid in transporting and solubilizing cholesterol esters and triglycerides in plasma(90). Plasma lipoproteins are categorized based on size, lipid, and protein composition: chylomicrons, chylomicron remnants, VLDL, intermediate-density lipoprotein (IDL), LDL, and HDL. In humans, the large lipoproteins (chylomicrons, VLDL, and LDL) are proathrogenic, whereas small lipoproteins (HDL) are anti-athogenic (Figure 1-6)(90). Lipoproteins are also characterized by their protein composition.

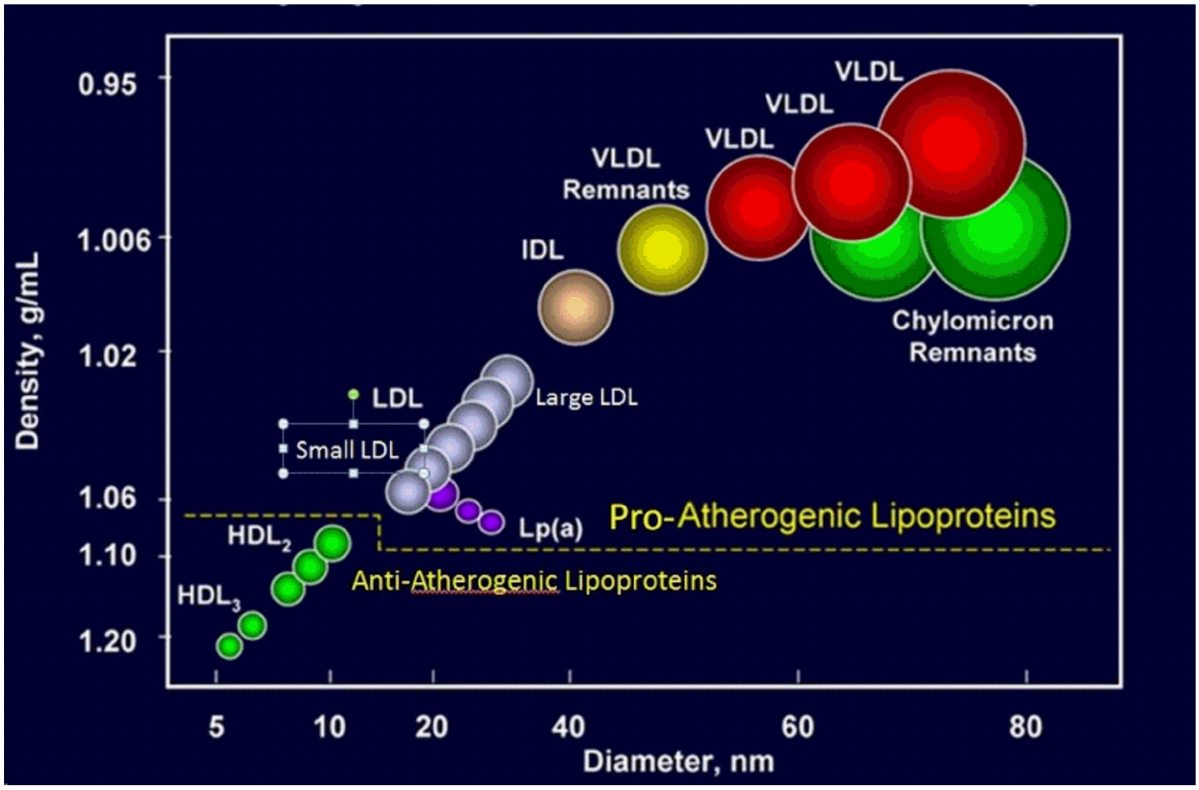

Figure 1-6. Size and density of lipoproteins. From Feingold, KR & Grunfeld, C. Introduction to Lipids and Lipoproteins. In: De Groot LJ, Chrousos G, Dungan K, Feingold KR, Grossman A, Hershman JM, Koch C, Korbonits M, McLachlan R, New M, Purnell J, Rebar R, Singer F, Vinik A, editors. SourceEndotext. South Dartmouth (MA): MDText.com, Inc.

Apolipoprotein B-100 (apoB-100), synthesized in the liver, is the main structural component of VLDL, IDL and LDL, whereas apoB-48, synthesized in the intestine is the main protein in chylomicrons(90). On HDL, apolipoprotein A-I (apoA-I) is the main protein accounting for 70% of HDL protein and apoA-II accounts for another 20% of total HDL protein(90). The field of lipoproteins is well studied, however, this dissertation focuses on non-cannonical cargo and function of HDL, but not the other lipoproteins. Therefore, further discussion of HDL's structure, function and non-cannonical function is provided next.

High density lipoproteins

The main structure function protein on HDL, apoA-I is synthesized predominantly in the liver and intestine and secreted to the circulation. This lipid-poor HDL acquires cholesterol and phospholipids that are effluxed from enterocytes and hepatocytes through the ATP-binding cassette transporter A1 (ABCA1) (90). Rodent studies have shown that most of the cholesterol efflux to nascent HDL occurs from hepatocytes, however, other cell types that express ABCA1, including muscle cells, adipocytes, and macrophages can also efflux cholesterol and phospholipids to nascent HDL(90). Cellular ATP-binding cassette transporter G1 (ABCG1) plays an important role in effluxing cholesterol to mature HDL particles(90). The cholesterol carried on HDL is primarily cleared through the liver. In the liver, HDL bindind to the scavenger receptor B-I (SR-BI) promotes the selective uptake of HDL cholesterol, without internalization of the particle, and a smaller particle is formed and released into circulation. Apo-AI, on the other hand, is catabolized by the kidneys, and to a lesser extent by the liver(90).

HDL research has predominantly focused on it's role in reverse cholesterol transport (RCT (91). Peripheral cells accumulate excess cholesterol through *de novo* cholesterol synthesis, as well as uptake of lipoproteins. However, most cell do not have ability to catabolize cholesterol(90). Therefore, the first step of RCT is efflux of cholesterol from peripheral cells to HDL, an important mechanism to rid the cell of excess cholesterol and prevent toxicity(90). During RCT, HDL also

undergoes structural modifications to the particle in response to lipid loading, which may alter its function(91). The final step of RCT is hepatic lipid uptake, where cholesterol is taken up by hepatocytes for excretion in bile and feces(91). Of clinical importance, RCT may aid in counteracting the development of atherosclerosis by promoting efflux of cholesterol from lipid loaded macrophages in the artery wall to HDL(91).

Epidemiological studies have shown an inverse association between HDL-cholesterol (HDL-C) and atherosclerosis and heart disease(91). For this reason, a number of new drug classes have aimed at raising HDL-C as a treatment for cardiovascular disease(92). However, while these drugs successfully raised HDL-C, they failed to reduce the risk of cardiovascular disease, calling into question whether raising HDL-C alone is an effective therapeutic strategy(92). Therefore, recently, there have been efforts to further understand the chemical composition and subclasses of HDL particles to better develop therapeutics for cardiovascular disease. Furthermore, beyond HDL's role in RCT, HDL also confers additional beneficial effects, including antioxidative, anti-inflammatory, antiapoptotic and improving endothelial cell dysfunction. It is currently not well understood how HDL confers these beneficial effects, but one theory is that the lipid, protein and RNA cargo on HDL may influence its function(93).

Seminal work from the Vickers laboratory in 2011 identified that HDL carries small RNAs, namely miRNAs, on HDL(94), and a follow-up study showed that HDL-mIRNAs have important anti-inflammatory effects in endothelial cells(95). Therefore, it is possible that HDL-miRNAs confer some of the beneficial properties of HDL. However, there are key questions still unanswered, including what cells release miRNAs to HDL, how this release is regulated, how miRNAs are carried and stabilized by HDL, and how HDL-miRNAs are delivered to recipient cells. Work in this dissertation aimed to answer the first two questions of miRNA export. As such, an introduction into miRNAs, their biogenesis, and function is provided next.

miRNAs

miRNAs are endogenous small non-coding RNAs approximately 20-25 nucleotides (nt) in length that function as guide molecules in RNA silencing(96). miRNAs are present in all tissues, and their regulation is tightly controlled, as miRNA dysregulation is associated with numerous human diseases. Primary miRNAs (pri-miR) are transcribed by Polymerase II (Pol II) either from their own promoter or processed from introns of protein coding genes and undergo several steps of maturation (Figure 1-7)(97). pri-miRs are often >1000kb and contain secondary stem loop structures that contain the mature miRNA sequence, and can consist of a single miRNA, or multiple related miRNAs (miRNA cluster) (98, 99). Similar to Pol II transcribed messenger RNAs (mRNAs), pri-miRs are 5' capped, polyadenylated and can be spliced(97). pri-miRs are processed in the nucleus by the microprocessor complex composed of the RNAse III enzyme Drosha and its double-stranded RNA binding cofactor DiGeorge syndrome critical region 8 (DGCR8) (Figure 1-7)(97). Following Drosha processing, the resulting stem loop precursor miRNA (pre-miRNA) is exported to the cytoplasm by the Ras-related nuclear protein-guanosine triphosphate (Ran-GTP) protein, exportin 5 (Figure 1-7) (98). In the cytoplasm, miRNA maturation continues, as the pre-miRNA is further processed by the RNAse III endonuclease Dicer to generate a small RNA duplex(98). The small RNA duplex generated by Dicer then is loaded onto an Argonaute (Ago) protein to form the RNA induced silencing complex (RISC) (Figure 1-7). The nomenclature for miRNAs is such that the miRNA derived from the 5' end is designated -5p and the miRNA from the 3' end is designated -3p. Generally, the miRNA strand with relatively lower thermodynamic stability on the 5' end is incorporated into Ago, and the ratio between the common and uncommon strand is on average 100:1(97, 98).

Once the mature single-stranded miRNA is incorporated into an Ago protein and the RISC complex, the miRNA guides the complex to its mRNA targets through sequence complementarity(97). In the case of perfect complementarity between the miRNA and its target

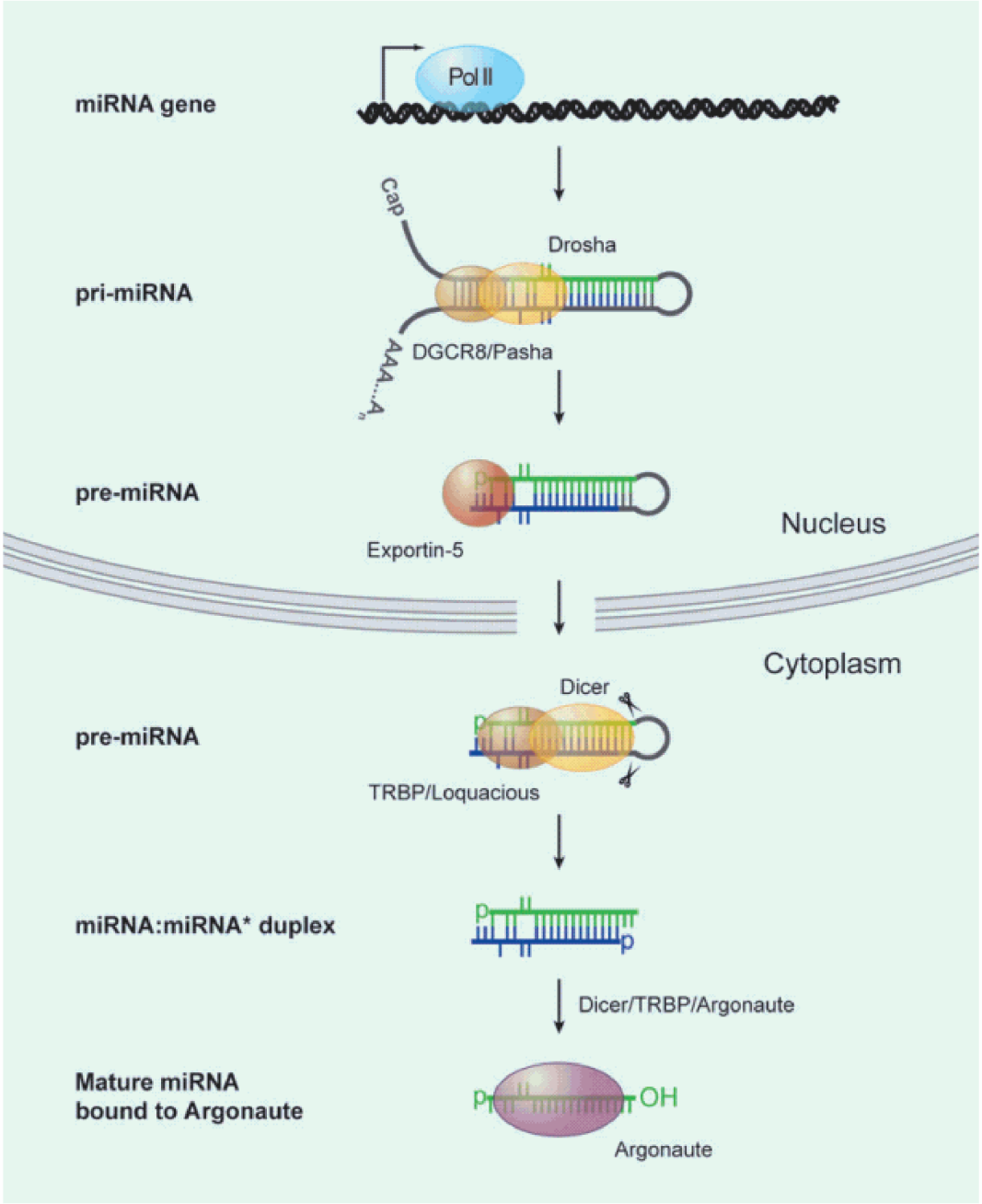

Figure 1-7. MicroRNA biogenesis. From Bushati, N. & Cohen SM. Annu Rev Cell Dev Biol. 2007;23:175-205.

sequence, the target mRNA can be cleaved and degraded. In mammals, Ago2 is the only Ago protein that is capable of endonucleolytic cleavage of the target RNA(97). However, endonucleolytic cleavage of target mRNAs is very uncommon in mammals, and only one miRNA target has been reported to be cleaved. This mechanism is mostly used as a research tool using silencing RNAs (siRNAs) designed to have perfect base pairing to the target mRNA to silence protein both *in vitro* and *in vivo*. In most mammalian cells, miRNAs pair imperfectly with their targets to repress translation(97). nts 2-8 are termed the seed region and are critical for initial target recognition; nts 9-10 are the intermediate region and do not have a significant role in target recognition; nts 13-16 are important to stabilizing the miRNA-RNA interaction, and nts beyond 16 are the tail region and do not bind to the target RNA(100). miRNAs generally target mRNAs in the 3' untranslated region (UTR). Although miRNAs can target the open reading frame (ORF) or the 5' UTR, miRNA activity does not normally occur in these regions as the translating ribosome allows limited residency time of silencing complex in the ORF. miRNAs suppress target mRNA activity by interfering with translation by blocking initiation, preventing elongation, or destabilizing the transcript resulting in mRNA decay(97). mRNA decay involves recruiting of the glycine-tryptophan protein of 182kDa (GW182), which interacts with the polyadenylate-binding protein (PABPC) and promotes deadenylation of the mRNA transcript(99). While it appears that blocking initiation and preventing elongation is a key mechanism of miRNA mediated regulation, mRNA decay is an irreversible process, and therefore likely accounts for the majority of miRNA silencing(101).

Due to the imperfect base pairing between miRNAs and target mRNAs, one miRNA can silence hundreds of genes, and multiple miRNAs can target the same mRNA. However, the effects of miRNAs are generally mild, and thus miRNAs have been termed "fine-tuners" of gene expression. But miRNAs can also have robust effects; often miRNAs or clusters of miRNAs regulate genes in the same cellular pathway to compound the small effects of a single miR-mRNA interaction(99). The work described in this dissertation focuses on four microRNAs: rno-, mmu-

and hsa-miR-375-3p, mmu-miR-96-5p, mmu-miR-182-5p and mmu-miR-183-5p. A review of the exisiting literature on the miR-96/182/183 cluster in metabolic tissues and miR-375-3p in islets is provided next.

The miR-96/182/183 cluster in metabolic tissues

The miR-96/182/183 cluster is a polycistronic miRNA cluster encoded on chromosome 6 in mouse and chromosome 7 in humans first identified in the eye(102). More recently, this cluster was shown to be associated with cholesterol metabolism(103). Jeon *et al*. recently reported that the promoter for miR-96/182/183 contains a sterol response element (SRE), which is transcriptionally activated by SREBPs(103). There are three major isoforms of SREBP: SREBP-1a and SREBP-1c which are encoded by the *SREBF1* gene but have unique promoters, and SRBEP-2 which is encoded by the *SREBF2* gene(104). SREBPs are transcription factors and are considered master regulators of cholesterol and fatty acid metabolism. SREBP-1c preferentially activates genes for fatty acid metabolism, SREBP-2 activates cholesterol genes and SREBP-1a regulates both cholesterol and fatty acid metabolism(105). This dissertation specifically focuses on SREBP-2.

Due to its important role in maintaining cholesterol homeostasis, SREBP-2 is regulated through a number of elegant mechanisms. SREBP-2 is transcribed and translated and retained in the endoplasmic reticulum (ER) in its inactive form(105). When cellular cholesterol levels are low, the SREBP cleavage-activating protein (Scap) forms a complex with SREBP2 that allows for its transport to the Golgi apparatus and for proteolytic cleavage(105). The active transcription factor can then translocate to the nucleus where it activates gene transcription(105). To restore cellular cholesterol levels, SREBP-2 activates transcription of genes encoding rate limiting enzymes in the *de novo* cholesterol biosynthesis pathway, 3-hydroxy-3-methylglutaryl-coA reductase (*HMGCR*) and squalene epoxidase (*SQLE*), and genes encoding cholesterol uptake proteins, such as LDLR(105). SREBP-2 also inhibits loss of cellular cholesterol through efflux to

HDL. In its intron, SREBP-2 encodes miR-33a, which was shown to target the *ABCA1*, a key protein in cholesterol efflux(106-108). Furthermore, through the miR-96/182/183 cluster, Jeon *et al*. showed that mouse SREBP-2 participates in a positive feedback loop by inhibiting suppressors of SREBP-2 activity(103). mmu-miR-182-5p was shown to target the E3 ubiquitin ligase F-box and WD repeat domain containing 7 (Fbxw7), a protein that degrades SREBP-2, and mmu-miR-96-5p targets the insulin induced gene 2 (Insig2) a protein that binds to Scap to prevent its association with SREBP-2 under conditions of elevated cellular cholesterol(103).

Beyond cholesterol regulation, members of the miR-96/182/183 cluster have also been found to play a role in glucose metabolism. miR-182-5p expression was reported to be downregulated in WAT, skeletal muscle, liver, pancreas, and blood from HFD fed rats(109). Furthermore, miR-182-5p is also decreased in blood from HFD fed non-human primates (NHP) and humans with T2D(109). Although not investigated directly in this study, the authors postulated that downregulation of miR-182-5p in T2D allows for upregulation of its target gene, FOXO1, a key gluconeogenic gene that has been reported to be upregulated in T2D(109-113). miR-182-5p has also been shown to target FOXO3, a protein that has been implicated in muscle atrophy(114, 115). More recently, Zhang *et al*. reported that miR-182 knockout mice have impaired glucose metabolism(116). miR-182-5p was shown to target FOXO1 and the pyruvate dehydrogenase kinase 4 (PDK4), and loss of miR-182-5p and upregulation of its target genes decreased glucose utilization in skeletal muscle and led to elevated plasma glucose levels(116). Unlike miR-182-5p, miR-96-5p has been shown to be upregulated, not downregulated in the livers of HFD fed mice, albeit this study was in mice, whereas the miR-182 study was in rats(109, 117). Nevertheless, in this study miR-96-5p was found to target INSR and IRS-1. Yang *et al*. proposed a model in which miR-96-5p upregulation with HFD feeding suppresses INSR and IRS-1 and promotes insulin resistance(117). Furthermore, FOXO1 has also been identified to be a target of miR-96-5p(118-120). At this time, there have been no reports of changes in miR-183-5p with HFD or in T2D, nor the effect of miR-183 on glucose control. As such, further work will be required to dissect the

effects of each of these miRNAs, and distinguish how cellular conditions alter their expression, as well as what miRNA-target networks are regulated under different conditions. In my studies, I found that this cluster is also upregulated in diabetic mice and rats treated with colesevelam, a BAS that stimulates *de novo* cholesterol synthesis to replenish lost BAs. Due to the established role of miR-182-5p in glucose metabolism in skeletal muscle, I hypothesized that hepatic miR-182 may contribute to the glucose lowering effects of colesevelam. This work is described in Chapter V.

Islet miR-375-3p

miR-375-3p is a miRNA encoded in an intergenic region of choromosome 1 in mouse and chromosome 2 in humans(121, 122). miR-375-3p is one of the most abundant miRNAs in the pancreatic islet and β cell(123, 124). In 2004, Poy *et al*. first reported that miR-375-3p is an islet specific miRNA (Figure 1-8A) and subsequently two more studies showed that while miR-375-3p is expressed in other organs in both mouse and humans, it is highly enriched in the pancreas and islet (Figure 1-8B-D)(125, 126). The first study by Poy *et al*. showed that miR-375-3p inversely regulates insulin secretion, as overexpression of miR-375-3p in MIN6 cells inhibited insulin secretion, whereas inhibition of miR-375-3p in these cells enhanced insulin secretion(127). miR-375-3p was also found to target myotrophin (Mtpn), a protein involved in insulin exocytosis(127). Subsequently in 2009, Poy *et al*. reported the generation of the miR-375 knockout (KO) mouse(128). These mice are hyperglycemic, have impairments in β cell development, increased total α cell numbers and elevated glucagon levels(128). Furthermore, the authors showed by crossing miR-375 KO mice onto an *ob/ob* background, that loss of miR-375-3p prevents the proliferation in β cells normally observed in *ob/ob* mice in response to increased insulin demand(128). Work from this same group later showed that overexpressing miR-375-3p 1.5-fold (Tg375) in β cells (Figure 1-7B) results in no apparent phenotype, but that rescuing miR-375-3p

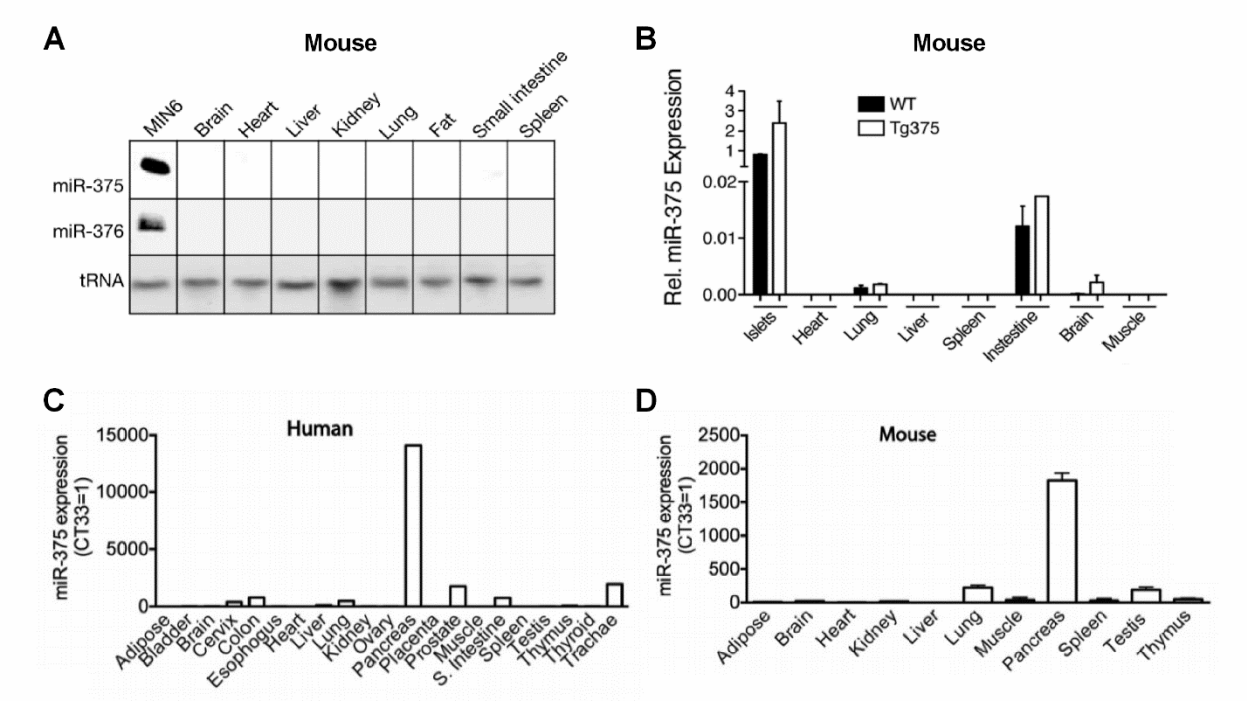

Figure 1-8. Tissue expression of miR-375-3p. (A) Mouse tissue expression of miR-375 and miR-376 by Northern blots. From Poy, MN. et. al. Nature. 2004 Nov 11;432(7014):226-30. (B) Mouse tissue expression of miR-375-3p in wildtype and miR-375 overexpressing mouse (Tg375) by qPCR. From Latreille et. al. J Mol Med (Berl). 2015 Oct;93(10):1159-69. (C) Human and (D) mouse expression of miR-375-3p by qPCR. From Erener, S. et. al. Endocrinology. 2013 Feb;154(2):603-8.

expression in beta cells alone (by crossing miR-375 KO with β cell Tg375) rescues the phenotype of the miR-375 KO mouse(125).

Due to its key role in the islet, a number of studies have aimed to define the transcriptional networks that regulate miR-375-3p expression in the islet. A study by Avnit-Sagi and colleagues suggested that regulation of miR-375-3p confers its enrichment in the islet, perhaps through the transcription factors Neurogenin-3 (Ngn3) and neuronal differentiation 1 (NeuroD)(129). Furthermore, both glucose and cAMP have both been shown to reduce miR-375-3p levels(130, 131). El Ouaamari *et al*. showed that in INS-1E cells and primary rat islets, pre-miR-375 and mature miR-375-3p are downregulated with high glucose treatment, whereas Keller *et al*. showed that miR-375-3p expression is suppressed with compounds that raise cAMP levels, such as GLP1R and cAMP agonists(131). This supports a model proposed by the *in vitro* functional studies described above, where miR-375 is low under conditions of high glucose, derepressing target genes, such as *Mtpn* and *Pdk1* that promote insulin secretion.

Due to its important role in the islet, miR-375-3p changes have also been studied in response to T2D. In islets from diabetic GK rats compared to control nondiabetic rats, one study reported a decrease in miR-375-3p, whereas another study reported no change(130, 132). In humans, there was no difference in miR-375-3p between islets isolated from T2D and control donors(133). Moreover, *ob/ob* mice have elevated levels of islet-miR-375-3p compared to controls. miR-375-3p targets a broad network of genes in the β cell, and its regulation is likely tightly controlled to both promote β cell development and allow for insulin secretion. Therefore it is still unknown how long-term metabolic alterations such as T2D alter the levels of this miRNA. The work described in Chapter III identifies that miR-375-3p may have a function outside of β cells and islets, as I show that these cells can export miR-375-3p to HDL. An introduction to extracellular miRNAs and its carriers is provided next.

Extracellular miRNAs

Beyond their canonical cellular role, miRNAs have also been found in the extracellular environment, including biological fluids, and have become known as extracellular miRNAs or circulating miRNAs(134, 135). miRNAs have been found in plasma, blood, saliva, tears, urine, breast milk, cerebrospinal fluid, bronchial lavage and follicular fluid(136-142). RNAs were known to be present in blood as early as the 1970s, however, it was assumed that these extracellular RNAs would be rapidly degraded due to the presence of RNAses in blood and other extracellular fluids(143, 144). However, in 2004, work by El-Hefnawy *et al.* reported that RNA in plasma is stable unless pre-treated with detergent, suggesting that plasma RNAs are bound to a lipid or protein carrier that confers its stability(145). Subsequently in 2008, Valadi *et al*. published the first report showing that both mRNAs and miRNAs are released from cells in exosomes and that mRNAs could be transferred to recipient cells and undergo mRNA translation to produce new proteins(137). Since then, the field of extracellular miRNAs has generated enormous excitement, as they hold great potential as hormone-like molecules in inter-cellular communication, as disease biomarkers, and potentially as novel drug targets.

To date, numerous extracellular miRNA carriers have been identified, including exosomes, microvesicles (MVs), lipoproteins and ribonucleoproteins (Figure 1-9). Exosomes are vesicles derived from multivesicular bodies (MVB) in endosomes and are the most well studied extracellular miRNA carrier(146). Exosomes are formed by the internalization of the cell membrane to produce endosomes (Figure 1-9). These endosomes then become part of the MVBs and can be released into the extracellular space after fusion of the MVB with the plasma membrane(146). Exosomes are less than 150 nm in diameter and their formation is ATP dependent(146). Furthermore, miRNA profiles of exosomes contain cargo distinct from the parent cell, thus suggesting that exosome cargo is actively sorted from the total cellular RNA and protein pool(135, 137). The main function for exosome-miRNAs has been hypothesized to be cell-to-cell

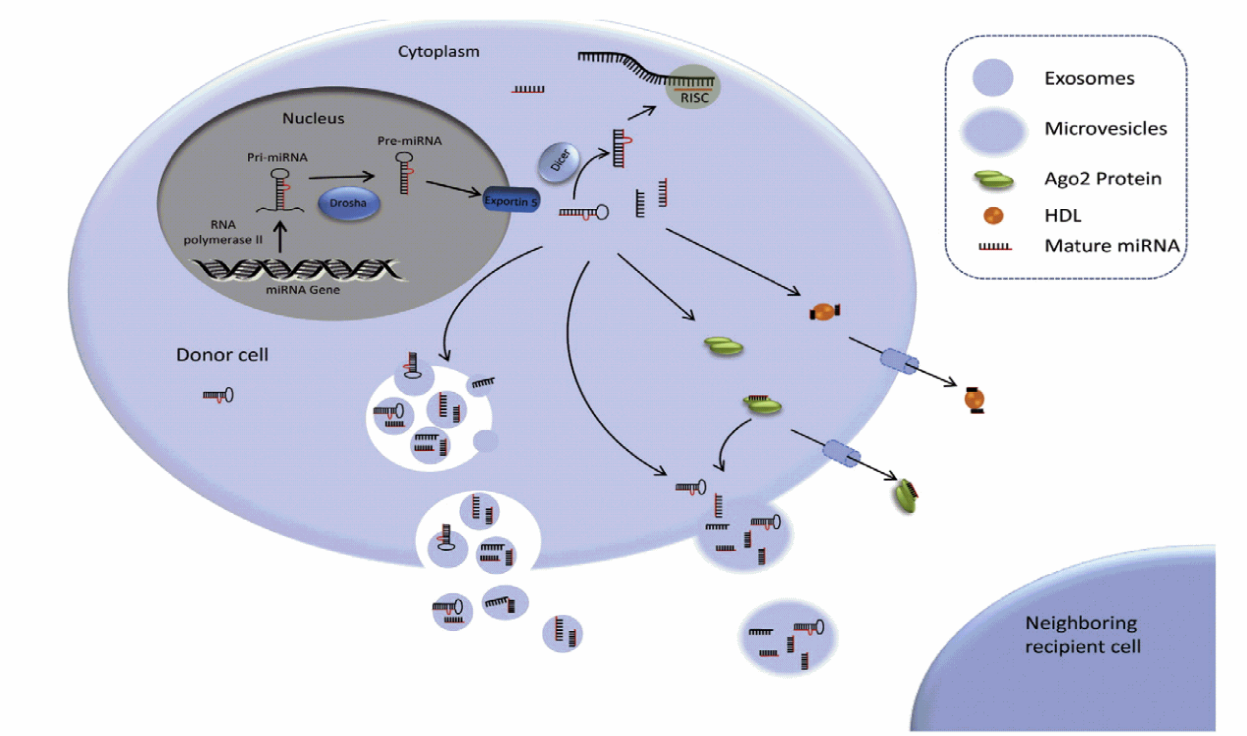

Figure 1-9. MicroRNA biogenesis and release to the extracellular environment. From Sohel, MH. Achievements in the Life Sciences 10 (2016) 175–186

communication, however, a recent study reported that exosomes, on average, contain less than 1 molecule of a given miRNA per exosome, and that over 100 exosomes would have to be profiled to observe one copy of a single abundant miRNA(147). This has called into question the stoichiometry of miRNAs carried by exosomes and their influence on distal gene expression. Furthermore, most of the work supporting miRNA transfer between cells via exosomes has come from *in vitro* studies, but recent studies have also examined the physiological role of exosome miRNAs by injecting miRNA-loaded exosomes into rodents(148-150). As such, a comprehensive understanding of the role of exosome miRNAs *in vivo* is still lacking.

MVs or microparticles are also membrane bound vesicles, but unlike exosomes, are shed by the plasma membrane of cells and the composition of surface markers is largely dependent on the cell of origin (Figure 1-9)(135). MVs are larger than exosomes, ranging from 100 to 1000 nm in diameter. MVs containing miRNAs have been reported to be released from endothelial cells, platelets, neurons, cancer cells, and stem cells, among other cells(136, 151-154), and evidence *in vitro* suggests they may be involved in intercellular communication(135, 155). Similarly, cells can also release apoptotic bodies as they undergo apoptosis. These membrane blebs are phosphatidylserine rich and the vesicle size ranges from 1 to 5 μm(135). Apoptotic bodies have also been shown to carry miRNAs, and have been postulated to function in cell-to-cell communication as a recent study showed that apoptotic bodies containing miR-146 altered atherosclerosis in a mouse(156).

In 2011, two studies showed that a large proportion of extracellular miRNAs are not associated with vesicle carriers, but rather associate with Ago2, the functional component of RISC. Arroyo *et al*. showed that three miRNAs studied in detail had distinct distribution in plasma; let-7a was found to associate predominantly with vesicles, whereas miR-16 and miR-92a associated with free protein, and they identified this free protein to be Ago2, but not Ago1, Ago3 or Ago4(139). Similarly, Turchinovich *et al*. identified that miR-16, miR-21 and miR-24 are associated with Ago2, however, unlike the study by Arroyo *et al*., this study suggested that the

other Ago proteins may also carry these miRNAs(157), and a follow-up study also showed that miRNAs associate with both Ago1 and Ago2(158). Additionally, while Arroyo *et al*. estimated that 10-25% of the total pool of miR-16 and miR-92a were contained in Ago2, Turchinovich *et al*. suggested that 90% of miRNAs are carried by Ago2(139, 157). It is unclear if this difference is due to a distinct distribution among the miRNAs in each study or due to technical limitations in estimating percent recovery from the enrichment techniques used, i.e. IP.

Also, in 2011, our lab identified that miRNAs are carried in circulation, protected from RNAses by HDL(94). HDL is clinically important as HDL-C is inversely associated with cardiovascular disease(159). HDL are the smallest of the family of lipoproteins and are characterized by their density of 1.063 g/mL to 1.210 g/mL, and by the presence of the major structural protein apoA-I(160). A number of other lipoproteins also contribute to the composition of HDL, including apoAII, apoAIV, apoB, apoCI and apoCII(160). HDL are mainly secreted by the liver and small intestine as free apoA-I and become lipidated to form pre-β HDL and mature HDL through the RCT(161). In the first step of RCT, cholesterol is effluxed to HDL from peripheral cells. Subsequently, cholesterol is carried back to the liver for recycling and excretion through bile(161). HDL aids in clearing cholesterol from atherosclerotic foam cells in the plaque and thereby reducing the atherosclerotic burden. HDL can also exchange cholesteryl esters and triglyceride with apoB containing particles (LDL and VLDL). Recently HDL has been found to transport a wide variety of cargo in addition to cholesterol and lipids, including miRNAs.

Prior to the discovery that HDL could transport miRNAs, Lee *et al*. reported that apoA-I could effectively be used to deliver siRNAs to mouse livers *in vivo(162)*. Shortly after, Vickers *et al*. reported that HDL carries RNAs, predominantly small RNAs <40 nt, in circulation(94). This study further showed that miR-223, an inflammatory cell miRNAs, is highly expressed on HDL, and is exported from macrophages to HDL. In addition, Vickers *et al*. showed that HDL-miR-223 can be delivered to recipient Huh7 hepatoma cells *in vitro*, and that this delivery requires HDL's receptor, SR-BI(94). In a follow-up study, Tabet *et al*. demonstrated that HDL-miR-223 is

transferred to endothelial cells *in vitro* and can downregulate the expression of two inflammatory genes, intercellular adhesion molecule-1 (*ICAM1*) and colony-stimulating factor 2(95). However, in an independent study, Wagner *et al*. reported that HDL-miR-223 is not transferred to endothelial cells, smooth muscle cells, or peripheral blood mononuclear cells(163). This difference is likely due to differing amounts of HDL used in these *in vitro* studies, and therefore a systematic approach to studying HDL-miRNA using tracer techniques *in vivo* would provide a better understanding of this process.

Furthermore, there is little known about the processes that regulate miRNA export to HDL. Vickers *et al*. reported that chemical inhibition of the neutral sphingomyelinase 2 (nSMase2), which inhibits exosome biogenesis, enhances miR-223 export to HDL(94, 164). Additionally, this study reported that miR-223 export to HDL was unaffected when ABCA1 or ABCG1 were induced using a liver-X-receptor (LXR) agonist(94). However, to date, there have not been any reports of pathways that are required for miRNA export to HDL. As such, I investigated the regulatory pathways of HDL-miR-375-3p export from pancreatic beta cells and found that promoting insulin secretion with high glucose (in the presence of Ca^{2+}), tolbutamide, or cAMP inhibited miR-375-3p export to HDL (Chapter III).

miRNA-mediated intercellular communication from islets

The idea that β cells release miRNAs to the circulation for cell-to-cell communication is not novel. In 2014, Figlioni *et al*. showed that EVs isolated from islet culture medium contained islet-specific proteins (insulin, C-peptide and GLP1R), mRNAs (insulin), and miRNAs (including miR-375, miR-200c and miR-21)(165). Furthermore, this study showed that *in vitro*, insulin mRNA, as well as miR-375-3p, miR-200c and miR-21 were delivered to islet endothelial cells, with the levels peaking 3h post incubation(165). In another study, Guay *et al*. profiled the miRNA composition of exosomes secreted from MIN6 β cells and found that exosome miRNAs do not reflect cell miRNAs, and that the miRNA cargo packaged in exosomes changes when cells are

treated with cytokines(166). Through the use of an exogenous non-mammalian miRNA, cel-miR-238, this study further demonstrated that exosomes can transfer this miRNA to recipient β cells. In addition, Guay *et al*. found that when donor β cells are treated with cytokines, exosomes released from these cells induce apoptosis in the recipient β cells(166). The authors propose that this is due to transfer of miRNAs in exosomes between β cells, as cytokine treated exosomes downregulated Ago2 in recipient cells(166). Finally a recent study by Lakhter *et al*. similarly found that miRNA secretion from β cells to exosomes was altered with cytokine treatment. Specifically, this study showed that β cell lines and human islets released increasing amounts of miR-21-5p in response to cytokine treatment, however, the authors did not measure delivery of this miRNA to recipient cells.

While each of these studies measured miRNA release from islets or β beta cells to exosomes or MVs, they do not overcome the key question in the field of whether this process occurs *in vivo*, and whether the amount of miRNAs released by β cells is sufficient to modulate gene expression in recipient cells. My work in Appendix Part 4 & 5 aimed to develop a method, first *in vitro*, and then *in vivo* to trace miRNAs transcribed in the β cell and delivered to recipient tissues. Unfortunately, I was unable to reliably distinguish signal from noise and the results were highly variable between studies. Therefore a comprehensive analysis into miRNA transfer between cells, and especially β cells, is still lacking.

Extracellular miR-375-3p

The studies mentioned above describe a potential role for β cell miRNAs as intercellular communication signals. Although the function of extracellular mIR-375-3p is currently unknown, a number of studies have investigated miR-375-3p release from β cells. Previous studies have proposed that miR-375-3p may be released from β cells in response to cell death. In support of this hypothesis, two independent studies have shown that extracellular miR-375-3p levels are increased in cell culture medium when islets or MIN6 cells were treated with the cytotoxic

compound STZ(126, 167). As shown in Figure 1-9, Erener *et al*. showed that miR-375-3p levels are upregulated approximately 20-fold when islets are treated with cytokines or STZ to induce cell death (Figure 1-10A)(126). Furthermore, release of miR-375-3p to the medium was decreased when cells were pretreated with compounds that partially blocked the effects of cytokines and STZ on cell viability (Figure 1-10B)(126). Similarly, Song *et al*. found that when MIN6 cells were treated with increasing concentrations of STZ to induce cell death, miR-375-3p levels in the cell culture medium increased (Figure 1-10C,D)(167). However, both of these studies induced very high levels of cytotoxicity (>50% cell death), much higher than what is observed *in vivo* under normal physiological conditions. Therefore, while it is likely that miR-375-3p is released from β cells upon cell death, this does not rule out the possibility that miR-375-3p is also released from β cells under non-cytotoxic conditions and that this export process is regulated.

In support of this, a recent study by Zhang *et al*. reported that miR-375-3p is selectively released in exosomes from MIN6 β cells and human islets (Figure 1-11)(168). This study also found that miR-375-3p release in exosomes is enhanced with conditions that promote insulin secretion, such as high glucose, potassium chloride (KCl) and arginine (Figure 1-11)(168). Similarly, miR-375-3p has been shown to be released from neurons in large dense-core vesicles and this export is enhanced with Ca^{2+}(169). Work from the Vickers lab has shown that miR-375-3p is among the most abundant HDL-miRNAs and data from our lab also suggests that miRNA export to HDL is regulated inversely to miRNA release in exosomes(94, 170). Therefore, I hypothesized that miR-375-3p export to HDL from β cells is suppressed by cellular conditions that enhance insulin secretion. My studies addressing this hypothesis are described in Chapter III.

Beyond its role in intercellular communication, there has also been great interest in studying extracellular miR-375-3p as a biomarker for diabetes. In T1D, studies consistently show in rodents and humans that miR-375-3p is upregulated(125, 126, 167, 171-173). However, in T2D, the data is less conclusive, with some studies showing increase, others decrease, and still

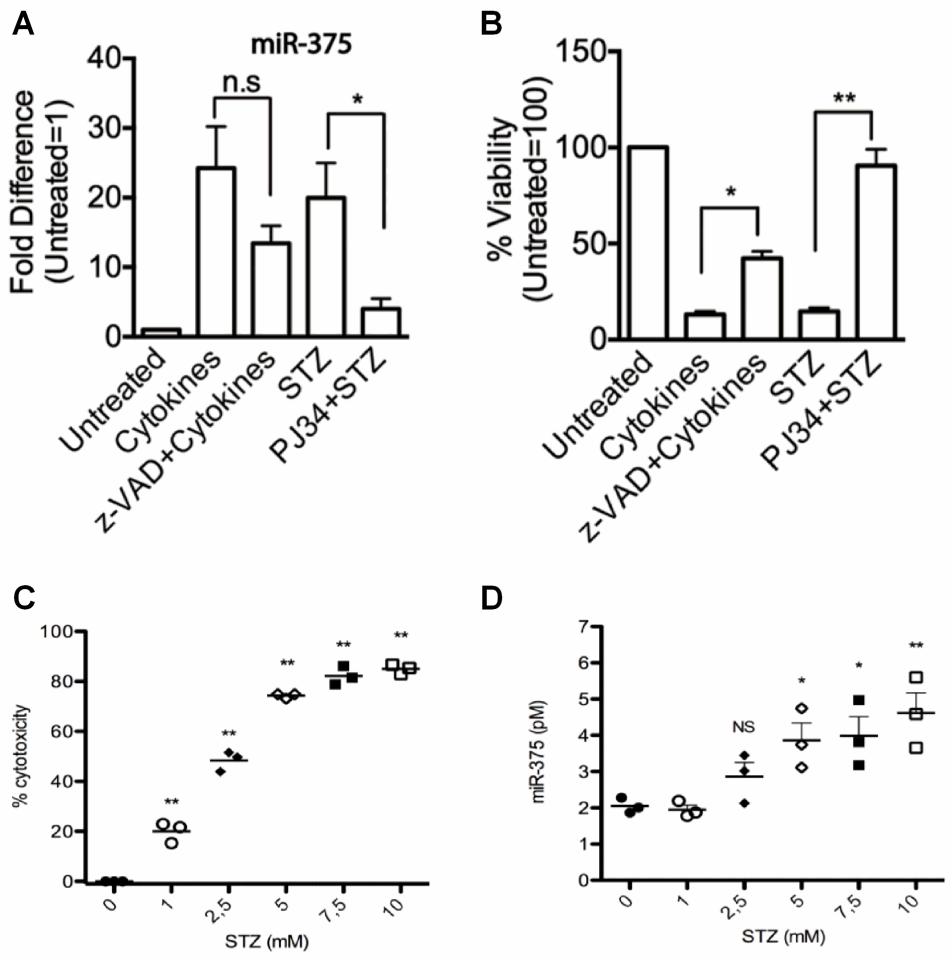

Figure 1-10. miR-375-3p release in response to cell death. (A) miR-375-3p levels measured from total RNA isolated from islet cell culture media. (B) Cell viabilty measured by staining with ethidium homodimer and calcein. From Erener, S. et. al. Endocrinology. 2013 Feb 154(2):603-608. (C) Percent cytotoxicity of MIN6 cells using crystal violet staining in response to increasing concentration of STZ. (D) miR-375-3p levels in media from MIN6 cells treated with increasing concentrations of STZ for 18h. From Song, I et. al. PLoS One. 2017 Oct 17;12(10):e0186480.

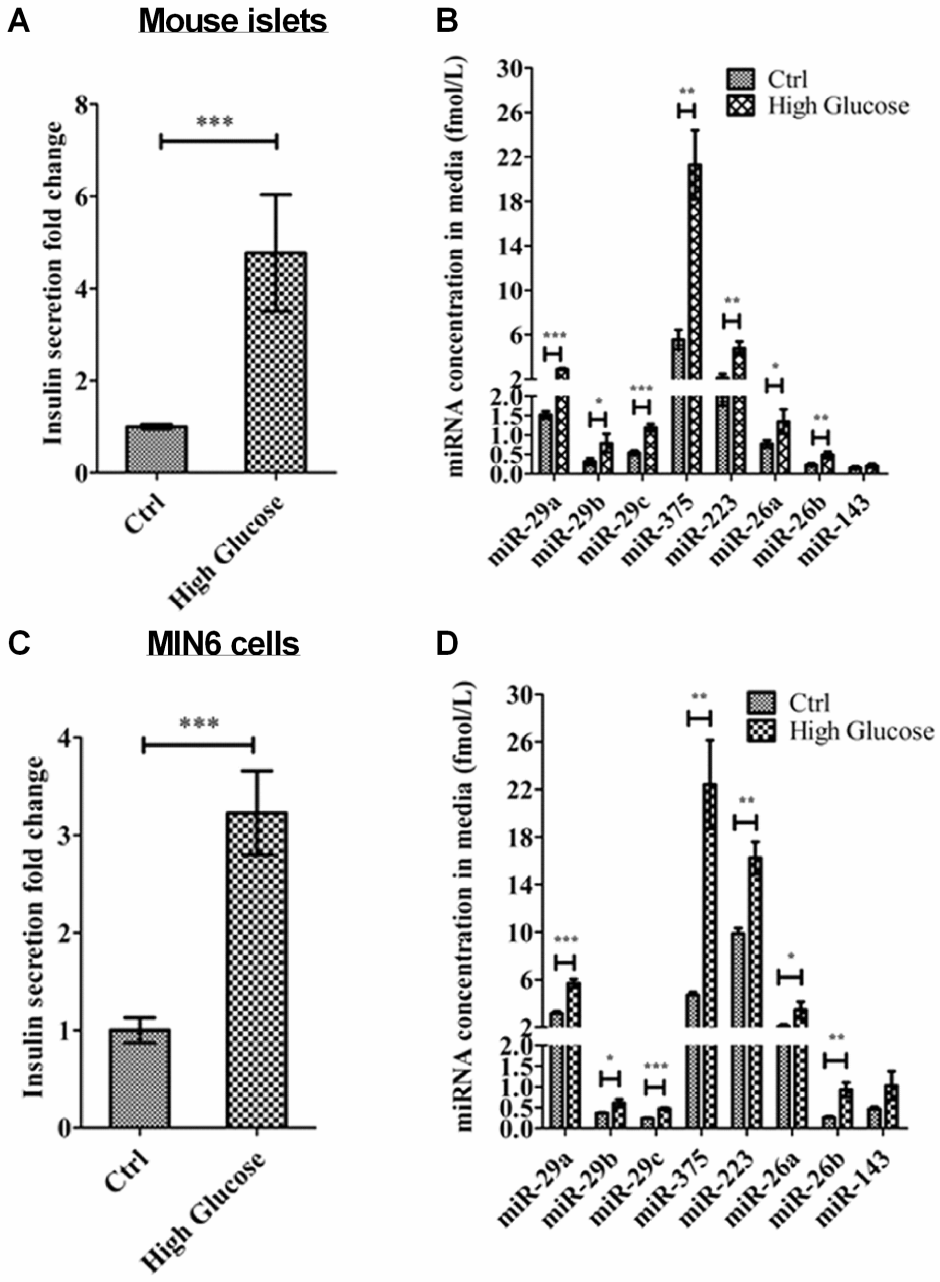

Figure 1-10. miR-375-3p release from islets and MIN6 in response to high glucose. (A) Insulin secretion from mouse primary islets (B) miRNA, including miR-375-3p, export from islets in exosomes in response to high glucose. (C) Insulin secretion from MIN6 cells (D) miRNA, including miR-375-3p, export from MIN6 cells in exosomes in response to high glucose. From Zhang, A et. al. Biochem Biophys Res Commun. 2018 Jan 8;495(2):1648-1654.

others no change in miR-375-3p levels in rodent models of T2D or human subjects with T2D(101, 125, 174-176). Due to my findings that miR-375-3p is exported to HDL from clonal β cells and islets, I investigated whether HDL-miR-375 is altered in *db/db* mice, ZDF rats, and human subjects with T2D. Additionally I investigated the effect of STZ treatment in mice on plasma- and HDL-miR-375-3p. My findings and a comparison to the existing studies is provided in Chapter IV.

Goals of the dissertation

The field has made enormous progress in defining the biogenesis, function and impact of disease on extracellular miRNAs, but many questions still remain, especially in the field of HDL-miRNAs. The studies described in this dissertation define an inverse relationship between insulin secretion and miR-375-3p export to HDL from β cells (Chapter III). Although the function of HDL-miR-375-3p is currently unknown, my work is the first to uncover a regulatory pathway by which a cell exports a miRNA to HDL. Part of my work also aimed to develop a method that could be used to label β cell originating miRNAs *in vitro* and *in vivo* and trace their delivery to recipient cells, as comprehensive data showing *in vivo* HDL-miRNA delivery and its function in physiology is desperately needed in the field (Appendix Part 4 & 5). Furthermore, due to the enormous interest in using extracellular miRNAs as biomarkers for disease, and my findings that β cells can export miR-375-3p to HDL, I profiled HDL- and plasma-miR-375-3p changes in both T1D and T2D rodent models, and in human subjects with T2D (Chapter IV). Finally, my work described in Chapter V aimed to study whether miR-182 contributes to the glucose lowering effects of the BAS, colesevelam. The methods utilized for these studies are described in Chapter II. Collectively, the work described in this dissertation provides a novel understanding of the mechanisms of β cell, extracellular and hepatic miRNA regulation in response to chronic and acute metabolic alterations.

CHAPTER II

MATERIALS AND METHODS

Methods for Chapters III & IV

HDL Isolation

Native HDL (nHDL) used for cell culture studies was isolated from healthy volunteers at Vanderbilt University Medical Center, purchased from Interstate Blood Bank, or obtained from the Vanderbilt blood bank. nHDL was isolated from human plasma by density-gradient ultra-centrifugation (DGUC, 1.061-1.21 g/mL), 330,000 x *g* followed by extensive dialysis at 4°C in 1X phosphate buffered saline (PBS). The study conformed to the guidelines set out in the Declaration of Helsinki and pertinent ethical regulations. The protocol was approved by the ethical committee of Vanderbilt University Medical Center (Institutional Review Board, IRB# 151573) and all volunteers gave written informed consent for participation in the study. Pooled mouse plasma (50 ml) was purchased from Equitech-Bio, Inc. HDL was isolated from mouse and human plasma by DGUC, as described above for nHDL. For human HDL-RNA analysis, blood was collected from healthy blood donors (n=10) at Vanderbilt University Medical Center under active IRB protocol. For human studies comparing healthy and T2D HDL and plasma, blood was collected from control (n=20) and T2D (n=20) subjects at KineMed, Inc. (Emeryville, CA) and at Vanderbilt University Medical Center as approved by IRB. T2D was defined as HbA1c 6.7%-10% and controlled by diet alone, stable dose of sulfonylurea and/or metformin. Immuno-affinity purification of HDL was achieved as previously described(94) using goat-anti-human apoA-I antibodies conjugated to Sepharose-4B beads (Academy Biomedical Company). RNA was isolated from 100 µg of HDL protein (Norgen Biotek).

Animal Experiments

All animal experimentation was approved by and carried out in accordance to the Vanderbilt Institutional Animal Care and Use Committee (IACUC). All transgenic lines were backcrossed to a C57BL/6 background for more than 10 generations. Female *Abcc8*$^{-/-}$ (*Abcc8*$^{tm1.1Mgn}$) and wildtype C57B6/J (WT) mice were used at 12 weeks old(177). Female *Kcnj11*$^{-/-}$ mice were used at 12 weeks old(178). *Scarb1*$^{+/-}$ mice were obtained from The Jackson Laboratory and bred to generate *Scarb1*$^{-/-}$ mice. Female *Scarb1*$^{-/-}$ and WT mice were used at 8 weeks old. Blood was collected from lean and ZDF rats as approved by KineMed Inc. IACUC protocol. Blood was collected from 10-wk old *db/db* mice and WT controls. 8-week old male C57B6/J mice (Jackson Laboratories) were treated with STZ or PBS control. Prior to each injection, mice were fasted for 4 hours. Mice were dosed i.p. with freshly made 50 mg/kg STZ (Sigma-Aldrich) dissolved in sodium-citrate buffer pH 4.5 (Sigma-Aldrich) for 5 consecutive days. Control mice were fasted and received injections of 1x PBS (Invitrogen) for 5 consecutive days. STZ treated mice were supplemented with 10% sucrose (Sigma-Aldrich) in drinking water to avoid sudden hypoglycemia. Body weight was measured daily and glucose was measured from the tail using the Aviva Plus ACCU-CHECK glucometer (Roche) biweekly and on the day of sacrifice. 10-days after the last STZ dose, mice were fasted and sacrificed and retro-orbital blood was collected. Glucose levels in the STZ treated mice varied substantially, and hence were divided into “low” and “high” glucose groups for the analysis. For fast-refed study, 11-week old male C57B6/J were divided into three groups: fasted (n=3), fed (n=3) and refed (n=3). Fed mice were allowed access to food *ad libitum* until sacrifice. Fasted, and refed mice were fasted for 16h. Fasted mice were sacrificed after 16h fast. Refed mice were give ad libitum access to food for 2h post fast, and then sacrificed. At sacrifice, retro-orbital blood was collected and livers were perfused and flash frozen. For correlation of plasma and HDL miR-375, blood was collected from 5 12-week old male WT mice.

HDL-miRNA Export Assays

Primary islets (human and rodent) or INS-1 cells were incubated with 1 mg/mL nHDL (isolated by DGUC) in serum-free media for 1-48 h and maintained at 37°C with 5% CO_2 for 24 h. Control nHDL was added to media and incubated in the absence of cells (cell free, cf) at 37°C with 5% CO_2 for 24 h. cf-nHDL and islet-nHDL or INS-1-nHDL were isolated from culture media by immunoprecipitation (IP) using goat-anti-human apoA-I antibodies conjugated to Sepharose-4B beads (Academy Biomedical Company). RNA was isolated from 100µg of HDL total protein (Norgen Biotek).

Primary Islet Culture

Primary human islets from three individual human donors were obtained through the Integrated Islet Distribution Program. Primary mouse islets were isolated from the following transgenic mice: *Abcc8*$^{-/-}$, *Kcnj11*$^{-/-}$, *Scarb1*$^{-/-}$ and WT mice as previously described(179). Primary islets (50) were added to each well in RPMI supplemented with 5.6 mM glucose, streptomycin (100 µg/ml), penicillin (100 U/ml), 10% lipoprotein deficient serum (LPDS) (DGUC 1.21 g/ml, bottom fraction), and 1mg/ml DGUC nHDL and maintained at 37°C with 5% CO_2 for 24 h. For the control group, nHDL was added to islet-free media and maintained at 37°C with 5% CO_2 for 24 h in cell-free conditions (cf-nHDL). Cf-nHDL and islet-nHDL were isolated by IP against apoA-I, and total RNA was isolated from 100 µg of nHDL. Total RNA was also isolated from islets to confirm genotype.

Cell Culture

MIN6 cells were cultured in DMEM supplemented with streptomycin (100 µg/ml), penicillin (100 U/ml) and 10% FBS. INS-1 832/13 cells were cultured in RPMI supplemented with streptomycin (100 µg/ml), penicillin (100 U/ml), 10% fetal bovine serum (FBS), and INS-1 supplement which consists of 10 mM HEPES, 2 mM L-glutamine, 1 mM sodium pyruvate, and

0.05 mM β-mercaptoethanol. All cells were maintained at 37°C with 5% CO_2. For miRNA export assay, INS1 and MIN6 cells were plated at 2 x 10^5 cells/mL for 24 h prior to HDL addition. Export experiments were performed at the following glucose concentrations: MIN6 cells – 5 mM D-glucose, INS1 cells – 11 mM glucose, except for experiment used for HDL-sequencing which was performed at 3 mM glucose. DGUC nHDL was added to cells at 1 mg/ml for 1-24h. For tolbutamide studies, cells were washed with 1x Hank's balanced salt solution (HBSS) for 2 h (0 mM glucose). Media was then added containing 3 mM glucose and either 25 µM, 150 µM tolbutamide or ethanol vehicle (veh) for 1 h. RPMI media was not supplemented with $CaCl_2$ for these experiments. 1 mg/mL nHDL was added for an additional 2 h. For low and high glucose studies, cells were wash with 1x HBSS, and then media containing 3 mM or 11 mM glucose supplemented with 1.8 mM $CaCl_2$ +/- 1 mg/ml nHDL was added for 24 h. For cAMP studies, INS-1 cells were pretreated with vehi, 100 µM 3-isobutyl-1-methylxanthine (IBMX), or 100 nM exendin-4 (ex-4) for 1 h in complete INS-1 media. Cells were then switched to serum free media +/- nHDL supplemented with 100 µM IBMX, or 100 nM ex-4 for an additional 2 h. nHDL was added to the media from each of the conditions, as described above, and maintained at 37°C with 5% CO_2 for 24 h (cf-nHDL). For diazoxide (DIA) studies: Media was added containing 11 mM glucose and either dimethyl sulfoxide (DMSO) (veh) or 200 µM DIA for 1 h +/- 1.8 Mm $CaCl_2$. 1 mg/mL nHDL was added for an additional 2 h. Cf-nHDL and INS-1-nHDL were isolated by IP for apoA-I or size exclusion chromatography (SEC), and total RNA was isolated from 100-300 µg of nHDL.

Cell Cycle Assays

Synchronization was performed as previously described(180). Briefly, cells were plated in INS-1 RMPI media containing 10% FBS. Asynchronous cells were plated at the same time, but remained in INS-1 media for the remainder of the study. After 24 h, synchronized cells were switched to INS-1 media + 0.1% FBS for 56 h, at which point cells were treated with 2 µg/ml aphidicolin (Sigma-Aldrich) for an additional 12 h. Following aphidicolin treatment, media was

changed to INS-1 media with 10% FBS and cells were collected at 0 h, 4 h, and 12 h for flow cytometry analysis of cell cycle phases and RNA content. To quantify miRNA export, media was changed to serum free media or serum free + 1 mg/mL nHDL 4 h prior to the final time-point for each condition. For analysis of cell cycle phases by flow cytometry, cells were trypsinized and counted, and $5x10^5$ cells were washed with 1X PBS and fixed in 80% methanol (Sigma-Aldrich) at -20°C overnight. Methanol was removed by centrifugation at 2000 x *g* for 10 min and cells were washed in 1X PBS twice. Cells were stained with 50 µg/ml propidium iodide (Invitrogen) in the presence of 50 µg/ml RNAse A (ThermoFisher) on ice for 2 h. Deoxyribose nucleic acid (DNA) content was analyzed using the 3-laser BD LSRII at the Vanderbilt Flow Cytometry Shared Resource Core.

Transfection Studies

Cells were plated at 2 x 10^5 cells/mL for 24 h prior to transfection (48 h) with DharmaFECT 4 (Dharmacon). Transient transfections (50 nM) were conducted with siRNA against Scarb1 (ON-TARGETplus SMARTpool L-098018-02), against Abca1 (ON-TARGETplus SMARTpool L-098018-02), and against Abcg1 (ON-TARGETplus SMARTpool L-098018-02).

Insulin Secretion Assays

INS-1 cells were plated onto 24-well plates and were grown to confluency prior to assay. The standard tissue culture medium was switched to medium containing 5 mM glucose for 18 h. Insulin secretion was performed in HBSS (114 mM NaCl, 4.7 mM KCl, 1.2 mM KH_2PO_4, 1.16 mM $MgSO_4$, 20mM HEPES, 2.5 mM $CaCl_2$, 25.5 mM $NaHCO_3$ and 0.2% bovine serum albumin, pH 7.2). Cells were washed with HBSS containing 3 mM glucose, followed by a 2 h incubation in the same buffer. Insulin secretion was then measured in static incubations of HBSS containing 3 mM or 15 mM glucose containing 200 µM tolbutamide or DIA for 2 h. Insulin levels were measured

using the porcine insulin radioimmunoassay (RIA) (Millipore, PI-12K). Human insulin was used for standard curves.

Transcriptomics and qPCR

HDL-RNA was isolated from equivalent amounts of HDL total protein and then quantified by real-time polymerase chain reaction (RT-PCR) or small RNA (sRNA) sequencing. Total RNA was isolated using either Total RNA Purification Kit (Norgen Biotek) or miRNeasy Mini Kit (Qiagen). HDL-RNA was isolated from equal HDL-protein amounts for each experiment. Cell and tissue RNA was diluted to equal concentrations. miRNA reverse transcription was performed using TaqMan miRNA Reverse Transcription Kit and predesigned TaqMan assays for each miRNA Mix (Applied Biosystems). mRNA complementary DNA (cDNA) was obtained using High-Capacity cDNA Reverse Transcription Kit (Applied Biosystems). RT-PCR was performed for 40 cycles using Taqman Universal PCR and predesigned Taqman assays for each miRNA or mRNA (Applied Biosystems). Threshold cycle (Ct) values were normalized to a housekeeping gene, U6 spliceosomal RNA (U6) for miRNAs and Ppia for mRNAs. Absolute quantification of miR-375 was performed by comparing Cts for samples of unknown miRNA concentration to a standard curve created with known concentration of miR-375 oligonucleotides, ranging from 3fM-400pM (Integrated DNA Technologies). Real-time PCR was performed on the QuantStudio 6 Real-Time PCR System, as per according to manufacturer's instructions (Life Technologies).

Western Blotting

Whole cell lysates were isolated using 150 mM NaCl, 1% NP-40, 0.1% SDS, 100 mM Tris-HCl, pH 7.4, supplemented with protease inhibitors (Roche) and cleared by centrifugation at 4°C for 10 min at 10,000×g. Proteins lysates were separated by 4-12% sodium dodecyl sulfate-polyacrylamide gel electrophoresis (SDS-PAGE) and then transferred to nitrocellulose membranes. The membranes were probed with monoclonal rabbit anti-SR-BI (Abcam, ab180383,

1:1,000), mouse monoclonal anti-ABCA1 (Abcam, ab18180, 1:1,000), rabbit polyclonal anti-ABCG1 (Novus Biologics, NB400-132, Lot F3, 1:1,000 dilution), or monoclonal mouse anti-glyceraldehyde 3-phosphate dehydrogenase (GAPDH) (Sigma, G8795, 1:10,000) in TBS-Tween20 containing 4% non-fat dry milk. Horseradish peroxidase (HRP)-conjugated secondary antibodies we used: anti-mouse (Promega, W4028, Lot 0000214819, 1:15,000) and anti-rabbit (Promega, W4018, Lot 0000212738, 1:20,000). Immune complexes were detected with Western Lightning Plus-ECL (Perkin Elmer) or Amersham ECL Prime Western Blotting Detection Reagent (GE Healthcare Life Sciences) chemiluminescent substrate.

Small RNA Sequencing

Total RNA from human HDL (Table A-1), human islets export (Figure 3-1, Table A-2), rat INS-1 cell export (Figure 3-2, Table A-4) were prepared with TruSeq small RNA library kits (Illumina) and sequenced on the HiSeq2500 sequencer SE50 (Illumina). Total RNA from human islets (Table A-3) were prepared with TruSeq sRNA kits (Illumina) and sequenced on the NextSeq500 sequencer SE75 (Illumina). All kits were performed as per manufacturer's instruction with added amplification cycles. Prior to sequencing samples were size-selected by Pippin-Prep (Sage Science) to collect cDNA 135-200 nts in length. Libraries were cleaned and concentrated (DNA Clean and Concentrator 5 kit, Zymo), tested for quality (High-Sensitivity DNA chips, 2100 Bioanalyzer, Agilent), and quantified (High-Sensitivity DNA assays, Qubit, Life Technologies). Equal concentrations samples were pooled for multiplex sequencing and concentrated (DNA Clean and Concentrator 5 kit, Zymo).

Informatics

miRNA sequencing data were analyzed by an in-house sRNA-seq data analysis pipeline(170). Briefly, Cutadapt was used to remove adapters and reads >16 nts in length were aligned to the rat (rno5) or human (Hg18) genome with 1 mismatch allowance by

Bowtie1(v1.1.2)(181) and DEseq2 (v1.18.1)(182) was used for differential expression between cf-nHDL and INS-1-nHDL or islet-nHDL. For human HDL and islets, reads were normalized and reported as reads per million total reads (RPM). For MAplots, log_2 fold change and log_2 normalized counts were calculated using DESEq2 v1.20.0. Circos plot was generated with R package Circlize v0.4.3. Briefly, log_2 fold change of miRNAs exported to HDL were calculated with DESEq2 v1.20.0 and sorted in descending order. Human islet miRNA counts were normalized by total reads per million, averaged among technical replicates, and sorted in descending abundance. Top 100 miRNAs were plotted. Links represent miRNAs exported to HDL that were also present in human islets.

Statistics

All data are presented in dot plots ± 95% confidence intervals (CI). Analysis between two groups was performed using two-tailed t-tests or Mann-Whitney non-parametic test. Analysis between three or more groups was performed using One-way ANOVA with Bonferonni post-correction, alpha=0.05. Spearman's tests were used to calculate correlations between two parameters. A $p<0.05$ was considered significant.

Methods for Chapter V

Animals

All animal studies were submitted to, approved by and completed under protocols by KineMed, Inc. or Vanderbilt IACUC. Rats and mice were maintained in a 12h/12h light/dark cycle with unrestricted access to food and water. Eight week-old male ZDF fa/fa rats (Charles River Laboratories International, Inc., Wilmington, MA) were maintained (*ad libitum*) on Purina 5001 chow diet (veh) (n=24) or chow diet supplemented with 2% colesevelam (n=24) for 4 weeks. Rats and food were weighed weekly to monitor body weight and food intake, respectively. Morning blood glucose concentrations (OneTouch Ultra, Lifescan, Inc. Milapitas, CA) and HbA1c (DCA

2000 analyzer, Bayer Healthcare LLC, Elkhart, IN) were measured weekly in fed rats. Portal blood was collected from all rats at sacrifice after a 12h fast to quantify blood glucose, plasma insulin and total GIP concentrations (Rat Metabolic Hormone MAG Bead Kit 2 Plex, Millipore Bioscience Division, St Charles, MO) and total GLP-1 and active GLP-1 (ECLIA, Pacific Biomarkers, Seattle, WA). For glucose tolerance tests, a subset of rats (n=12) were fasted for 4h and given a bolus of [6,6-$^2H_2$] glucose (2g/kg body weight, BW) by oral gavage. Blood glucose, plasma insulin, and plasma total GIP concentrations were measured at 0, 10, 20 and 60 min and plasma active GLP-1 concentrations were quantified at 10 min post-glucose injection. Whole-body glycolytic disposal of the administered glucose was determined by measuring the production of deuterated water (^2H_2O) from the administered [6,6-$^2H_2$] glucose during the glucose tolerance tests. Islet cell proliferation was measured by heavy water (^2H_2O) labeling as described by Chen et al.(183). Briefly, rats received ^2H_2O in the drinking water for four weeks. At the end of the heavy water labeling period, rats were sacrificed, pancreatic islet cells and bone marrow cells were isolated and the incorporation of ^2H from ^2H_2O into the deoxyribose moiety of purine deoxyribonucleotides in genomic DNA was measured by gas chromatography-mass spectrometry (GC-MS). The fraction of newly divided islet cells was then calculated from the ratio of ^2H incorporation into DNA from islets to ^2H incorporation into bone marrow cells. Hepatic free cholesterol synthesis was measured by heavy water (^2H_2O) labeling as described by Lee et al(184). Briefly, rats received ^2H_2O in the drinking water for four weeks. At the end of the heavy water labeling period, rats were sacrificed, free cholesterol was extracted from the liver and the incorporation of ^2H in free cholesterol was compared to the ^2H incorporation of body water to determine the fraction of free cholesterol that was newly synthesized in the liver during the labeling period. Adult male BKS.Cg-*Dock7^m* +/+ *Lepr^{db}*/J (*db/db*) mice were obtained from Jackson Laboratories and maintained (*ad libitum)* on NIH31 chow diet alone or supplemented with 2% colesevelam (Envigo) for 9 weeks. Mice were injected (intravenously) at retro-orbital site with 10 mg/kg *in vivo* grade locked-nucleic acid (LNA) miRNA inhibitor against mmu-miR-182-5p (Exiqon). Glucose tolerance tests were

performed at 4 and 8 weeks; fasted (5h) mice were injected intraperitoneally (i.p.) with glucose (1.5g/kg BW) and blood glucose levels were quantified at 0, 15, 30, 60 and 120 min post-injection. Insulin tolerance tests were completed at 5 weeks; fasted (5h) mice were injected (i.p.) with 1.5U/kg BW insulin (Humalin, Eli Lilly) and blood glucose levels were quantified at 0, 15, 30, 45, 60, 90 and 120 min post-injection. To quantify plasma incretin levels, fasted mice were assayed at 6 weeks, before and after 1.5g/kg BW glucose injection i.p., and insulin and GIP levels were quantified by multiplex immunoassays (Luminex). GLP-1 levels were undetectable. At the termination of the study, blood was collected from retro-orbital site and tissues were harvested and flash-frozen in liquid nitrogen and stored at -80^{o}C. Blood glucose concentrations were assayed within 2 freeze-thaw cycles using the glucose colorimetric assay kit (Cayman Chemical).

Cell Culture

Huh7 and human embryonic kidney 293 (HEK293) cells were maintained in DMEM supplemented with 10% FBS and 1% Penicillin and Streptomycin. Huh7 cells were transfected with 20nM miRNA mimics (Dharmacon) or LNAs (Qiagen) using Dhamafect1 (Dharmacon). HEK293 cells were transfected with 50nM miRNA mimics (Dharmacon) and 1µg/ml gene reporter (luciferase) plasmids using Dhamafect Duo (Dhamacon). Mouse primary hepatocytes were isolated from chow-fed male C57B/6J mice (Jackson Laboratory) by perfusion and digestion (137mM NaCl, 7mM KCl, 0.7mM Na_2HPO_4-$12H_2O$, 10mM HEPES, 5.1mM $CaCl_2$ and 0.4mg/ml Collagenase from Clostridium histolyticum type IV), as previously described(185). Cells were seeded in 12- or 6-well BioCoat Collagen I plates (BD) and incubated at 37°C with 5% CO_2 in William's E media + hepatocyte supplements (Invitrogen). 5h post-plating, cells were transiently transfected with 50nM miRNA mimics (Dharmacon), 50nM LNAs (Qiagen), 50nM ON-TARGET Plus *Med1* siRNAs (Set of 4), or scramble control siRNAs (Dharmacon) using Lipofectamine RNAiMAX Transfection Reagent (ThermoFisher) for 48h.

Transcriptomics

Total RNA was isolated from cells or 30mg of tissue using the miRNeasy Mini kits (Qiagen). cDNAs were generated as described above. U6 and *Ppia* were used as internal controls for miRNA and mRNA reactions, respectively, and relative quantitative values (RQV) were calculated by delta Ct method ($RQV=2^{-dCt}$) and reported as fold changes.

Small RNA Sequencing

Total RNA from rat liver (n=6) was prepared for high-throughput small RNA sequencing (sRNA-seq) using TruSeq small RNA library kits (Illumina). Library preparation was performed according to manufacturer's protocol from 1 μg of input total RNA and 11 amplification cycles were used. Library preparation, sequencing and analysis were performed as described above. DEseq2 (v1.18.1)(182) was used to identify significant ($p<0.05$) differentially (absolute fold change >1.5) expressed liver miRNAs. Raw and processed data from this sequencing experiment has been deposited to Gene Expression Omnibus: GSE116826; processed data from this experiment is found in Table A-10.

Proteomics

Cell lysates were collected using protein extraction buffer (50mM HEPES, 150mM NaCl, 0.2mM EDTA, 2mM MgCl2, 1% Triton X-100 and 1x protease inhibitors). Protein extracts from livers were collected in radioimmunoprecipitation assay (RIPA) buffer (150mM NaCl, 1% NP-40, 0.5% sodium deoxycholate, 0.1% SDS 50mM Tris-HCl, 1x protease inhibitors, pH 8.0). Protein lysates were incubated for 1h at 4°C and cell debris was pelleted through centrifugation; 40-100μg of protein lysates were separated on 3-8% Tris-Acetate gels (ThermoFisher). Rabbit anti-mouse antibodies against MED1 (Abnova PAB8661, lot 2G073735, polyclonal, 1:1000 dilution in Odyssey blocking buffer) and β-Actin (Cell Signaling 13E5, lot 14, monoclonal, 1:5000 dilution in

Odyssey blocking buffer) were used for western blotting and detected using the LICOR system. Med1 antibody was validated in cell culture using a *Med1* siRNA.

Gene Reporter (Luciferase) Assays

Putative miR-182/183/96 target sites (30-40bp fragments) within the human *MED1* 3'-UTR were cloned down-stream of Firefly luciferase (pEZX-MT01 vector, GeneCopoeia) and confirmed by Sanger sequencing (GeneWiz). Luciferase assays were performed in HEK293 cells dually transfected with gene reporter (luciferase) plasmids and miRNA mimics (miR-182/183/96) using the Luc-Pair Duo-Luciferase Assay Kit 2.0 (GeneCopoeia). Firefly luciferase activity was normalized to *Renilla* (transfection control) luciferase activity and expressed as fold changes.

Statistics

Data are shown as mean ± standard error of the mean (SEM). Differences between two groups were analyzed by Student's t-test with ($N<4$) or Mann-Whitney non-parametric test ($N\geq4$) correction, and differences between >2 groups were analyzed by One-way ANOVA with Dunn's post-test. Area under the curve for glucose tolerance tests were calculated using GraphPad Prism.

CHAPTER III

MECHANISMS OF β CELL EXPORT OF HDL-MIR-375

Adapted from Sedgeman *et al*., "Beta cell secretion of miR-375 to HDL is inversely associated with insulin secretion". Under revision at *Scientific Reports*

Introduction

Islets of Langerhans in the pancreas control systemic energy homeostasis primarily through two cell types: insulin-producing β cells and glucagon-producing α cells. In response to high glucose, β cells secrete insulin in a process known as GSIS; however, chronic exposure to supraphysiological concentrations of glucose, e.g. conditions of systemic insulin resistance, can result in damage to the β cell, and the development of T2D(186, 187). HDL have many beneficial properties in various biological processes that underlie pancreatic β cell integrity and function, including enhancing GSIS(188, 189). HDL's regulation of β cell integrity and insulin secretion have been reported to be both dependent and independent of cholesterol transporters - ABCA1 and SR-BI(189, 190). HDL also have a wide-variety of alternative functions in many different cell-types conferred in part through the transport of non-cholesterol cargo, e.g. miRNAs(93-95), suggesting there may be a relationship between insulin secretion and HDL-miRNAs.

miRNAs are small non-coding RNAs (18-22 nts in length) that post-transcriptionally regulate gene expression and are key factors in many (patho)physiologies(96). In pancreatic β cells, miRNAs have emerged as critical regulators of insulin secretion and cellular proliferation(191, 192). miR-375-3p is highly expressed in pancreatic islets and β cells(124, 193), and is a key regulator of β cell proliferation and function. Extracellular miRNAs are also detected in plasma, where they are protected from RNase digestion by protein and/or lipid complexes(94, 137, 139). Recently, miR-375-3p was also found to be released from β cells in exosomes(168),

suggesting that miR-375-3p may have both cellular and extracellular roles. Nevertheless, extracellular miR-375-3p is not limited to just exosomes, as we have previously reported that HDL also transport miR-375-3p(94). Furthermore, we have previously demonstrated that HDL can transfer miRNAs, including miR-375-3p, to recipient cells, e.g. hepatocytes(94). HDL-transferred miRNAs are also functional in recipient cells, as we have previously demonstrated that HDL-miRNAs delivered to coronary artery endothelial cells regulate key inflammatory genes, thus conferring, in part, HDL's anti-inflammatory properties(95). Collectively, our previous studies support that HDL transports miRNAs in circulation, that HDL-miRNA signatures are altered in metabolic disease, and that HDL-miRNAs serve as cell-to-cell signals within potential intercellular communication networks. Despite these findings, very little is understood about how cells export miRNAs to HDL.

Here, we demonstrate that pancreatic islets and β cells export miRNAs, specifically miR-375-3p, to HDL and report key insights into processes that regulate export. Remarkably, contrary to exosomes in which miR-375-3p export was increased under cellular conditions that promote with insulin secretion(168), we found that β cell miR-375-3p export to HDL is suppressed by these same mechanisms that promote insulin secretion. Multiple conditions that stimulate insulin secretion from pancreatic β cells - high glucose, tolbutamide, and persistent membrane depolarization - inhibited miRNA export to HDL. Moreover, we found that high glucose inhibition of HDL-miR-375-3p export required extracellular Ca^{2+}, which is also critical for insulin secretion, thus further establishing the negative relationship between insulin secretion and HDL-miR-375 export. Nonetheless, despite the importance of cholesterol flux for insulin secretion from β cells, miRNA export to HDL was found to be independent of cholesterol transporters. Collectively, these findings establish that the pancreatic β cells contribute to extracellular miRNAs on circulating HDL and that β cell miRNA export is inversely regulated by the cellular processes that promote insulin secretion.

Results

Pancreatic β cells export miRNAs to HDL

High-throughput sRNA-seq was used to quantify miRNAs on HDL from humans, and miR-375-3p was identified as a top-ranked HDL-miRNA (Table A-1). To quantify the concentration of miR-375-3p on HDL, miR-375-3p levels were measured by quantitative PCR (qPCR) using 1 mg of HDL from human and mouse HDL isolated by SEC or DGUC followed by SEC. We detected 10^5-10^6 copies / mg HDL (total protein) for miR-375-3p in both mouse and human samples (Figure 3-1A). Based on miR-375's link to β cell biology and our previous study demonstrating that miR-375-3p was highly abundant on HDL, we hypothesized that pancreatic islets and β cells contribute miR-375-3p to HDL. To test this hypothesis, we developed an HDL-miRNA export assay to measure miRNA efflux to HDL. Briefly, primary islets or β cell lines were incubated with serum-free medium containing 1 mg/mL native HDL (islet-nHDL or INS-1-nHDL) for 24h, or in cell free conditions (cf-nHDL). We then re-isolated nHDL from the culture media by SEC or apoA-I-IP. To determine if primary human islets export miRNAs to HDL *ex vivo*, miRNA levels were quantified (by sRNA-seq) on cf-nHDL and on islet-nHDL, and differential expression analysis identified that 17 miRNAs were detected at levels >1.5 fold on HDL after incubation with islets compared to cf-nHDL (Figure 3-1B, Table A-2). Strikingly, miR-375-3p was found to be the only miRNA that was detected with a large fold change and at high abundance. Real-time PCR was used to confirm that miR-375-3p levels were significantly increased (donor 1: 135-fold, p=0.0007; donor 2: 3.5-fold, p=0.008; donor 3: 609-fold, p=0.02) on nHDL after incubation with islets from three individual islet donors (Figure 3-1C). Other top exported miRNAs (Table A-2), let-7d-5p, miR-126-5p, miR-183-5p, miR-223-3p were measured by real-time PCR, and only miR-183-5p was found to be exported to HDL, albeit at much lower levels than miR-375-3p (Figure 3-1D). To assess the specificity of human islet miRNA export to HDL, miRNA profiles from sRNA sequencing of the human islets from donor 1 and their exported HDL-miRNAs were linked using a circos plot (Figure 3-1E, Table A-2, Table A-3). Each of the miRNAs expressed in human islets are shown below the

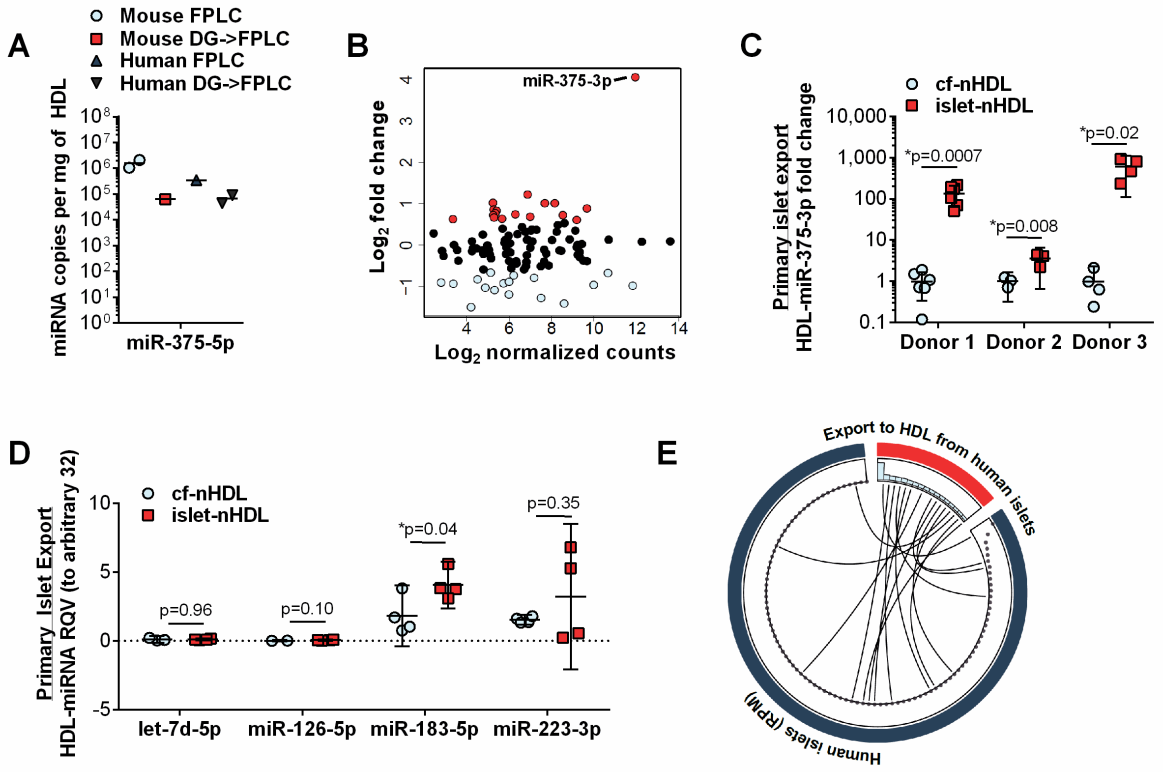

Figure 3-1. Pancreatic islets export miR-375-3p to HDL. (A) Absolute quantification (qPCR) of mouse and human HDL-miRNAs from 1mg of HDL isolated by fast-protein liquid chromatography (FPLC) or density-gradient ultracentrifugation (DGUC) followed by FPLC. n=1-2 (B) MA plot of miRNA changes between cf-nHDL and islet-nHDL. Each dot represents a single miRNAs. Red, upregulated >1.5 fold; black, no change; blue, downregulated >1.5 fold. n=1 human donor. (C) miR-375-3p levels on cf-nHDL and islet-nHDL from three islet preps from individual donors. Donor 1: n=6, donor 2: n=3, donor: 3, n=4; Two-tailed t-test. (D) let-7d-5p, miR-126-5p, miR-183-5p, miR-223-3p levels on cf-nHDL and islet-nHDL from islet preps from donor 3. n=4; Two-tailed t-test. (E) Circos depicting top 100 islet miRNAs from 1 human donor (blue) and exported miRNAs from the same islets. sRNA-seq; dots represent RPM in islets and blue bars depict log2 HDL-miRNA fold change in islet-nHDL compared to cf-nHDL.

blue bar, and each of the miRNAs exported to HDL (Figure 3-1B) were graphed below the blue part. This graph allows us to visualize which cellular miRNAs (blue) are also export to HDL (red). We found that of the 1491 miRNAs detected in islets, only 17 were exported to nHDL (>1.5-fold islet-nHDL vs. cf-nHDL levels), suggesting that miRNA export to nHDL is likely to be specific, and not simply reflecting cellular miRNA concentrations (Figure 3-1E).

To determine if pancreatic β cells export miR-375-3p and other miRNAs to HDL, HDL-miRNA export assays were performed in rat INS-1 832/13 cells and sRNA-seq was used to quantify miRNAs on cf-nHDL and INS-1-nHDL. Strikingly, the levels of 61 miRNAs were increased >1.5-fold on INS-1-nHDL compared to cf-nHDL. (Figure 3-2A, Table A-4). Similar to our findings of islet exported miRNAs (Figure 3-1B), miR-375-3p export was robust and distinct from other miRNAs. Real-time PCR was used to confirm that INS-1 cells exported miR-375-3p to nHDL (81.48-fold, p=0.0007) (Figure 3-2B). Furthermore, miR-145-5p was used as a negative control, as we found that miR-145-5p was consistently not exported to INS-1-nHDL by RT-PCR (Figure 3-2B). We quantified additional exported miRNAs by RT-PCR, miR-16-5p, miR-107-3p, miR-30d-5p, miR-182-5p, miR-21-5p, miR-27b-3p, miR-25-3p, miR-132-3p, miR-22-3p (Figure 3-2C). Similar to our findings in islets, only one miRNA, miR-132-3p was found to be significantly exported (p=0.01) and at much lower levels than miR-375-3p (Figure 3-2C). Based on the striking observation that miR-375-3p is the most abundantly exported miRNA, we next investigated how its export is regulated.

miR-375-3p regulates β cell development, and its levels have been found to be inversely associated with insulin secretion(124, 128, 194). To determine if β cell export of miR-375-3p to HDL reduces cellular miR-375-3p levels, mature miR-375-3p levels were quantified by RT-PCR in INS-1 cells treated with nHDL for 24h. Cellular levels of mature miR-375-3p were not altered by nHDL treatments (Figure 3-2D), suggesting that export of miR-375-3p to HDL is not likely a mechanism for the regulation or depletion of cellular miRNA levels. Nevertheless, miR-375 transcription was found to be inhibited by nHDL treatments, as the levels of the primary miR-375

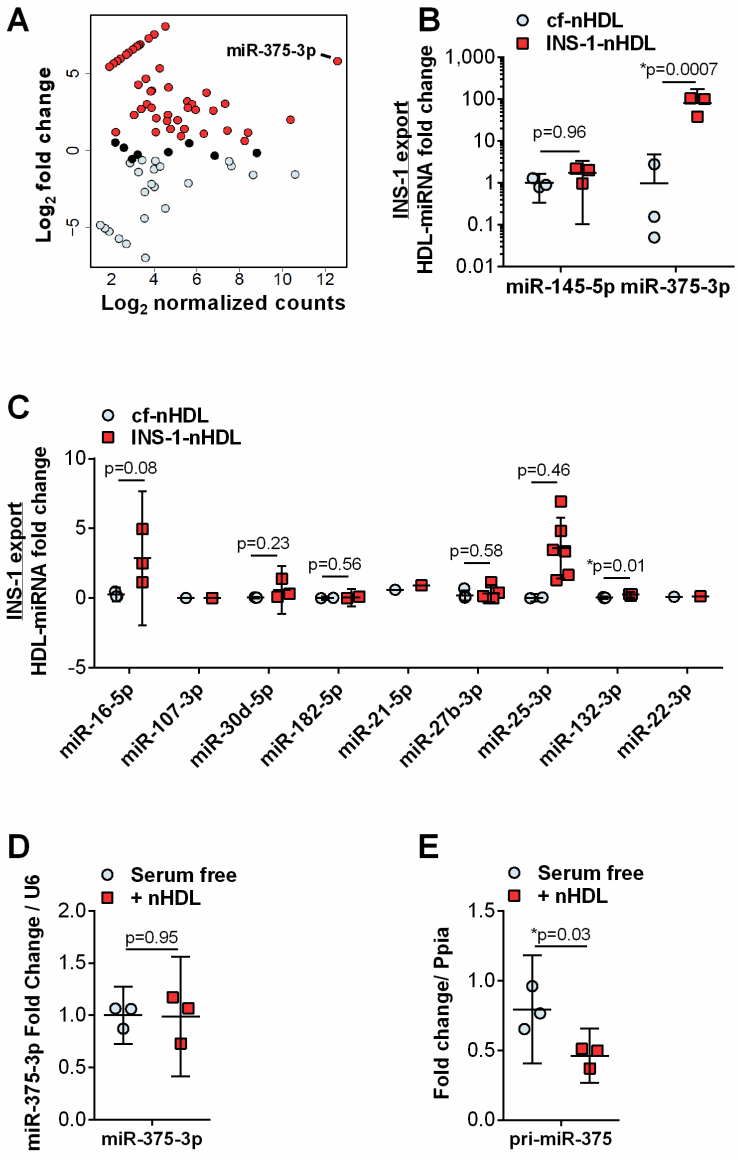

Figure 3-2. INS-1 (832/13) β cells export miR-375-3p to HDL. (A) MA plot of miRNA changes between cf-nHDL and INS-1-nHDL. Each dot represents a single miRNAs. Red, upregulated >1.5 fold; black, no change; blue, downregulated >1.5 fold. n=1. (B) HDL miR-145-5p and miR-375-3p levels on cf-nHDL and INS-1-nHDL. n=3; two-tailed t-test. (C) miR-16-5p, miR-107-3p, miR-30d-5p, miR-182-5p, miR-21-5p, miR-27b-3p, miR-25-3p, miR-132-3p, miR-22-3p export to nHDL from INS-1 cells. n=1-6; two-tailed t-test. (D,E) INS-1 cellular levels of (D) mature miR-375-3p and (E) primary-miR-375. n=3; two-tailed t-test

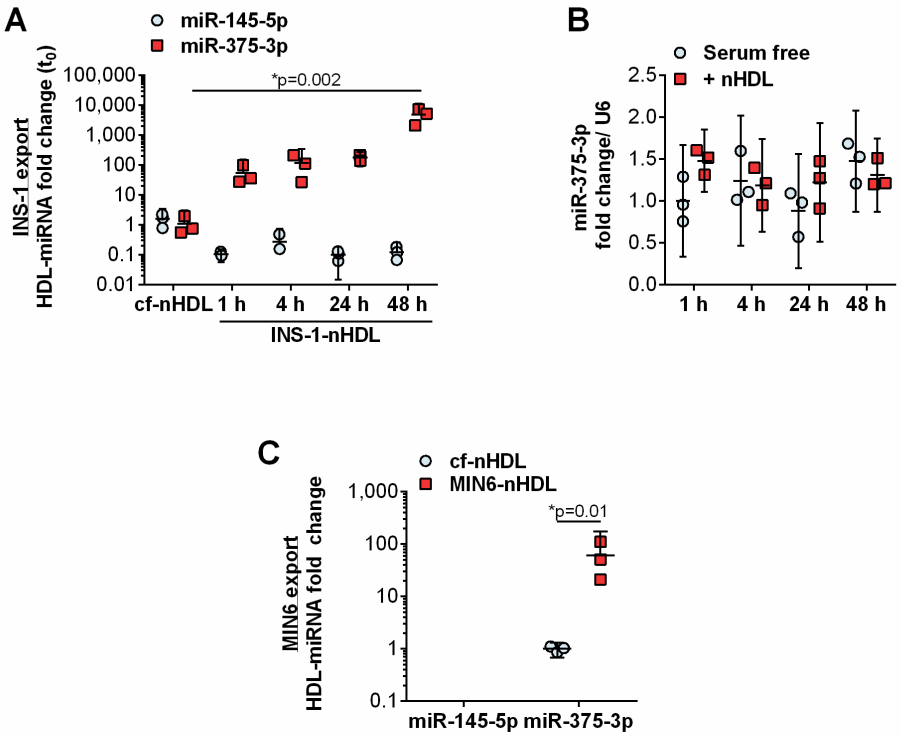

Figure 3-3. INS-1 and MIN6 β cells export miR-375-3p to HDL. (A) INS-1 miR-145-5p and miR-375-3p export to nHDL: cf-nHDL and INS-1-nHDL after 1, 4, 24, or 48h after incubation with INS-1 cells. n=3; one-way ANOVA with Bonferroni post-test, alpha = 0.05. (B) Cellular miR-375 levels in INS-1 cells treated with or without nHDL for 1, 4, 24 and 48h. n=3; one-way ANOVA with Bonferroni post-test, alpha = 0.05. (C) HDL miR-145-5p and miR-375-3p levels on cf-nHDL and INS-1-nHDL. n=3; mean ± 95% CI; two-tailed t-test.

transcript (pri-miR-375) were significantly decreased (p=0.03) in INS-1 cells treated with nHDL compared to untreated cells (Figure 3-2E). To determine the temporal dynamics of β cell HDL-miR-375-3p export, INS-1-nHDL was purified at multiple time-points. We found that miR-375-3p levels steadily increased on INS-1-HDL over 24h – 54-fold at 1 h, 116.3-fold at 4 h, 180.5-fold at 24 h, and 4,874.2–fold at 48 h compared to cf-nHDL levels - whereas miR-145-5p was not exported to HDL at any time-point (Figure 3-3A). Cellular miR-375-3p levels were unaffected at any time-point, and miR-145-5p levels were considerably decreased at 24h. (Figure 3-3B). To confirm that β cell miR-375-3p export to HDL is not limited to rat INS-1 cells, HDL-miRNA export assays were also performed in mouse MIN6 cells, and we found that MIN6 cells also export miR-375-3p (46.19-fold), but not miR-145-5p, to nHDL (Figure 3-3C). These results strongly support that pancreatic islets and INS-1 cells robustly and selectively export miR-375-3p to HDL.

Unlike native β cells in the islets which are not proliferative, INS-1 and MIN6 cells are mitotically active(180). We found that in unsynchronized INS-1 cells, approximately 77% of cells are in G1 phase, whereas approximately 6-8% of cells are in S and G2 phases (Figure 3-4, Figure 3-5A). We next tested whether INS-1 cells that are enriched in G1 (0h), S (4h) or G2 (12h) phases differentially export miR-375-3p to HDL. Of note, we did not observe any differences in cell cycle states when cells were treated with FBS, serum free, or serum free + nHDL media for the last 4h of the experiments (Figure 3-4, Figure 3-5A). Most importantly, we found that miR-375-3p levels on INS-1-nHDL are not affected by the cell cycle (Figure 3-5B), whereas cellular levels of miR-375-3p were found to be increased at 0h ($p<0.0001$) compared to asynchronous cells (Figure 3-5C). Pri-miR-375 levels were not altered across the time points studied (Figure 3-5D). Due to the observation that despite the differences in proliferation between islets and INS-1 cells, miR-375-3p is the main miRNA exported from both islets and INS-1 cells at high levels, we sought to characterize whether miR-375-3p export is regulated by insulin secretion.

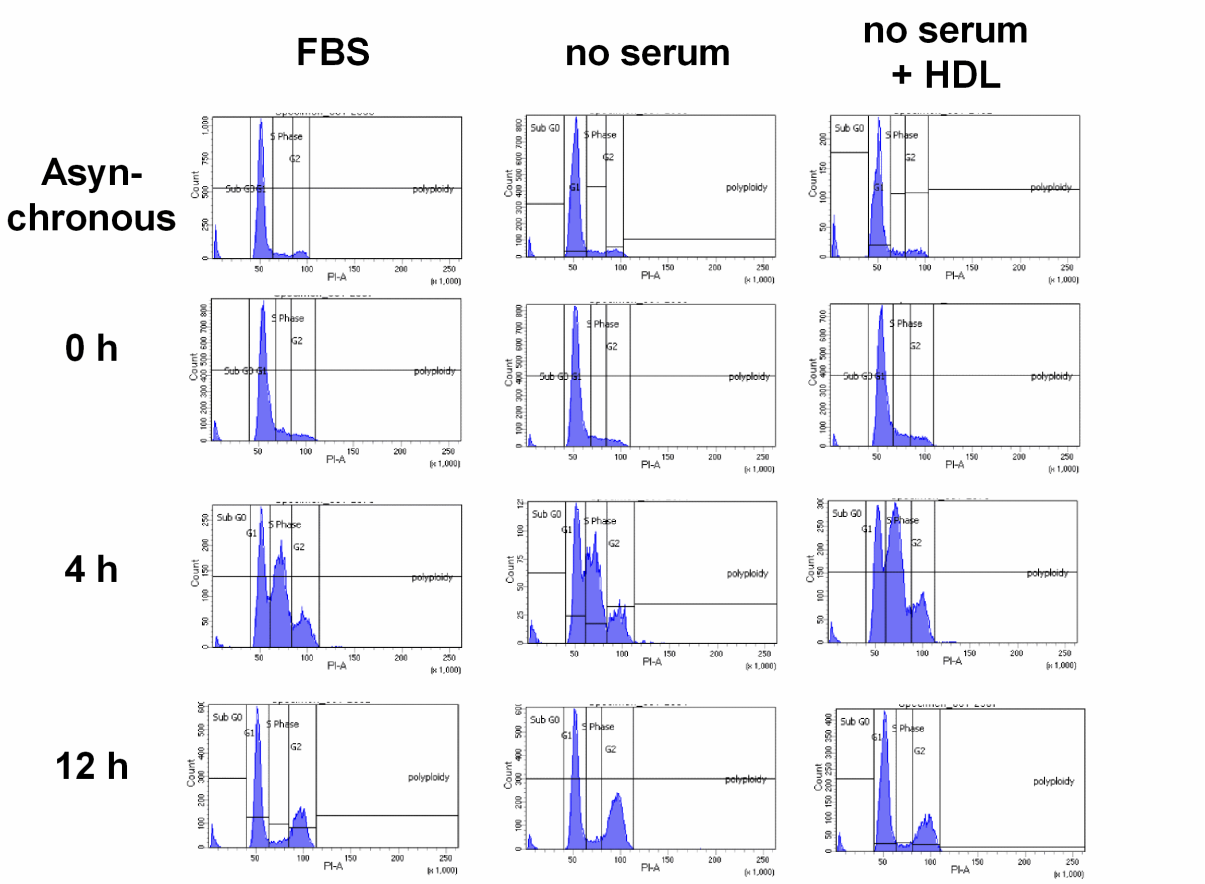

Figure 3-4. Flow cytometry quantification of cell cycle. Representative flow cytometry plots of cells in G1, S and G2 phase in asynchronous or after 0h, 4h or 12h after G1 arrest.

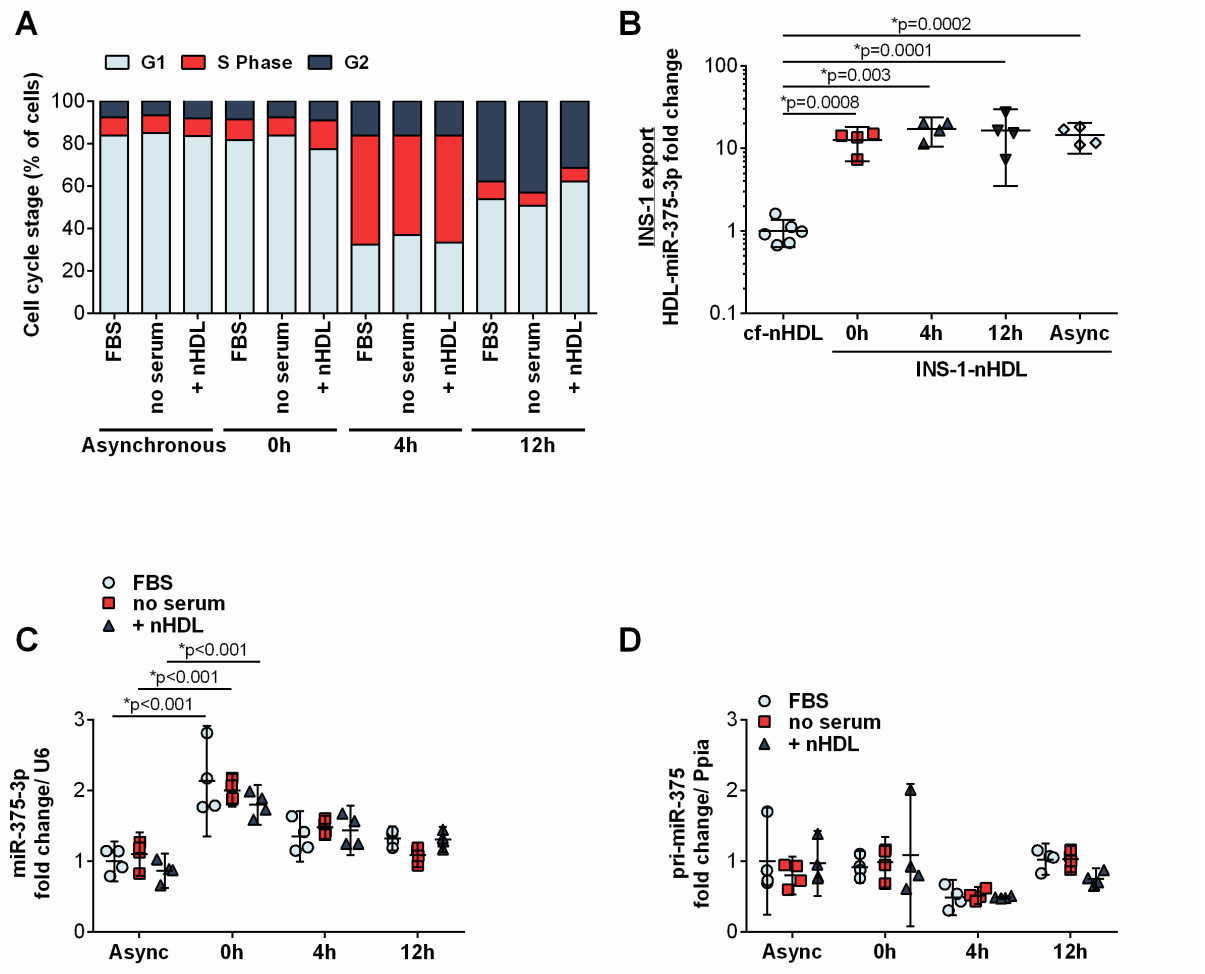

Figure 3-5. Effect of cell cycle on miR-375-3p export to HDL. (A) Percentage of INS-1 cells in G1, S and G2 phase determined by flow cytometry quantification of propidium iodide stain. n=4; mean. (B) Export of miR-375-3p to nHDL after cell cycle synchronization and enrichment in G1 (0h), S (4h) and G2 (12h) phase. n=4; one-way ANOVA with Bonferroni post-test, alpha = 0.05. (C) Cellular miR-375 and (D) pri-miR-375 in asynchronous INS-1 cells or after 0, 4, or 12h after G1 arrest with or without serum and HDL. n=4; one-way ANOVA with Bonferroni post-test, alpha = 0.05.

Insulin secretion suppresses β cell miRNA export to HDL

Pancreatic β cells maintain systemic energy homeostasis through glucose sensing and insulin secretion; therefore, we sought to determine if the cellular mechanisms that control insulin secretion (i.e. GSIS) also regulate miRNA export to HDL. To determine the impact of high glucose conditions on β cell miR-375-3p export to HDL, export assays were completed in INS-1 cells with RPMI media containing normal (3 mM) or high (11 mM) glucose levels. In these assays, we failed to find a difference in HDL-miR-375-3p export between the two conditions (Figure 3-6A). However, RPMI medium is hypocalcemic (0.45mM $Ca(NO_3)_2$) and GSIS requires extracellular Ca^{2+} for membrane depolarization. Therefore, we tested whether high glucose (11 mM) media supplemented with 1.8mM $CaCl_2$ alters β cell miR-375-3p export to HDL. The addition of 1.8mM $CaCl_2$ to the medium raises the extracellular levels to physiological levels, allowing for a rise in $[Ca^{2+}]_i$ in response to high glucose stimulation. Remarkably, in the presence of extracellular Ca^{2+}, high glucose conditions suppressed β cell miR-375-3p export to nHDL (p=0.02 between INS-1-nHDL 3mM glucose + 1.8mM $CaCl_2$ and 11mM glucose + 1.8mM $CaCl_2$) (Figure 3-6A). In response to high glucose, β cells trigger a series of cellular processes that result in the secretion of insulin, including the closure of K_{ATP} channels, depolarization of the plasma membrane, and influx of extracellular Ca^{2+} through VGCC(55). To determine whether the observed inhibition of HDL-miR-375-3p export by high glucose conditions is regulated by cellular mechanisms that regulate insulin secretion, the role of K_{ATP} channels in miRNA export to HDL was investigated. HDL-miRNA export assays were performed in INS-1 cells treated with a chemical inhibitor of the K_{ATP} channel (tolbutamide)(21), which results in depolarization of the plasma membrane. Strikingly, tolbutamide treatment resulted in a significant decrease in β cell miR-375-3p export to nHDL (p=0.0.004 INS-1-nHDL veh compared to INS-1-nHDL 25 μM tolbutamide; p=0.008 INS-1-nHDL vehicle compared to INS-1-nHDL 100 μM tolbutamide) (Figure 3-6B), without any changes in cellular miR-375-3p levels (Figure 3-6C). Conversely, DIA, a K_{ATP} channel activator, prevented the suppression of miR-375-3p export to HDL observed with vehicle (Veh) + $CaCl_2$ (p=0.74

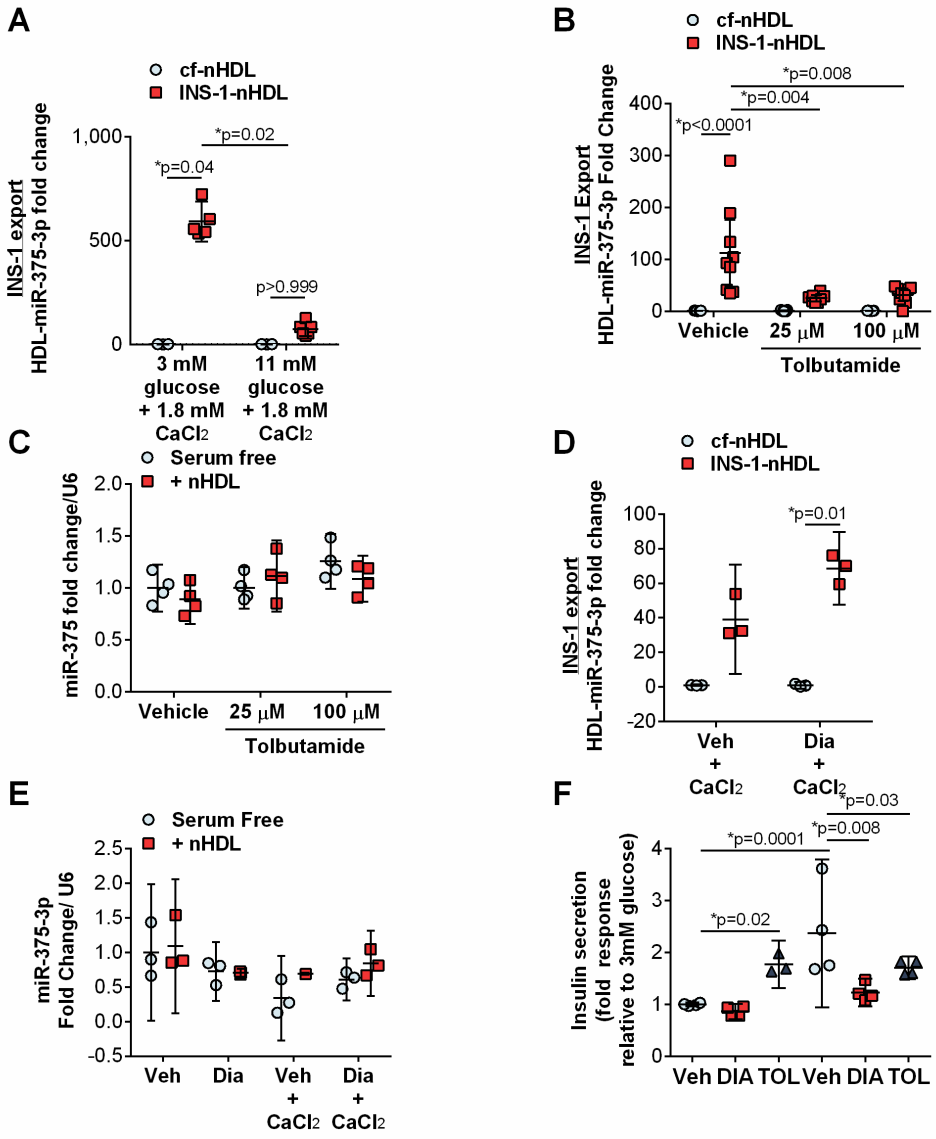

Figure 3-6 Stimulation of insulin secretion blocks INS-1 export of miR-375-3p to HDL. (A) miR-375-3p levels on cf-nHDL and INS-1-nHDL after INS-1 cell treatment with 3mM or 11mM D-glucose in the presence or absence of 1.8mM $CaCl_2$. n=3-6; one-way ANOVA with Bonferroni post-test, alpha = 0.05. (B) HDL-miR-375-3p levels on cf-nHDL and INS-1-nHDL from INS-1 cells treated with tolbutamide for 2h. n=7-9; one-way ANOVA with Bonferroni post-test, alpha = 0.05. (C) Cellular miR-375-3p levels in INS-1 cells treated with tolbutamide for 3h. n=4; one-way ANOVA with Bonferroni post-test, alpha = 0.05. (D) miR-375-3p levels on cf-nHDL and INS-1-nHDL after INS-1 cell treatment with vehicle or diazoxide (DIA) in the presence or absence of 1.8mM CaCl2. n=3; one-way ANOVA with Bonferroni post-test, alpha = 0.05. (E) Cellular levels of miR-375-3p in INS-1 cells treated diazoxide (Dia) with or without HDL for 3h in the presence or absence of CaCl2. n=3; one-way ANOVA with Bonferroni post-test, alpha = 0.05. (F) Insulin secretion to media from INS-1 cells in low (3mM) or high (15mM) glucose supplemented with 200uM diazoxide (DIA) or tolbutamide (TOL). n=3-4; one-way ANOVA with Bonferroni post-test, alpha = 0.05.

between cf-nHDL and INS-1-nHDL in Veh + $CaCl_2$; p=0.01 between cf-nHDL and INS-1-nHDL in Dia + $CaCl_2$) (Figure 3-6D). DIA also failed to alter cellular levels of mature miR-375-3p in INS-1 cells with or without $CaCl_2$ (Figure 3-6E). In addition, we confirmed that both high glucose conditions and tolbutamide treatments stimulated insulin secretion from INS-1 cells (Figure 3-6F).

The K_{ATP} channel is a hetero-octameric protein composed of four SUR1 and four Kir6.2 subunits, and deletion of either channel component results in incomplete trafficking to the plasma membrane and complete loss of channel activity(195). To replicate our chemical inhibition findings using an orthogonal approach, we tested whether genetic deletion of a K_{ATP} channel subunit in mice (SUR1 KO, *Abcc8*$^{-/-}$) impacts pancreatic islet miR-375-3p export to nHDL. Primary islets were isolated from *Abcc8*$^{-/-}$ mice (Figure 3-7A), and miR-375-3p export to HDL was quantified *ex vivo*, as described above. In agreement with our *in vitro* studies, loss of the K_{ATP} channel in SUR1 knockout islets, significantly reduced miR-375-3p export to nHDL *ex vivo* (p=0.04 between WT and *Abcc8*$^{-/-}$ islet-n-HDL) (Figure 3-7B). K_{ATP}–deficiency in mice (*Abcc8*$^{-/-}$) has been reported to cause Ca^{2+}-associated changes in the β cell transcriptome(177); therefore, we confirmed that the observed loss of HDL-miR-375-3p export was not merely due to decreased miR-375-3p expression in islets isolated from *Abcc8*$^{-/-}$ mice compared to WT mice. In fact, miR-375-3p levels were found to be increased, not decreased, in *Abcc8*$^{-/-}$ islets (Figure 3-7C). Similarly, we found that islets with loss of the other subunit in the K_{ATP} channel, Kir6.2 KO, also had significantly reduced miR-375-3p export to nHDL *ex vivo* (p=0.02 between WT and *Kcnj11*$^{-/-}$ islet-n-HDL) (Figure 3-7D).These findings suggest that miR-375-3p export to nHDL is inverse to insulin secretion. To further test this association, the role of cAMP was investigated.

As a second messenger molecule, cAMP enhances GSIS in β cells through both PKA dependent and independent mechanisms that regulate the exocytotic machinery and membrane depolarization(196, 197). A rise in cellular cAMP levels can be triggered by increased $[Ca^{2+}]_i$ concentrations or through hormone signaling, e.g. GLP-1. cAMP also alters gene expression and recently, cAMP has been shown to repress transcription of pri-miR-375(131). Therefore, we

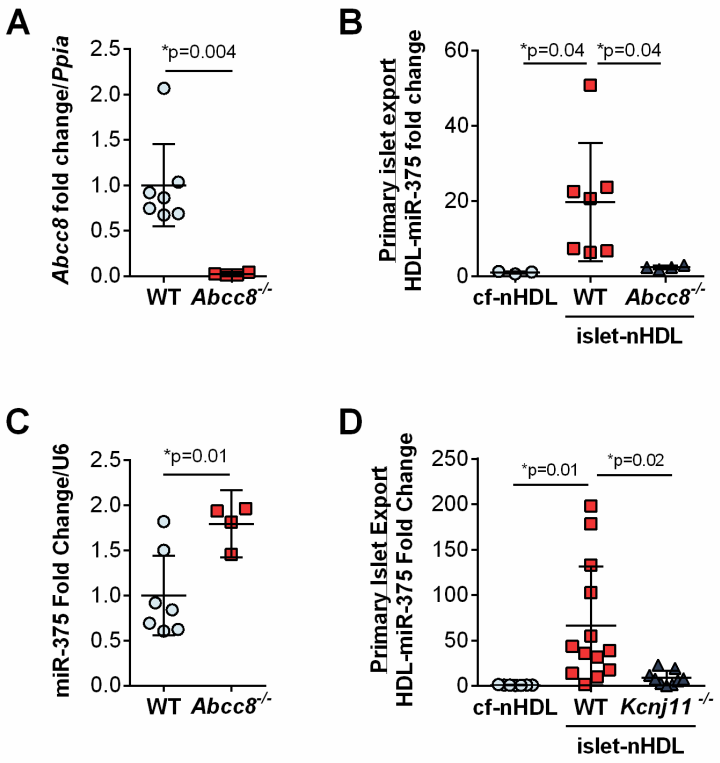

Figure 3-7. miR-375-3p export to HDL from K_{ATP} deficient islets. (A) Expression of Abcc8 in primary islets from WT (wildtype) or *Abcc8*$^{-/-}$ mice. n=3; two-tailed t-test. (B) miR-375-3p levels on cf-nHDL and islet-nHDL from mouse WT (wildtype) or SUR1 KO (*Abcc8*$^{-/-}$) mice. n=3; one-way ANOVA with Bonferroni post-test, alpha = 0.05. (C) miR-375-3p in primary islets from WT (wildtype) or *Abcc8*$^{-/-}$ mice. n=3; two-tailed t-test. (D) miR-375-3p levels on cf-nHDL and islet-nHDL from mouse WT (wildtype) or KIR6.2 KO (*Kcnj11*$^{-/-}$) mice. n=3; one-way ANOVA with Bonferroni post-test, alpha = 0.05.

investigated whether miR-375-3p export to nHDL is regulated by cAMP. Two different compounds were used to stimulate cAMP in INS-1 cells, ex-4, a GLP1R agonist, and IBMX, a phosphodiesterases inhibitor. As a positive control, the expression of c-fos was quantified, as this gene was previously reported to be increased with ex-4 and IBMX treatments(131, 198). IBMX treatments, but not ex-4, increased *Fos* mRNA levels in INS-1 cells ($p<0.0001$), perhaps due to low level of expression of GLP1R in INS-1 cells(199) (Figure 3-8A). Were found that pri-miR-375, but not mature miR-375-3p levels were down-regulated in INS-1 cells treated with ex-4 or IBMX in serum-free media +nHDL (Figure 3-8B, Figure 3-8C). Most interestingly, IBMX, but not ex-4, was found to repress miR-375-3p export to nHDL ($p=0.01$) (Figure 3-8D). These results further support a model in which stimulation of GSIS from β cells, either through glucose, membrane depolarization, or cAMP inhibit miR-375-3p export to nHDL. Furthermore, these results established an inverse link between β cell miRNA export to HDL and insulin secretion.

β cell HDL-miRNA export is independent of cholesterol flux

Previously, studies have demonstrated that HDL enhances β cell insulin secretion which requires cholesterol transporters(189). Based on these findings, we sought to examine the roles of HDL's primary receptor, SR-BI, and key cholesterol transporters, ABCA1 and ABCG1, in regulating β cell miRNA export to nHDL. SR-BI is a bidirectional transporter of cholesterol and lipids, and mediates HDL-induced cell signaling(200, 201). We have previously demonstrated that HDL-miRNA delivery to recipient hepatocytes was dependent upon SR-BI(94). SR-BI is also expressed in pancreatic β cells and could, therefore, directly transport miRNAs to nHDL or indirectly facilitate HDL-induced cell signaling to promote miRNA export. To determine if SR-BI in mouse islets is required for trafficking of miR-375-3p to nHDL, pancreatic islets were collected from *Scarb1*$^{-/-}$ (SR-BI KO) and c57Bl/6 WT mice, and incubated with nHDL *ex vivo* (Figure 3-9A). Surprisingly, islets from both SR-BI KO and WT mice were found to export miR-375-3p to nHDL and we found no difference between islet genotype ($p=0.69$ between WT and *Scarb1*$^{-/-}$ islet-nHDL)

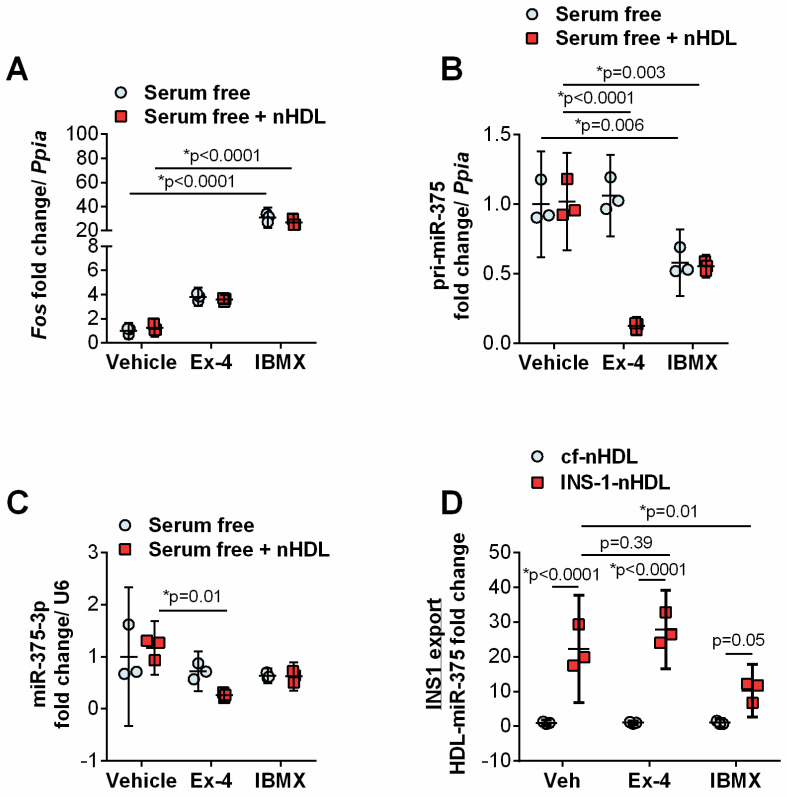

Figure 3-8. Export of miR-375-3p with cAMP stimulation. (A) Cellular levels of *Fos*, (B) pri-miR-375 and (C) miR-375-3p in INS-1 cells treated with ex-4 or IBMX with or without HDL for 3 h. n=3; one-way ANOVA with Bonferroni post-test, alpha = 0.05. (D) HDL-miR-375-3p levels on cf-nHDL and INS-1-nHDL from INS-1 cells treated with exendin-4 (ex-4) or IBMX for 3h. n=3; one-way ANOVA with Bonferroni post-test, alpha = 0.05.

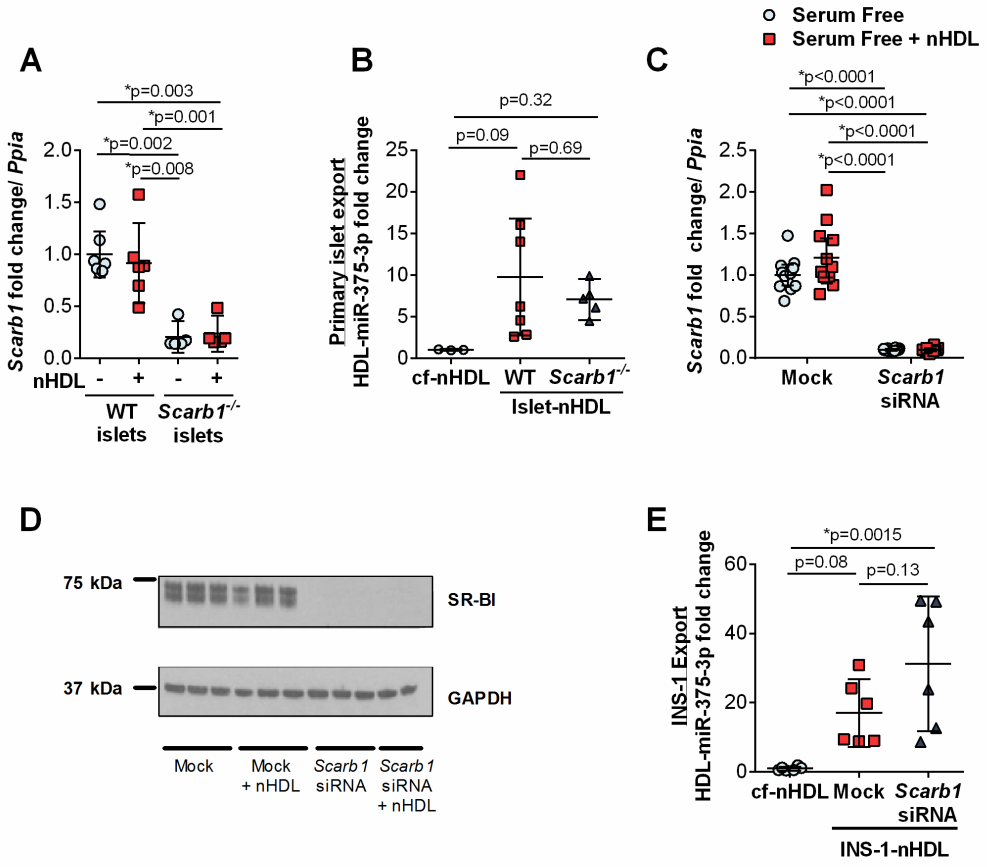

Figure 3-9. β cell miR-375-3p export to HDL does not require SR-BI. (A) SR-BI and wildtype islet levels of Scarb1 mRNA. n=3; one-way ANOVA with Bonferroni post-test, alpha = 0.05. (B) miR-375-3p levels on cf-nHDL and islet-nHDL from mouse WT (wildtype) or SR-BI KO (Scarb1-/-) mice. n=3; one-way ANOVA with Bonferroni post-test, alpha = 0.05. (C) INS-1 cellular levels of Scarb1 mRNA and (D) SR-BI protein (western blotting) after transfection with mock or 50 nM siRNA against Scarb1. Cropped images are of the same blot at different exposures. n=12; one-way ANOVA with Bonferroni post-test, alpha = 0.05. (E) miR-375-3p levels on cf-nHDL and INS-1-nHDL after knockdown of Scarb1; cells were transfected with mock or 50 nM Scarb1 siRNA. n=6; one-way ANOVA with Bonferroni post-test, alpha = 0.05.

(Figure 3-9B). Moreover, we tested whether β cell SR-BI regulates HDL-miR-375-3p export *in vitro*; siRNAs were used to knockdown SR-BI expression in INS-1 cells, which was confirmed at the mRNA and protein levels by RT-PCR and western blotting, respectively (Figure 3-9C, Figure 3-9D). Similar to our findings in primary islets *ex vivo*, SR-BI was not required for miR-375-3p export to nHDL from INS-1 cells (p=0.13 between mock and *Scarb1* siRNA INS-1-nHDL) (Figure 3-9E).

We next sought to investigate the role of cholesterol transporters ABCA1 and ABCG1 in regulating miRNA export to HDL. ABCA1 and ABCG1 mediate cholesterol and lipid efflux to discoidal nascent HDL and spherical HDL particles, respectively(202). ABCA1 is also a key mediator of HDL-induced anti-inflammatory cell signaling. We have previously reported that LXR activation, which increases ABCA1 and ABCG1 expression, failed to alter miR-223-3p export from macrophages to nHDL(94). Nonetheless, ABCA1 and/or ABCG1 might regulate miR-375-3p export to nHDL in pancreatic β cells; therefore, siRNAs were used to knockdown ABCA1 and ABCG1 expression in INS-1 cells, which was confirmed by loss of mRNA (Figure 3-10A, Figure 3-10B) and protein levels (Figure 3-10C, Figure 3-10D). Due to low basal levels of ABCG1 expression in β cells, we also studied the effect of transporter over-expression using LXR/retinoid-X-receptor (RXR) agonists which promote the transcription of *Abca1* and *Abcg1* (TO901317, LXR agonist; 9-cis-retinoic acid, RXR agonist) (Figure 3-10A, Figure 3-10B, Figure 3-10C, Figure 3-10D). HDL-miRNA export assays were performed in conditions of dual *Abca1* and *Abcg1* knockdown or over-expression; however, neither silencing, nor over-expression of these cholesterol transporters had any effect on β cell HDL-miR-375-3p export (Figure 3-10E). Thus, SR-BI, ABCA1, and ABCG1 do not likely regulate HDL-miR-375-3p export from pancreatic β cells. Combined, these results support a model in which β cell miR-375-3p export and cholesterol efflux to HDL are mediated by distinct transporters and/or pathways.

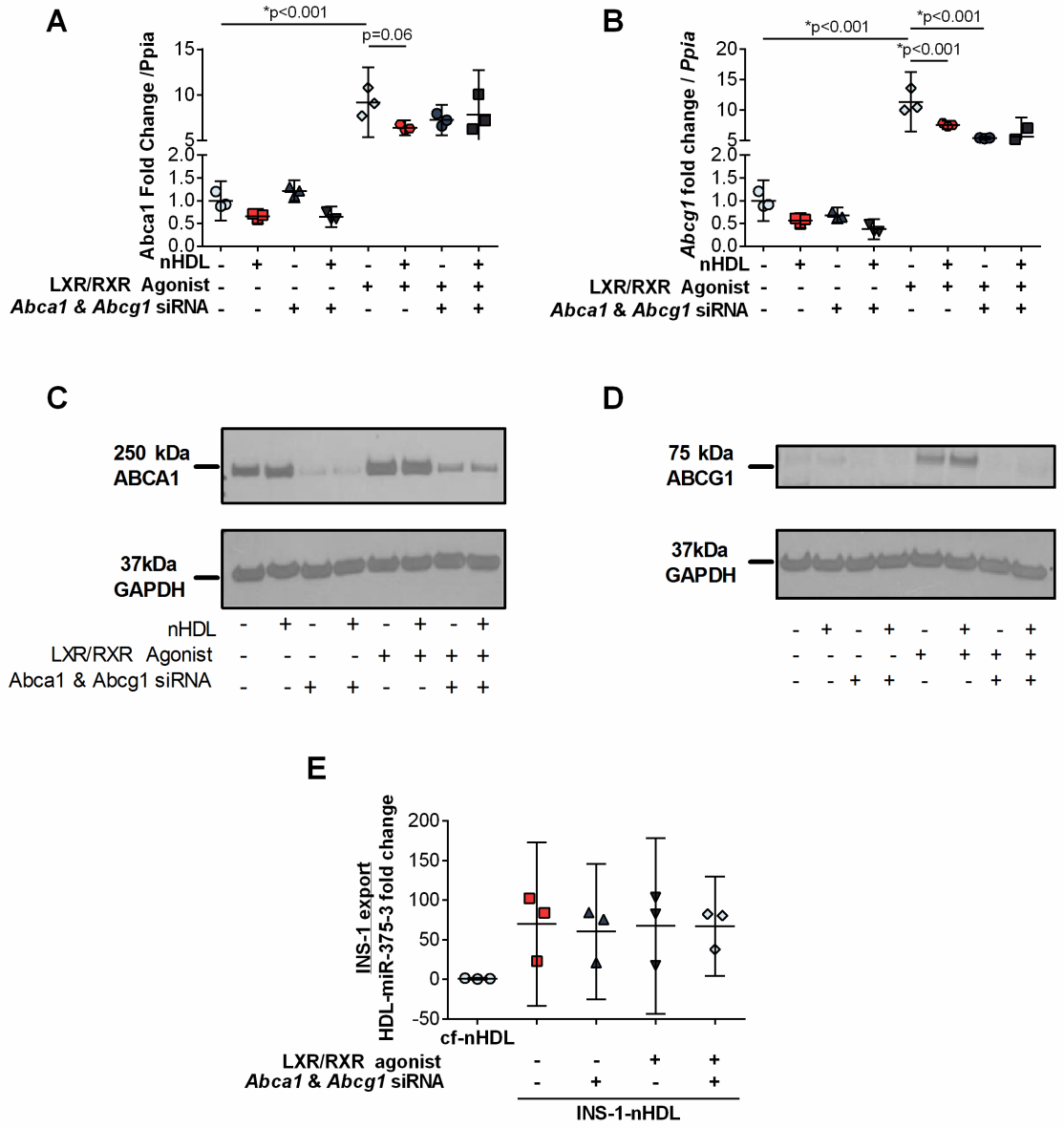

Figure 3-10. β cell miR-375-3p export to HDL does not require ABCA1 and ABCG1. (A) *Abca1* and (B) *Abcg1* mRNA levels in INS-1 cells treated with *Abca1* and *Abcg1* siRNA and/or LXR and RXR agonist. n=3; one-way ANOVA with Bonferroni post-test, alpha = 0.05. (C) ABCA1 and (D) ABCG1 protein (western blotting) after transfection with mock or 50 nM siRNA against *Abca1* and *Abcg1*, in the presence or absence of TO901317 (LXR agonist) and 9-cis-retinoic acid (RXR agonist). Representative of n=3. Cropped images are of the same blots at different exposures. (E) miR-145-5p and miR-375-3p levels on cf-nHDL and INS-1-nHDL after INS-1 cells transfection with mock or 50 nM siRNAs against *Abca1* and *Abcg1* and/or LXR/RXR agonists. n=6; one-way ANOVA with Bonferroni post-test, alpha = 0.05.

Discussion

HDL particles have many diverse beneficial properties with regard to anti-inflammatory and anti-oxidant capacities(188). In the β cell, HDL promotes cell integrity and proper function, e.g. protection against cellular toxicity and maintenance of GSIS(188). Although most of the beneficial properties of HDL are attributed to cholesterol metabolism, HDL transports many types of non-cholesterol cargo, including proteins, vitamins, bioactive lipids, and non-coding sRNAs, which also likely contribute to HDL's beneficial properties(93). Previously, we reported that HDL transport miRNAs and deliver them to recipient cells where they regulate target gene expression(94, 95). Nevertheless, very little is known about the origin of HDL-miRNAs and the mechanisms of cellular miRNA export to HDL. In this study, we demonstrate that pancreatic islets and β cells export selected miRNAs, e.g. miR-375-3p, to HDL. Using sRNA-seq, we profiled miRNA expression in pancreatic islets and on HDL. Comparisons of miRNAs detected in both HDL and islets showed considerable overlap. Based on this overlap, sRNA-seq was further used to identify the miRNAs that are exported from primary islets and β cells to HDL *ex vivo* and *in vitro*, and we found that miR-375-3p is a highly and the most abundant exported miRNA to HDL. Results suggest that β cell miRNA export to HDL is inversely linked to insulin secretion. For example, β cell miRNA export to HDL likely occurs during cellular conditions in which insulin secretion is low, as HDL-miR-375-3p export was inhibited under conditions that stimulate insulin secretion. Although we hypothesized that cholesterol transporters facilitate miRNA transport across the plasma membrane, we found that inhibition of SR-BI, ABCA1, and ABCG1 failed to alter β cell miRNA export to HDL. Overall, these observations markedly advance our fundamental understanding of HDL-miRNA secretion.

Many of the most abundant miRNAs in pancreatic islets and β cells were found circulating on HDL, including miR-375-3p. Due to miR-375-3p's critical importance to β cell integrity and function, extracellular circulating miR-375-3p levels have been reported as a biomarker of β cell function(167, 194). miR-375-3p has previously been detected in plasma, as well as exosomes

and MVs, prompting renewed interest in the role of miR-375-3p as an intercellular signaling molecule and for its utility as a biomarker of disease (and pre-disease)(168). In patients with T2D, no clear consensus exists as to the regulation of extracellular miR-375-3p levels, as different studies have reported an increase, decrease, or no change in extracellular miR-375-3p levels in T2D human subjects and rodent models of T2D(194). Nevertheless, in both humans with T1D and murine models of T1D, miR-375-3p was consistently found to be upregulated in plasma samples(203). For this reason, circulating (plasma/serum) miR-375-3p has been proposed as a biomarker of β cell death(125, 167). Despite reports that β cells may release miR-375-3p during cell death and serum-free conditions used in our studies may promote some level of cell death, we did not observe substantial cell death in our cell culture conditions. Moreover, in this study, we found that β cell miRNA export is selective for miR-375-3p, and that many of the other highly-abundant miRNAs in the β cells and islets are not exported to HDL, as determined by sRNA-seq.

Due to the secretory phenotype of the endocrine β cell, we sought to determine whether cellular mechanisms that control insulin secretion also regulate miRNA export to HDL. We found that while miR-375-3p was readily exported to HDL in low glucose conditions, export was inhibited at high glucose in the presence of physiologic Ca^{2+} concentrations. In β cells, under basal, low glucose conditions, the plasma membrane is hyperpolarized and insulin secretion is low. Increases in glucose concentrations above 5 mM result in glucose metabolism and a rise in the ATP/ADP ratio. ATP closes the K_{ATP} channels resulting in the depolarization of the plasma membrane. This activates VGCC, and leads to increased $[Ca^{2+}]_i$ levels which result in insulin granule secretion. Many pharmacologic agents have been developed to modulate this process: sulfonylureas promote insulin secretion by binding to the SUR1 subunit and closing the K_{ATP} channel, whereas DIA opens the channel(195, 204). Here, chemical inhibition of the K_{ATP} channel, independent of high glucose, significantly inhibited miR-375-3p export to HDL. Conversely, DIA in high glucose prevent the suppresion of miR-375-3p export caused by $CaCl_2$. It should also be noted that we were able to readily detect GSIS in the INS-1 cells, and tolbutamide also increased

insulin secretion in low glucose conditions, whereas DIA inhibited insulin secretion in high glucose. Nevertheless, tolbutamide was found to inhibit GSIS in the high glucose condition and this was not expected. One possible explanation could be that tolbutamide treatments resulted in complete K_{ATP} inhibition and the membrane potential was depolarized to a level that resulted in voltage-dependent inactivation of Ca^{2+} channels and reduced Ca^{2+} influx and insulin secretion. We further tested the requirement of the K_{ATP} channel using islets isolated from SUR1 (*Abcc8*$^{-/-}$) KO mice and Kir6.2 (*Kcnj11*$^{-/-}$) KO mice. Islets lacking the K_{ATP} channel had a decreased capacity to export miR-375-3p to HDL. We also found that IBMX, but not ex-4, suppressed miR-375-3p export to nHDL. Of note, IBMX resulted in a strong induction of c-fos, a cAMP responsive gene, whereas ex-4 did not, suggesting that a large increase in cAMP may be required in INS-1 cells to inhibit miR-375-3p export to HDL. Based on these observations, a few models can be proposed. Firstly, that the K_{ATP} channel itself may be responsible for directly transporting miRNAs across the plasma membrane; however, the size of the channel is likely not large enough to facilitate miRNA transport across the plasma membrane. Secondly, that K_{ATP} channel may indirectly aid the transport of miRNAs across the plasma membrane through interaction with a currently unknown membrane transporter, potentially through an allosteric regulatory mechanism. Thirdly, inhibition (closure) or absence of the K_{ATP} channel alters the cell polarization state and ion concentrations leading to insulin secretion, while indirectly affecting miRNA release or retention in the cell. Although our studies cannot distinguish between these three models, our findings suggest that ion dynamics likely are involved, as glucose-induced suppression of HDL-miR-375-3p export also required extracellular Ca^{2+} and occurred with elevated cAMP.

Although this is the first study to report critical regulators of β cell miRNA export to HDL, a recent study found that β cell secretion of exosomes containing miR-375-3p was increased under conditions that promoted insulin secretion, i.e. high glucose, arginine and KCl(168). This observed discrepancy - decreased miRNA export to HDL compared to increased exosome miRNA release with GSIS - is in agreement with our previous study in which we reported that

inhibition of the ceramide signaling pathway by GW4869 (attenuates exosome secretion) increased miRNA release to HDL(94). Although further work is required to fully define the relationship between insulin secretion, miRNA export to HDL, and exosome secretion, results presented here and our proposed model support that β cell miRNA export though exosomes and HDL occur through distinct routes under opposing cellular stimuli and regulation.

Based on the results presented here and in previous studies from our laboratory(94), β cell-derived miRNAs are likely transported by HDL in circulation, and thus, may regulate target genes in cells that take up HDL-miRNAs. We have previously demonstrated that miR-223-3p, a miRNA detected on HDL at comparable levels to miR-375-3p, is biologically active on HDL and regulates inflammatory target genes in recipient endothelial cells(95), thus supporting a potential role for β cell-derived HDL-miR-375-3p in intercellular gene regulation. Nevertheless, the functional impact of HDL-miR-375-3p on cell-to-cell communication networks remains to be determined. In exosomes, miR-375-3p has been reported to be the 3rd most abundant miRNA originating from pancreatic β cells (following miR-709 and miR-1224)(166),and miRNAs that are detected in exosomes at 8-10 times lower concentration than miR-375-3p, e.g. miR-15a, have been shown to have biological function in miRNA-mediated communication originating from β cells(205). For example, an exogenous miRNA, cel-miR-238, when expressed in pancreatic β cells has been shown to be released into exosomes to promote apoptosis in recipient cells(166). Similarly, exosomes released from human islets and β cells have also been reported to be taken up by recipient dendritic cells(206). Furthermore, INS-1 β cells were demonstrated to release exosomes containing miR-15a, which was increased in high glucose conditions(205). These INS-1 cell exosomes were demonstrated to target Akt3 and promote apoptosis in recipient retinal glial cells (Muller cells), thus representing a potential underlying mechanism of diabetic complication resulting from β cell-originating intercellular communication(205). Although these miRNAs have been demonstrated to have physiological function in cell-to-cell communication pathways, they are found in exosomes at concentrations much lower than miR-375-3p. In addition, a recent study

by Chevillet *et al.,* found that the levels of miR-375-3p carried in exosomes represent a small percentage (2.7%) of total plasma miR-375-3 levels, thus leaving 97.3% to be associated with other carriers, e.g. lipoproteins and RNA-binding proteins(147).

Nevertheless, essential questions regarding the biological functions of HDL-bound miR-375-3p remain to be determined. HDL-miR-375-3p is abundantly detected in plasma, and likely regulates cell-to-cell communication in some capacity(94). We hypothesize that HDL-miR-375 is transported from the β cell to recipient cells where miR-375-3p regulates target gene expression; however, at this time the identity of the recipient cells/tissues are unknown. miR-375-3p has been extensively studied in pancreatic β cells, however, a few studies in other cell-types offer clues to the potential physiological effects of HDL-miR-375-3p. For example, miR-375-3p has been shown to negatively regulate osteogenesis, the process of bone formation, by targeting Wnt signaling proteins(207). Wnt signaling is also involved in epithelial cell differentiation in the lung and rheumatoid arthritis (RA) pathogenesis(208). miR-375-3p was also shown to target Frizzled 8, a component of canonical Wnt signaling, and inhibit epithelial cell differentiation in response to lung injury(208). In fibroblasts, miR-375-3p suppression of Frizzled 8 inhibited disease pathogenesis in a rat model of RA(209). In the brain, miR-375-3p is associated with neuroprotection in a rat model of cerebral ischemia/reperfusion(210).

In summary, this study provides regulatory insight into the cellular process that affect miR-375-3p export to HDL from human islets and pancreatic β cells. Results suggest that miR-375-3p export to HDL is inhibited by glucose-stimulation (high glucose), but only in the presence of extracellular Ca^{2+}. Furthermore, through multiple different approaches, we demonstrate that miR-375-3p export to HDL occurs only under conditions of low insulin secretion, as demonstrated by modulating K_{ATP} channel activity and cAMP levels. Moreover, we found that miR-375-3p export to HDL was independent of cholesterol transporters - ABCA1, ABCG1 and SR-BI. Together, these results support that pancreatic β cell miR-375-3p export to HDL is inversely regulated by the cellular mechanisms that control insulin secretion.

CHAPTER IV

PROFILING OF HDL AND TISSUE miR-375 IN RESPONSE TO METABOLIC ALTERATIONS

Introduction

miRNAs exert actions in different tissues, and miR-375-3p has garnered attention in the diabetes field because levels are highly enriched in the endocrine cells of the pancreas(125, 126). Expression studies of miRNAs in islets and β cells have consistently identified miR-375-3p as the most abundant islet (Table A-3) and β cell miRNA(123, 124). miR-375-3p was first cloned in the pancreatic β cell line, MIN6 cells(127), and was later found to be expressed in β cells and endocrine non-β cells in the islet(128, 211). Global miR-375 KO mice have a reduction in insulin-producing β cells (31% decrease compared to WT at 10 wks), a concomitant 1.7-fold increase in α cells, and are hyperglycemic(128). Furthermore, when *ob/ob* mice were bred with miR-375 KO mice, these miR-375 KO/*ob* mice had severely diminished β cell proliferative capacity normally observed in *ob/ob* mice, suggesting that miR-375 is critical for β cell development and proliferation(128). miR-375-3p has also been shown to play a key role in the adult β cell, regulating insulin secretion(127). Poy *et al*. first showed that miR-375-3p inversely regulates insulin secretion(127). miR-375-3p is elevated under conditions of low glucose and has been proposed to regulate insulin secretion through its target gene *Mtpn*(127). Similarly, El Ouaamari *et al*. have shown that miR-375-3p also directly regulates synthesis of the insulin gene through its direct targeting of *Pdk1* and by decreasing insulin synthesis, miR-375-3p thereby inhibits insulin secretion(130). And through a third approach, Keller *et al*. have further shown the inverse relationship between insulin secretion and miR-375-3p expression(131). This study showed that cAMP, a second messenger molecule that potentiates insulin secretion, inhibits miR-375 transcription through the cAMP-PKA pathway(131). Together these studies have shown a critical

role for miR-375-3p in the islet, which has prompted numerous research groups, including ours, to study the relationship between diabetes, islet miR-375-3p and circulating miR-375-3p.

In the introduction of this dissertation, research on HDL-miRNAs was discussed extensively. Furthermore, Chapter III presented the β cell as a cell type that exports miR-375-3p to HDL. However, to date, there has not been an investigation into how diabetes affects HDL-miRNAs and specifically, HDL-miR-375. Below, I discuss the findings presented on how metabolic alterations in rodents and humans affects HDL-miRNAs, namely, HDL-miR-375-3p and discuss these findings in the context of published results examining circulating miR-375-3p changes in response to T1D and T2D. Furthermore, a key question in the field of extracellular RNAs is what proportion of plasma miRNAs are localized and/or bound to each of the extracellular compartments, i.e. exosomes, plasma, protein-bound. Here, I provide the first stoichiometric quantification of a miRNA in both plasma and HDL and relate the relative abundances to estimate what proportion of plasma miR-375-3p is contained within the HDL compartment. Furthermore, I provide a discussion of how these results compares to similar stoichiometric analysis of miRNAs in exosomes.

Results

HDL-miRNA changes in leptin deficient rodent models

Numerous studies have examined the effects of T1D and T2D on total extracellular miRNAs and exosome miRNAs. However, to date, there have been no reports quantifying changes in miRNAs in T1D and T2D in the HDL compartment. Therefore, to investigate the changes in HDL-miRNAs in T2D, plasma was collected from two rodent models of T2D, ZDF rats and *db/db* mice and lean controls. HDL was isolated from ZDF and lean rats and sRNA sequencing was performed on HDL-RNA. Twelve (9 upregulated, 3 downregulated) miRNAs were found to be significantly altered in ZDF compared to lean rats by sRNA sequencing (Figure 4-1A and Table A-5). Surprisingly, miR-375-3p, a miRNA that has been found to be enriched in

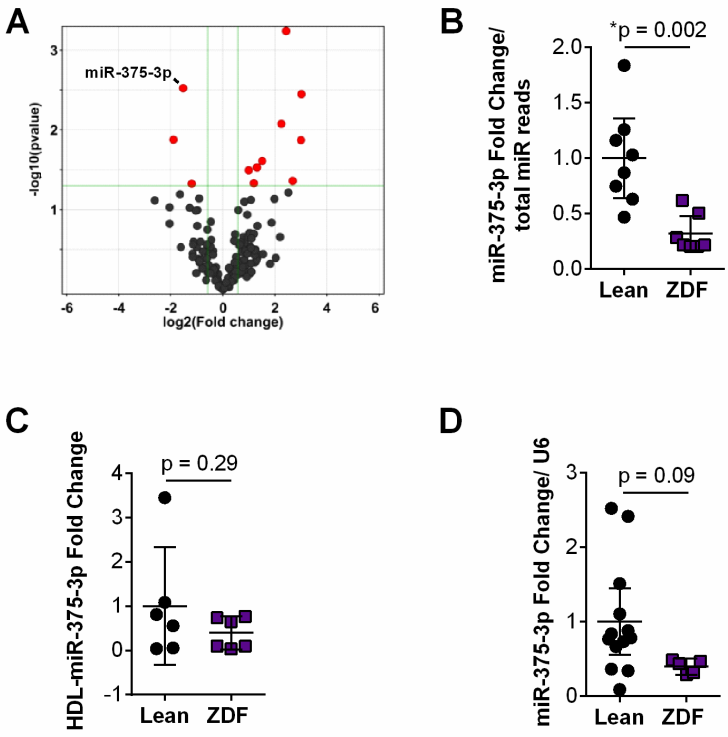

Figure 4-1. miR-375 changes in islet and HDL from lean and ZDF rats. (A) Volcano plot of small RNA sequencing of HDL-RNA from lean and ZDF rats. Red dots indicate miRNAs with fold change >1.5, and $p<0.05$; n=7-8; two-tailed t-test. (B) HDL-miR-375-3p reads from small RNA sequencing. n=7-8; two-tailed t-test. (C) HDL-miR-375-3p levels by real time PCR from lean and ZDF rats. n=6; two-tailed t-test. (D) miR-375-3p levels from lean and ZDF rat islets. n=5-13; two-tailed t-test.

pancreatic islets was one of the miRNAs that was significantly downregulated in ZDF rat HDL (Figure 4-1B). To confirm the sequencing findings by RT-PCR, miR-375-3p levels were measured in HDL from lean and ZDF rats. Using this complementary technique, I found miR-375-3p was decreased, albeit not significantly (Figure 4-1C). Since miR-375-3p has been reported to be most abundant in pancreatic islets, I next tested whether miR-375 was altered in the islets of ZDF rats. I performed sRNA sequencing on islet RNA from lean and ZDF rats and found 110 significantly altered miRNAs (46 down, 94 up; Table A-6). Among them, miR-375-3p was found to be decreased in ZDF rat islets, compared to lean (Table A-6). I performed RT-PCR to validate these changes, and found that miR-375-3p was decreased in ZDF islets compared to lean, but the difference did not reach statistical significance with the low sample size (n=3) (Figure 4-1D).

Both *db/db* mice and ZDF rats are a model of T2D due to leptin receptor mutations, and therefore I sought to test whether the decrease in HDL-miR-375-3p observed in ZDF rats also occurred in *db/db* mice. HDL-miR-375-3p, was found to be slightly, but not significantly decreased in *db/db* mice compared to controls (Figure 4-2). Together, this data suggests that HDL-miR-375-3p may be decreased in rodent models of T2D, but that further studies with larger sample sizes are required to accurately assess the effect of leptin-deficiency on HDL-miR-375-3p.

HDL and plasma miRNA changes in human T2D subjects

There has been an enormous interest in exploring extracellular miRNAs as biomarkers of human disease. To this end, human donors were recruited to collect blood samples from 20 healthy and 20 diabetic subjects (donor characteristics are shown in Table A-7). sRNA sequencing was performed to measure miRNAs in plasma and HDL from healthy and T2D subjects. 149 miRNAs were detected in plasma at >5 reads per sample (Table A-8). miR-27a-3p (2.7 fold, p=0.01) and miR-369-3p (3.0 fold, p=0.02) were found to be downregulated, whereas miR-122-5p (2.7 fold, p=0.002), miR-1246 (3.1 fold, p=0.02) and miR-486-5p (3.3 fold, p<0.0001) were found to be upregulated in plasma from T2D subjects compared to controls (Table A-8).

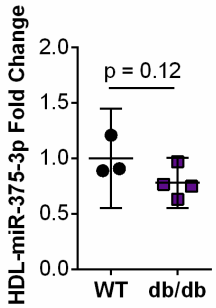

Figure 4-2. miR-375 changes on HDL from WT and db/db mice. HDL-miR-375-3p levels by real time PCR from wildtype (WT) and db/db mice. n=3-4; two-tailed t-test.

sRNA sequencing was also performed on HDL-RNA isolated from the same blood samples and 16 miRNAs were detected on HDL at >5 reads per sample (Table A-9). Of these, all but one miRNA, miR-203a-3p, were also detected in plasma. Only one miRNA was found to be significantly altered; miR-320a was downregulated (2.9 fold, p=0.03) in T2D HDL compared to healthy HDL (Table A-9). Surprisingly, miR-320a was also detected in plasma from these donors, but contrary to the changes observed in HDL, miR-320a was unchanged in plasma between healthy and T2D (upregulated 1.4 fold, p=0.3) (Table A-9). This suggests that miRNA changes with T2D in plasma may not reflect changes in the HDL compartment, and vice versa.

Due to my findings that HDL-miR-375-3p levels are trending towards downregulation in rodent models of T2D (Figure 4-1, 4-2), and that previous studies have found discrepant results in plasma miR-375-3p in T2D humans(121), I investigated whether miR-375-3p is altered in plasma and HDL by qPCR from T2D subjects compared to controls. Plasma miR-375-3p levels were found to be unchanged between healthy and T2D subjects (Figure 3-3A). Recent studies have implicated a role for gender in differential promoter methylation of miR-375(212). Although it is currently unknown how promoter methylation of this loci affects expression levels between genders, I divided this cohort of subjects into males and females to determine whether plasma expression levels were different in males and females with and without T2D. However, there was no differences in plasma miR-375-3p levels between males and females in either control or T2D subjects (Figure 4-3B). Next, I investigated whether HDL-miR-375-3p levels were altered in T2D subjects, however, similar to the findings in plasma, I did not detect any difference in miR-375-3p levels in this cohort (Figure 4-3C). Moreover, I separated males and females, and failed to find any difference between genders in miR-375-3p levels on HDL (Figure 4-3D). Taken together, these results suggest that while there is a slight decrease in HDL-miR-375-3p levels in rodent models of T2D, the variability in genetics and environment in humans coupled with the low number of miRNAs detected by sequencing severely underpowered these studies. Further studies with larger sample size and greater sequencing depth will be required to adequately profile the

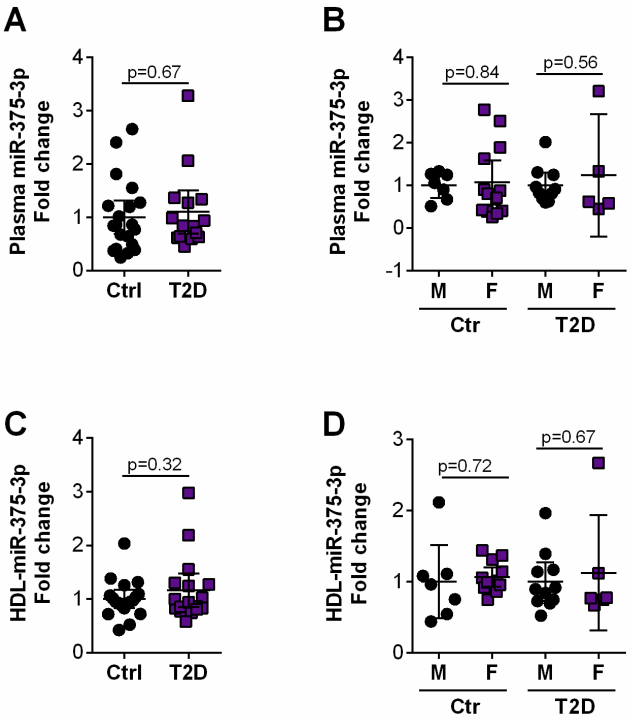

Figure 4-3. Plasma- and HDL-miR-375-3p from control and T2D human subjects. (A) Plasma miR-375-3p levels from control and T2D human subjects. n=15-20; two-tailed t-test. (B) Plasma miR-375-3p levels from control and T2D human subjects divided into M (male) and F (female). n=5-13; two-tailed t-test. (C) HDL-miR-375-3p levels from control and T2D human subjects. n=17-19; two-tailed t-test. (D) HDL-miR-375-3p levels from control and T2D human subjects divided into M (male) and F (female). n=6-12; two-tailed t-test.

changes in HDL miRNAs to compare them to published results reporting changes in plasma miRNAs in T2D.

HDL-miR-375-3p changes in response to STZ as a model of β cell death

Next, I examined miR-375-3p changes in mice treated with a β cell toxin, STZ. STZ treated mice represent a model of T1D, as they lose β cells and develop hyperglycemia. The goal of using this model was two-fold; to measure miR-375-3p changes in plasma and HDL in response to T1D, and to test whether β cells contribute the majority of miR-375-3p to HDL. Male WT mice were divided into two group, PBS (controls) and STZ such that there was no difference in fasting plasma glucose levels or body weights prior to STZ treatment (Figure 4-4A,B). Fasting glucose levels were measured at sacrifice (10 days post injection) and mice were divided into two groups based on glucose levels, low (mean glucose 177mg/dl) and high (mean glucose 255mg/dl) groups (Figure 4-4A). Only the STZ high group had fasting glucose levels significantly elevated compared to PBS controls (Figure 4-4A), whereas the random fed glucose levels were higher in both STZ groups compared to PBS controls (Figure 4-4C). Similar to previous reports, STZ treated mice had small reductions in body weight (Figure 4-4B)(126). This provided a model in which to study miRNA changes in plasma and HDL in response to STZ. Similar to previous reports(125, 126, 167), plasma miR-375-3p levels were found to be elevated in both groups of STZ treated mice, albeit the results were not significant in either STZ group (Figure 4-4D). I next measured HDL-miR-375-3p levels. Although the samples had enormous variability, there appeared to be a trend towards increased levels of miR-375-3p on HDL from STZ treated mice (Figure 4-4E), however, further studies will be required to better understand the effect of STZ on HDL-miR-375-3p.

Acute changes in HDL-miR-375-3p with fasting and feeding

Previous work presented in this dissertation points to glucose and insulin secretion regulating export of miR-375-3p to HDL from β cells (Chapter III). To test whether systemic

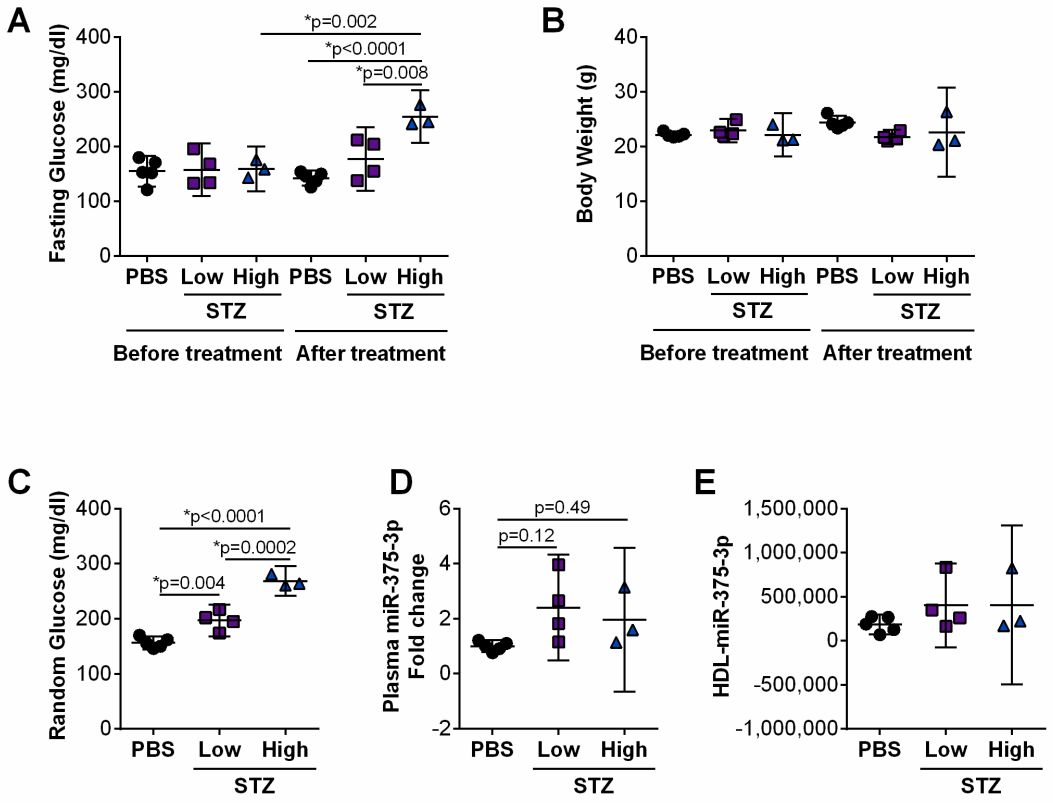

Figure 4-4. miR-375 changes in HDL and plasma from wildtype (WT) mice treated with streptozotocin (STZ). (A) Fasting glucose levels in mice treated with STZ or PBS before and after treatment. STZ mice were stratisfied into two groups: low and high based on their glucose levels (<250mg/dl: low; >250mg/dl: high). n=3-5; one-way ANOVA with Bonferonni post-test. (B) Body weights from mice treated with STZ or PBS. n=3-5; one-way ANOVA with Bonferonni post-test. (C) Non-fasted glucose levels 10-days post STZ injections. n=3-5; one-way ANOVA with Bonferonni post-test. (D) Plasma miR-375-3p levels in PBS and STZ treated mice. n=3-5; one-way ANOVA with Bonferonni post-test. (E) HDL-miR-375-3p levels from PBS and STZ treated mice. n=3-5; one-way ANOVA with Bonferonni post-test.

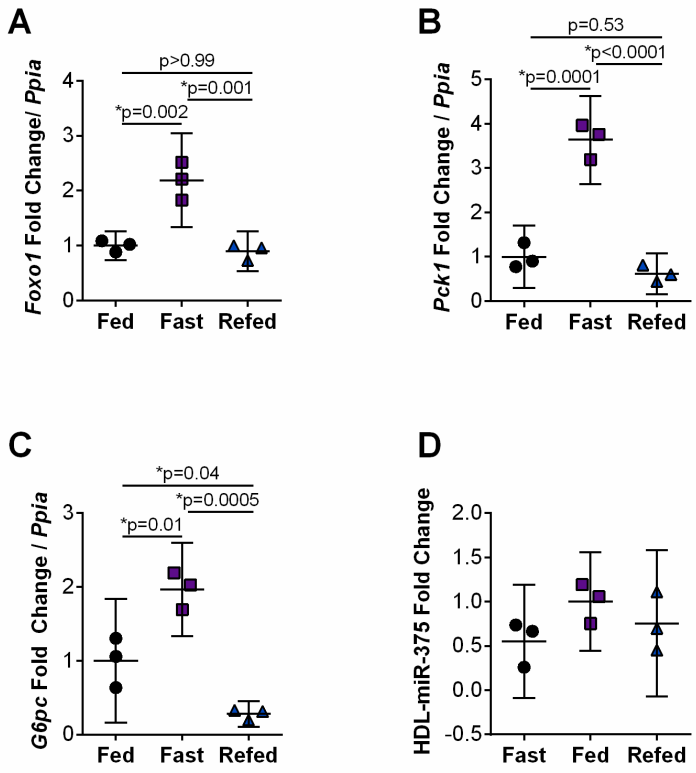

Figure 4-5. miR-375-3p changes on HDL in response to fasting and feeding. (A) Hepatic expression of *Foxo1*, (B) *Pck1*, and (C) *G6PC* from wildtype mice, ad lib fed (fed), fasted for 16h (fast) or fasted for 16h and and refed for 2h (refed). n=3; one-way ANOVA with Bonferonni post-test. (D) HDL-miR-375-3p levels from fast, fed and refed mice. n=3; one-way ANOVA with Bonferonni post-test.

changes to glucose and insulin alter HDL-miR-375-3p levels, mice were fasted and fed and HDL-miR-375-3p was quantified. Fasting represents a β cell state of low insulin secretion, whereas the fed, and refed states represent conditions of high insulin secretion and acutely elevated glucose and insulin levels. Therefore, I hypothesized that under fasted conditions (low insulin secretion), β cell miR-375-3p secretion levels would be increased resulting in an elevation in HDL-miR-375-3p levels. To test this, male C57B/6J mice were given free access to food (fed) or fasted for 16h (fast and refed groups); post-fast, refed mice were then given free access to food for 2h. To confirm that the mice were adequately fasted, three gluconeogenic genes were measured in the liver, *Foxo1*, *Pck1* and *G6Pase*. As expected *Foxo1*, *Pck1* and *G6Pase* were elevated in fasted compared to fed and refed mice (Figure 4-5A-C). Next, I isolated HDL from plasma and measured miR-375-3p levels on HDL. However, with a small sample size (n=3), there was no difference in HDL-miR-375-3p in any of the three groups, and the fasted mice trended towards a decrease in HDL-miR-375-3p, not an increase, as hypothesized.

Stoichiometric quantification of HDL and plasma miR-375-3p

Another key question in the field of extracellular miRNAs is what proportion of plasma miRNAs are contained within each compartment, i.e. exosomes, MVs, HDL, other lipoproteins, and bound to RNA-binding proteins. To address this question in the context of HDL-miR-375-3p, miR-375-3p was quantified in five WT mice in plasma and HDL. 1ml of plasma contains approximately 1mg of HDL protein, and therefore the absolute concentrations of miR-375-3p for HDL and plasma were plotted to test their correlation (Figure 4-6). HDL-miR-375-3p levels were found to reflect plasma miR-375-3p levels, as HDL-miR-375-3p and plasma miR-375-3p levels were highly correlated in mice (Spearman r=0.7, P=0.07) (Figure 4-6). Furthermore, this approach allowed me to approximate the percentage of plasma miR-375-3p that is bound to HDL. Using this correlation, I estimate that approximately 3.7-6.0% of plasma miR-375-3p is bound to HDL (Figure 4-6); however, some miRNAs may be lost during HDL isolation and these values may

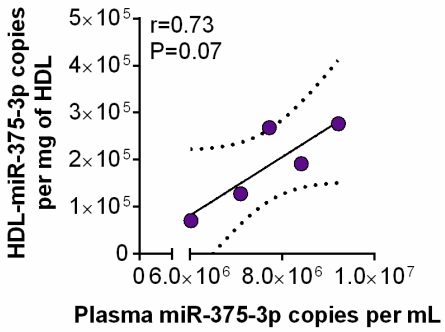

Figure 4-6. Quantification of miR-375-3p in plasma and HDL from WT mice. Correlation of plasma miR-375-3p levels and HDL-miR-375-3p levels. n=5; Linear regression analysis.

underestimate HDL content. Together this data suggests that a small amount of plasma miR-375-3p is bound to HDL and that at least under normal conditions in WT mice, plasma miR-375-3p levels correlate with HDL miR-375-3p levels.

Discussion

Previous studies have examined changes in miR-375-3p levels in rodent models as well as humans with T1D and T2D, however, this is the first study to quantify changes in HDL-miR-375-3p in response to T1D and T2D. Here, I find that HDL-miR-375-3p is decreased, albeit not significantly in ZDF rats and *db/db* mice, two models of T2D. However, in human subjects with T2D I found no difference in HDL and plasma miR-375-3p levels. Contrary to my prediction that STZ treated mice lacking β cells would have a reduction in HDL-miR-375-3p, an increase was observed. Similarly, mice that were fasted did not have an elevation in HDL-miR-375-3p as predicted from *in vitro* studies showing the β cells export of miR-375 is enhanced under conditions of low glucose (Chapter II). Finally, I find that in WT mice, HDL-miR-375-3p correlates strongly with plasma levels of miR-375-3p, and 3.7-6.0% of extracellular miR-375-3p is isolated with HDL.

In this study I identified that miR-375-3p is decreased on HDL from ZDF rats compared to lean (Figure 3-1A-C). ZDF rats undergo four distinct phases in diabetes development: early on the rats are pre-diabetic (6 weeks of age), then they develop hyperinsulenimia (8 weeks of age), followed by β cell failure where plasma insulin levels are decreased and hyperglycemia develops (11 weeks of age) and finally, late-stage diabetes and severe hyperglycemia (17 weeks of age)(50). A recent study by Delic *et al*. compared plasma miR-375-3p levels in diabetec rats in the hyperinsulinemic, β cell failure and late-stage diabetes time points compared to expression levels with pre-diabetes(50). This study reported no change in circulating levels of miR-375-3p in ZDF rats until the late-stage diabetes (17 weeks), when circulating miR-375-3p levels were found to be increased, compared to pre-diabetes(50). Although this study appears to be in conflict with these findings, there are a number of key differences in experimental design: firstly, my study

investigated HDL-miR-375-3p levels whereas the Delic *et al*. study analyzed total circulating miR-375-3p levels. Secondly, I compared the levels of HDL-miR-375-3p between 8 week old ZDF rats and lean rats, whereas the Delic *et al*. study examined changes in plasma miR-375-3p over time compared to 6 week old pre-diabetic ZDF rats(50). At this time it is unknown whether there are changes in miR-375-3p expression either in plasma or HDL between pre-diabetic ZDF rats and lean controls that may contribute to the apparent discrepancies. Additionally, I find that miR-375-3p levels are reduced in ZDF rat islets, whereas the only other report of miR-375-3p islet expression in a T2D model, showed no change in islet miR-375-3p between GK rats, a non-obese spontaneous T2D animal model and control Wistar rats. While both rats are models of T2D, there are key differences; ZDF rats develop obesity and hyperglycemia as early as 10-11 weeks of age(50), whereas GK rats are non-obese, and don't develop diabetes until 14-16 weeks of age(213), and it is possible that islet miR-375-3p vary throughout disease progression, similar to circulating levels. Therefore, future studies with larger sample sizes and examining ZDF rats across multiple time points will be required to uncover the changes in HDL-miR-375-3p with disease and the relationship between islet, plasma and HDL miR-375-3p levels.

I hypothesized that since both ZDF rats and *db/db* mice are leptin-deficient models of T2D, HDL-miR-375-3p would be similarly altered. With a small cohort of mice, I found a slight, but not significant reduction in the levels of miR-375-3p on HDL in *db/db* mice compared to WT controls. Although no other studies have investigated HDL-miR-375-3p changes in *db/db* mice, a recent study reported that plasma miR-375-3p levels are upregulated in *db/db* mice compared to WT(125). Similar to the discrepancies observed between my HDL-miR-375-3p findings and the reported plasma miR-375 changes in ZDF rats, it is unclear whether these effects are due to differences between HDL and plasma levels, or due to physiological differences from studying rodents at different timepoints in disease development. Of note, in this study, Latrielle *et al*. reported that two other mouse models of metabolic dysfunction, *ob/ob* mice and DIO mice have reduced miR-375-3p levels in plasma(125). The key distinction between *db/db* mice and *ob/ob*

and DIO mice is that *db/db* mice, similar to ZDF rats, display severe hyperglycemia due to β cell dysfunction, whereas ob/ob and DIO mice are normoglycemic and have increased β cell function. It is possible that this analysis in 10 week old *db/db* mice captured circulating miR-375-3p changes in a physiological state of β cell compensation, rather than dysfunction, more similar to *ob/ob* and DIO mice, than *db/db* mice. In fact, a recent study analyzed *db/db* mice aged 13-18 weeks and found large phenotypic variability among individual animals, with disease development ranging from β cell compensation (slightly elevated fasting blood glucose) to severe diabetes(214). Therefore, future studies examining HDL-miR-375-3p levels should also investigate the correlation of HDL-miR-375-3p not only with plasma-miR-375-3p levels, but also with glucose, and β cell function in individual animals to better understand the physiologic changes that alter HDL-miR-375-3p levels.

Extracellular miRNAs are a novel class of disease biomarkers and circulating miRNA levels have been extensively profiled for many metabolic diseases, including T2D(194, 215). However, due to conflicting data, at this time there is no consensus on circulating miR-375-3p and T2D(194). Multiple groups have reported that miR-375-3p levels are increased in serum(175, 216) and plasma(217) from T2D subjects. Similar to my findings, two recent studies reported that plasma miR-375-3p levels are not affected by T2D(125, 218). These discrepancies may be due to genetic, demographic, disease state progression and/or therapy differences between the subjects examined in each study, however, miRNAs still hold potential as a circulating biomarkers of β cell function and T2D. Therefore, I also performed sRNA-sequencing on plasma and HDL RNA from healthy and T2D donors. In this study, 55 plasma miRNAs were identified whose levels were significantly altered (13 increased, 41 decreased) in T2D subjects. Most of the miRNAs discovered have not previously been reported to be altered in T2D. Similar to my results, plasma miR-195, miR-126-3p and miR-320b have been shown to be decreased in T2D subjects and plasma miR-320a, miR-375 and miR-486 have been shown to be increased in T2D and insulin resistant individuals(219-222). However, contrary to my findings, previous studies have found

miR-122 and miR-486 to be inversely associated with glycemic progression and T2D(223, 224). A number of miRNA changes observed in my study are in opposition to published results; I observed miR-22-3p, miR-140-5p, miR-27a and miR-374a-5p to be decreased in T2D, but studies report these miRNAs are increased in T2D and insulin resistance(219, 221, 222, 225). Similarly, I observed miR-423a-5p and let-7a to be increased in T2D patients, whereas this miRNA has previously been found to be decreased in T2D(219, 225, 226). A pertinent issue with profiling extracellular miRNAs with sequencing is the validation of observed changes with a secondary method, e.g. RT-PCR. Indeed, in this study, we were not able to confirm by RT-PCR the observed 3-fold increase in plasma miR-375-3p levels in T2D subjects with sRNA-seq. Results from both sRNA-seq and RT-PCR suggest that HDL-miR-375-3p levels are not altered in the setting of T2D in humans and rodent models. Nevertheless, I identified 3 HDL-miRNAs that were significantly decreased in T2D subjects – hsa-miR-451a, hsa-miR-486-5p, hsa-miR-320b. These three HDL-miRNAs may hold value as extracellular markers of T2D or represent changes to HDL function within potential intercellular communication networks in T2D.

Based on the high expression of miR-375-3p in pancreatic β cells, numerous groups have hypothesized that extracellular (plasma/serum) miR-375-3p may be a marker of β cell death and a biomarker for T1D. Two recent studies have reported an increase in circulating miR-375-3p levels(125, 218), whereas one study reported a decrease(172), and yet another reported a correlation between C-peptide and miR-375-3p levels in newly diagnosed T1D subjects, but did not compare these levels to healthy controls(173). For mice, however, the results are much more consistent. Similar to my study, four other studies have reported increased plasma miR-375-3p levels in response to STZ treatment(125, 126, 167, 171). While we examined plasma- and HDL-miR-375-3p levels after 10 days of STZ treatment, Song *et al*. reported that levels rise as early as 4h post STZ(167). In a separate study, Erener *et al*. tracked plasma miR-375-3p levels after STZ treatment and found that levels were increased at D1, decreased at D7, and then increased again at D14 and remained elevated until D63 when mice were treated with insulin to normalize

glucose(126), supporting that plasma miR-375-3p levels are elevated both acutely and chronically in response to STZ.

The goal of measuring plasma- and HDL-miR-375-3p was to compare HDL-miR-375-3p levels in response to STZ to published results of plasma-miR-375-3p and to test whether β cells contributed a substantial amount of the circulating miR-375-3p. The hypothesis was that if β cells contribute most of the circulating miR-375 to the circulation (and specifically HDL), STZ treated mice would have acutely elevated circulating miR-375-3p levels during β cell lysis and then a reduction in plasma-miR-375 once β cells are mostly destroyed and circulating miR-375-3p is turned over. However, Erener *et al*. found that miR-375-3p levels remain elevated in the blood for as many as 63 days post STZ treatment(126). Although β cell number was not quantified in this study, plasma glucose levels reached 30mM by D14 and remained at this level until D63, suggesting that no further β cell loss occurred between these timepoints(126). Similarly, Latreille *et al*. addressed this question using a miR-375 global knockout mouse (375-KO) in which circulating miR-375-3p levels were undetectable(125). When these mice were crossed with transgenic mice expressing miR-375 only in the β cell (β-rescue), many of the physiological abnormalities of the 375-KO mice were restored, but only 1% of the circulating levels of miR-375-3p in a WT mouse were restored in the β-rescue mouse(125). Together, these two studies suggest that while the β cells likely contributes some proportion of miR-375 to the circulation, it is not the sole contributor, and other tissues, perhaps even other endocrine cells in the islet, can also release this miRNA to circulation. A key outstanding question is whether the same is true of HDL-miR-375-3p and whether the majority of miR-375-3p released to HDL originates from the β cell and via the mechanisms uncovered *in vitro* in Chapter III. Future studies will be required to further examine the relationship between HDL-miR-375-3p and plasma-miR-375-3p to understand whether the source of these two pools of circulating miR-375-3p are the same or not.

While most of the models discussed thus far have examined chronic changes in miR-375-3p levels in response to diabetes models (T1D & T2D), we also sought to investigate whether HDL-miR-375-3p levels were regulated acutely in response to glucose changes. However, similar to previous studies that reported no change in plasma-miR-375-3p in response to fasting and refeding(126), we did not observe any change in HDL-miR-375-3p levels with fasting or refeeding. Contrary to this, a recent study in humans, observed that plasma levels of miR-375-3p were upregulated 60 and 120 minutes after an oral (OGTT), but not intravenous (IGTT), glucose bolus(227). This suggests that gut incretins may contribute to the release of miR-375-3p to the circulation, as GPL-1, GLP-2, and GIP were elevated in response to OGTT, but not IGTT(227). Although it is unknown whether incretins stimulate miR-375-3p to circulation from β cells or other cells types, our *in vitro* data supports that incretins may contribute, as we found that β cells export miR-375-3p to HDL in the presence of the GLP-1 analogue, ex-4, but not in response to high glucose (Chapter III). Beyond the effect of incretins, Yan *et al*. postulated the insulin may also contribute to the rise in circulating miR-375-3p with OGTT, as subjects had higher insulin levels in response to OGTT than IGTT(227). However, this is likely not the main contributor, as Erener *et al*. found that in mice treated with STZ, insulin treatment reduced circulating levels of miR-375-3p(126). While numerous studies have examined circulating miR-375-3p levels and hypothesized the molecular mechanism that regulate these levels, further work using a combination of *in vivo* and *in vitro* tools will be required to uncouple the chronic and acute effects of metabolic alterations, as well as the contribution of different cell types to circulating miR-375-3p levels and the dynamics between cellular secretion and turnover of this miRNA.

Finally, I examined what percentage of miR-375-3p in the circulation of WT mice is bound to HDL. Here, I report that HDL makes up approximately 4-6% of circulating miR-375-3p. While I did not investigate the contribution of exosome miR-375-3p to the total circulating pool of miR-375-3p directly, I have used published studies of stoichometric analysis to estimate this. My analysis suggest that exosomes, the best studied miRNA carrier in plasma, contains

approximately 2% of plasma miR-375(151). While this study shows a strong correlation between HDL-miR-375 and plasma miR-375 (Linear regression, r=0.7), these authors found much lower correlation between plasma miR-375 and exosome miR-375 (Spearman correlation, r=0.4)(151). Furthermore, the miRNA found at the highest ratio of exosome to plasma content was let-7a-5p; 6.36% of plasma let-7a-5p was contained within exosomes, similar to the 4-6% we calculated for HDL-miR-375(151). However, the authors claim this does not reflect the ratio of EV-enclosed to EV-free ratio as the efficiency of the EV isolation method likely affects the miRNA recovery. Nevertheless, the amount of miR-375 contained within HDL is either greater than what is contained in exosomes, or similar levels, if we assume loss of 50% of EVs during the isolation protocol. Additionally, the authors report that their study recovered more EVs than other similar studies, suggesting HDL and exosomes make up about the same percentage of total plasma miR-375-3p (and perhaps other miRNAs as well). Therefore, although it appears that only 4-6% of plasma miR-375-3p being contained on HDL is low, these levels are similar to levels found in exosomes, and therefore likely biologically relevant. Furthermore, while exosome- and HDL-miRNAs have been found to be transported to recipient cells to mediate gene expression and physiological changes(95, 166, 228), it is unclear at this time whether free-miRNAs in plasma can be transferred to recipient cells, and what the miRNA turnover levels are for HDL-miRNAs, exosome-miRNAs, and other plasma miRNAs.

While I find that HDL-miR-375-3p levels correlate strongly with plasma miR-375-3p in WT mice, this may not be the case in response to metabolic stressors. For example, I find that human T2D plasma changes were not the same as HDL changes in the same subjects, suggesting that there may be an RNA sorting mechanism that may enrich or deplete different miRNAs either at the export, stability or uptake stage and that this may be altered in response to disease. While this dissertation mostly focused on the mechanisms of miRNA release (Chapter III) and steady state levels (this Chapter), in the future, it will be interesting to investigate how release, stability and turnover are regulated and how they affect steady-state HDL and circulating miRNA.

CHAPTER V

INTESTINAL BILE ACID SEQUESTRATION IMPROVES GLUCOSE CONTROL BY STIMULATING HEPATIC MIR-182-5P IN TYPE 2 DIABETES

Adapted from Sedgeman *et al*., "Intestinal bile acid sequestration improves glucose control by stimulating hepatic miR-182-5p in type 2 diabetes". Am J Physiol Gastrointest Liver Physiol. 2018 Aug 30. *In press* (89)

Introduction

T2D is a major health problem worldwide, and will continue to expand due to rising obesity levels(229). The pathophysiology of T2D is characterized by decreased glycemic control and hyperglycemia, which arises from loss of pancreatic β cell integrity, insulin resistance, and metabolic dysfunction(229). Key dysfunctions include insufficient insulin secretion from pancreatic β cells, impaired suppression of hepatic gluconeogenesis in response to insulin, and defects in glucose uptake by skeletal muscle and adipocytes. Each of these metabolic processes has been targeted by drug therapy to improve glycemic control. Nonetheless, some drugs that are indicated to treat other diseases have been repositioned to treat T2D despite a lack of clear mechanism for their glucose lowering properties. Colesevelam, a BAS, has emerged from clinical data to lower blood glucose levels; however, the mechanisms for its glycemic effects have yet to be determined(230).

BAS are a class of drugs that bind to BAs in the intestine and prevent their reabsorption. In the liver, *CYP7A1* converts cholesterol to BAs which are secreted into the bile to facilitate absorption of lipids and lipid-soluble vitamins in the intestine(29). Approximately 95% of BAs are reabsorbed by the intestine and transported back to the liver via enterohepatic circulation(29).

Absorbed bile-acids activate farnesoid X receptor (FXR), which promotes biliary secretion and represses BA synthesis to prevent BA overload and toxicity(231). Colesevelam binds and sequesters BAs in the gut and prevents their absorption. In turn, decreased BA absorption limits the activation of FXR and promotes increased BA synthesis through activation of CYP7A1. Increased hepatic sterol flux promotes activation of SREBP2 activity and transcription of its target genes, *HMGCR*, *SQLE*, and *LDLR*. This transcriptional program results in increase cholesterol biosynthesis, increased LDL-C uptake, and increased cholesterol conversion to BAs(30, 31). As a result of promoting LDL-C uptake for cholesterol conversion to BA, colesevelam reduces plasma LDL-C levels, which lowers the risk for cardiovascular disease. In clinical trials, colesevelam decreased LDL-C levels by 15% and total plasma cholesterol levels by 10%(32). In 2000, Colesevelam was FDA approved as a monotherapy with diet and exercise to treat primary hyperlipidemia and is prescribed with statins to manage hypercholesterolemia and lower LDL-C levels. Subsequently in 2008, based upon the results of three pivotal clinical studies showing that colesevelam improves glycemia(33-35), colesevelam was approved as adjunct therapy for T2D and is the only BAS currently approved to treat T2D. Although colesevelam is not first line therapy for either hypercholesterolemia or T2D, colesevelam is the only single ingredient drug approved to treat both diseases. Nevertheless, the molecular mechanism(s) of colesevelam-mediated glycemic control are unknown.

Work in the last decade has demonstrated that hepatic sterol metabolism is tightly regulated by miRNAs(103, 232). miRNAs are small, non-coding RNAs that regulate gene expression by binding to and destabilizing mRNA targets(233, 234). In the liver, miRNAs have emerged as critical regulators of both glucose and cholesterol metabolism(235, 236). For example, miRNAs have been found to regulate insulin signaling, glucose uptake, glycogen synthesis and gluconeogenesis in the liver(236-238). Moreover, many of the nuclear receptors that respond to changes in sterol metabolism, also regulate miRNA expression(239-241). Therefore, we hypothesized that investigating hepatic miRNAs may provide a link between the

intestinal, liver and systemic effects of colesevelam on sterol and glucose regulation. We found that the poly-cistronic miRNA cluster, miR-96/182/183, composed of miR-96-5p, miR-182-5p, and miR-183-5p(103), is elevated in the liver of diabetic rats treated with colesevelam. The promoter for this cluster contains an SRE and is a transcriptional target of SREBP-2(103). Moreover, these miRNAs have been reported to be suppressed in numerous tissues in rodent models and humans with T2D(109). In liver and islets, dysregulation of miR-182-5p has been proposed to contribute to T2D, in part, through altered regulation of Foxo1, a key transcription factor regulating gluconeogenesis in the liver and insulin secretion in islets(119, 242, 243). Furthermore, miR-182 KO mice have impaired glucose tolerance, a phenotype that was attributed to decreased glucose oxidation and glycolytic capacity in muscle(116). Thus far the influence of colesevalam on hepatic miRNA expression has not been explored, and as such, we designed a study to assess hepatic miRNA changes in colesevelam treated rodents and their impact on glucose metabolism.

In this study, improvements in glucose control with colesevelam were associated with a significant increase in hepatic expression of miR-96/182/183. Most importantly, inhibition of miR-182-5p partially inhibited colesevelam's glucose lowering effects in *db/db* mice. Moreover, we found that miRNAs in the miR-96/182/183 cluster directly target mediator complex subunit 1 (Med1), a RNA Pol II cofactor that links nuclear receptor activity to transcription(244). Therefore, colesevelam-induced activation of SREBP-2 may drive miR-96/182/183 regulation of glucose metabolism through Med1 and other target genes. This pathway likely contributes to colesevalam's effects on glucose and supports a paradigm in which miRNAs link cholesterol and glucose regulation.

Results

Colesevelam reduces plasma glucose levels and increases glycolysis in ZDF rats

To assess the impact of colesevelam on glucose metabolism, ZDF rats were treated with colesevelam or veh (control) for 4 weeks. Colesevelam-treated rats maintained glycemic control

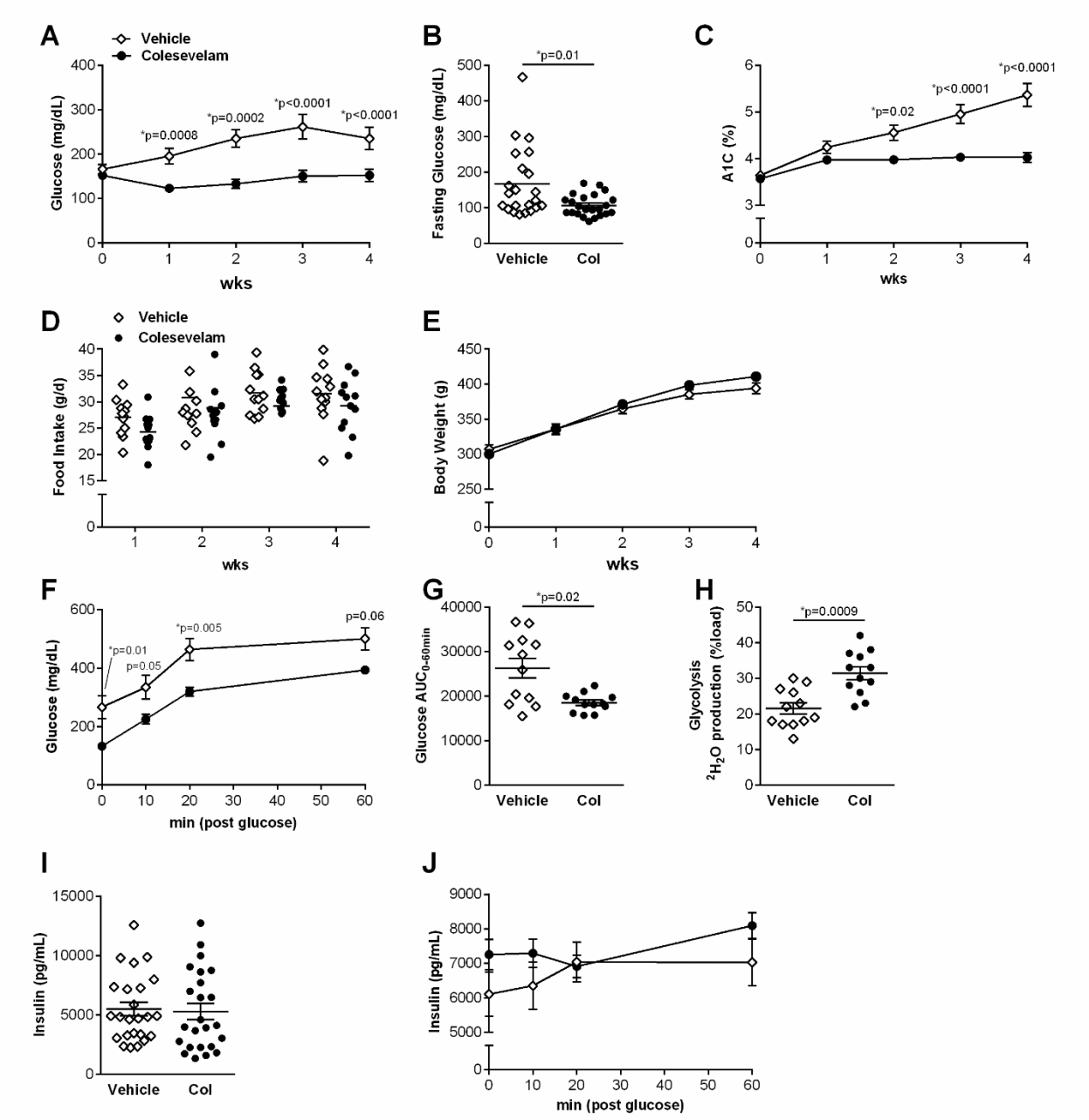

Figure 5-1. Colesevelam treatment improves glucose tolerance in ZDF rats. (A) Morning glucose levels in ZDF rats treated with vehicle or 2% colesevelam-supplemented diet. n=24. (B) Fasting glucose in portal blood after 12h fast. n=22-23. (C) Hemoglobin A1c levels. n=24. (D) Food intake of ZDF rats treated with vehicle or 2% colesevelam supplemented diet. n=12. (E) Body weights. n=24. (F) Plasma glucose levels after IP glucose challenge. n=12 (G) Area under the curve of glucose tolerance tests. n=12. (H) Total glucose disposal via glycolytic pathway following glucose disposal tests. n=12. (I) Insulin levels during glucose tolerance test. n=12 (J) 12-hr fasting insulin levels. n=24. For comparisons between 2 groups, Mann-Whitney non-parametric tests were used, and for repeated measures across time, 2-way ANOVA with Bonferonni's post-tests were used.

over the course of study, whereas vehicle-treated ZDF rats had significantly elevated morning blood glucose levels beginning at 1 week (Figure 5-1A). Fasting blood glucose concentrations were also decreased in colesevelam, compared to vehicle-treated ZDF rats after a 12h fast (Figure 5-1B). Moreover, for vehicle-treated ZDF rats, HbA1c levels increased over 4 weeks, whereas colesevelam-treated rats had decreased HbA1c levels for the duration of the study (Figure 5-1C). There were no differences in food intake (Figure 5-1D) or BW gain (Figure 5-1E) between the 2 groups. To further investigate colesevelam's impact on glycemic control in ZDF rats, glucose tolerance tests were performed, and colesevelam-treated ZDF rats were found to have improved glucose tolerance (Figure 5-1F,G) and increased glycolytic disposal of glucose compared to vehicle-treated rats (Figure 5-1H) during the tests**.** The changes in glucose tolerance and glycolysis were despite no changes in fasting or post-glucose plasma insulin levels (Figure 5-1I,J).

Previous studies have suggested that colesevelam's glucose lowering effects are linked to intestinal production of incretins, GLP-1 and GIP(37, 40). To quantify the impact of colesevelam on incretin levels in ZDF rats, GLP-1 and GIP were quantified in the fasting state and during a glucose tolerance test (Figure 5-2A-C). We failed to detect any significant differences in levels of either fasting GLP-1 or GIP or post-glucose active GLP-1 concentrations with colesevelam treatments (Figure 5-2A,B). Total GIP levels were, however, increased 20 min after an oral glucose bolus in colesevelam-treated rats compared to vehicle-treated rats (Figure 5-2C). Pharmacological agents that increase circulating incretins, i.e. DPP4 inhibitors and GLP-1 receptor agonists, have been shown to stimulate β cell proliferation(24). However, no significant difference in islet cell proliferation was found after 4 weeks of colesevelam or veh treatment in ZDF rats (Figure 5-2D). Similarly, HOMA-IR (primarily reflecting hepatic insulin sensitivity) and β cell function (HOMA-β) were not significantly different between the two groups (Figure 5-2E,F). In addition, ZDF rats treated with colesevelam were found to have significantly increased hepatic *de novo* cholesterol biosynthesis compared to vehicle-treated rats, as well as a slight, albeit not

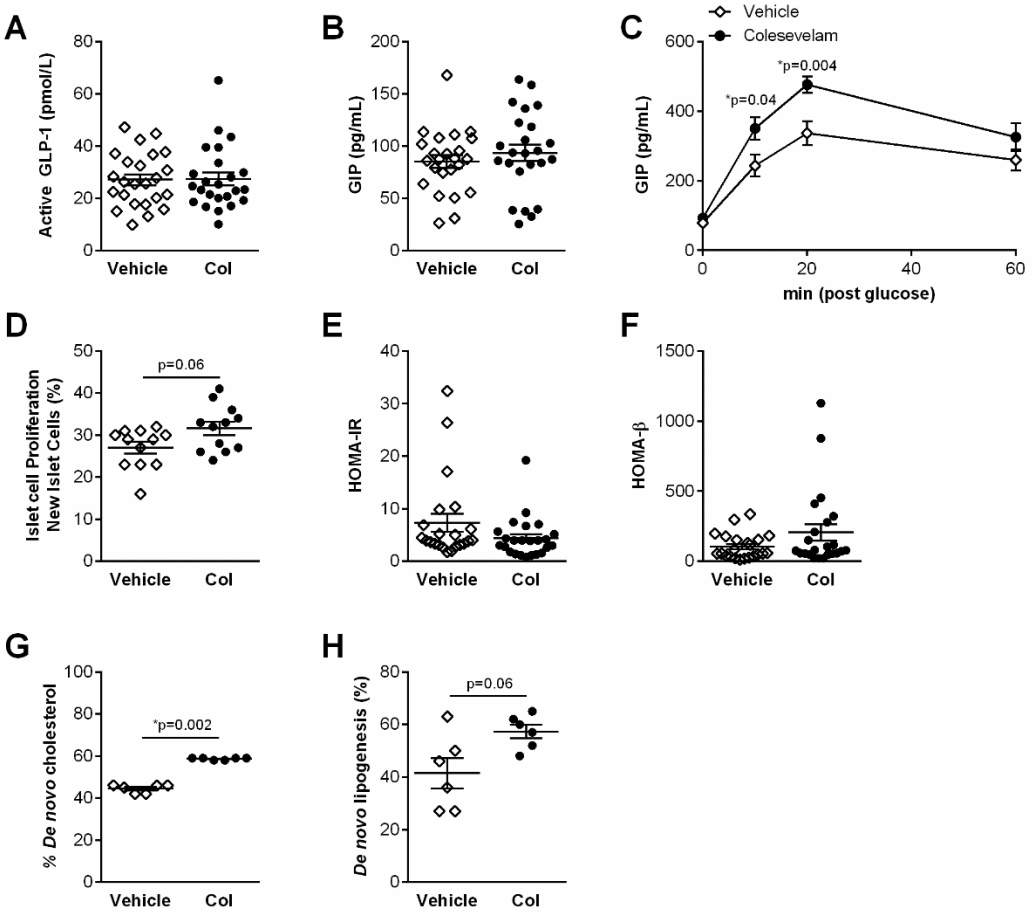

Figure 5-2. Colesevelam alters hepatic lipid metabolism but has modest effects on incretins. (A) Levels of GLP-1 in portal blood from overnight fasted animals. n=24. (B) Levels of GIP in portal blood from overnight fasted animals. n=24. (C) Plasma GIP levels after IP glucose challenge. n=12. (D) Percentage of new islets by BRDU labelling. n=12. (E) Homeostatic model assessment (HOMA) method for assessing insulin resistance (IR) from basal (fasting) glucose and insulin concentrations. n=22-24 (F) Homeostatic model assessment (HOMA) method for assessing insulin ?-cell function from basal (fasting) glucose and C-peptide concentrations. n=22-23. (G) Percent de novo cholesterol synthesis over 4 wks. n=6. (H) De novo lipogenesis, percentage new triglyceride-palmitate after 4 wks of labeling. n=6. For comparisons between 2 groups, Mann-Whitney non-parametric tests were used, and for repeated measures across time, 2-way ANOVA with Bonferonni's post-tests were used.

significant (p=0.06), increase in hepatic *de novo* lipogenesis (Figure 5-2G,H). Together these data suggest that colesevelam treatments significantly alter hepatic lipid metabolism and improve glucose control by increasing whole-body glycolysis independent of any changes in β cell functionality, and only modest changes in incretin concentrations. Therefore it is likely that other mechanisms contribute to these early metabolic effects of this drug.

Colesevelam induces hepatic expression of the miR-96/182/183 cluster

Due to the hepatic effects of colesevelam *in vivo*, hepatic miRNA changes were investigated. To quantify the impact of colesevelam on hepatic miRNAs, sRNA-seq was performed on livers from ZDF rats (n=6) after colesevelam or veh treatments for 4 weeks. Strikingly, colesevelam treatments significantly altered 29 hepatic miRNAs (4 up, 25 down) compared to vehicle-treated rats (Figure 5-3A, Table A-10). Two of the most up-regulated hepatic miRNAs were rno-miR-182 and rno-miR-183-5p, which are part of a poly-cistronic miRNA cluster on chromosome 4 with rno-miR-96-5p in rats(245). Rno-miR-182 is expressed at levels 10-times higher than rno-miR-183-5p, and rno-miR-96-5p was not detectable by sequencing in livers of ZDF rats (Figure 5-3A). Real-time PCR was used to validate sequencing results, and rno-miR-182 and rno-miR-183-5p were confirmed to be significantly increased in livers from colesevelam-treated compared to veh-treated ZDF rats (Figure 5-3B,C). Hepatic rno-miR-96-5p levels were also found to be significantly increased with colesevelam treatments, as quantified by RT-PCR (Figure 5-3D). Similar to sequencing, results from RT-PCR assays suggest that rno-miR-182-5p was the most abundantly expressed miRNA from the cluster (Figure 5-3B-D). The miR-96/182/183 cluster has previously been reported to harbor an SRE in its promoter and be directly activated by the nuclear receptor, SREBP2(103). Most interestingly, colesevelam's lipid lowering effects in humans are attributable to changes in sterol metabolism that increase activity of SREBP2. To link changes in miRNA expression with SREBP2 activity, we measured the expression of *Srebf2* and down-stream SREBP2 target genes, *Sqle*, *Ldlr*, and *Hmgcr*, and we

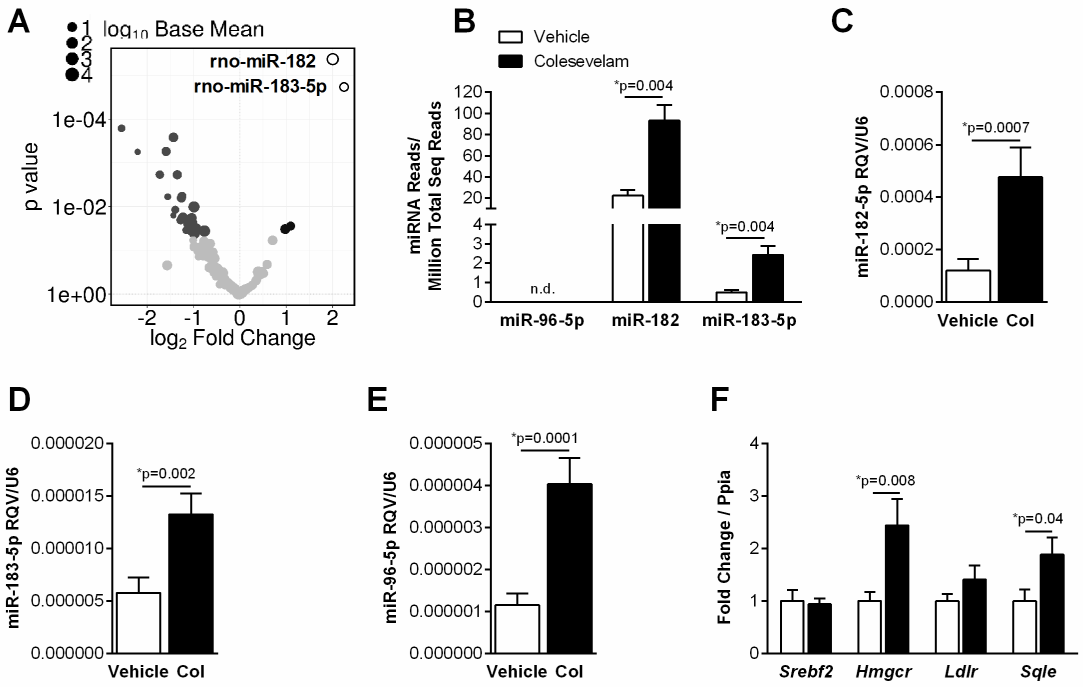

Figure 5-3. The miR-96/182/183 cluster is up-regulated in the livers of colesevelam-treated ZDF rats. (A) Volcano plot depicting significantly altered miRNAs between colesevelam and vehicle-treated ZDF rat livers (left) and expression (reads per million total reads) of the miR-96/182/183 cluster (left) n=6. (B) Liver expression of the miR-96/182/183 cluster by real-time PCR. n=9-12. (C) Liver gene (mRNA) expression changes of Srebf2 and it's target genes Hmgcr, Ldlr, and Sqle. n=8-12. For sequencing data, unpaired t-tests were used. For comparisons between 2 groups, Mann-Whitney non-parametric tests were used. n.d.= not detectable

found that *Sqle* and *Hmgcr* mRNA levels were significantly increased in the livers of colesevelam-treated ZDF rats (Figure 5-3E). These results suggest that colesevelam stimulates expression of hepatic miR-96/182/183 in ZDF rats, likely through SREBP2.

Inhibition of miR-182 blocks colesevelam's glucose lowering effects

miR-182 is the most abundant hepatic miRNA in the cluster. Therefore, to next determine if miR-182-5p contributes to the glucose lowering effects of colesevelam, leptin receptor-deficient (*db/db*) mice were co-treated with colesevelam and miR-182-5p inhibitors. Adult male *db/db* mice were fed control diet (Chow) or diet supplemented with 2% colesevelam (Col) for 9 wks. Mice were intravenously injected bi-weekly with 10 mg/kg BW LNA miRNA inhibitors against mmu-miR-182-5p (LNA-182) or PBS (control) (Figure 5-4A). Three groups were studied, *db/db* mice treated with vehicle (Chow + PBS), colesevelam (Col + PBS), or colesevelam + LNA-182 (Col + LNA). Similar to observations in ZDF rats, hepatic levels of all three miRNAs were significantly up-regulated in the livers of Col + PBS *db/db* mice (Figure 5-4B). Real-time PCR was also used to confirm that mmu-miR-182-5p levels were significantly decreased in mice that received Col + LNA treatment, compared to Col + PBS (Figure 5-4B). Surprisingly, LNAs against mmu-miR-182-5p also decreased mmu-miR-183-5p levels in *db/db* mouse livers, however, mmu-miR-96-5p levels were not significantly affected (Figure 5-4B). Furthermore, the expected changes in SREBP2 target genes, *Hmgcr*, *Ldlr,* and *Sqle* were observed, and LNA-182 treatment did not interfere with these effects (Figure 5-4C). Although SREBP2 likely promotes its own transcription, the *Srebf2* mRNA levels were not altered in livers from *db/db* mice treated with colesevelam (Col +PBS) or LNA-182 (Col + LNA-182) as compared to control treated mice (Chow +PBS) (Fig.4C). To determine if miRNAs from the miR-96/182/183 cluster were also up-regulated in other metabolic tissues in response to colesevelam treatments, miR-96-5p, miR-182-5p and miR-183-5p were measured in WAT from treated *db/db* mice. Colesevelam treatments failed to increase the expression of miRNAs in the miR-182/183/96 cluster in WAT; however, miR-182-5p levels were

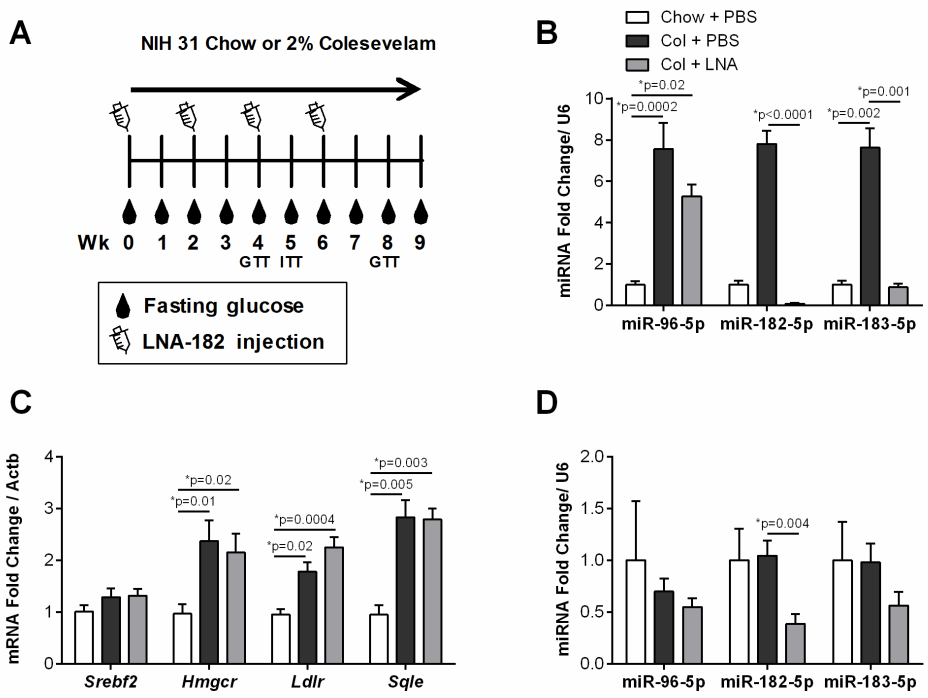

Figure 5-4. Colesevelam stimulates the miR-96/182/183 cluster in livers of db/db mice, and is inhibited with LNA-182 treatment. A) Schematic of animal study. 12 wk old db/db mice treated with vehicle or 2% colesevelam-supplemented diet for 9 wks. (B) Liver expression of miR-96/182/183 cluster miRNAs. n=8-9. (C) Liver gene (mRNA) expression changes for SREBP2 target genes Hmgcr, Ldlr, Sqle and Srebf2. n=8-9. (D) White adipose tissue (WAT) miRNA expression of miR-182/183/96 cluster. n=8-9. For comparisons between 3 groups, Kruskal-Wallis One-way ANOVA with Dunn's post-test, alpha 0.05.

decreased by 50% in Col + LNA compared to Col + PBS *db/db* mice (Figure 5-4D). These results suggest that the induction of the miR-96/182/183 cluster is specific to liver, likely due to increased hepatic SREBP2 activity.

To determine if colesevelam's glucose lowering properties are mediated by miR-182-5p in mice, we performed metabolic studies in these *db/db* mice. Prior to injections, there was no difference in plasma glucose or body weights between groups (Figure 5-5A,B). In Chow + PBS *db/db* mice, glucose levels steadily increased over the 9 week study, and these mice lost a significant amount of weight beginning at 6 weeks (Figure 5-5A,B). Conversely, Col + PBS mice displayed variable glucose levels over 9 weeks; as glucose levels were decreased at 1, 2, 6, and 7 weeks of treatments, but not at 3, 4, 5, and 8 weeks (Figure 5-5A). Most importantly, LNA-182 treatments blocked colesvelam's glucose lowering effects early in the study at 1 and 2 weeks, but failed to alter colesevelam's effects on fasting glucose levels later in the study (Figure 5-5A). The high variability in fasting glucose may be due to repeated testing on these severely diabetic mice, including glucose tolerance test (week 4 and 8), insulin tolerance test (week 5), glucose bolus for incretin measurements (week 6). Nonetheless, colesevelam treatments prevented the observed weight loss (likely a result of diabetic wasting) in the Col + PBS *db/db* mice, and LNA-182 treatments did not affect this parameter (Figure 5-5B). To determine if colesevelam improves glucose metabolism in *db/db* mice, glucose tolerance tests were performed at 4 and 8 week time-points within the study. At 4 weeks, Col + PBS mice, but not Col + LNA mice, showed improved glucose tolerance compared to Chow + PBS mice (Figure 5-5C,D). LNA treatments were found to partially reverse the beneficial effects of colesevelam ($p=0.08$), as we did not find a significant difference between Chow + PBS and Col + LNA-treated mice (Figure 5-5D). These results suggest that miR-182-5p is at least partially required for improved glucose tolerance associated with colesevelam treatments in mice (Figure 5-5C,D).

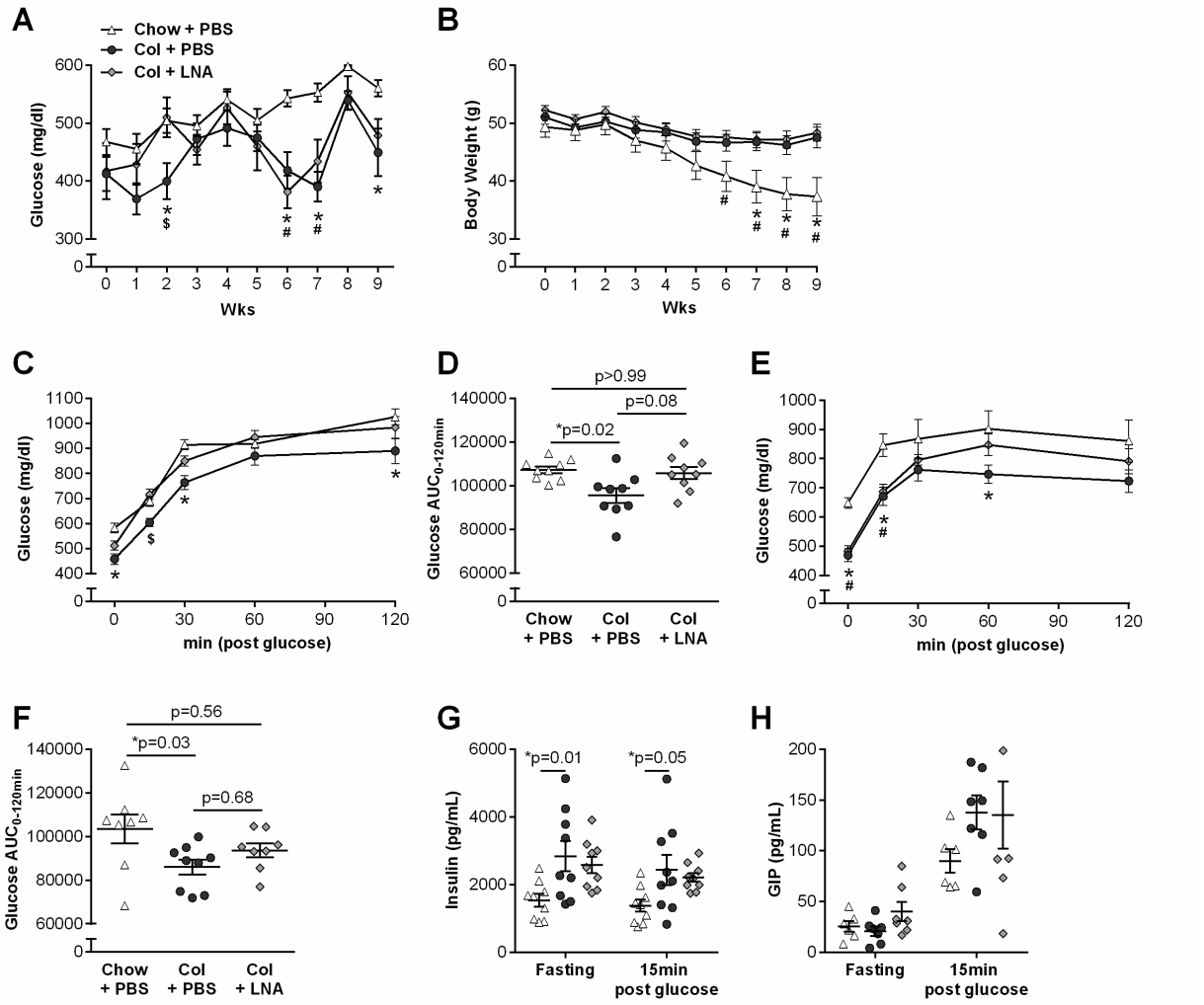

Figure 5-5. Inhibition of miR-182 in vivo abrogates the early improvements in glucose tolerance conferred by colesevelam in db/db mice. (A) 4h fasted glucose levels in Chow + PBS, Col + PBS and Col + LNA treated db/db mice. n=7-9. (B) Body weight of db/db mice. n=8-9. (C) Plasma glucose levels after IP glucose challenge at wk 4 of study. n=9. (D) Area under the curve of glucose tolerance test at wk 4. n=9. (E) Plasma glucose levels after IP glucose challenge at wk 4 of study. n=9. (F) Area under the curve of glucose tolerance test at wk 4. n=9. (G) Plasma insulin levels after 4h fast, and 15 min post glucose bolus at wk 5 of study. n=9. Plasma GIP levels after 4h fast, and 15 min post glucose bolus at wk 5 of study. n=6-7. For comparisons between 3 groups, Kruskal-Wallis One-way ANOVA with Dunn's post-test, alpha 0.05 or 2-Way ANOVA with Bonferonni's post-test for repeated measures across time. *#$ $p<0.05$; For D & E: * = chow PBS vs. col PBS, # = chow PBS vs. col LNA, $ = col PBS vs. Col LNA.

At 8 weeks, glucose tolerance levels were significantly improved in Col + PBS-treated mice compared to Chow + PBS-treated mice; however, glucose tolerance levels in Col + LNA-treated mice were not significantly different compared to either Chow + PBS or Col + PBS (Figure 5-5E,F). To determine if colesevelam and/or LNA-182 treatments altered fasting or post-glucose incretin or insulin levels in *db/db* mice, insulin, GLP-1, and GIP levels were measured in fasted (4h) mice before and after (15 min) glucose injections at 6 wks of treatment (Figure 5-5G,H). Col + PBS *db/db* mice, but not Col + LNA mice, were found to have elevated fasting and post-glucose insulin levels, compared to Chow + PBS mice (Figure 5-5G). GLP-1 levels were undetectable in either fasting or post-glucose samples, and no significant differences in GIP were detected between Col + PBS and Chow + PBS mice in fasted and post-glucose states (Figure 5-5H). Together these results suggest that miR-182 partially mediates the effects of colesevelam on glucose metabolism.

The miR-96/182/183 cluster directly regulates Med1

miRNAs have emerged as critical regulators of metabolic gene expression and represent a new class of drug targets to treat metabolic dysfunction(246). To demonstrate that colesevelam-induced miR-182-5p likely mediates hepatic gene expression changes, we sought to experimentally validate miR-182-5p regulation of a novel predicted target gene *in vitro* that is suppressed by colesevelam *in vivo*. Therefore, *in silico* miRNA prediction studies were used with RT-PCR to identify potential gene targets that are expressed in the liver. Using this approach, we identified *Med1* as a potential target of miR-182-5p, as well as miR-183-5p, and miR-96-5p, the two other members of the miRNA cluster. In humans, the *MED1* 3'-UTR harbors multiple putative binding sites for each of the miRNAs in the miR-96/182/183 cluster; 2 for hsa-miR-182-5p, 1 for hsa-miR-183-5p, and 2 for hsa-miR-96-5p (TargetScanSv7.2). In humans and rodents, miR-182-5p and miR-96-5p share the same seed sequence (bases 2-7 on the 5' end of the mature miRNA)

- a critical region used to recognize mRNA targets - and, thus, are predicted to regulate the same genes at the same putative target sites. We validated the Med1 antibody using siRNA knockdown of *Med1* in primary hepatocytes (Figure 5-6A,B). To test whether the miR-96/182/183 cluster regulates hepatic *Med1* in mice, real-time PCR was used to quantify gene expression in the livers of *db/db* mice treated with Chow + PBS, Col + PBS, and Col + LNA. In Col + PBS treated mice, miR-96/182/183 expression levels were increased (Figure 5-4B), and hepatic *Med1* mRNA levels were found to be significantly decreased compared to Chow + PBS mice (Figure 5-6C). A modest, but not statistically significant restoration, was observed in Col + LNA treated mice (Figure 5-6C). Furthermore, Med1 protein levels were significantly reduced in Col + PBS mice compared to Chow + PBS-treated mice, as determined by western blotting and densitometry (Figure 5-6D,E). Most interestingly, LNA-182 treatments were found to partially reverse the observed colesevelam (Col)- mediated decrease in Med1 protein levels, as we found no significant differences between Col + LNA-182-treated mice and Chow + PBS-treated mice; however, we also failed to find a significant difference between Col + LNA-182 and Col + PBS-treated mice (Figure 5-6D,E).

To experimentally test whether miR-96/182/183 directly target *Med1* in mice, *in vitro* studies were performed in mouse primary hepatocytes. Primary hepatocytes were isolated from male c57BL/6J wild-type (WT) mice and transiently transfected with 50nM miRNA mimics of mmu-miR-182-5p, mmu-miR-183-5p, and mmu-miR-96-5p individually or in combination for 48h (Figure 5-6F). We validated successful transfection of miRNA mimics and observed significantly decreased *Med1* mRNA levels (Figure 5-6F,G). Furthermore, over-expression of all three miRNAs resulted in a significant reduction in Med1 protein levels in mouse primary hepatocytes (Figure 5-6H). These results support that miRNAs in the miR-96/182/183 cluster regulate Med1 expression in mouse liver.

To determine if miR-96/182/183 directly regulates *MED1* in humans, putative *MED1* 3'-UTR targets sites were cloned down-stream of luciferase in gene reporter plasmids. In humans, *MED1* 3'-UTR is predicted to harbor 3 distinct regions that contain predicted target sites for the

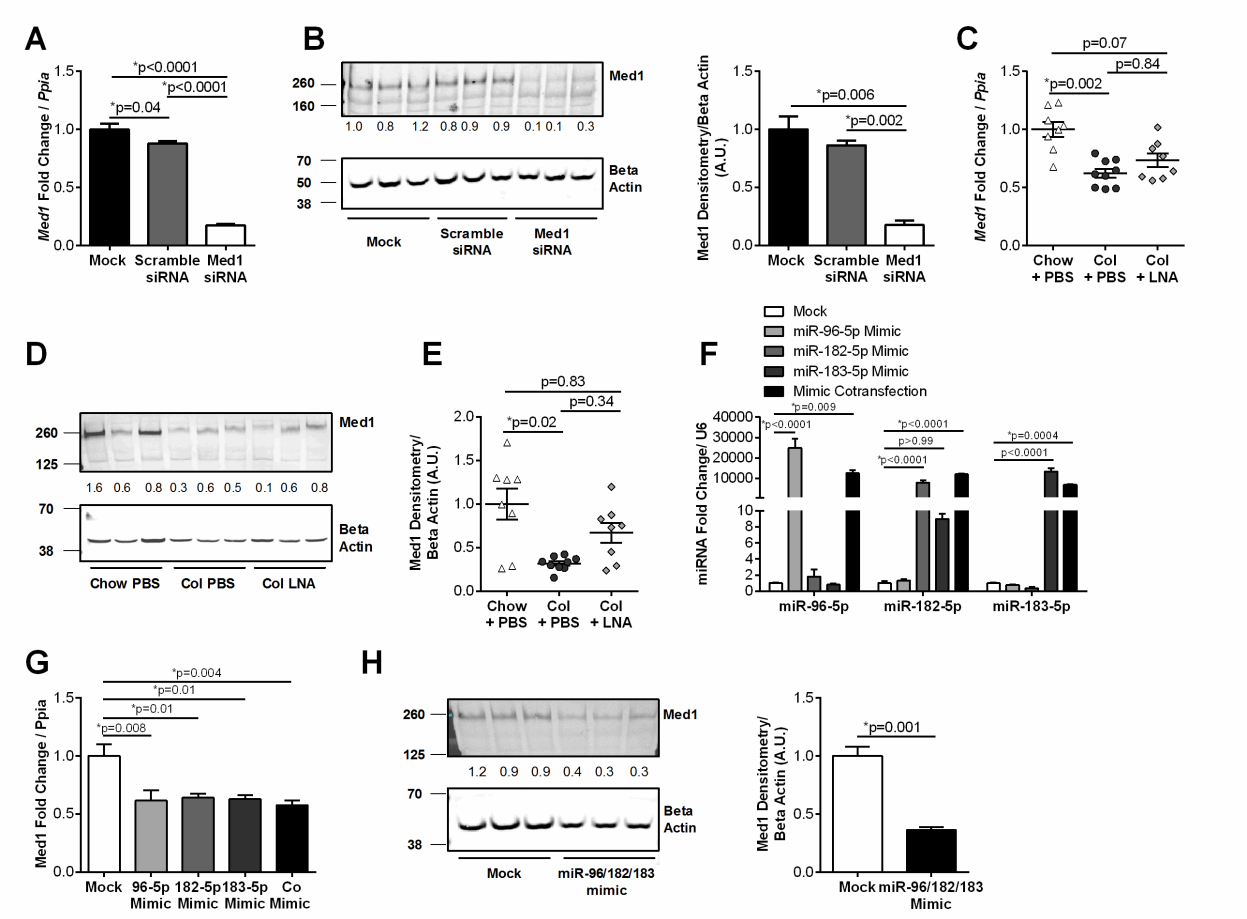

Figure 5-6. Med1 is regulated by miR-96/182/183 in mice. (A) Expression of Med1 by real-time PCR in mouse primary hepatocytes transfected with 50nM of Med1 or scramble siRNA. n=3 (B) Western blot of Med1 and beta actin (loading control) from protein samples of primary hepatocytes transfected with Med1 or scramble siRNA. Ratio of Med1/beta actin densitometry is indicated between the blots and graphed on the right. n=3 (C) Hepatic Med1 mRNA levels in db/db mice treated with vehicle or 2% colesevelam-supplemented diet and PBS or LNA-182-5p. Real-time PCR. n=8-9. (D) Hepatic Med1 and beta actin (loading control) protein levels from 3 representative liver protein samples for chow + PBS, col + PBS and col + LNA-182. Western blotting. Ratio of Med1/beta actin densitometry is indicated between the blots. (E) Densitometry quantification of Med1 protein levels normalized to beta actin. n=8-9. (F) Expression of miR-96-5p, miR-182-5p, and miR-183-5p in mouse primary hepatocytes transfected with 50nM miR-96-5p, miR-182-5p, miR-183-5p mimics individually or in combination. Real-time PCR. n=3. (G) Med1 mRNA levels in mouse primary hepatocytes transfected with 50nM miR-96-5p, miR-182-5p, miR-183-5p mimics individually or in combination. Real-time PCR. n=3. (H) Protein levels of Med1 and beta actin (loading control) from protein samples of primary hepatocytes transfected with mock or 50nM miR-96-5p, miR-182-5p, miR-183-5p mimics individually or in combination. Western blotting. Ratio of Med1/beta actin densitometry is indicated between the blots and graphed on the right. n=3. For comparisons between 2 groups, Students' t-tests were used, and for >2 groups, Kruskal-Wallis One-way ANOVA with Dunn's post-test, alpha 0.05 or One-Way ANOVA with Bonferonni's post-test for comparison to mock group only, alpha 0.05.

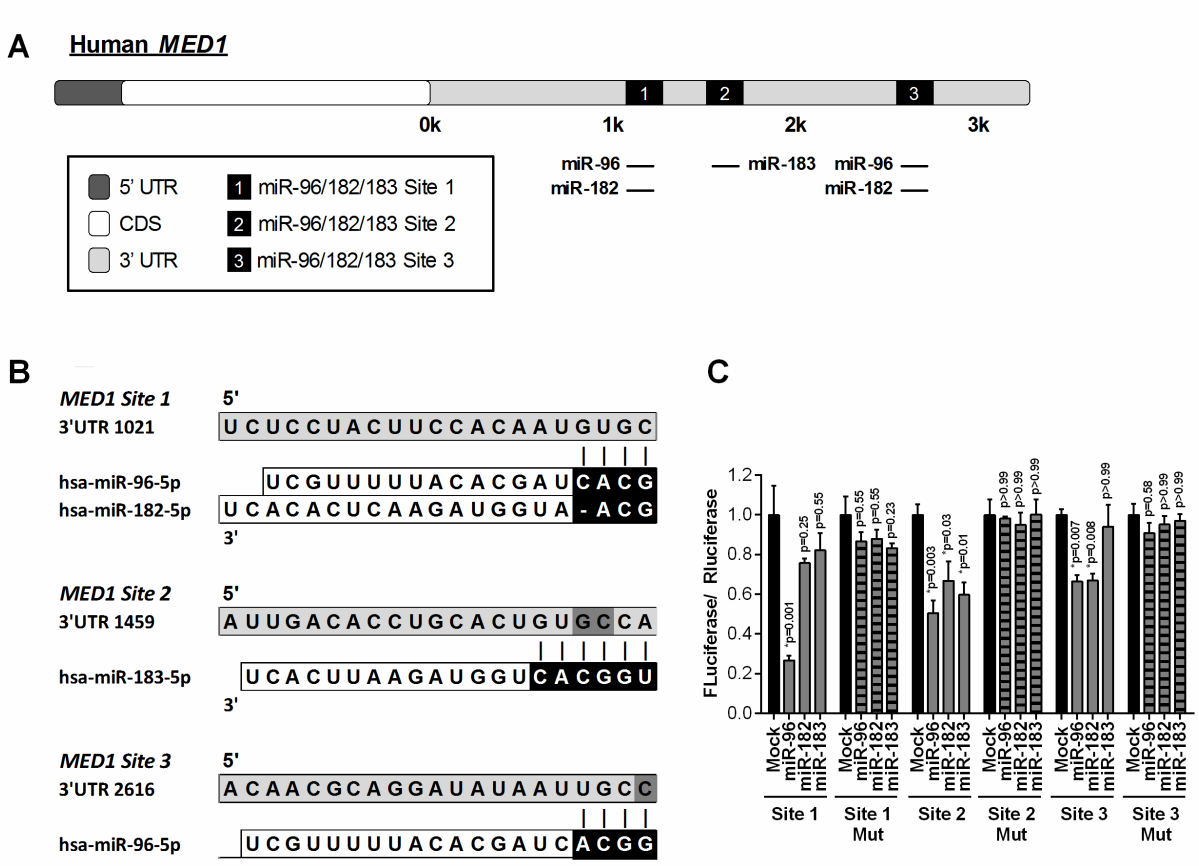

Figure 5-7. MED1 is a direct target of miR-182-5p, miR-183-5p, and miR-96-5p in humans. (A) Schematic of human MED1 mRNA and the three putative miR-182/183/96 target sites in the 3'-UTR. (B) Predicted MED1 3'-UTR target sites. Bases highlighted in dark grey represent mutations for gene reporter (luciferase) assays. (C) Normalized luciferase activity in HEK293 cells after dual transfection of miR-96/182/183 mimics and gene (luciferase) reporters harboring putative target sites for miR-96-5p, miR-182-5p, and/or miR-183-5p. n=4. For comparisons between >2 groups to mock only, One-Way ANOVA with Bonferonni's post-test was used, alpha 0.05.

miR-96/182/183 cluster miRNAs (Figure 5-7A). Gene reporter (luciferase) assays were performed in HEK293 cells dually transfected with the luciferase reporters and 50nM miRNA mimics. Site 1 contains the putative binding sites for hsa-miR-182-5p and hsa-miR-96-5p (Figure 5-7B), and we found that only over-expression of miR-96-3p, but not miR-182-5p suppressed luciferase activity (Figure 5-7C). Site 2 is a putative binding site only for hsa-miR-183-5p, but we found that overexpression of all three miRNAs suppressed normalized luciferase activity (Figure 5-7B,C). Similar to site 1, site 3 contains predicted binding sites for hsa-miR-182-5p and hsa-miR-96-5p, but not hsa-miR-183-5p; however, unlike site 1 where only miR-96-3p suppressed luciferase activity, both hsa-miR-182-5p and hsa-miR-96-5p suppressed normalized luciferase activity in gene reporter assays (Figure 5-7B,C). To demonstrate that the miRNAs suppress reporter luciferase activity through these putative target sites, two bases of the predicted seed sites were mutated for each of the loci (sites 1-3) (Figure 5-7B). Most importantly, miRNA over-expression failed to suppress luciferase activity when the predicted target sites were mutated, indicating that this regulation is likely direct (Figure 5-7C). Together these data suggest that all three miRNAs in the miR-96/182/183 cluster directly target and suppress *MED1* at multiple target sites within the 3'-UTR.

To further demonstrate that the miR-96/182/183 cluster regulates *MED1* in human hepatocytes, miRNA mimics were transiently transfected into Huh7 hepatoma cells (Figure 5-8A). In Huh7 cells, over-expression of both hsa-miR-182-5p and hsa-miR-183-5p were required to significantly decrease *MED1* mRNA levels (Figure 5-8B). Conversely, LNAs against hsa-miR-182-5p and hsa-miR-183-5p were transiently transfected in Huh7 cells, individually and in combination. Markedly, inhibition of hsa-miR-182-5p (LNA-182) alone or in combination with LNA-183 significantly increased *MED1* mRNA levels (Figure 5-8C,D). Most importantly, LNA inhibition of miR-96, miR-182, and miR-183 (in combination) resulted in a significant increase in Med1 protein levels in Huh7 cells (Figure 5-8E). Together these data support that *MED1* is a novel target of the miR-96/182/183 cluster in both mice and humans.

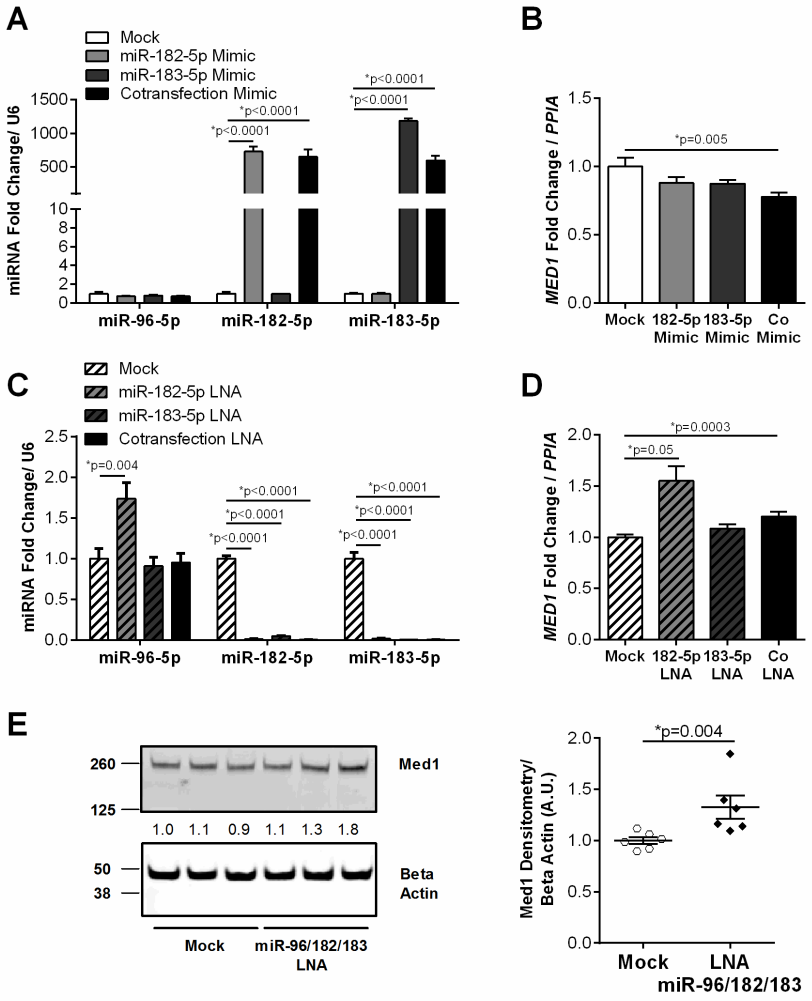

Figure 5-8. MED1 is regulated by miR-96/182/183 in human Huh7 cells. (A) miR-96-5p, miR-182-5p, miR-183-5p levels in Huh7 cells transfected with 50nM miR-96-5p, miR-182-5p, miR-183-5p mimics individually or in combination. Real-time PCR. n=6. (B) MED1 mRNA levels in Huh7 cells transfected with 50nM miR-96-5p, miR-182-5p, miR-183-5p mimics individually or in combination. Real-time PCR. n=6. (C) miR-96-5p, miR-182-5p, and miR-183-5p levels in Huh7 cells transfected with mock or 50nM LNAs against miR-182-5p and/or miR-183-5p. Real-time PCR. n=6. (D) MED1 mRNA levels in Huh7 cells transfected mock or 50nM LNAs against miR-182-5p and/or miR-183-5p. Real-time PCR. n=6. (E) Protein levels of Med1 and beta actin (loading control) from protein lysates of Huh7 cells transfected with mock or 50nM miR-96, miR-182 and miR-183 LNAs. Ratio of Med1/beta actin densitometry is indicated between the blots and graphed on the right. N=6 For comparisons between >2 groups to mock only, One-Way ANOVA with Bonferonni's post-test was used, alpha 0.05. For comparisons between two groups Mann-Whitney non-parametric tests were used.

Discussion

Colesevelam hydrochloride is a BAS approved for the treatment of T2D (37, 40, 85, 247). Nevertheless, the molecular mechanisms by which colesevelam improves glucose metabolism remain unclear. Both human studies and studies in diabetic rodent models suggest that colesevelam likely mediates its metabolic effects, in part, through the liver(37, 39, 85, 248, 249). Thus, the goal of this study was to investigate whether a hepatic mechanism contributes to colesevelam's glucose lowering capacity. Strikingly, we discovered a mechanism that bridges both cholesterol and glucose metabolic pathways in the liver. We found that colesevelam induces the expression of the miR-96/182/183 cluster of miRNAs in the liver, likely though increased SREBP-2 activity, known to be associated with colesevelam. We found that colesevelam-induced changes to glucose metabolism in *db/db* mice were partially blocked by LNA inhibition of miR-182 *in vivo*. Next, we demonstrated that miR-96/182/183 directly targets and suppresses *MED1* in humans and mice, a gene previously linked to hepatic lipid metabolism(250). Results from this study support that colesevelam improves glycemic control through cholesterol-linked post-transcriptional gene regulation in the liver.

Although a variety of hypotheses have been proposed(39, 230, 247), the specific mechanism(s) by which colesevelam improves glycemic control remains unknown. Colesevelam is not absorbed in the intestine; therefore, it has been postulated that colesevelam's effects are mediated through the intestine, and previous studies have implicated gut incretins. We and others have previously reported that colesevelam treatment increases plasma levels of gut-derived incretins that promote insulin secretion, e.g. GLP-1 and GIP in humans (39) and animal models(40). However, the observed increase in circulating incretins are modest, especially compared to DDP4 inhibitors and while they may contribute to the improved glycemic control with colesevelam treatment, signals beyond incretins are likely involved in the metabolic benefits of colesevelam(39). In human studies, we previously suggested an effect on gluconeogenesis and glycogenolysis(39) and these effects were confirmed in rodents(37). Similarly, Yamakawa *et al.*

recently reported that colestimide, another BAS, improved glycemic control, and suggested this effect is driven by hepatic changes(249, 251).In this study, hepatic *Srebf2* mRNA levels were found to be increased with colestimide treatments by PCR; however, in our study, we failed to find a significant increase in *Srebf2* mRNA levels in mice treated with colesevelam, despite evidence that other SREBP-2 transcriptional target genes (e.g. *Hmgcr*) were significantly increased with BAS (colesevelam) treatments(249, 251). Here, we present evidence that colesevelam lowered plasma glucose levels and increased glycolysis in ZDF rats. This could occur through either improvements in hepatic or peripheral insulin sensitivity or improvements in β cell function. However, it's unlikely that colesevelam affects peripheral insulin sensitivity, as previous studies showed no difference in clamp studies in humans. Furthermore, we observed only modest effects on gut incretin levels, no difference in islet proliferation rate, HOMA-IR or HOMA-β, suggesting that at least at 4-weeks, β cell function and insulin sensitivity are not substantially improved. However, longer treatments periods may be required to observe changes in these parameters. Therefore, taken together, these studies suggest that colesevelam improves glucose metabolism through incretin-dependent and incretin-independent mechanisms. As discussed above, the effects on incretins have been inconsistent in the literature and other factors likely also contribute to the glucose lowering effects of colesevelam. Therefore, 4 wks of colesevelam treatments in ZDF rats provides a window to study new incretin-independent mechanisms, particularly in the liver, that contribute to colesevelam's metabolic effects.

High-throughput sRNA-seq and real-time PCR studies identified a hepatic miRNA cluster that contributes to the glucose lowering effects of colesevelam. We found that miR-182, miR-183-5p, and miR-96-5p, which form the poly-cistronic miRNA cluster miR-96/182/183, are up-regulated in the livers of colesevelam-treated diabetic rodents, ZDF rats and *db/db* mice. Furthermore, inhibition of miR-182-5p *in vivo* was found to partially reverse the beneficial effects of colesevelam on glucose control. miR-182-5p is expressed at levels 10-100-fold greater than miR-183-5p and miR-96-5p in the liver, and therefore it is likely that the physiologic and hepatic

effects observed in this study are driven by changes in miR-182-5p and its accompanying effect's on gene expression. However, due to the observed decrease in miR-183-5p in LNA-182 treated mice and the sequence similarity between the miRNAs, we cannot rule that miR-183-5p may contribute to some of the effects on glucose metabolism observed *in vivo*. Nevertheless, whether the effect is specific to miR-182-5p or whether miR-183-5p contributes to the effects observed *in vivo*, our findings suggest that the glucose lowering properties of colesevelam are likely mediated through its effects on cholesterol metabolism as the miR-96/182/183 miRNA cluster is directly regulated in the liver by the master transcriptional regulator of cholesterol metabolism, SREBP2(103). Colesevelam has previously been demonstrated to indirectly promote SREBP2 activity in the liver(251). Our results suggest that SREBP2 mediated expression of the miRNA cluster in response to colesevelam improves glycemic control through suppression of target gene(s) that promote metabolic dysfunction(109, 116). Paradoxically, statins, which classically induce SREBP2 activity and have been shown to induce miR-96/182/183 expression, have been associated with increased risk of T2D (103, 252). Jeon *et al.* first demonstrated that SREBP2 transcriptionally regulates the miR-96/182/183 cluster in the liver in response to statins(103). They proposed that these miRNAs coordinate hepatic lipid metabolism by directly targeting negative regulators of SREBP2, Insig2 and Fbxw7, as a feed-forward network(103). However, we failed to find changes in *Insig2* or *Fbxw7* mRNA expression in the livers of colesevelam-treated mice (data not shown). These discrepancies are likely due to differences in cellular metabolic conditions that may affect miRNA-mRNA interactions. Moreover, statins inhibits, while colesevelam promotes, hepatic cholesterol synthesis, which may contribute to the differential effects on glycemia. Colesevelam and statins also differ in their effects on BAs(253), signaling molecules that have been implicated in glucose control and have also been shown to regulate miRNAs-gene networks(241). Colesevelam may also mediate the effects on the miR-96/182/183 miRNA cluster through changes in the FXR transcriptional network, as FXR signaling is reduced with BAS. The expression of the BA enzyme, CYP7A1, is increased with reduced FXR activation, and recently,

Cyp7a1 over-expressing mice were shown to have increased hepatic SREBP2 (mRNA) expression compared to control mice(254). Moreover, miR-33, an intronic miRNA harbored by and co-transcribed with SREBF2, was also found to be increased with Cyp7a1 over-expression(254), suggesting that Cyp7a1 may also contribute to the observed induction of SREBP2 activity and the increase in miR-96/182/183 cluster in our study. As such, further work will be required to fully elucidate differences in metabolic physiology between colesevelam and statins and to understand whether the changes in BAs contribute to the regulation of this miRNA cluster and its target genes.

Previous studies have linked individual miRNAs of the miR-96/182/183 cluster to glucose metabolism. For example, miR-182 knockout mice have impairments in glucose tolerance(116). Furthermore, miR-182-5p has been reported to be down-regulated in numerous tissues (blood, adipose tissue, pancreas, muscle, and liver) in DIO mouse models. Likewise, miR-182-5p levels have been found to be decreased in blood from DIO non-human primates and T2D patients(109). Recently, Zhang *et al*. reported the miR-182 knockout mice have impaired glucose tolerance which they linked to decreased glucose utilization by skeletal muscle(116). Similarly, we observed an increase in glycolysis in colesevelam-treated ZDF rats, which may also be due to improvements in whole-body insulin sensitivity. In addition, miR-182 targets a member of the forkhead box family of transcription factors, FoxO3, which has been implicated in muscle atrophy(114). Therefore, it is possible that miR-96/182/183 in non-hepatic tissues may contribute to glucose control. However, the amount of cholesterol flux in other peripheral tissues (i.e. muscle and WAT) in response to colesevelam and T2D is unlikely to be elevated. Nevertheless, miR-96/182/183 expression in these tissues may be independent of SREBP2 and influence glucose metabolism through unique mechanisms.

Results from this study identified *MED1* as a novel target of all three miRNAs in the miR-96/182/183 cluster in both rodents and humans. MED1 is a large multi-subunit protein, originally identified as a peroxisome proliferator-activated receptor (PPARs) binding protein(255). MED1

has been found to bind to a number of nuclear receptors, including PPARα, PPARγ, estrogen receptor α (ERα), glucocorticoid receptor (GR), constitutive androstane receptor (CAR), and thyroid hormone receptor α, among others, and its function has been proposed as integrating ligand-dependent activity of nuclear receptors with transcription(244, 255-257). MED1 is also a cofactor of the RNA Pol II; therefore, it is likely that through MED1, miR-96/182/183 regulates numerous, unexplored genes and biological pathways. Nonetheless, mice with mutations in the nuclear receptor binding motif of Med1 are viable, and it is postulated that these mice are protected from insulin resistance and glucose intolerance that occur in WT mice fed a high-fat diet(244, 258). These observations are in line with our findings that diabetic mice treated with colesevelam have increased miR-182-5p expression, decreased hepatic *Med1* expression, and improvements in glucose tolerance. Nevertheless, further work will be required to understand whether hepatic Med1 regulates glucose metabolism. *Med1*-null mice are embryonic lethal(259); however, tissue-specific Med1 knock-out mice have been generated. For example, skeletal muscle-specific *Med1* knockout mice showed improved glucose tolerance, insulin sensitivity, and resistance to high-fat diet-induced obesity(260). Liver-specific *Med1* knockout mice have been used to demonstrate a role for Med1 in liver regeneration, hepatocellular proliferation, induction of PPARα responsive genes in the liver and development of hepatic steatosis; however no glucose phenotypes were reported for these mice(250, 257, 261). Of note, liver specific *Med1* knockout mice were found to phenocopy PPARα knockout mice(257, 259), and were reported to have decreased expression of genes involved in fatty acid oxidation, fatty acyl-CoA oxidase (*ACOX*), and *PDK4*(257). In addition, liver specific *Med1* knockout mice are protected from developing hepatic steatosis(250). Although we did not find alterations in fatty acid oxidation or lipogenic genes in this study (data not shown), it is possible that miR-96/182/183-dependent down-regulation of *Med1* alters PPARα or PPARγ gene regulation under conditions distinct from those assessed in this study, e.g. stress, PPARα or PPARγ activation, or an earlier diabetic

phenotype. Furthermore, Med1 has also been shown to be post-translationally regulated by phosphorylation and cellular localization(262), and it is possible that while a 50% reduction in *Med1* mRNA and protein levels were observed in response to miR-96/182/183 over-expression, these post-translational regulatory mechanisms maintain the regulation of PPARα or PPARγ gene expression intact.

One key limitation to this study is that we only investigated the effects of colesevelam on hepatic gene expression. While it is unlikely that SREBP2 is altered in other tissues in response to colesevelam, further studies will be required to elucidate whether BA changes and signaling through the TGR5 alter miR-96/182/183 expression in other metabolic tissues, e.g. islet, adipose, and muscle. Similarly, the regulation of Med1 by miR-96/182/183 in these tissues also requires further investigation, as Med1 has also been found to affect metabolic phenotypes outside the liver, e.g. regulation of glucose metabolism through mitochondrial uncoupling in muscle(260), and PPARγ gene transcription and adipogenesis in adipose tissue(263). As further insight into the gene regulatory networks between miRNAs and mRNAs are uncovered, it is likely that we will further appreciate that miRNAs may not regulate the same set of genes in every cell type or under all cellular conditions, as stoichiometry and RNA-protein interactions likely affect miRNA-mRNA interactions.

Taken together, we propose a model in which colesevelam up-regulates the miR-96/182/183 cluster in the livers of diabetic mice (*db/db*) and rats (ZDF). Inhibition of miR-182 *in vivo* partially reverses the beneficial effects of colesevelam on glucose tolerance. While we cannot rule out that miR-183-5p and miR-96-5p may contribute to colesevelam's glucose lowering effect, the low levels of expression and physiological effects observed with inhibition of miR-182-5p alone *in vivo* suggest that miR-182-5p is the main contributor to these effects. Nevertheless, we have identified *MED1* as a novel direct target of all members of the miR-96/182/183 cluster in both mice and humans. Therefore, we propose that miR-182-5p alters hepatic gene expression, likely

through Med1 and other target genes, and contributes to the beneficial effects of colesevelam in systemic glucose metabolism.

CHAPTER VI

SUMMARY AND FUTURE DIRECTIONS

Thesis Summary

The work described in this dissertation aims to provide insights into the role of extracellular HDL-miR-375 and the function of the hepatic miR-96/182/183 cluster in glucose control. As described in this introduction, the Vickers lab has previously reported that miRNAs are carried in circulation on HDL and can be delivered to recipient cells to modulate gene expression(94, 95). Profiling of HDL through sRNA sequencing has revealed that miR-375-3p is one of the most abundant miRNAs on HDL (Table A-1). miR-375-3p is highly enriched in the endocrine cells of the pancreas, and has been shown to play a critical role in islet development and insulin secretion(121, 127, 128). miR-375-3p has also been reported to be released from β cells to the circulation via exosomes, and this process occurs under the same conditions that promote insulin secretion(168). The work described here aimed to understand whether islets, and specifically, β cells could export miR-375-3p to HDL, and what regulatory processes alter this export. I found that primary human and mouse islets, as well as clonal β cell lines, INS-1 and MIN6 cells, robustly export miR-375-3p to HDL. I further profiled the miRNAs that are released to HDL from human islets and INS-1 cells, and found that miR-375-3p is the most abundantly exported miRNA (Figures 3-1B, 3-2A). Importantly, unlike export of miR-375-3p to exosomes, miR-375-3p export to HDL occurs under conditions in which insulin secretion and β cell electrical activity is low, i.e. low glucose.

While the mechanisms of export of miRNAs to HDL is currently unknown, our lab has previously shown that SR-BI is required for miRNA uptake from HDL(94, 95). SR-BI is a bidirectional cholesterol transporter with a functional role in the β cell. Loss of SR-BI, Abca1, and Abcg1 have been shown impair GSIS from the β cells(189, 264, 265), therefore I investigated

whether cholesterol transporters in the islet, ABCA1, ABCG1 and SR-BI could transport miR-375-3p across the plasma membrane. However, I did not find any impairments in miR-375-3p export to HDL in the absence of these transporters. Although I did not identify the direct mechanism by which miRNAs cross the plasma membrane in β cells and how they become bound to HDL in cell culture medium or plasma, this work is the first to uncover novel mechanisms that regulate how miRNAs are released to HDL from β cells (Figure 6-1). While many of these regulatory mechanisms, i.e. insulin secretion, are specific to the β cell, it will be interesting to understand how these regulatory pathways are conserved in other cell types that have been proposed to contribute miRNAs to HDL in the circulation.

A key outstanding question is whether miRNAs, and specifically the quantity of miR-375-3p released from β cells is sufficient to regulate gene expression in distal tissues. My work described in Part 4 & 5 of the Appendix aimed to develop a method to label and trace miRNAs transcribed in the β cell and transferred via HDL to hepatocytes and endothelial cells both *in vitro* and *in vivo*. For this, I used a modified PARCLIP protocol, which we termed Trans-PAR-CLIP. To date, the methods used for measuring delivery of extracellular miRNAs to recipient tissues *in vivo* have largely been injecting labelled miRNAs in exosomes and/or MVs and tracking their delivery to recipient cells(148, 149). However, this likely does not recapitulate the stoichiometry of circulating miRNAs, as the number of injected miRNAs is much more than endogenous levels. Therefore, I aimed to label both *in vivo* and *in vitro* miRNAs transcribed in the β cell using a 4-thiol modified uridine and trace their delivery to recipient cells. However, this technique presented numerous problems, most critically that labelling of nascent miRNAs is rather low (up to 4%)(266) and that not enough is known about miRNAs transfer via HDL to confidently distinguish signal from noise. It will be interesting to perform these studies and quantitate miRNA transfer once these technical challenges are overcome.

Moreover, there is enormous interest in understanding how circulating miRNAs are altered in response to metabolic disease. Therefore, I investigated how both chronic (T2D) and acute

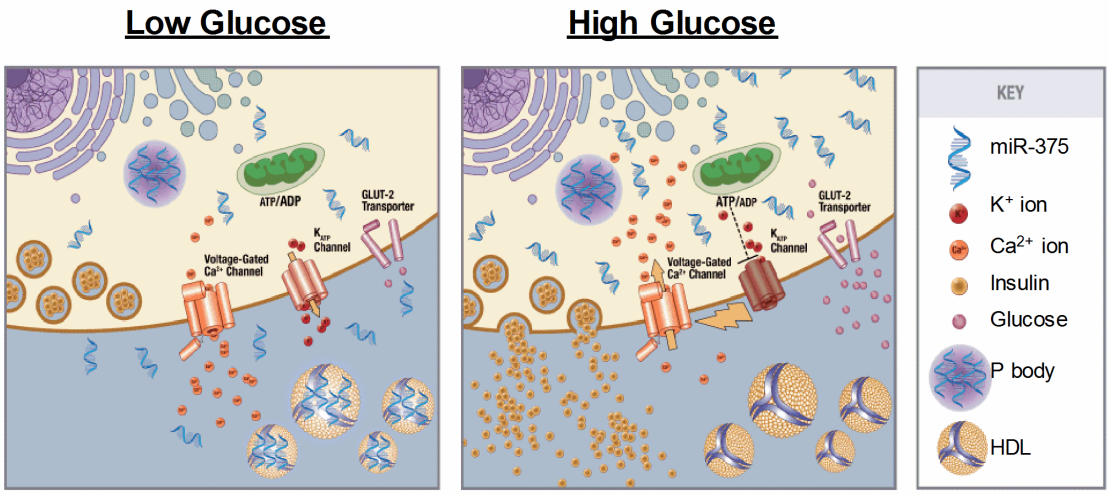

Figure 6-1. Regulation of miR-375-3p export to HDL in low and high glucose. Schematic depicting miRNA export to HDL in low glucose (left panel), and suppression of export in high glucose (right panel).

(fasting/refeding) metabolic alterations affected both plasma and HDL miRNAs, namely miR-375-3p (Chapter IV). In ZDF rats, I found that HDL-miR-375 is downregulated (Figure 4-1), whereas a recent study reported no change in circulating miR-375-3p levels in ZDF rats. In *db/db* mice and humans with T2D, I found no difference in HDL-miR-375-3p or plasma miR-375-3p (humans only) (Figures 4-2, 4-3). Previous studies have found a decrease in plasma miR-375-3p in *db/db* mice(125), whereas the findings in humans are discrepant, with some studies reporting an increase, and others reporting a decrease or no change(121). However, in agreement with the literature I found an elevation in plasma miR-375-3p levels in a T1D model, the STZ mouse, but no change in HDL-miR-375-3p (Figure 4-4)(125, 126, 167, 171). The work described here aimed to test how metabolic alterations alter HDL-miRNA-375-3p, however, due to the low study size, future studies will be required to test whether miRNA changes on HDL reflect plasma miRNA changes, or whether these measurements are independent.

Finally, my aim was to test whether profiling of hepatic miRNAs could aid in elucidating the glucose lowering mechanism of colesevelam. My work found that the miR-96/182/183 cluster is upregulated in ZDF rats treated with colesevelam for 4-weeks. The miR-96/182/183 cluster contains a sterol response element in its promoter and has been shown to be induced by the master cholesterol regulator SREBP2(103). Colesevelam has been shown to promote SREBP-2 activity to stimulate hepatic cholesterol biosynthesis in response to increased BA synthesis from cholesterol(251, 267). As such, I investigated whether miR-182-5p, the most abundant member of the cluster (Figure 5-3), was required for colesevelam's glucose lowering effects. Inhibition of miR-182-5p partially reversed the improvements in glucose tolerance observed with colesevelam in *db/db* mice. Paradoxically, the miR-96/182/183 cluster is also induced with statins(103), which contrary to colesevelam, can result in worsened glucose tolerance(252). Therefore, it is possible that the hepatic gene regulatory networks that are altered with BAS are distinct from those altered with statins and/or that alterations in other tissues also contribute to the divergent phenotypes of each of these drug classes.

Future Directions

Future studies to elucidate the export mechanisms of miR-375-3p

The studies described here are the first to uncover the regulatory processes that regulate how a miRNA, miR-375-3p, is exported from pancreatic β cells to HDL. While the data presented in Chapter III are a significant advance in our understanding of miRNA release to HDL, there is still more work to be done to identify the transporter(s) by which miRNAs cross the plasma membrane. However, a key limitation to these studies are that the assay developed by Vickers *et al*. and adapted for my studies require IP or chromatography isolation of HDL from cell culture medium(94). Both of these techniques are cumbersome and neither is suited for high-throughput screening. Some of my work (not presented here) aimed to develop an assay that could be used to screen miRNA export to HDL without isolating HDL from the medium. However, these attempts were limited by the use of non-PCR techniques to detect miRNAs, and a poor signal-to-noise ratio as the abundance of exported miRNAs is rather low. Another limitation is that we are interested in identifying miRNAs that are specifically exported to HDL, and it is likely that any method that detects miRNAs in the medium and not just bound to HDL will also detect miRNAs on exosomes, MVs and apoptotic bodies. This distinction is key as contrary to export to HDL, miR-375 has been shown to be released in exosomes under conditions that promote insulin secretion(168). Nevertheless, if these technical limitations are overcome and a high-throughput assay is developed to detect HDL-miRNAs, a siRNA screen could be used to identify candidate miRNA transporters. One potential approach is to reconstitute HDL using phospholipids tagged with biotin and to use to biotin-streptavidin pulldowns paired with 96-well automated RNA isolation techniques to screen for HDL-miRNAs. Using this approach it would be possible to not only screen for total HDL-miRNA using a high-sensitivity RNA dye, such as RiboGreen, but also to later measure specific miRNAs, such as miR-375-3p.

Two candidate miRNA transporters that were of interest are homologs of the *C. elegans* RNA transporter SID-1 (systemic RNA interference deficient-1), SID-1 Transmembrane Family

Member 1 and 2 (*Sidt1* and *Sidt2*). In *C. elegans*, SID-1 has been proposed as an RNA channel which enables the passive uptake of dsRNA ranging from 20nt to 700nt(268). In humans, SIDT1 localizes to the plasma membrane and has been shown to facilitate the uptake of a miRNA into HEK cells(269, 270), whereas SIDT2 been proposed to localize to the lysosome and take up RNA for degradation via RNA mediated autophagy(271). Furthermore, knockout mice of *Sidt2* have impaired glucose tolerance and dysfunctional insulin secretion(272). Although SIDT1 and SIDT2 have been proposed to function in RNA uptake, due to their importance in islet function, I hypothesized that SIDT1 and/or SIDT2 may transport RNA across the β cell plasma membrane to export miR-375-3p to HDL. To test this, I transfected MIN6 cells with siRNAs against *Sidt2* or *Sidt1* and *Sidt2* (Figure 6-2A,B), but I did not detect any impairments in miR-375-3p export to HDL (Figure 6-2C). This experiment was limited by poor knockdown of these two transporters and future studies should try to optimize the siRNA knockdown, or use isolated islets from *Sidt1*$^{-/-}$ and/or *Sidt2*$^{-/-}$ mice. These studies would be especially interesting now in light of a new study that proposed that SIDT1 and SIDT2 are not RNA transporters, but rather that they function to traffic cholesterol across the plasma membrane(273), making this transporter potentially relevant to the link between HDL and miRNAs. Further analysis into SIDT1 and SIDT2 and other potential RNA or cholesterol transporters may provide insight into how these miRNAs cross the plasma membrane.

An alternative hypothesis that merits consideration is that miRNAs are released from cells due to cell death and lysis. This hypothesis has been proposed in the β cell field in response to data from T1D humans and rodents showing that plasma miR-375-3p is increased(125, 126, 167, 171-173). Erener *et al*. showed that miR-375-3p levels increased approximately 20-fold when cells were treated with cytokines or STZ to induce about 80% cell death(126). Similarly, Song *et al*. reported that media levels of miR-375-3p correlate well with MIN6 cell cytotoxicity(167). However, in this study, Song *et al*. reported that 50-80% of cell death from 2.5-5mM STZ was required before media-miR-375-3p levels were elevated above control(167). While this issue is

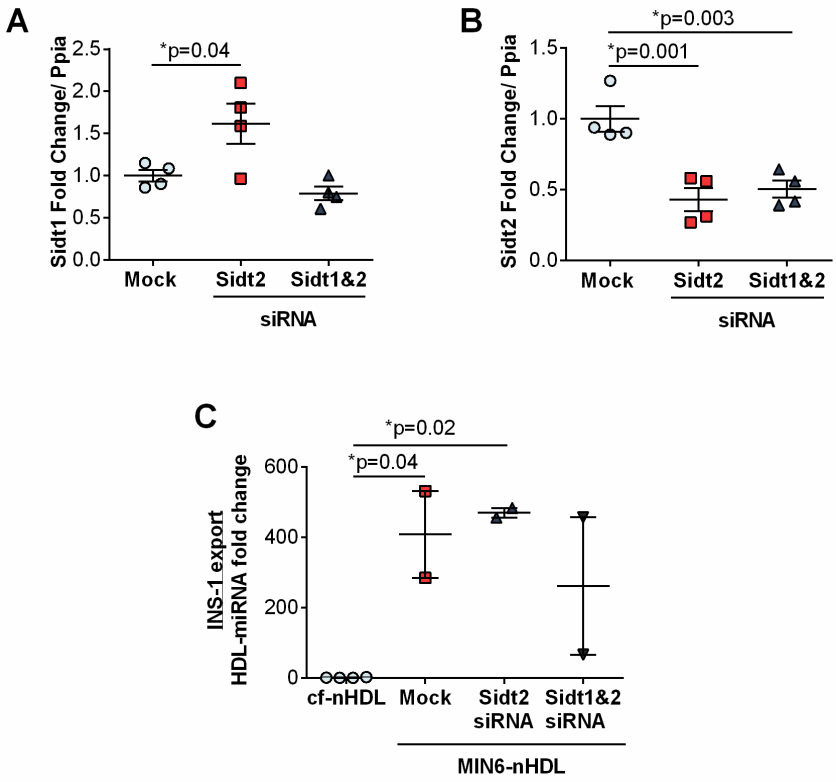

Figure 6-2. Sidt1 and Sidt2 do not alter MIN6 beta cells export of miR-375-3p to HDL. (A) Expression of Sidt1 and (B) Sidt2 with siRNA against Sidt2 and Sidt1 and 2. n=4; One-way ANOVA compared to mock only with Bonferoni post-test. Alpha 0.05. (C) HDL miR-375-3p levels on cf-nHDL and MIN6-nHDL with Sidt2 or Sidt1 and 2 siRNA. n=2-4; One-way ANOVA compared to mock only with Bonferoni post-test. Alpha 0.05. Mean ± SEM.

not directly addressed in this dissertation, I have measured cell death in my assays, and found the levels of cell death to be negligible. Nevertheless, it will be important to assess this issue directly, by treating INS-1 cells with STZ and measuring HDL-miR-375-3p export or by measuring cell death under conditions of both high and low export levels.

While my work presented in Chapter III defines an inverse relationship between miR-375-3p export to HDL, further studies will be required to parse out what signals regulate miRNA release to HDL from β cells and other cells. I identified that when INS-1 cells are treated with high glucose and Ca^{2+}, or when the K_{ATP} channel is inhibited, miR-375-3p export to HDL is suppressed. From this data, I proposed three models: firstly, that the K_{ATP} channel itself transports miRNAs across the plasma membrane, secondly, that the K_{ATP} channel indirectly aids in transport, or that cell membrane depolarization alters ion concentrations in the cell to retain miR-375-3p in the cell during insulin secretion. While it is likely that the K_{ATP} channel pore size is too small to traffic miRNAs, the SUR1, but not Kir6.2 subunit has also been reported to be localized to the insulin granule, suggesting that SUR1 also has K_{ATP} channel independent functions(274). Unfortunately, this will be difficult to distinguish experimentally, as loss of SUR1 also inhibits formation of the K_{ATP} channel. The second model proposes that the K_{ATP} channel may indirectly alter membrane dynamics. One way to study this would be to alter lipid rafts. Lipid rafts contain much greater levels of cholesterol than the surrounding bilayer, and cholesterol depletion can be performed using pharmacological agents, such as methyl-β-cyclodextrin (MβCD) or by inhibiting cholesterol biosynthesis using statins or inhibitors of the squalene epoxidase. Importantly, SUR1 and Kir6.2 are not targeted to cholesterol rich lipid rafts, thereby providing a way to study membrane dynamics independent of the K_{ATP} channel(275). Lastly, the third model proposes that the alterations in ion concentration downstream of membrane polarization may help to retain miRNAs in the cell during insulin secretion. This could be tested using compounds that modulate activity of the L-type Ca^{2+} channels. Bay K 8644 is a Ca^{2+} channel agonist which enhances GSIS (276), whereas nifedipine is a L-type Ca^{2+} channel blocker that inhibits insulin secretion(277) and

investigations using these compounds to alter Ca^{2+} dynamics in the β cell may aid in further uncovering the mechanisms of miR-375-3p export to HDL. Further insight into the mechanisms that regulate miR-375-3p to HDL from the β cell may aid in understanding how other non-insulin secretory cells may also regulate the export of miRNAs to HDL.

Another key consideration is how the mechanisms that regulate miR-375-3p export to HDL are conserved between humans and mouse. While my work identified that miR-375-3p was the most abundantly exported miRNA to HDL (Figure 3-1B), all of the mechanistic studies were performed in clonal β cells or rodent islets. Moreover, I investigated whether miR-375-3p export occurred from numerous donors, and found that human islet from three individual donors exported miR-375-3p to HDL, albeit at vastly different amounts (Figure 3-1C). As such, it is likely that genetic and/or environmental heterogeneity in humans also contributes to the variability observed.

Although I did not observe any differences in HDL-miR-375-3p levels between healthy and diabetic patients (Figure 4-3), it well established that T2D causes both β cell and HDL dysfunction(278-280). Therefore, I investigated whether HDL from a diabetic donor (T2D-HDL) also had the ability to take up miR-375-3p from INS-1 cells. I found no difference between miR-375-3p export to healthy or T2D-HDL (Figure 6-3). One key caveat is that the blood glucose concentrations of this donor were well controlled, and at this time it is not known what properties of HDL are required for miRNA binding and whether those are disturbed by prolonged glucose or insulin. Additionally, it would also be interesting to study whether islets from T2D patients have any dysfunction in miR-375-3p export to HDL, especially due to the discrepant data on plasma miR-375(121) and my findings that HDL-miR-375-3p is decreased in ZDF rats compared to lean (Figure 4-1). Importantly, T2D is not only hyperglycemia (the focus of Chapter III), and many other circulating factors are also altered in T2D patients, including lipids and insulin, and it would be interesting to understand whether these factors also influence miR-375-3p export to HDL.

Finally, it is important to acknowledge the difference between the chronic miRNA export assay (hs) and the acute timeframe for insulin secretion (min-h) and ion dynamics (sec). While I

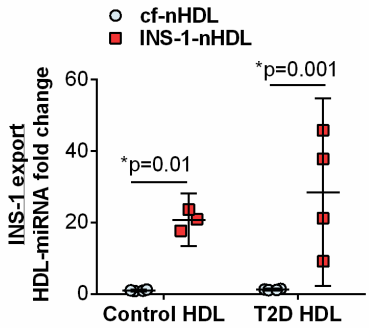

Figure 6-3. INS-1 cells export miR-375-3p to healthy and T2D HDL. HDL miR-375-3p levels on cf-nHDL and INS-1-nHDL. nHDL isolated from control of T2D subject. n=4; Student's t-test. Mean ± SEM.

propose a model in which miRNA export is regulated inversely to insulin secretion, all of the miRNA export assays described in Chapter III were performed between 2-24 h, whereas insulin secretion assays are performed for 15-30 min. This difference is important because I observed that miR-375-3p export to HDL occurred as early as 1h and increased at 4h, 24h and 48h (Figure 3-3A). There are a number of models that could explain these results: 1) that a few cells export miR-375-3p to HDL and over time more cells can export miR-375-3p, 2) that all cells export a basal amount of miR-375-3p to HDL, but the amount each cell exports over time increases, or 3) that cells continuously export miR-375-3p to HDL and it accumulates over time without turnover/degradation. Currently, the kinetics of HDL-miRNA binding are unknown, and with the steady-state measurements used in this study it is impossible to distinguish between these models. However, future studies into miRNA export, HDL-miRNA stability and turnover should provide further insight into these mechanisms.

Future studies to define the contribution of β -cell derived miR-375-3p to the total extracellular miR-375-3p pool

The work described in this dissertation focused on miR-375-3p export from the β cell, but miR-375-3p is also highly abundant in the α cell(281), and may also be expressed in other islet cells. Because β cells make up the largest percentage of islet cells, it is likely that most of the islet-originating miR-375 comes from β cells, but it will be important to study the contribution of miR-375-3p to HDL from each of these cells. Furthermore, although islets have been shown to contain much more miR-375-3p than other tissues(125, 126), Latreille *et al*. recently showed that extracellular miR-375-3p was absent in a miR-375 KO mouse, but only 1% ($5.0x10^4$ compared to $6.0x10^6$ in WT) of extracellular miR-375-3p was restored when miR-375-3p was selectively rescued in β cells using a β cell miR-375-Tg mouse(125). Therefore, it is likely that other cells, perhaps the intestine, or other islet cells that also have high expression levels of miR-375-3p may contribute this miRNA to the circulating pool. To address the question of how much miR-375-3p

beta cells contribute to HDL, we are currently breeding *Dicer* (*Dcr*) floxed mice with an inducible beta cell specific cre (β-Dcr KO). Not only will this model allow for quantification of beta cell originating miR-375-3p, and any other DICER-dependent miRNAs, but it will also allow for temporal regulation of *Dcr* deletion which may enable us to study the turnover of beta-cell originating miRNAs using this model.

The β-Dcr KO mouse will also enable us to study whether loss of beta cell miR-375-3p causes any physiological alterations in other tissues, which may shed light into the role of beta cell originating miR-375-3p. Three groups have now shown that β-cell Dicer-null mice are hyperglycemic, have reduced β cell mass, altered β cell morphology, and impaired insulin synthesis (282-284), but there have been no reports of effects in other tissues. Due to these abnormalities in beta cell development with deletion of *Dcr* during development, we chose to use an inducible cre to allow for normal *Dcr* expression and miRNA processing until adulthood. This will allow us to study the role of *Dcr* independent of developmental effects, and to investigate whether there are any physiological effects in other tissues, due to loss of beta cell miRNAs. While these experiments will not directly address whether extracellular HDL-miR-375-3p regulates gene expression in distal tissues, and which ones, coupling these physiological experiments with injection of HDL bound fluorescent or radioactive miR-375-3p oligos into mice to track miRNA delivery to recipient tissues may aid in uncovering function of HDL-miR-375-3p.

Future studies to elucidate the effect of colesevelam and the miR-96/182/183 cluster in the liver

My work described in this dissertation also uncovered a novel mechanism for glucose regulation by colesevelam and miR-182-5p. Colesevelam is a BAS used to treat hyperlipidemia and hyperglycemia(33, 34, 247), however the mechanism of action remains unclear. My work identified that the SREBP-2 regulated miRNA cluster, miR-96/182/183 is upregulated in the livers of colesevelam treated mice and rats and that inhibition of miR-182 *in vivo* partially reverses the glucose lowering effects of colesevelam(89). This work also identified that Med1, a protein that

links nuclear receptor activity to Pol II transcription, is a direct target of this miRNA cluster(89). A key question that has emerged from this work is how does upregulation of miR-182 with both statins and colesevelam result in differing effects on glucose control.

While we propose that miR-96/182/183 upregulation occurs in response to cholesterol changes in the liver and upregulation of the transcription factor SREBP-2, another key distinction between statins and colesevelam is the effect of colesevelam on BAs. Normally 95% of BAs are reabsorbed by the intestine and transported back to the liver through enterohepatic circulation and FXR is the primary sensor for endogenous BAs(29). Colesevelam inhibits BA reabsorption and promotes their excretion, resulting in decreased FXR signaling(37). In response to BAs, FXR represses CYP7A1 to inhibit BA synthesis in the liver(285). FXR and CYP7A1 have both in turn been reported to regulate miRNAs(240). FXR knockout mice were shown to have increased levels of miR-34a(286), and *Cyp7a1* overexpressing mice were reported to have increased levels of miR-33a(254). Therefore it is possible that loss of FXR or activation of CYP7A1 with colesevelam may also contribute to upregulation of the miR-96/182/183 cluster through distinct mechanisms from statins. Microarray data comparing miRNAs altered in WT and FXR knockout livers did not detect miR-96-5p, miR-182-5p, nor miR-183-5p(240, 286), but the upregulation in miR-33 in Cyp7a1 overexpressing mice was proposed to be due to Cyp7a1 induction of SREBP-2(254). Hence, this BA regulated pathway may also contribute to the upregulation of this cluster in the liver of colesevelam treated rodents, and may distinguish the effects of BAS and statins.

Members of the miR-96/182/183 cluster have also been shown to have effects in non-hepatic tissues. miR-182-5p has been shown to be downregulated in diabetic compared to healthy human and NHP blood as well as rat blood, muscle, adipose, pancreas and liver(109). Similarly, Zhang *et al*. recently reported that HFD feeding resulted in a downregulation of miR-182-5p in gastrocnemius muscle of WT mice(116). This study further showed that global loss of miR-182 resulted in glucose impairments, whereas restoration of miR-182 expression in HFD fed mice reversed the glucose phenotype(116). In the islets, miR-182-5p and miR-183-5p are among the

most highly abundant miRNAs (Table A-3), and have been shown to be downregulated in islets from T2D rodents(124, 287).

Most of the effects of this cluster in metabolism have been proposed to be mediated by the target gene, *FoxO1(109)*. Zhang *et al*. proposed that miR-182-5p alters glucose utilization by inhibiting its target genes Foxo1 and Pdk4(116), and Karolina *et al*. showed an inverse relationship between miR-182 expression and *FoxO1* expression in islets. In the islet, FoxO1 is critical for beta cell function, proliferation and compensation in response to increased insulin demand(288). As such, downregulation of miR-182-5p, and upregulation of FoxO1 in the islet of T2D rodents may be a mechanism for beta cell compensation. In muscle, FoxO1 and the other FoxO family members, are key factors in the control of muscle energy metabolism through glycolytic flux and mitochondrial metabolism(115). Moreover, in the liver, FoxO1 also plays a critical role in glucose regulation, by promoting the expression of key gluconeogenic genes, G6Pase and PEPCK (Figure 6-4) (289). In my studies I tested whether miR-96-5p, miR-182-5p and miR-183-5p regulate *Foxo1* in primary hepatocytes and in the liver in response to colesevelam. I found that overexpression of each of the miRNAs from the cluster downregulate *FoxO1* expression in primary hepatocytes (Figure 6-5A). However, in the livers, I did not detect any difference in *Foxo1* expression between Chow + PBS, Col + PBS and Col + LNA (Figure 6-5B). One reason why we may not observe regulation of Foxo1 in the mouse livers, is that FoxO1 is robustly induced by fasting(289), and the mice in this study were not fasted at sacrifice. Nevertheless, this data suggests that other target genes likely contribute the physiological effects of miR-182-5p *in vivo*. For this reason, I investigated other target genes in the liver, and identified Med1 as a target of miR-96/182/183 (discussed in Chapter V).

Finally, independent of colesevelam, I investigated whether the miR-96/182/183 cluster is regulated acutely in response to fasting and feeding. Zhang *et al*. have shown that in muscle, miR-182-5p levels are upregulated during fasting(116). In the liver, SREBP-2 activity has been shown to be suppressed under fasting conditions(290), which leads to the hypothesis that the

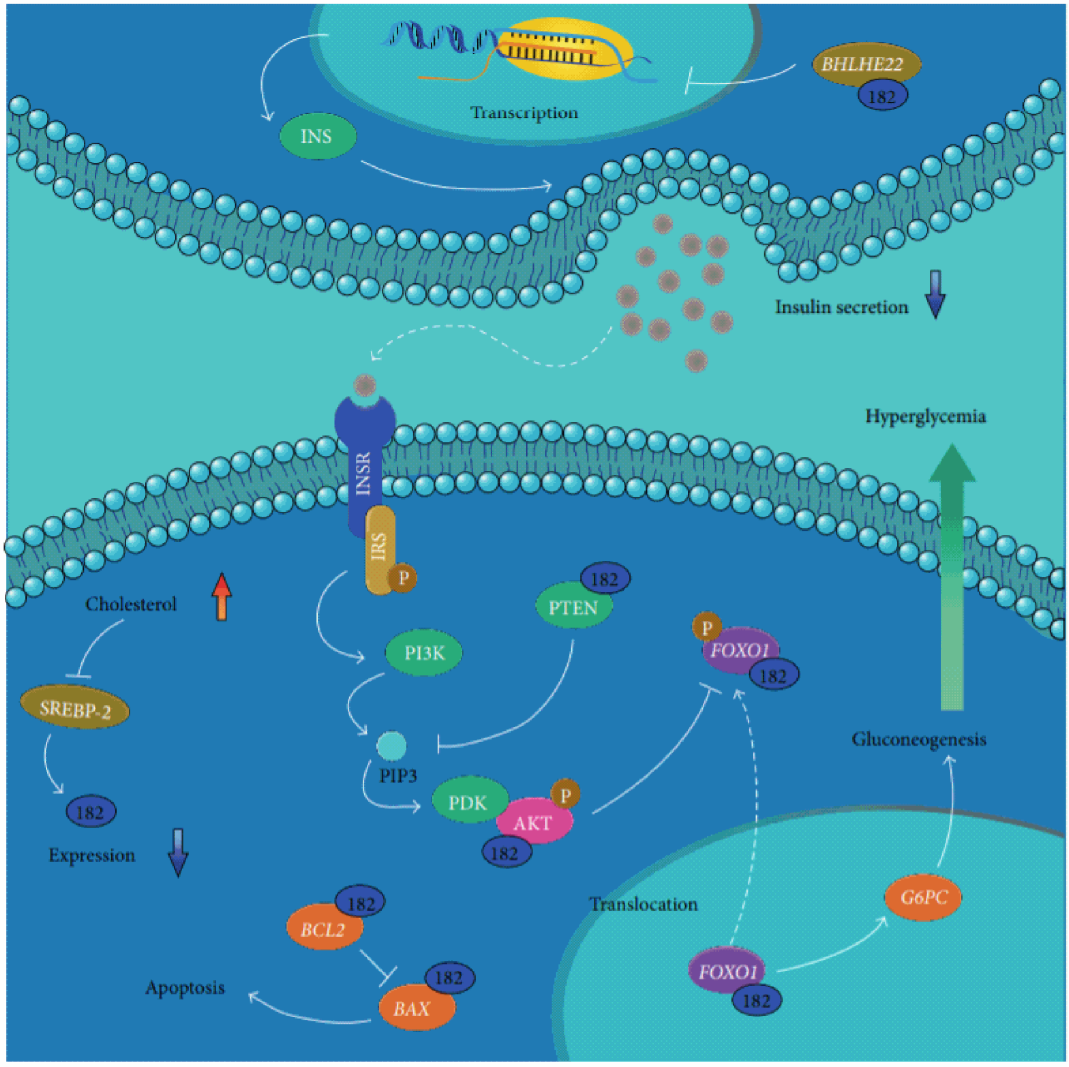

Figure 6-4. Proposed mechanism for miR-182-5p regulation of gluconeogenesis. From Zhou et., J Diabetes Res. 2014;2014:760397.

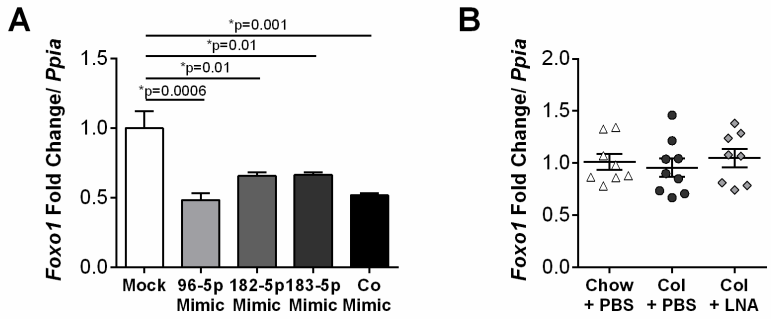

Figure 6-5. Foxo1 regulation by miR-96, miR-182 and miR-183. (A) FoxO1 mRNA levels in mouse primary hepatocytes transfected with 50nM miR-96-5p, miR-182-5p, miR-183-5p mimics individually or in combination. Real-time PCR. n=3. One-Way ANOVA with Bonferonni's post-test compared to mock group only, alpha 0.05. (B) Hepatic FoxO1 mRNA levels in db/db mice treated with vehicle or 2% colesevelam-supplemented diet and PBS or LNA-182-5p. Real-time PCR. n=8-9.

miR-96/182/183 cluster is downregulated, not upregulated as in muscle, during fasting in the liver. However, I did not observe any differences in hepatic miR-96-5p, miR-182-5p, nor miR-183-5p between fed, fasted and refed samples (Figure 6-6). This may be due to the long half-life of miRNAs, or due to other factors besides SREBP-2 in regulating miR-96/182/183 transcription. As such, future studies should study how these miRNAs are regulated in different metabolic tissues in response to both chronic and acute metabolic alterations to fully understand the role of this cluster in regulating physiology.

Future studies into the function of β cell derived HDL-miR-375-3p

Since its inception, the field of extracellular RNAs has postulated that extracullar miRNAs function in cell-to-cell communication. While many miRNAs have been reported to have roles in cell-to-cell communication, to date it is unknown what tissues or cells miR-375-3p is delivered to. Functional studies of miR-375-3p in non-β cells suggests that miR-375-3p may impact bone formation, epithelial cell differentiation, Wnt signaling, hormone secretion from neuronal cells or neuroprotection during cerebral ischemia(207-210, 291). However, it is likely that miR-375-3p has currently undefined functional roles in other cell types beyond those described above. Research from the cancer literature suggests miR-375-3p impacts autophagy and carcinogenesis, as well as a number of signaling pathways, including connective-tissue groth factor (CTGF)-epidermal growth factor receptor (EGFR), Akt, Janus kinase 2 (JAK2)-Signal transducer and activator of transcription 3 (STAT3), and Mitogen-Activated Protein Kinase Kinase Kinase 8 (MAP3K8)-extracellular signal–regulated kinase (ERK) signalling(292-296). Therefore it is likely that miR-375-3p is important for regulating critical cell processes, although it is currently unknown if extracellular miR-375-3p also regulates these same process. Moreover, it is known that exosomes, HDL and microvesicles can transport miR-375-3p but it is currently unknown whether miR-375-3p bound to each of these carriers has similar or distinct functional roles in tissues(94, 168, 169).

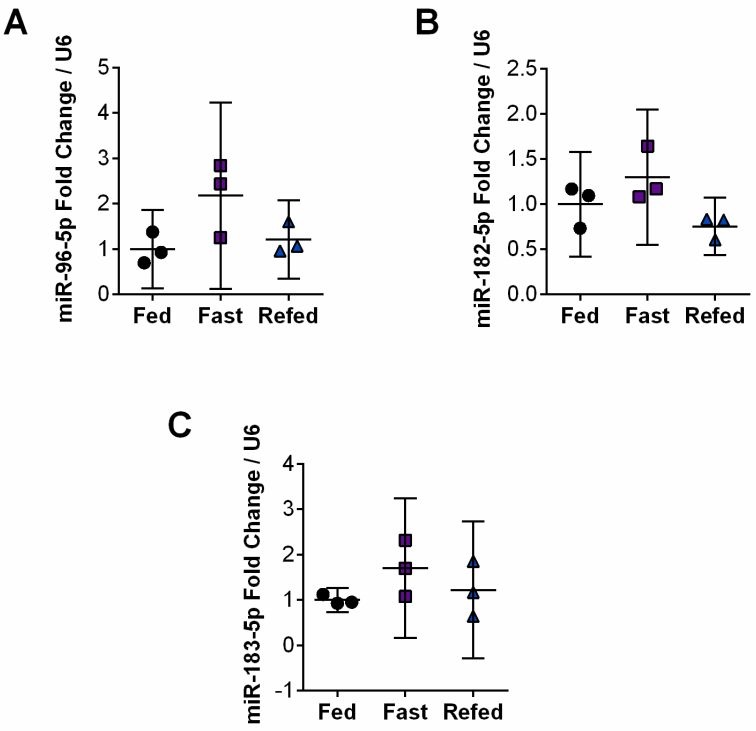

Figure 6-6. Hepatic miR-96/182/183 changes in response to fasting and feeding. (A) Hepatic expression of miR-96-5p, (B) miR-182-5p, and (C) miR-183-5p from wildtype mice, ad lib fed (fed), fasted for 16h (fast) or fasted for 16h and and refed for 2h (refed). n=3; one-way ANOVA with Bonferonni post-test.

Alternatively, HDL-bound miRNAs as well as other extracellular miRNAs may not function via delivery to tissues for gene expression, but rather may contribute to cell signaling. One hypothesis is that HDL-miRNAs may function as receptor agonists or antagonists for toll-like receptors (TLRs), independent of sequence(297). In support of this hypothesis, extracellular let-7b have been shown to activate TLR7 in neurons(298), and viral miRNAs activate TLR8 in macrophages to induce inflammation(299). Furthermore, HDL-miRNAs may be turned over during HDL clearance through the kidney, or by RNAses in the blood. As such, many questions still remain about the role of circulating HDL-miRNAs in physiology and further work will be required to define the functional role of β cell originating HDL-miR-375-3p.

APPENDIX

Part 1: Tables associated with Chapter III

Table A-1. Normalized miRNA rank (RPM) in human (healthy) HDL by sRNA-seq. Mean from n=10

This table contains small RNA sequencing results of miRNAs from healthy human HDL (n=10) ranked based on abudance. Textual citation is located on page 58.

Feature	Mean RPM	Standard Deviation
hsa-miR-486-5p	788.0112	456.7136
hsa-miR-27b-3p	345.1239	178.1848
hsa-miR-423-5p	319.4812	281.671
hsa-miR-92a-3p	281.4443	244.7793
hsa-miR-3168	195.0576	152.0776
hsa-miR-22-3p	173.6318	140.1347
hsa-miR-26a-5p	161.2463	162.8545
hsa-miR-16-5p	133.8386	74.41697
hsa-miR-191-5p	119.7854	105.1068
hsa-let-7f-5p	108.0859	116.4362
hsa-miR-126-5p	71.14003	55.7222
hsa-miR-21-5p	69.68608	88.02777
hsa-miR-30d-5p	61.40914	85.8951
hsa-let-7i-5p	57.19072	81.51391
hsa-let-7a-5p	52.71567	62.44602
hsa-miR-181a-5p	51.00064	59.93619
hsa-miR-30e-5p	46.35006	58.70766
hsa-miR-375	44.40288	17.06922
hsa-miR-320a	41.24771	48.00825
hsa-miR-146a-5p	39.45484	47.21153
hsa-miR-203a	34.63446	10.18178
hsa-miR-320b	29.35724	18.41114
hsa-miR-151a-3p	27.6612	25.07574

hsa-miR-451a	26.84648	18.20303
hsa-miR-25-3p	19.52505	11.03535
hsa-let-7g-5p	17.10731	18.65177
hsa-miR-127-3p	16.93047	34.60336
hsa-miR-182-5p	16.74405	12.31013
hsa-miR-26b-5p	14.79317	15.6524
hsa-miR-146b-5p	14.56165	17.50995
hsa-miR-222-3p	14.31521	19.17382
hsa-miR-130a-3p	13.66696	7.699563
hsa-miR-423-3p	13.18309	14.12278
hsa-miR-28-3p	12.58219	15.78282
hsa-miR-10a-5p	12.55418	10.21123
hsa-miR-10b-5p	12.48325	9.664026
hsa-miR-143-3p	12.41597	9.269474
hsa-miR-584-5p	12.39155	19.99658
hsa-miR-103a-3p	12.32826	14.61766
hsa-miR-151a-5p	11.81064	16.00837
hsa-miR-148a-3p	11.57163	9.780746
hsa-miR-3621	11.4806	5.934623
hsa-miR-186-5p	10.89291	15.13651
hsa-miR-148a-5p	10.56691	12.71385
hsa-miR-15a-5p	10.44135	9.346207
hsa-miR-192-5p	9.9571	7.213854
hsa-miR-199a-3p;hsa-miR-199b-3p	9.835791	12.65265
hsa-let-7b-5p	9.015215	12.82158
hsa-miR-126-3p	8.308532	9.860342
hsa-miR-27a-3p	7.972251	3.4671
hsa-miR-92b-3p	7.087933	4.789983
hsa-let-7d-5p	7.001503	11.70697
hsa-miR-125a-3p	6.29544	6.96409
hsa-miR-744-5p	5.786959	7.174524
hsa-miR-181b-5p	5.745241	7.154621
hsa-miR-148b-3p	5.511017	9.116341
hsa-miR-30c-5p	5.040731	7.490189
hsa-miR-140-3p	4.971965	6.836437
hsa-miR-30a-5p	4.825282	4.719443
hsa-miR-93-5p	4.43947	5.802726
hsa-let-7e-5p	4.387744	4.778715
hsa-miR-877-5p	4.125504	9.271787
hsa-miR-409-3p	3.578761	4.523906
hsa-miR-378a-3p	3.436597	2.949803
hsa-miR-101-3p	3.249335	3.962054
hsa-miR-432-5p	3.210909	7.056805

hsa-miR-17-5p	3.156199	3.161019
hsa-miR-23a-3p	3.101793	2.11827
hsa-miR-142-5p	3.085366	4.266771
hsa-miR-223-3p	2.996284	5.238771
hsa-miR-1246	2.757549	2.71853
hsa-miR-301a-3p	2.698945	2.51427
hsa-miR-184	2.426209	3.493294
hsa-miR-484	2.417394	5.216184
hsa-miR-98-5p	2.375291	5.016895
hsa-miR-142-3p	2.276818	3.146609
hsa-miR-221-3p	2.251317	4.004715
hsa-miR-130b-3p	2.124789	2.825755
hsa-miR-425-5p	1.933646	5.026174
hsa-miR-23b-3p	1.885075	1.789049
hsa-miR-155-5p	1.80416	2.732211
hsa-miR-100-5p	1.758465	5.560754
hsa-miR-107	1.745213	0.718582
hsa-miR-410-3p	1.659829	4.051417
hsa-miR-486-3p	1.639299	2.703247
hsa-miR-20a-5p	1.620598	2.73591
hsa-miR-128-3p	1.514984	2.654882
hsa-miR-421	1.480628	3.214629
hsa-miR-30e-3p	1.374828	2.630024
hsa-miR-28-5p	1.363409	2.404024
hsa-miR-221-5p	1.284207	2.719184
hsa-miR-340-5p	1.230565	2.626052
hsa-miR-19a-3p	1.204221	2.756621
hsa-miR-15b-5p	1.202127	2.605209
hsa-miR-144-3p	1.192036	1.546762
hsa-miR-433-3p	1.156504	2.439425
hsa-miR-7977	1.14226	1.158401
hsa-miR-133a-3p	1.089457	1.775504
hsa-miR-654-3p	1.057014	1.921373
hsa-miR-224-5p	0.994556	2.293266
hsa-miR-136-3p	0.936677	2.081764
hsa-miR-323b-3p	0.888826	2.810715
hsa-miR-627-5p	0.861207	1.825931
hsa-miR-342-3p	0.847269	2.679301
hsa-miR-766-5p	0.842046	2.662783
hsa-miR-93-3p	0.837221	1.822078
hsa-miR-181c-3p	0.83713	1.777149
hsa-miR-885-3p	0.810446	1.710193
hsa-miR-125a-5p	0.795265	2.51485

hsa-miR-361-3p	0.795265	2.51485
hsa-miR-629-5p	0.793521	2.509333
hsa-miR-4732-3p	0.778847	2.462929
hsa-miR-1307-3p	0.770245	2.182074
hsa-miR-194-5p	0.767475	1.634957
hsa-miR-4516	0.767334	1.369029
hsa-miR-185-5p	0.760457	2.404777
hsa-miR-21-3p	0.751251	1.248465
hsa-miR-3615	0.734768	2.209812
hsa-miR-891a-5p	0.734547	2.322842
hsa-miR-4520a-3p	0.72119	2.280602
hsa-miR-106b-5p	0.717454	1.439748
hsa-miR-335-3p	0.702211	2.220586
hsa-miR-889-3p	0.701705	2.218985
hsa-let-7c-5p	0.683756	1.211577
hsa-miR-103b	0.681772	1.566444
hsa-miR-30b-5p	0.672703	1.770978
hsa-miR-215-5p	0.666892	1.225463
hsa-miR-106b-3p	0.637828	1.144105
hsa-miR-652-3p	0.628433	1.376372
hsa-miR-146b-3p	0.628204	1.986555
hsa-miR-374b-5p	0.612364	1.936466
hsa-miR-181c-5p	0.608144	1.923121
hsa-miR-5010-3p	0.608144	1.923121
hsa-miR-1304-3p	0.600451	1.898794
hsa-miR-151b	0.592301	0.634469
hsa-miR-99b-5p	0.584135	1.847197
hsa-miR-6852-5p	0.581105	1.212846
hsa-miR-181a-2-3p	0.579217	1.369252
hsa-miR-744-3p	0.56936	1.800475
hsa-miR-425-3p	0.561364	1.775188
hsa-miR-500a-3p	0.561364	1.775188
hsa-miR-3688-3p	0.557562	1.763166
hsa-miR-4446-3p	0.538702	1.185676
hsa-miR-411-5p	0.502102	0.817138
hsa-miR-4532	0.500773	0.75705
hsa-miR-6748-3p	0.476222	0.88888
hsa-let-7d-3p	0.474467	1.500396
hsa-miR-197-5p	0.474467	1.500396
hsa-miR-660-5p	0.472779	1.435334
hsa-miR-199b-5p	0.448907	1.247594
hsa-miR-548n	0.445356	1.408339
hsa-miR-671-3p	0.433076	0.994592

hsa-miR-625-5p	0.422487	1.224265
hsa-miR-485-5p	0.421023	1.331391
hsa-miR-1343-3p	0.408534	0.334219
hsa-miR-150-5p	0.389423	1.231464
hsa-miR-200a-3p	0.389423	1.231464
hsa-miR-125b-5p	0.386005	1.220653
hsa-miR-26b-3p	0.386005	1.220653
hsa-miR-363-3p	0.374924	0.823524
hsa-miR-4485	0.363697	1.150111
hsa-miR-4757-3p	0.354887	0.991115
hsa-miR-5189-3p	0.354755	1.121835
hsa-miR-4772-3p	0.349526	0.737021
hsa-miR-183-5p	0.346803	0.49908
hsa-miR-301b	0.341616	1.080285
hsa-miR-19b-3p	0.336163	1.063041
hsa-miR-4433b-3p	0.330634	1.045555
hsa-miR-370-3p	0.327462	1.035527
hsa-miR-378i	0.327462	1.035527
hsa-miR-505-3p	0.327462	1.035527
hsa-miR-7975	0.325754	0.705431
hsa-miR-381-3p	0.280682	0.887594
hsa-miR-4742-3p	0.280682	0.887594
hsa-miR-5010-5p	0.280682	0.887594
hsa-miR-483-3p	0.275921	0.872538
hsa-miR-187-5p	0.264507	0.836444
hsa-miR-496	0.257336	0.813769
hsa-miR-760	0.233902	0.739662
hsa-miR-17-3p	0.23372	0.739086
hsa-miR-141-3p	0.214447	0.678141
hsa-miR-6791-3p	0.194843	0.616148
hsa-miR-369-3p	0.187121	0.591729
hsa-miR-431-5p	0.187121	0.591729
hsa-miR-769-5p	0.187121	0.591729
hsa-miR-6869-5p	0.170524	0.369907
hsa-miR-320d	0.169824	0.248057
hsa-miR-24-3p	0.161693	0.341672
hsa-miR-1260b	0.140341	0.443797
hsa-miR-6087	0.119845	0.281921
hsa-miR-4530	0.118646	0.375191
hsa-miR-384	0.118252	0.373945
hsa-miR-7704	0.093561	0.295865
hsa-miR-3191-3p	0.083504	0.264064
hsa-miR-6791-5p	0.078835	0.249297

hsa-miR-511-3p	0.075953	0.161789
hsa-miR-320c	0.073291	0.083652
hsa-miR-4508	0.069165	0.218718
hsa-miR-497-5p	0.059323	0.187596
hsa-miR-3610	0.056936	0.180048
hsa-miR-4492	0.055669	0.176042
hsa-miR-323a-3p	0.04678	0.147932
hsa-miR-6073	0.04678	0.147932
hsa-miR-205-5p	0.039417	0.124648
hsa-miR-3150b-5p	0.039417	0.124648
hsa-miR-4783-3p	0.039417	0.124648
hsa-miR-193a-3p	0.033389	0.105584
hsa-miR-4662b	0.033063	0.104556
hsa-miR-3074-3p	0.027835	0.088021
hsa-miR-1247-3p	0.019774	0.062532
hsa-miR-3150b-3p	0.019774	0.062532
hsa-miR-3184-3p	0.019774	0.062532
hsa-miR-6516-5p	0.018979	0.060016
hsa-miR-6851-5p	0.018979	0.060016
hsa-miR-7641	0.018979	0.060016
hsa-miR-145-3p	0.017291	0.05468
hsa-miR-3622b-3p	0.017291	0.05468
hsa-miR-6834-5p	0.017291	0.05468

Table A-2. Primary human islet miRNA export to HDL. Fold change of islet-nHDL versus cf-nHDL from 1 human islet donor.

This table contains small RNA sequencing results of miRNAs exported to HDL from primary human islets (n=1). Base mean represents abundance. Fold change of miRNA export between cf-nHDL and islet-nHDL. Textual citation is located on page 58.

miRNA	DEseq2 (BaseMean)	Fold Change	cf-nHDL (RPM)	Islet-nHDL (RPM)
hsa-miR-375	3937.38	16.77	160.00	3944.76
hsa-let-7d-5p	117.55	2.34	50.02	94.32
hsa-miR-200a-3p	37.91	2.03	17.32	35.74
hsa-miR-148a-3p	285.12	2.02	145.47	203.56
hsa-miR-30c-5p	205.87	2.02	118.93	160.70
hsa-miR-30a-5p	812.26	1.85	441.25	606.52
hsa-miR-223-3p	38.69	1.81	18.28	33.09
hsa-miR-101-3p	42.64	1.78	9.03	32.21
hsa-let-7d-3p	40.84	1.71	23.93	33.41
hsa-miR-125a-5p	78.79	1.68	31.70	63.91
hsa-miR-92b-3p	38.20	1.65	15.13	36.73
hsa-let-7f-5p	370.57	1.65	216.53	262.95
hsa-miR-126-5p	127.87	1.61	54.55	87.93
hsa-miR-425-5p	39.13	1.60	21.07	30.59
hsa-miR-181b-5p	50.86	1.56	30.08	36.89
hsa-miR-183-5p	10.27	1.55	4.12	8.81
hsa-miR-30e-5p	583.44	1.53	427.29	440.71
hsa-miR-30d-5p	390.14	1.45	248.94	285.87
hsa-miR-191-5p	314.15	1.41	181.99	234.27
hsa-miR-127-3p	97.64	1.36	61.42	59.74
hsa-let-7b-5p	51.90	1.32	36.03	38.72
hsa-miR-205-5p	134.97	1.30	86.85	94.08
hsa-let-7a-5p	156.81	1.29	108.85	94.95
hsa-miR-93-5p	130.65	1.28	89.93	84.75
hsa-let-7i-5p	555.92	1.27	369.73	334.91
hsa-miR-215-5p	109.33	1.26	79.99	67.74
hsa-miR-423-5p	303.25	1.25	211.53	178.56
hsa-miR-194-5p	5.45	1.22	3.88	5.83
hsa-miR-186-5p	83.96	1.20	51.49	49.76
hsa-miR-145-5p	27.27	1.20	19.36	18.09
hsa-miR-128-3p	63.12	1.17	51.30	41.06

hsa-miR-451a	462.89	1.10	324.83	282.24
hsa-miR-92a-3p	1649.47	1.10	1190.28	983.81
hsa-miR-30b-5p	114.52	1.10	94.52	65.59
hsa-miR-200b-3p	119.81	1.09	72.27	75.69
hsa-miR-143-3p	260.78	1.09	169.79	152.12
hsa-miR-146a-5p	56.07	1.09	39.36	38.21
hsa-miR-574-3p	19.10	1.07	16.58	13.22
hsa-let-7g-5p	137.53	1.07	51.22	71.36
hsa-miR-486-5p	12316.90	1.07	9388.91	7232.77
hsa-miR-22-3p	4882.67	1.06	3506.36	2930.14
hsa-miR-199a-3p;hsa-miR-199b-3p	55.42	1.04	45.44	36.90
hsa-miR-182-5p	65.81	1.04	59.00	39.72
hsa-miR-192-5p	689.27	1.02	463.31	445.19
hsa-miR-378c	10.62	1.01	9.62	6.80
hsa-miR-27b-3p	594.52	1.00	432.58	355.21
hsa-miR-144-5p	31.70	1.00	32.20	13.40
hsa-let-7e-5p	31.25	0.99	12.23	11.40
hsa-miR-532-5p	58.47	0.98	19.76	28.44
hsa-miR-10b-5p	583.80	0.96	450.35	353.54
hsa-miR-15a-5p	128.49	0.96	124.88	74.53
hsa-miR-138-5p	19.92	0.96	7.75	10.60
hsa-miR-125b-5p	22.18	0.95	23.09	15.80
hsa-let-7c-5p	201.63	0.93	190.98	134.83
hsa-miR-187-3p	33.46	0.93	18.61	16.62
hsa-miR-181d-5p	11.77	0.92	12.48	3.68
hsa-miR-378a-3p	333.65	0.92	249.31	200.30
hsa-miR-149-5p	26.93	0.92	32.41	14.02
hsa-miR-26a-5p	352.49	0.91	257.85	189.49
hsa-miR-100-5p	7.19	0.91	8.65	2.99
hsa-miR-132-3p	19.11	0.90	13.05	11.64
hsa-miR-150-5p	641.35	0.90	489.70	361.33
hsa-miR-328-3p	66.67	0.88	67.60	39.32
hsa-miR-29a-3p	215.21	0.87	165.77	119.96
hsa-miR-410-3p	27.71	0.87	12.46	7.30
hsa-miR-181c-5p	57.91	0.86	46.33	29.33
hsa-miR-107	34.19	0.86	29.08	19.38
hsa-miR-25-3p	599.40	0.85	569.82	313.53
hsa-miR-151a-3p	114.08	0.85	71.05	59.18
hsa-miR-152-3p	7.55	0.84	6.82	3.49
hsa-miR-133a-3p	641.86	0.82	464.52	338.32
hsa-miR-99b-5p	35.57	0.80	29.10	21.57
hsa-miR-181a-5p	725.44	0.77	579.05	380.52

hsa-miR-106b-5p	12.24	0.77	15.44	3.84
hsa-miR-21-5p	813.50	0.77	576.76	382.25
hsa-miR-744-5p	64.55	0.77	32.73	31.40
hsa-miR-484	80.88	0.77	87.46	39.27
hsa-miR-142-5p	201.37	0.76	191.56	95.54
hsa-miR-320a	112.84	0.76	92.99	47.59
hsa-miR-130a-3p	81.47	0.74	72.69	38.11
hsa-miR-140-3p	233.31	0.71	190.94	113.81
hsa-miR-423-3p	111.14	0.71	90.71	54.98
hsa-miR-27a-3p	180.26	0.70	139.38	75.33
hsa-miR-342-3p	68.78	0.68	43.67	30.53
hsa-miR-1226-3p	27.74	0.67	19.88	11.69
hsa-miR-103a-3p	104.45	0.67	92.26	50.12
hsa-miR-23b-3p	35.02	0.63	30.80	14.81
hsa-miR-3168	1616.76	0.63	1191.11	676.32
hsa-miR-23a-3p	74.50	0.60	58.51	29.73
hsa-miR-320b	145.45	0.58	122.96	40.92
hsa-miR-106b-3p	22.94	0.57	28.78	6.25
hsa-miR-221-3p	64.08	0.54	60.90	24.23
hsa-miR-320d	6.97	0.53	12.39	1.31
hsa-miR-125b-2-3p	53.56	0.53	40.30	17.59
hsa-miR-381-3p	10.39	0.52	17.23	1.93
hsa-miR-10a-5p	1016.35	0.52	861.64	373.73
hsa-miR-16-5p	3630.80	0.51	2930.93	1313.72
hsa-miR-222-3p	29.47	0.49	34.51	3.03
hsa-miR-26b-5p	39.96	0.47	38.46	9.96
hsa-miR-126-3p	63.91	0.44	70.26	20.19
hsa-miR-141-3p	182.00	0.41	178.44	50.97
hsa-miR-203a-3p	387.08	0.38	372.92	91.65
hsa-miR-210-3p	18.49	0.36	14.90	1.91

Table A-3. Normalized miRNA rank (RPM) in primary human islets by sRNA-seq. n=1 human donor.

This table contains small RNA sequencing results of miRNAs expressed in primary islets, ranked by abundance. Textual citation is located on page 58.

Rank	Feature	RPM
1	hsa-miR-375	115165.4
2	hsa-miR-26a-5p	67691.51
3	hsa-miR-22-3p	39888.83
4	hsa-miR-27b-3p	33335.49
5	hsa-let-7a-5p	24821.51
6	hsa-let-7f-5p	18039.81
7	hsa-miR-125a-5p	18030.24
8	hsa-miR-141-3p	12378.82
9	hsa-miR-16-5p	11041.81
10	hsa-miR-151a-5p	10598.18
11	hsa-miR-192-5p	10378.69
12	hsa-miR-148a-3p	8673.186
13	hsa-miR-191-5p	8299.377
14	hsa-miR-21-5p	8141.678
15	hsa-miR-143-3p	7441.399
16	hsa-miR-182-5p	7029.85
17	hsa-miR-125b-5p	6649.971
18	hsa-miR-30d-5p	5892.425
19	hsa-let-7b-5p	5528.996
20	hsa-miR-29a-3p	5139.805
21	hsa-miR-99b-5p	4652.784
22	hsa-miR-181a-5p	4641.751
23	hsa-miR-200b-3p	4439.209
24	hsa-let-7g-5p	3876.618
25	hsa-miR-10a-5p	3677.62
26	hsa-let-7e-5p	3283.382
27	hsa-miR-126-5p	3254.887
28	hsa-let-7i-5p	3251.6
29	hsa-miR-98-5p	3056.06
30	hsa-miR-30b-5p	3041.764
31	hsa-miR-183-5p	3040.656
32	hsa-miR-30c-5p	2953.583
33	hsa-miR-423-5p	2835.993

34	hsa-miR-29c-3p	2696.512
35	hsa-miR-23b-3p	2683.83
36	hsa-miR-92a-3p	2681.71
37	hsa-miR-186-5p	2419.887
38	hsa-miR-26b-5p	2398.655
39	hsa-miR-200a-3p	2089.876
40	hsa-miR-222-3p	2087.633
41	hsa-miR-27a-3p	2083.216
42	hsa-miR-30a-5p	1980.771
43	hsa-miR-92b-3p	1935.638
44	hsa-miR-30e-5p	1751.66
45	hsa-miR-335-5p	1627.754
46	hsa-let-7d-5p	1619.637
47	hsa-miR-153-3p	1538.779
48	hsa-miR-423-3p	1503.004
49	hsa-miR-151a-3p	1403.599
50	hsa-miR-200c-3p	1339.256
51	hsa-miR-204-5p	1277.235
52	hsa-miR-127-3p	1173.747
53	hsa-miR-487b-3p	1135.028
54	hsa-miR-338-3p	1050.98
55	hsa-miR-23a-3p	1024.262
56	hsa-miR-101-3p	1001.408
57	hsa-miR-126-3p	978.9712
58	hsa-miR-15a-5p	921.1897
59	hsa-miR-132-3p	885.1281
60	hsa-let-7c-5p	882.5081
61	hsa-miR-7-5p	862.6641
62	hsa-miR-103a-3p	841.0173
63	hsa-miR-181c-5p	787.4481
64	hsa-miR-136-3p	783.6147
65	hsa-miR-361-5p	771.282
66	hsa-miR-10b-5p	760.0214
67	hsa-miR-28-3p	702.5677
68	hsa-miR-410-3p	702.5494
69	hsa-miR-409-3p	685.2376
70	hsa-miR-24-3p	665.2599
71	hsa-miR-194-5p	634.4039
72	hsa-miR-429	634.0176
73	hsa-miR-29b-3p	612.2177
74	hsa-miR-136-5p	600.5248
75	hsa-miR-484	580.7374
76	hsa-miR-411-5p	579.5778

77	hsa-miR-432-5p	542.7362
78	hsa-miR-342-3p	533.9539
79	hsa-miR-3168	464.4544
80	hsa-miR-181b-5p	462.2785
81	hsa-miR-320a	460.6484
82	hsa-miR-28-5p	460.326
83	hsa-miR-199a-3p;hsa-miR-199b-3p	450.9452
84	hsa-miR-376c-3p	448.2679
85	hsa-miR-148b-3p	442.8233
86	hsa-miR-199a-5p	440.5607
87	hsa-miR-130a-3p	416.9796
88	hsa-miR-146b-5p	416.6273
89	hsa-miR-744-5p	414.4475
90	hsa-miR-381-3p	409.2744
91	hsa-miR-221-3p	389.9197
92	hsa-miR-485-5p	356.8929
93	hsa-miR-574-3p	335.9766
94	hsa-miR-128-3p	327.2629
95	hsa-miR-301a-3p	323.908
96	hsa-miR-486-5p	307.2739
97	hsa-miR-421	301.1576
98	hsa-miR-425-5p	299.8963
99	hsa-miR-874-3p	280.8262
100	hsa-miR-3607-5p	266.8123

Table A-4. INS-1 cell miRNA export to HDL. Fold change of INS-1-nHDL versus cf-nHDL from n=1 pool of 3 samples.

This table contains small RNA sequencing results of miRNAs exported to HDL from INS-1 cells (n=1). Base mean represents abundance. Fold change of miRNA export between cf-nHDL and INS-1-nHDL. Textual citation is located on page 60.

Feature	DEseq2 (BaseMean)	Fold Change	cf-nHDL (RPM)	INS-1-nHDL (RPM)
rno-miR-375-3p	6132.951	56.03596	14.10	755.72
rno-miR-16-5p	1555.169	0.343913	151.78	49.91
rno-miR-203a-3p	1337.862	4.042332	34.80	134.52
rno-miR-21-5p	449.1478	0.899418	31.02	26.67
rno-miR-10a-5p	397.4127	0.338184	38.95	12.60
rno-miR-22-3p	336.4992	2.271046	13.49	29.30
rno-miR-27b-3p	302.4495	1.55808	15.54	23.10
rno-miR-320-3p	195.859	0.502728	17.10	8.22
rno-miR-125b-2-3p	183.0042	0.624578	14.78	8.82
rno-miR-130a-3p	172.2597	2.458554	6.53	15.36
rno-miR-192-5p	160.0844	8.294808	2.26	17.92
rno-miR-27a-3p	114.328	0.805963	8.33	6.40
rno-miR-378a-3p	109.3488	6.118584	2.01	11.79
rno-miR-182	87.68644	13.49039	0.79	10.24
rno-miR-92a-3p	80.38319	2.139767	3.36	6.87
rno-let-7i-5p	61.54899	6.345834	1.10	6.67
rno-miR-340-5p	54.92498	8.076497	0.79	6.13
rno-miR-26a-5p	49.94882	1.384559	2.75	3.64
rno-miR-141-3p	48.69655	0.230763	5.19	1.15
rno-let-7f-5p	47.94302	6.922716	0.79	5.25
rno-miR-30a-5p	47.08364	9.114886	0.61	5.32
rno-miR-25-3p	42.78739	2.676803	1.53	3.91
rno-miR-30e-5p	38.27605	1.93673	1.71	3.17
rno-miR-103-3p	34.37302	3.922887	0.93	3.46
rno-miR-181a-5p	27.31948	2.668148	0.98	2.49
rno-let-7b-5p	25.56475	17.30648	0.16	3.00
rno-miR-423-5p	25.38629	0.947768	1.71	1.55
rno-miR-30d-5p	25.13523	4.999737	0.55	2.63
rno-let-7c-5p	24.45498	3.776037	0.68	2.44
rno-miR-1224	23.09415	269.6946	0.00	2.90
rno-miR-423-3p	23.02357	0.07525	2.81	0.20

rno-miR-23a-3p	19.47848	0.494492	1.71	0.84
rno-miR-328a-3p	19.26305	40.38068	0.06	2.36
rno-miR-107-3p	17.2223	4.285485	0.41	1.73
rno-miR-92b-3p	16.93596	2.307589	0.67	1.48
rno-miR-23b-3p	16.68557	0.629353	1.34	0.84
rno-miR-148a-3p	16.18446	0.198937	1.77	0.34
rno-miR-664-2-5p	16.1122	188.1568	0.00	0.00
rno-miR-205	16.00532	0.432682	1.47	0.61
rno-let-7d-3p	14.89487	14.9988	0.12	1.75
rno-miR-451-5p	14.788	0.221891	1.59	0.34
rno-miR-140-3p	14.7517	6.922635	0.24	1.62
rno-miR-93-5p	14.3578	14.42192	0.12	1.68
rno-miR-98-5p	13.42683	156.7962	0.00	1.68
rno-miR-151-3p	12.67499	8.076356	0.18	1.41
rno-miR-532-5p	12.2811	25.382	0.06	1.48
rno-miR-26b-5p	12.10263	0.008164	1.59	0.00
rno-let-7g-5p	11.85191	0.157343	1.34	0.20
rno-miR-125a-5p	11.70874	0.048078	1.47	0.07
rno-let-7a-5p	10.81339	0.659325	0.87	0.55
rno-miR-29a-3p	10.5267	6.538005	0.18	1.15
rno-miR-488-3p	10.20439	119.1634	0.00	0.00
rno-miR-142-5p	9.667655	0.384611	0.92	0.34
rno-miR-222-3p	9.667317	112.8912	0.00	1.21
rno-miR-128-3p	9.59573	19.61329	0.06	1.15
rno-miR-133a-3p	9.41693	0.839138	0.67	0.54
rno-miR-132-3p	9.130244	106.6191	0.00	1.15
rno-miR-30d-3p	9.130244	106.6191	0.00	1.15
rno-miR-326-3p	9.130244	106.6191	0.00	1.15
rno-miR-221-3p	8.378409	4.999656	0.18	0.88
rno-miR-106b-3p	8.056098	94.07489	0.00	1.01
rno-miR-421-3p	8.056098	94.07489	0.00	1.01
rno-miR-10b-5p	7.877298	0.692293	0.61	0.40
rno-miR-150-5p	7.340225	0.576914	0.61	0.34
rno-miR-101a-3p	6.981951	81.53067	0.00	0.88
rno-miR-186-5p	6.516803	0.015162	0.85	0.00
rno-miR-1839-5p	6.444878	75.25857	0.00	0.81
rno-miR-191a-5p	6.015355	1.15381	0.37	0.40
rno-miR-409a-3p	5.370732	62.7144	0.00	0.67
rno-miR-101b-3p	5.120345	0.019297	0.67	0.00
rno-miR-129-5p	4.833659	56.44233	0.00	0.61
rno-miR-877	4.833659	56.44233	0.00	0.61
rno-miR-143-3p	4.618897	2.307558	0.18	0.40
rno-miR-126a-5p	4.54731	1.442251	0.24	0.34

rno-miR-652-3p	4.296585	50.17028	0.00	0.54
rno-miR-183-5p	3.759512	43.899	0.00	0.47
rno-miR-127-3p	3.723887	0.026534	0.49	0.00
rno-miR-100-5p	3.258401	0.030324	0.43	0.00
rno-miR-130b-5p	3.258401	0.030324	0.43	0.00
rno-miR-223-3p	3.258401	0.030324	0.43	0.00
rno-let-7e-5p	2.792915	0.035378	0.37	0.00

Part 2: Tables associated with Chapter IV

Table A-5: miRNAs significantly altered between lean and ZDF rat HDL

This table contains small RNA sequencing results of miRNAs altered between lean and ZDF rat HDL. Fold change represents changes in ZDF compared to vehicle. Textual citation is located on page 81.

miRNA	p value	Fold Change	Regulation (vehicle over lean)
rno-miR-126a-5p	0.047122	2.2754908	down
rno-miR-141-3p	0.013316	3.7128687	down
rno-miR-375-3p	0.003009	2.8698032	down
rno-miR-17-5p	0.032104	2.004263	up
rno-miR-181c-5p	0.024541	2.876959	up
rno-miR-181d-5p	5.75E-04	5.433555	up
rno-miR-20a-5p	0.008464	4.769224	up
rno-miR-30c-5p	0.029798	2.5105093	up
rno-miR-32-5p	0.04363	6.4316854	up
rno-miR-328a-3p	0.046543	2.2938426	up
rno-miR-383-5p	0.003591	8.109223	up
rno-miR-6328	0.013518	8.072154	up

Table A-6: miRNAs significantly altered between lean and ZDF rat islets

This table contains small RNA sequencing results of miRNAs altered between lean and ZDF rat islets. Fold change represents changes in ZDF compared to vehicle. Textual citation is located on page 83.

miRNA	p value	Fold Change	Regulation (vehicle over lean)
rno-miR-802-5p	0.021721	1.556291	down
rno-let-7a-1-3p	0.044429	1.579436	down
rno-miR-375-3p	0.005421	1.581197	down
rno-miR-376a-3p	0.043186	1.606522	down
rno-miR-19b-3p	0.018715	1.667735	down
rno-miR-3068-3p	0.025842	1.673637	down
rno-miR-7a-2-3p	0.023498	1.711185	down
rno-miR-29b-3p	0.005431	1.770244	down
rno-miR-379-3p	0.026497	1.832335	down
rno-miR-664-3p	0.029199	1.885253	down
rno-miR-376c-3p	0.029402	1.929296	down
rno-miR-673-5p	0.038315	2.057227	down
rno-miR-377-3p	0.007857	2.083654	down
rno-miR-369-3p	0.023357	2.14252	down
rno-miR-879-5p	0.038309	2.215309	down
rno-miR-127-5p	0.040027	2.330875	down
rno-miR-543-3p	0.007728	2.456091	down
rno-miR-376b-3p	0.014473	2.463802	down
rno-miR-136-3p	0.023427	2.479688	down
rno-miR-6331	0.019655	2.556968	down
rno-miR-141-3p	0.008437	2.628847	down
rno-miR-29c-3p	0.00654	2.638748	down
rno-miR-879-3p	0.026022	2.689521	down
rno-miR-32-5p	0.013021	2.721235	down
rno-miR-16-3p	0.041145	2.781271	down
rno-miR-19a-3p	0.024939	2.926305	down
rno-miR-429	0.011613	3.03188	down
rno-miR-541-3p	0.036023	3.032576	down
rno-miR-129-2-3p	0.016983	3.069091	down
rno-let-7f-2-3p	0.017762	3.086363	down
rno-miR-539-5p	0.003295	3.23044	down
rno-miR-96-5p	0.004131	3.265816	down
rno-miR-184	0.021382	3.564035	down

rno-miR-455-5p	0.006807	3.638431	down
rno-miR-325-3p	0.00719	3.824028	down
rno-miR-582-3p	2.16E-04	3.949415	down
rno-miR-98-3p	0.01266	4.058248	down
rno-miR-129-1-3p	0.004562	4.737846	down
rno-miR-153-5p	0.00413	4.75185	down
rno-miR-374-3p	0.02311	5.592897	down
rno-miR-153-3p	0.003836	5.712057	down
rno-miR-190a-5p	0.024041	6.2499	down
rno-miR-384-5p	0.006157	6.72385	down
rno-miR-137-3p	0.012135	7.864126	down
rno-miR-384-3p	0.003825	9.299411	down
rno-miR-135a-5p	0.004	14.61787	down
rno-miR-194-5p	0.021423	1.529984	up
rno-miR-181c-3p	0.006163	1.571665	up
rno-miR-103-3p	0.007399	1.584178	up
rno-miR-151-5p	0.003539	1.598805	up
rno-miR-30e-3p	0.021546	1.604084	up
rno-miR-24-2-5p	0.004113	1.607601	up
rno-miR-143-3p	0.041226	1.625579	up
rno-miR-125b-2-3p	0.008863	1.641434	up
rno-miR-132-3p	0.00422	1.652053	up
rno-miR-425-5p	0.044211	1.671677	up
rno-miR-30c-2-3p	0.03138	1.679434	up
rno-miR-450a-5p	0.044191	1.681366	up
rno-miR-15b-5p	2.81E-05	1.716578	up
rno-let-7i-5p	9.00E-04	1.747268	up
rno-let-7d-5p	0.004151	1.767884	up
rno-miR-16-5p	0.00817	1.786828	up
rno-miR-653-5p	0.036792	1.798326	up
rno-miR-191a-5p	0.030341	1.815817	up
rno-miR-212-3p	0.029503	1.822599	up
rno-miR-17-5p	0.04512	1.893059	up
rno-miR-181c-5p	0.027256	1.924673	up
rno-miR-28-3p	5.52E-04	1.964873	up
rno-miR-322-5p	0.008399	1.971495	up
rno-miR-10a-5p	0.004099	2.000766	up
rno-miR-181a-1-3p	0.01823	2.041981	up
rno-miR-30a-3p	0.010438	2.062502	up
rno-miR-541-5p	0.001133	2.066275	up
rno-miR-181d-5p	0.005312	2.157162	up
rno-miR-200a-5p	0.01215	2.159839	up
rno-miR-378b	0.026696	2.202257	up

rno-miR-383-5p	0.001772	2.205044	up
rno-let-7c-5p	0.007822	2.224868	up
rno-miR-351-5p	0.048204	2.228974	up
rno-miR-1839-5p	0.019383	2.270553	up
rno-miR-378a-3p	0.012848	2.283531	up
rno-miR-217-5p	0.027759	2.299917	up
rno-miR-99b-3p	0.015309	2.303878	up
rno-miR-100-5p	0.002962	2.343879	up
rno-miR-540-3p	7.90E-04	2.353819	up
rno-miR-23a-3p	0.003714	2.360713	up
rno-miR-667-5p	0.022102	2.3872	up
rno-miR-221-3p	0.004663	2.467702	up
rno-miR-130a-3p	1.19E-06	2.484824	up
rno-miR-10a-3p	0.01002	2.511794	up
rno-miR-140-3p	4.35E-04	2.520984	up
rno-miR-3074	0.01378	2.557747	up
rno-miR-6328	0.027372	2.572884	up
rno-miR-125b-1-3p	0.037125	2.641316	up
rno-miR-3559-3p	0.028854	2.697952	up
rno-miR-151-3p	0.002291	2.706763	up
rno-miR-28-5p	2.82E-04	2.738832	up
rno-miR-146a-5p	0.007764	2.752401	up
rno-let-7b-5p	0.010688	2.755107	up
rno-miR-770-3p	0.007998	2.79297	up
rno-miR-181b-5p	0.0066	2.848137	up
rno-miR-379-5p	0.018845	2.862084	up
rno-miR-21-5p	0.001609	2.944074	up
rno-miR-483-5p	0.015251	2.955508	up
rno-miR-30b-3p	0.005522	3.01701	up
rno-miR-34c-5p	0.002911	3.024271	up
rno-miR-195-3p	0.009773	3.061512	up
rno-miR-25-5p	0.01416	3.115965	up
rno-miR-320-3p	0.02899	3.199146	up
rno-miR-145-5p	0.0198	3.236525	up
rno-miR-139-5p	0.003848	3.255921	up
rno-miR-93-5p	0.006766	3.274971	up
rno-miR-542-3p	0.025075	3.343873	up
rno-miR-133a-3p	5.53E-04	3.416051	up
rno-miR-322-3p	0.003361	3.435008	up
rno-miR-195-5p	9.45E-05	3.437073	up
rno-miR-216a-3p	0.016143	3.516965	up
rno-miR-674-5p	0.009708	3.607291	up
rno-miR-382-5p	0.009822	3.689679	up

rno-miR-199a-5p	0.006853	3.697531	up
rno-miR-378a-5p	0.03975	3.826814	up
rno-miR-130b-3p	0.003938	3.828429	up
rno-miR-150-3p	0.038751	4.000069	up
rno-miR-497-5p	9.15E-04	4.04014	up
rno-miR-218a-5p	6.00E-04	4.164922	up
rno-miR-542-5p	0.005916	4.289298	up
rno-miR-3585-5p	0.00655	4.42236	up
rno-miR-181a-5p	0.003282	4.606157	up
rno-miR-511-3p	0.001723	4.923221	up
rno-miR-10b-3p	0.004665	5.065116	up
rno-miR-92a-1-5p	0.001993	5.351742	up
rno-miR-326-3p	0.03207	5.503743	up
rno-miR-383-3p	0.025087	5.648245	up
rno-miR-218a-1-3p	0.002393	5.810829	up
rno-miR-3585-3p	0.028813	6.304665	up
rno-miR-708-5p	0.005808	6.659512	up
rno-miR-504	0.002308	6.759511	up
rno-miR-199a-3p	4.30E-04	6.989774	up
rno-miR-214-3p	2.58E-04	8.999195	up
rno-miR-708-3p	0.001855	23.97926	up

Table A-7: Human subject characteristics

This table contains subject characteristics of control and T2D subjects, including treatment, gender, race, age, and fasting glucose levels. Textual citation is located on page 83.

Group	Naïve/washout	Gender	Race	Age	HbA1c (%)	Fasting Glucose (mmol/l)
Control	-	M 7; F 13	White 18; Black 2	42 +/-10.06		-
T2D	Naïve 13; Washout 3	M 11; F 5	White 14; Black 1; Asian 1	51 +/-11.27	7.86 +/-0.84	7.84 +/-1.94

Table A-8: miRNAs expressed in plasma from healthy and T2D human subjects

This table contains small RNA sequencing results of miRNAs altered between healthy and T2D plasma. Fold change represents changes in T2D compared to healthy. Textual citation is located on page 83.

miRNA	Base Mean	P value	Bonferonni adjusted pvalue	Fold Change	Regulation (T2D over healthy)
hsa-miR-423-3p	6836.569095	0.993429	0.993429	1.003346	down
hsa-let-7d-3p	3395.365985	0.981693	0.988326	1.00837	down
hsa-miR-16-2-3p	951.5858763	0.980352	0.988326	1.011575	down
hsa-let-7g-5p	21434.76665	0.901016	0.952137	1.044609	down
hsa-miR-222-3p	3074.087025	0.909225	0.954045	1.047828	down
hsa-miR-181a-5p	1982.280195	0.895941	0.952137	1.056305	down
hsa-miR-128-3p	1833.523848	0.888225	0.952126	1.057756	down
hsa-miR-484	3376.456548	0.868721	0.937967	1.06042	down
hsa-miR-146a-5p	13038.92803	0.827518	0.913335	1.072658	down
hsa-let-7i-5p	17696.75283	0.8258	0.913335	1.079837	down
hsa-miR-99b-5p	763.4798084	0.856918	0.931977	1.084641	down
hsa-miR-16-5p	26690.46301	0.78515	0.906879	1.10291	down
hsa-miR-107	260.2403781	0.819118	0.913335	1.106829	down
hsa-miR-501-3p	284.8829421	0.824212	0.913335	1.112472	down
hsa-miR-328-3p	556.7696553	0.827006	0.913335	1.113121	down
hsa-miR-221-3p	11118.51803	0.714103	0.879972	1.133634	down
hsa-miR-1307-3p	370.7156113	0.773488	0.900388	1.150593	down
hsa-miR-4433b-5p	3830.096671	0.685861	0.869679	1.156942	down
hsa-miR-431-5p	157.2400775	0.765798	0.900388	1.157839	down
hsa-miR-15b-3p	338.1771526	0.755781	0.900388	1.164921	down
hsa-miR-150-5p	1403.105748	0.722552	0.882462	1.165387	down
hsa-miR-30c-5p	4211.569032	0.67167	0.869679	1.173209	down
hsa-miR-744-5p	165.094308	0.740681	0.897248	1.175437	down
hsa-miR-877-5p	332.5686205	0.714608	0.879972	1.195242	down
hsa-miR-340-3p	248.1859434	0.707799	0.879972	1.202557	down
hsa-miR-30a-5p	1166.852588	0.640186	0.847034	1.204666	down
hsa-miR-574-3p	208.7569705	0.688508	0.869679	1.217606	down
hsa-miR-185-5p	2122.664598	0.629212	0.847034	1.223195	down
hsa-miR-30d-5p	38494.60356	0.509326	0.816018	1.238348	down
hsa-miR-363-3p	617.3140764	0.651471	0.851484	1.246829	down
hsa-miR-340-5p	997.6118432	0.633615	0.847034	1.24998	down
hsa-miR-361-5p	591.5848274	0.642381	0.847034	1.250539	down
hsa-miR-543	590.8481312	0.627099	0.847034	1.267628	down

hsa-miR-382-5p	1043.187067	0.606052	0.845489	1.271294	down
hsa-miR-532-5p	303.4917168	0.607163	0.845489	1.287802	down
hsa-miR-425-3p	289.9160709	0.594324	0.843375	1.298643	down
hsa-miR-335-5p	866.3113851	0.588116	0.842589	1.298668	down
hsa-miR-151a-5p	2980.7239	0.556806	0.821014	1.300838	down
hsa-miR-191-5p	8032.867153	0.484373	0.793094	1.307481	down
hsa-miR-197-3p	584.4946091	0.559443	0.821014	1.318302	down
hsa-miR-323a-3p	402.4579312	0.561041	0.821014	1.329264	down
hsa-miR-335-3p	451.9320244	0.56022	0.821014	1.332043	down
hsa-miR-130b-5p	315.7665149	0.541572	0.821014	1.337926	down
hsa-miR-146b-5p	2674.228441	0.470943	0.789349	1.354624	down
hsa-miR-3615	318.8373353	0.524532	0.821014	1.364163	down
hsa-miR-140-3p	5061.427943	0.411154	0.789349	1.380966	down
hsa-miR-505-3p	335.1560155	0.499017	0.808191	1.394894	down
hsa-miR-1260a	382.5090561	0.471576	0.789349	1.396443	down
hsa-miR-652-3p	2724.302389	0.447144	0.789349	1.40722	down
hsa-miR-99a-5p	251.6698083	0.474639	0.789349	1.407822	down
hsa-miR-23b-3p	1810.285647	0.430432	0.789349	1.411348	down
hsa-miR-224-5p	829.2069518	0.476788	0.789349	1.417451	down
hsa-miR-409-3p	2726.918028	0.452424	0.789349	1.42041	down
hsa-miR-103a-3p	8003.742456	0.318757	0.765592	1.423556	down
hsa-miR-432-5p	2334.548437	0.429917	0.789349	1.428776	down
hsa-miR-485-3p	383.7591172	0.467569	0.789349	1.42991	down
hsa-miR-26b-5p	16841.7105	0.306349	0.765592	1.441639	down
hsa-miR-584-5p	2873.144832	0.342829	0.765592	1.441864	down
hsa-miR-106b-5p	410.7050552	0.452509	0.789349	1.447072	down
hsa-miR-329-3p	462.8143144	0.445554	0.789349	1.455937	down
hsa-miR-29a-3p	756.3502444	0.384611	0.774419	1.460582	down
hsa-miR-28-5p	433.9256812	0.438066	0.789349	1.463182	down
hsa-miR-28-3p	2515.684291	0.406672	0.789349	1.473468	down
hsa-miR-151a-3p	6999.095666	0.256366	0.694518	1.492993	down
hsa-miR-106b-3p	732.9412366	0.371155	0.766893	1.518665	down
hsa-miR-30b-5p	936.9901684	0.351503	0.765592	1.54229	down
hsa-miR-654-3p	419.0047899	0.375726	0.766893	1.54305	down
hsa-miR-1260b	1082.159824	0.264163	0.698959	1.546352	down
hsa-miR-142-5p	2811.502087	0.243008	0.694518	1.546637	down
hsa-miR-326	504.9167528	0.369295	0.766893	1.555802	down
hsa-miR-3613-5p	588.2123757	0.339942	0.765592	1.556368	down
hsa-miR-323b-3p	446.6858584	0.353929	0.765592	1.573654	down
hsa-miR-19b-3p	683.0367165	0.349388	0.765592	1.576251	down
hsa-miR-144-3p	1103.834759	0.343605	0.765592	1.57829	down
hsa-miR-361-3p	552.5422202	0.334453	0.765592	1.604864	down
hsa-miR-126-5p	4215.262083	0.180724	0.668282	1.627098	down

hsa-miR-495-3p	363.1001669	0.321502	0.765592	1.628215	down
hsa-miR-425-5p	3149.578914	0.21277	0.668282	1.658486	down
hsa-miR-101-3p	2662.624429	0.192182	0.668282	1.670338	down
hsa-miR-23a-3p	17941.03373	0.122631	0.666191	1.709289	down
hsa-miR-143-3p	5143.602452	0.224256	0.668282	1.710563	down
hsa-miR-148a-3p	2460.572444	0.180174	0.668282	1.720683	down
hsa-miR-29c-3p	300.8374122	0.267387	0.698959	1.725268	down
hsa-miR-148b-3p	1789.647047	0.210354	0.668282	1.750177	down
hsa-miR-181b-5p	277.6322056	0.252356	0.694518	1.751797	down
hsa-miR-324-3p	257.3362696	0.254774	0.694518	1.751881	down
hsa-miR-30e-3p	1013.41431	0.217465	0.668282	1.784133	down
hsa-miR-98-5p	5470.265032	0.141176	0.668282	1.799488	down
hsa-miR-142-3p	1610.083323	0.230006	0.671977	1.80088	down
hsa-miR-21-5p	36812.29494	0.085972	0.661615	1.809298	down
hsa-miR-27b-3p	3601.122129	0.111121	0.662282	1.818253	down
hsa-miR-22-3p	10987.0613	0.087685	0.661615	1.831674	down
hsa-miR-155-5p	570.5318604	0.210907	0.668282	1.851489	down
hsa-miR-24-3p	13950.76301	0.100024	0.662282	1.872671	down
hsa-miR-30e-5p	8085.802316	0.052984	0.661615	1.89425	down
hsa-miR-379-5p	645.1586706	0.191195	0.668282	1.900198	down
hsa-miR-199a-3p	4895.254177	0.12519	0.666191	1.906343	down
hsa-miR-26a-5p	37871.64267	0.069979	0.661615	1.915695	down
hsa-miR-20a-5p	985.6463465	0.165317	0.668282	1.91634	down
hsa-miR-186-5p	1622.675731	0.150583	0.668282	1.923134	down
hsa-miR-487b-3p	997.9372715	0.157168	0.668282	1.988158	down
hsa-miR-223-3p	25387.90224	0.054393	0.661615	2.035641	down
hsa-miR-17-5p	793.755845	0.136622	0.668282	2.072876	down
hsa-miR-145-5p	271.7650446	0.133299	0.668282	2.093974	down
hsa-miR-126-3p	8439.304915	0.067112	0.661615	2.121866	down
hsa-miR-15b-5p	2694.056217	0.076343	0.661615	2.169048	down
hsa-miR-374b-5p	590.6402211	0.098098	0.662282	2.250344	down
hsa-miR-15a-5p	2440.93375	0.082219	0.661615	2.293848	down
hsa-miR-493-5p	1185.926321	0.058739	0.661615	2.472929	down
hsa-miR-199a-5p	965.5631731	0.059311	0.661615	2.503594	down
hsa-miR-339-5p	598.0365487	0.053096	0.661615	2.562983	down
hsa-miR-27a-3p	3470.344366	**0.01469**	0.62919	2.796367	down
hsa-miR-369-3p	1591.574448	**0.020749**	0.62919	3.029218	down
hsa-miR-4433b-3p	574.1665184	0.960588	0.980326	1.024529	up
hsa-let-7f-5p	42877.26027	0.945079	0.97115	1.02465	up
hsa-miR-1-3p	817.9044739	0.936665	0.969188	1.03316	up
hsa-miR-93-5p	5082.610401	0.929227	0.968215	1.036943	up
hsa-miR-574-5p	473.6117764	0.848127	0.929198	1.095222	up
hsa-miR-182-5p	1712.245401	0.813948	0.913335	1.1104	up

hsa-miR-183-5p	651.4491727	0.772559	0.900388	1.151354	up
hsa-miR-342-3p	1274.365097	0.747373	0.898053	1.155929	up
hsa-miR-625-3p	337.7914492	0.688739	0.869679	1.217856	up
hsa-miR-125a-5p	1507.831346	0.583506	0.842589	1.247883	up
hsa-miR-139-5p	531.7945486	0.638755	0.847034	1.259383	up
hsa-let-7d-5p	7109.533138	0.528135	0.821014	1.279634	up
hsa-miR-92a-3p	92393.49477	0.361427	0.766893	1.298197	up
hsa-let-7e-5p	2144.488585	0.542457	0.821014	1.305187	up
hsa-miR-7-5p	504.6959124	0.562037	0.821014	1.319625	up
hsa-miR-320a	46287.16221	0.304295	0.765592	1.391275	up
hsa-miR-10a-5p	3125.288163	0.354536	0.765592	1.40012	up
hsa-miR-320c	199.25222	0.407776	0.789349	1.426849	up
hsa-miR-320d	75.28992301	0.423358	0.789349	1.453709	up
hsa-miR-25-3p	13409.62117	0.221788	0.668282	1.490837	up
hsa-miR-10b-5p	2804.993137	0.150885	0.668282	1.519749	up
hsa-let-7a-5p	59654.62939	0.17096	0.668282	1.61247	up
hsa-miR-423-5p	25765.5141	0.060407	0.661615	1.723934	up
hsa-miR-92b-3p	431.4677023	0.20234	0.668282	1.724695	up
hsa-let-7b-5p	62349.74241	0.088807	0.661615	1.730362	up
hsa-miR-486-3p	280.4834484	0.197041	0.668282	1.840286	up
hsa-miR-192-5p	322.103084	0.196799	0.668282	1.850974	up
hsa-miR-451a	105579.1735	0.056878	0.661615	1.87352	up
hsa-miR-375	589.7221614	0.162728	0.668282	1.885627	up
hsa-miR-320b	388.1569362	0.107449	0.662282	1.896215	up
hsa-let-7c-5p	1065.612802	0.077085	0.661615	2.062636	up
hsa-miR-100-5p	859.1912333	0.117401	0.666191	2.079814	up
hsa-miR-483-5p	223.500445	0.105419	0.662282	2.219623	up
hsa-miR-122-5p	21024.43168	**0.001887**	0.140613	2.707334	up
hsa-miR-1246	188.8651491	**0.021114**	0.62919	3.069861	up
hsa-miR-486-5p	81186.82517	**4.31E-06**	0.000641	3.299544	up

Bold denotes statistical significance ($p<0.05$)

Table A-9: miRNAs expressed on HDL from healthy and T2D human subjects

This table contains small RNA sequencing results of miRNAs altered between healthy and T2D HDL. Fold change represents changes in T2D compared to healthy. Textual citation is located on page 85.

miRNA	Base Mean	P value	Bonferonni adjusted pvalue	Fold Change	Regulation (T2D over healthy)
hsa-let-7b-5p	265.7055	0.978777	0.978777	1.012645	down
hsa-miR-92a-3p	464.5135	0.950506	0.978777	1.028771	down
hsa-miR-451a	625.4701	0.917017	0.978777	1.043321	down
hsa-miR-423-5p	155.5234	0.812266	0.978777	1.125674	down
hsa-let-7a-5p	386.1547	0.702914	0.954184	1.184615	down
hsa-let-7f-5p	159.6857	0.708202	0.954184	1.203293	down
hsa-miR-30d-5p	249.2574	0.635364	0.954184	1.250871	down
hsa-miR-16-5p	116.9788	0.650126	0.954184	1.251063	down
hsa-miR-486-5p	511.1525	0.199811	0.53283	1.804153	down
hsa-miR-203a-3p	260.2914	0.189238	0.53283	1.826724	down
hsa-miR-21-5p	434.3783	0.152948	0.53283	1.94085	down
hsa-miR-100-5p	337.5996	0.160032	0.53283	2.009662	down
hsa-miR-1-3p	360.0855	0.093021	0.53283	2.140136	down
hsa-miR-27a-3p	57.44772	0.715638	0.954184	1.184142	up
hsa-miR-27b-3p	97.59753	0.53041	0.954184	1.341738	up
hsa-miR-320a	203.6793	**0.02793**	0.446874	2.927267	up

Bold denotes statistical significance ($p<0.05$)

Part 3: Tables associated with Chapter V

Table A-10: Colesevelam-induced liver miRNA changes in ZDF rats.

This table contains small RNA sequencing results of hepatic miRNAs altered between ZDF vehicle and colesevelam treated rats. Fold change represents changes with colesevelam compared to vehicle treatment. Textual citation is located on page 105.

miRNA	Fold Change	p value
rno-miR-183-5p	4.74	1.85E-05
rno-miR-182	4.00	4.27E-06
rno-miR-146b-5p	2.13	2.78E-02
rno-miR-146a-5p	1.97	3.25E-02
rno-miR-92a-3p	0.59	3.62E-02
rno-miR-145-5p	0.53	3.08E-02
rno-miR-30c-2-3p	0.51	3.09E-02
rno-miR-30c-5p	0.51	4.14E-02
rno-miR-30d-5p	0.50	1.01E-02
rno-miR-122-3p	0.49	2.28E-02
rno-miR-31a-5p	0.49	1.83E-02
rno-miR-339-5p	0.48	2.86E-02
rno-miR-322-3p	0.48	3.84E-02
rno-miR-320-3p	0.48	2.62E-02
rno-miR-1247-5p	0.46	2.52E-02
rno-miR-139-5p	0.45	3.43E-02
rno-miR-148a-5p	0.43	1.77E-02
rno-miR-28-5p	0.42	5.76E-03
rno-miR-21-3p	0.42	6.35E-03
rno-miR-181c-5p	0.41	2.02E-02
rno-let-7d-3p	0.39	1.86E-03
rno-miR-532-5p	0.38	1.18E-02
rno-miR-423-3p	0.37	2.62E-04
rno-miR-674-3p	0.37	1.59E-02
rno-miR-361-3p	0.34	5.95E-03
rno-miR-150-5p	0.33	5.46E-04
rno-miR-423-5p	0.30	1.85E-03
rno-miR-3577	0.22	5.62E-04
rno-miR-193a-3p	0.17	1.62E-04

Part 4: Modified PAR-CLIP protocol to trace INS-1 originating miRNAs to Huh7 and HCAECs *in vitro*

Preface

A key question in the field of HDL-miRNAs is whether HDL-miRNAs can be delivered to recipient tissues and whether HDL-miRNAs function as canonical miRNAs once they are delivered to cells. Seminal studies from the Vickers lab have shown that a myeloid-enriched miRNA, miR-223, is exported from J774 macrophages to HDL and that HDL can deliver miR-223 to Huh7 hepatoma cells *in vitro*(94). Additionally, the lab has shown that HDL-miR-223, can be delivered to human coronary aortic endothelial cells (HCAECs) and directly target ICAM1(95). Despite these advances suggesting that HDL-miRNAs can be delivered to recipient cells, to date, no one has definitively shown through labelling approaches that miRNAs secreted from one cell can be delivered to a recipient cell *in vitro* or *in vivo*.

To address this question, a modification was introduced to the technique for photoactivatable ribonucleoside-enhanced crosslinking and IP (PAR-CLIP)(266) to label miRNAs in beta cell lines and trace their trafficking and loading into the RISC in recipient hepatoma and endothelial cells. In 2010, Hafner and colleagues published a study reporting a protocol which uses a photoactivatable nucleoside analog, 4-thiouridine (4SU) incorporated into transcripts of cultured cells that upon crosslinking undergoes a thymidine (T) to cytidine (C) transition that can be identified by sequencing(266) (Figure A-1A). The goal of this study was to modify this technique to label beta cells (INS-1 or MIN6) in culture with 4SU and then allow labelled RNAs to be exported to HDL and taken up by recipient cells (Huh7 or HCAECs). The recipient cells were then crosslinked with 365nm light which results in a covalent bond between 4SU and adjacent amino acids, prior to Ago2 IP(266). As such, only beta cell originating miRNAs would contain the photoactivatable base and hence, reads containing a T->C mutation would correspond to RNAs transcribed in either INS-1 or MIN6 cells depending on the experiment (Figure A-1B). The goal of

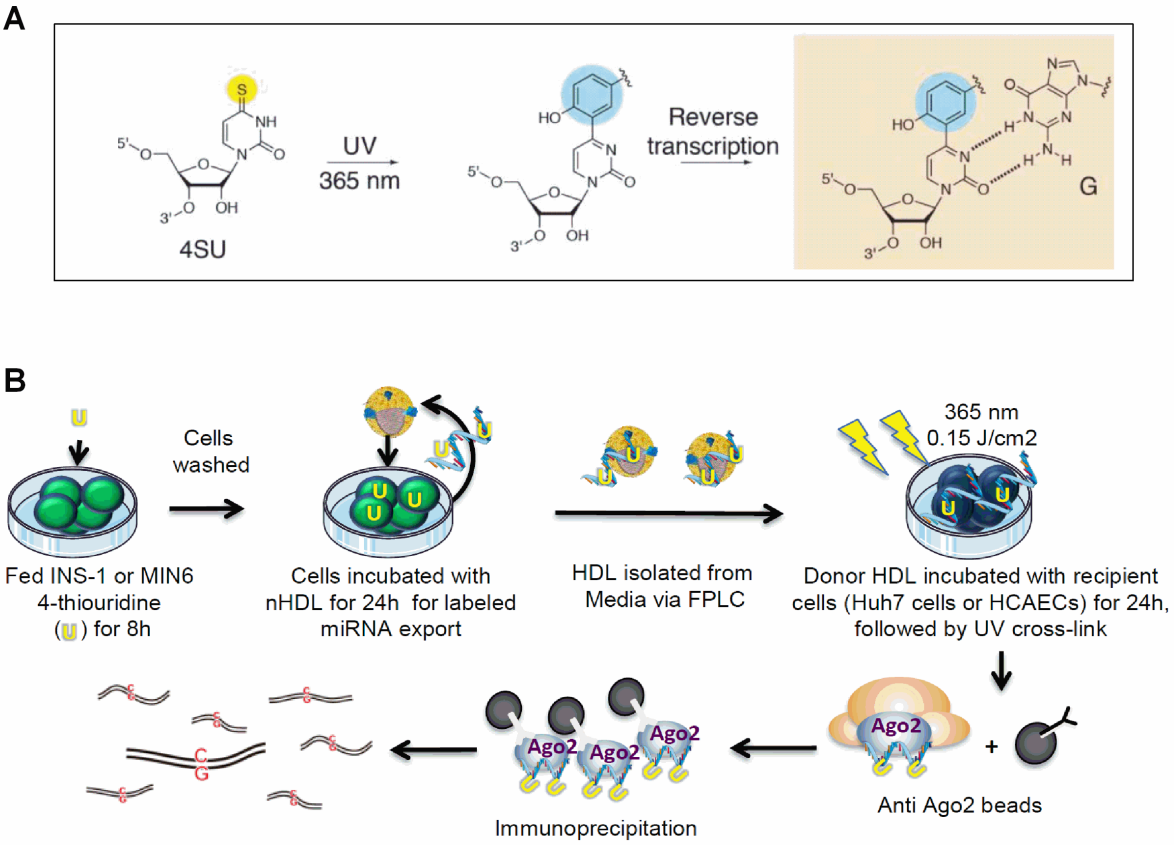

Figure A-1. Schematic of Trans-PAR-CLIP protocol modified from Modified from Hafner et. al. Cell 2010. (A) Chemical structure of 4SU (left), structure upon crosslinking to amino acids (middle) and base pairing to guanine (right). From: Ascano et. al., Identification of RNA-protein interaction networks using PAR-CLIP, WIREs RNA 2012, 3:159–177. (B) Graphical schematic of Trans-PAR-CLIP steps. Briefly, INS-1 or MIN6 cells were labelled with 4-thiouridine for 48h, and then washed and incubated with nHDL for 24h to allow for export of labelled miRNAs to HDL. HDL was then isolated from the medium by FPLC. Donor cells (Huh7 or HCAECs) were then incubated with HDL for 24h to allow delivery of labelled beta-cell originating HDL-miRNA to Huh7 or HCAECs. Recipient cells were then crosslinked and immunoprecipitated using Ago2 antibodies, and Ago2-bound small-RNAs were sequenced for presence of T-C mutation originating from crosslink of the 4-thiouridine label.

using trans-PARCLIP was two-fold; to develop a proof of concept to use this technique for tracing miRNAs delivery via HDL, and to test whether HDL-miRNAs are loaded into Ago2 or Ago3 complexes in recipient cells.

Materials and Methods

Cell Culture

INS-1 832/13 were cultured in RPMI (Invitrogen) supplemented with 10% FBS, 100 U/ml penicillin and 100 ug/ml streptomycin (Invitrogen), 10mM HEPES (Invitrogen), 2mM L-glutamine (Invitrogen), 1mM Sodium-pyruvate (Invitrogen), 0.05mM 2-mercaptoethanol (Sigma) and maintained at 37°C with 5% CO_2. MIN6 cells were cultured in DMEM (Invitrogen) supplemented with 10% FBS, 100 U/ml penicillin and 100 ug/ml streptomycin (Invitrogen), 1mM Sodium-pyruvate (Invitrogen), 0.05mM 2-mercaptoethanol (Sigma) and maintained at 37°C with 5% CO_2. HCAECs (Lonza) were cultured in Endothelial Basal Medium supplemented with EGM-2 bullet kit (Lonza), 5% FBS (Lonza) and 100 U/ml penicillin and 100 ug/ml streptomycin (Invitrogen). Huh7 cells were cultured in DMEM (Invitrogen) supplemented with with 10% FBS, 100 U/ml penicillin and 100 ug/ml streptomycin (Invitrogen).

HDL Isolation

HDL used for these studies was isolated from normal patients at Vanderbilt University Medical Center as approved by IRB# 151573 or obtained from Vanderbilt blood bank discarded plasma. Blood collections were carried out in accordance with the IRB guidelines and informed consent was obtained from all participants and/or their legal guardians. HDL was isolated from human plasma by density gradient ultra-centrifugation (DGUC, 1.061-1.21 g/mL), 330,000 x g followed by 3 days of dialysis at 4°C in 1x PBS.

Trans-PAR-CLIP

The following protocol was adapted from a methods publication describing the step-by-step protocol for PAR-CLIP(300, 301), with additional steps to label miRNAs in MIN6 or INS-1 cells and then perform the PAR-CLIP protocol in recipient Huh7 or HCAECs. MIN6, INS-1, Huh7 or HCAEC cells were seeded in 150mm cell culture plates ($5x10^6$/dish) and grown to confluency for 3 days. Donor cells (INS-1 or MIN6) were washed with 1x PBS and then treated with 100mM 4SU for 8h. Cells were then incubated in FBS-free medium supplemented with 1mg/ml HDL for 24h. The medium was then removed, concentrated and HDL was isolated using FPLC. HDL fractions were concentrated and 1mg/ml was used to treat recipient cells (Huh7 or HCAECs) for 24h. Cells were washed with 1x PBS and crosslinked with 365nm UV light ($0.15J/cm^2$) and scraped in 1x PBS. Cells were pelleted by centrifugation and lysed with 1x NP lysis buffer (5x NP lysis buffer: 50mM HEPES, pH 7.5, 150mM KCl, 2mM EDTA, 1mM NaF, 0.5% (v/v) NP40, 0.5mM DTT, complete EDTA-free protease inhibitory cocktail (Roche)) on ice for 10 minutes. Cell lysates were cleared by centrifugation and incubated with 1U/ul RNAse T1 (ThermoFisher) at 22 °C for 15 min and then on ice for 5 min. PureProteome NHS FlexiBind Magnetic Beads (Millipore) were complexed to either 75ug Ago2 (Monoclonal Anti-Ago2, clone 11A9, Batch 023M4810V, Sigma) or 50ug Ago3 (Monoclonal Anti-Ago3, Cat# MABE144, Lot 2006946, Millipore) antibodies according to manufacturer's recommendations. Ago2- and Ago3-bound magnetic beads were then incubated with partial RNase T1-treated cell lysate at 4°C overnight. Beads were washed with 1x NP lysis buffer 4 times and were then incubated with 100U/µl RNAse T1 at 22 °C for 15 min and then on ice for 5 min. Beads were then washed in high salt wash buffer (50mM HEPES–KOH, pH 7.5, 500mM KCl, 0.05% (v/v) NP40, 0.5mM DTT, complete EDTA-free protease inhibitor cocktail (Roche)) and dephosphorylated in dephosphorylation buffer (50mM Tris–HCl, pH 7.9, 100mM NaCl, 10mM MgCl2, 1mM DTT) with 0.5U/ul calf intestinal alkaline phosphatase (New England Biolabs) at 37°C for 10 min. Beads were then washed twice with 1x NP lysis buffer and twice with polynucleotide kinase (PNK) buffer (50mM Tris–HCl, pH 7.5, 50mM NaCl, 10mM

$MgCl_2$). Radiolabeling of RNA was performed in PNK buffer with DTT (50mM Tris–HCl, pH 7.5, 50mM NaCl, 10mM $MgCl_2$, 5 mM DTT) with 1U/ul T4 PNK (New England Biolabs), 0.5 µCi/µl (1.6 µM ATP) γ-^{32}P-ATP (Perkin Elmer) for 30 minutes at 37°C. Non-radioactive ATP (New England Biolabs) was then added to obtain a final concentration of 100µM and incubated at 37 °C for another 5 min. Beads were then washed five times with PNK buffer. Samples were then denatured in 1x NuPAGE LDS Sample Buffer (ThermoFisher) at 95°C for 5 mins. Supernatants containing radiolabeled RNAs were then loaded onto 4–12 % Bis-Tris polyacrylamide gel and separated by gel electrophoresis. Gels were imaged for ^{32}P and bands containing radiolabel at expected Ago2 or Ago3 size were excised from gel and electroeluted in D-Tube Dialyzer Mini tubes (Millipore) at 100V. Proteins were digested in 1x proteinase K digestion buffer (2x proteinase K buffer: 100 mM Tris–HCl, pH 7.5 150 mM NaCl, 12.5 mM EDTA, 2 % (w/v) SDS) containing 1.2mg/ml of proteinase K (stock 20mg/ml, Macherey-Nagel) at 55°C for 30 minutes followed by incubation on ice. RNA was isolated using the Total RNA purification kit (Norgen Biotek) according to manufacturer's instruction.

Library Preparation and Sequencing

RNA from Trans-PAR-CLIP was prepared for sequencing using the TruSeq Small RNA Library preparation kits according to manufacturer's instructions with minor modifications described next (Illumina). 20ng of immunoprecipitated RNA was used for library preparation, rather than the recommended 1ug of total RNA. To reduce the likelihood or adapter-adapter dimers, one tenth of the recommended 3' and 5' adapter concentrations were used in the library preparation. PCR amplification of cDNA libraries were performed for 25 cycles. Prior to sequencing samples, small-RNA sequencing libraries were size-selected by Pippin-Prep (Sage Science) to collect cDNA 135-200 nts in length. Individual libraries were purified and concentrated using the DNA Clean and Concentrator 5 kit (Zymo), tested for quality (High-Sensitivity DNA chips, 2100 Bioanalyzer, Agilent), and quantified (High-Sensitivity DNA assays, Qubit, Life

Technologies). Equal concentrations samples were pooled for multiplex sequencing and concentrated using the DNA Clean and Concentrator 5 kit (Zymo). Single-end sequencing of multiplexed libraries was performed on an Illumina HiSeq2500 sequencer SE50 at the Vanderbilt Technologies for Advanced Genomics (VANTAGE) core. Cutadapt(302) was used to trim 3' adapters for raw reads. Quality control on both raw reads and adaptor-trimmed reads was performed using FastQC (www.bioinformatics.babraham.ac.uk/projects/fastqc). All reads with lengths less than 16nts in length were discarded. The adaptor-trimmed reads were formatted into a non-redundant FASTQ file, where the read sequence and copy number was recorded for each unique tag. The usable unique reads were mapped to the whole mouse genome by Bowtie1 (v1.1.2)(181) allowing only one mismatch. T->C mutations were analyzed using PARALYZER(303). 6 nucleotide sequences containing the seed sequences of miRNAs were queried in annotated 3' UTR of genes to pair miRNAs with predicted mRNA binding sequences.

Results and Discussion

This protocol took advantage of random incorporation of photoactivatable nucleoside analogs into RNA *in vitro* in beta cell lines (Figure A-1B). MIN6 and INS-1 cells were treated with 4SU to allow labeling of actively transcribed RNAs with this nucleoside analog. I have previously shown that MIN6 and INS-1 cells can export miRNAs to HDL (Chapter III), therefore these cells were treated with HDL for 24h to allow for export of labelled (and unlabeled) miRNAs. HDL was then repurified from conditioned medium and used to treat Huh7 or HCAECs to trace labelled miRNAs delivered to hepatoma (Huh7) or endothelial (HCAECs) cells.

PAR-CLIP takes advantage of the chemical properties of 4SU; upon crosslinking, the thiol group in 4SU forms a covalent bond with adjacent amino acids (phenylalanine, tyrosine, tryptophan, lysine and cysteine) that shift the hydrogen bonding capacity to favor base pairing with guanine over adenosine, resulting in a T->C mutation detectable by sequencing (Figure A-1A) (304). Three experiments were performed to track miRNAs from INS-1 cells to Huh7, INS-1

cells to HCAECs and MIN6 cells to Huh7 cells and incorporated into Ago2 and Ago3 in the recipient cells (Table A-11). With the exception of INS1 to Huh7 in Ago3, greater than 2000 sequenced reads were mapped to miRNAs. Of these, 2.63% to 13.5% of reads contained a T->C mutation (Table A-11). I have previously shown that INS-1 and MIN6 cells export miR-375-3p to HDL (Chapter III), therefore the number of miR-375-3p reads containing T->C mutations were also examined. The number of miR-375-3p reads containing the T->C mutation ranged from 25.46% to 91.30% (Table A-11). INS-1 to Huh7 in Ago2 and Ago3 had the lowest rates of T->C, and surprisingly, there was very little difference between the T->C rates in Ago2 versus Ago3; in fact, the number of reads, and the T->C mutation rate was rather consistent within the same experiment, regardless of the protein used to IP miRNAs (Table A-11). Three other miRNAs were found with high rates of T->C, miR-532-5p (INS-1 to Huh7; Ago2, 100%), miR-182 (INS-1 to Huh7; Ago2, 2.03% and INS-1 to HCAEC; Ago3, 2.26%) and miR-30a-5p (MIN6 to Huh7; Ago3, 5.06%) (Table A-11). While this study was able to generate results and detect a T->C mutation, trans-PAR-CLIP contains multiple steps that will need to be optimized for further use and to facilitate interpretation of the data.

This study did not measure the rate of incorporation of 4SU into MIN6 or INS-1 cells, but Hafner *et al.* reported that at 100mM, 4SU resulted in up to 4% incorporation into nascent RNAs in HEK cells(266, 304). Using this approximation, I estimate that for every 25 U, 1 will be labelled with 4SU; factoring in that U make up 25% of the RNA bases, on average, for every 100 bases, 1 base will be 4SU labelled. miRNAs are 20-25 nts in length, and based on the above calculation, only 1 in every 4-5 miRNA transcripts will contain a label. Furthermore, it is likely that incorporation efficiency varies by cell type, and it is unknown whether 4SU-labelled miRNAs are exported with the same efficiency to HDL, and whether these labelled miRNAs can bind to HDL with the same efficiency. Moreover, it is currently unknown what percentage of recipient cell RNA is endogenously transcribed versus a product of transfer from other cells. Future studies will be

Table A-11: miRNAs containing T>C mutation in Ago2 and Ago3 IPs from Huh7 or HCAECs

	β–cell	Recipient	RISC	sRNA	Total Reads	T2C Reads	% T>C
Total	INS-1	Huh7	AGO2	miRNA	92153	2427	2.63
	INS-1	Huh7	AGO3	miRNA	143	65	45.45
	INS-1	HCAEC	AGO2	miRNA	2462	334	13.57
	INS-1	HCAEC	AGO3	miRNA	6740	363	5.39
	MIN6	Huh7	AGO2	miRNA	2857	281	9.84
	MIN6	Huh7	AGO3	miRNA	8188	466	5.69
	β–cell	**Recipient**	**RISC**	**sRNA**	**Total Reads**	**T2C Reads**	**% T>C**
miR-375-3p	INS-1	Huh7	AGO2	rno-miR-375-3p	381	97	25.46
	INS-1	Huh7	AGO3	rno-miR-375-3p	93	35	37.63
	INS-1	HCAEC	AGO2	rno-miR-375-3p	249	193	77.51
	INS-1	HCAEC	AGO3	rno-miR-375-3p	185	117	63.24
	MIN6	Huh7	AGO2	mmu-miR-375-3p	19	12	63.16
	MIN6	Huh7	AGO3	mmu-miR-375-3p	23	21	91.30
Other	INS-1	Huh7	AGO2	rno-miR-532-5p	109	109	100.00
	INS-1	Huh7	AGO2	rno-miR-182	14045	285	2.03
	INS-1	HCAEC	AGO3	rno-miR-182	1017	23	2.26
	MIN6	Huh7	AGO3	mmu-miR-30a-5p	474	24	5.06

required to titrate the 4SU concentration to improve labeling efficiency, without toxicity or changes in gene expression.

Distinguishing signal from noise is a key challenge in IP and sequencing based experiments(304). T->C mutations can be introduced from single-nucleotide polymorphisms, UV damaged RNA, RNA damaged by RNAse digestion or misincorporations of bases during cDNA synthesis or PCR that would be indistinguishable from 4SU-originating signal. Hafner *et al*. estimated that the background rate of T->C mutations is 1.3%(266), lower than the rates detected for miR-375-3p in these experiments (Table A-11). To determine the background levels of T->C mutations, future experiments should compare the experimental conditions to cells that were not treated with 4SU, not crosslinked or cells in which miRNA export to HDL has been inhibited to detect T->C enrichment over control. In addition, bioinformatically, T->C rates should be compared to other mutation combinations, i.e. T->A, T->G, C->A, C->G, C->T, etc to confidently measure T->C rates above background.

Despite the shortcomings of this experimental approach, I sought to investigate whether the information contained in the Ago2 and Ago3 IPs could also be helpful in identifying miRNA target genes. An attractive, and so far unused property of using PAR-CLIP, is that it could provide a snapshot into the mRNAs that were bound to the miRNAs at the time of crosslink, as fragments of mRNAs that are bound to the miRNAs can also be captured during the IP, albeit with less efficiency as they do not contain the 4SU and therefore are not covalently bound to the protein. From our sequencing data of INS-1 to Huh7 in Ago2, the reads that did not align to miRNAs were mapped to the 3' UTR of human mRNAs, and these reads were then mined for sequences complementary to the miR-375-3p seed sequence to identify potential miR-375-3p target genes. MTRNR2L6 and MTRNR2L8, two nuclear pseudogene of the mitochondrial MT-RNR2 gene were found to contain 63 and 53 reads complementary to miR-375-3p seed sequence in their 3' UTR, respectively (Table A-12). For protein coding genes, 17 reads from the RAD1, a checkpoint DNA exonuclease, 3' UTR were found in Ago2. A key limitation of this study is that the complementary

Table A-12: miR-375-3p predicted target 3'UTR found in Ago2 IP (Huh7, from INS-1)

Recipient Cell	Target Gene	Target Coverage
Huh7	MTRNR2L6	65
Huh7	MTRNR2L8	53
Huh7	RAD1	17
Huh7	NFYA	13
Huh7	SRFBP1	10
Huh7	CSNK2A1	7
Huh7	GTF2H3	7
Huh7	CLDN1	6
Huh7	GOLGB1	6
Huh7	MIB1	6
Huh7	MYCBP	6
Huh7	MAP4	5
Huh7	TOR1AIP2	4
Huh7	UBR5	4
Huh7	ZNF652	4

seed sequence that was used to search in the 3' UTRs was only 6 bases long, making the probability of identifying false positives very high. As such, further work will be required to determine whether these genes captured in Ago2 are in fact target genes of miR-375-3p and to analyze whether these is any specificity of targeting of these genes by endogenous miR-375-3p compared to HDL-delivered miR-375-3p.

Finally, through this study, I sought to address whether HDL-transferred miRNAs function similarly to endogenous miRNAs and are loaded into Ago2 and/or Ago3. Previous work from the Vickers lab has shown that HDL can be delivered to Huh7 and HCAECs and that delivery of HDL-miRNAs to recipient cells requires SR-BI(94, 95). A key unanswered question is how these HDL-delivered miRNAs escape the plasma membrane and whether they are incorporated into RISC and use the canonical posttranscriptional machinery. The lab has postulated that HDL-miRNAs are likely single stranded, as we do not detect the 3p and 5p miRNAs at comparable levels by qPCR or sequencing. Although it was thought that Ago2 required RNA duplexes for formation of active silencing complexes, recent studies have shown that single-stranded RNAs (ssRNA) can also be loaded into Ago2 when mixed in vitro in the absence of cellular RNases(305). Similarly, the lab has found that HDL-miR-223, likely single-stranded, can be delivered to endothelial cells and regulate gene expression(95). Contrary to this however, a recent study found that transfecting unmodified ssRNA oligonucleotides into cells did not achieve mRNA knockdown, whereas ssRNA containing modifications that made the ssRNA resistant to RNAses (phosphorothioate, 2' flouro, 2' O-methyl, or 2' O- methoxyethyl) were effective in reducing target mRNA levels(306). Together, these studies suggest that while Ago2 can load ssRNAs, *in vivo*, RNAses likely degrade the ssRNAs before they become bound to Ago2 and RISC. Therefore, it is likely that HDL-miRNAs contain as of yet, undefined modifications or protein-protein interactions between SR-BI (or other proteins) and the RISC complex protect the ssRNAs until they are loaded into Ago2. Further optimization of trans-PAR-CLIP as a technique to trace HDL-miRNAs may also aid in answering these questions and gaining greater understanding of HDL-miRNA delivery.

Part 5: Developing a method to trace beta cell originating miRNA delivery to distal tissues *in vivo*

Preface

Evidence of HDL-miRNA transfer between tissues has come from *in vitro* studies from our laboratory(94, 95), however, *in vivo* evidence is completely lacking, even in mouse models. A major challenge for the HDL-miRNA field and for the extracellular RNA field in general is being able to demonstrate RNA transfer between cells *in vivo*. Studies from the Vickers lab using HDL (unpublished) and from the EV fields using concentrated vesicle preparations, have been conducted to measure extracellular RNA delivery to tissues after injection of vesicles or HDL loaded with RNAs(148, 149). However, while this approach can address whether HDL or EVs can transfer RNAs to recipient cells, it does not truly address the question of whether RNA transfer occurs endogenously, and under what physiological conditions.

To overcome this challenge, in 2014, Ridder *et al*., reported an experimental model that could be used to trace mRNA delivery *in vivo* between transplanted tumor cells and leukocytes(307). In this study, glioma or carcinoma tumor cells were engineered to express Cre recombinase (Cre) and then transplanted into mice that will express a reporter (EGFP, EYFP, or LacZ) upon Cre recombination(307). This study found that Cre mRNA (but not protein) was contained in exosomes, and delivered to leukocytes that then translated the mRNA into protein. Furthermore, Cre protein was detected in leukocyte nuclei where recombination occurred to induce the reporter expression. This was the first model to show intracellular communication *in vivo* mediated by RNA, but unfortunately, we could not apply it to HDL-mediated transfer as HDL only carries small RNAs (<100nt)(94), and Cre is approximately 1000nt in length. Therefore, I sought to adapt Trans-PAR-CLIP (Appendix Part 4) to label and trace miRNA delivery *in vivo*.

The goal of this study was to label nascent RNAs in beta cells and trace their delivery to hepatocytes. A recent technique has been established taking advantage of the nt salvage enzyme uracil phosphoribosyltransferase (UPRT) to biosynthetically label newly synthesized RNA *in vivo*(308). UPRT catalyzes the conversion of uracil and 5-phosphoribosyl-1-R-diphosphate to uridine monophosphate (UMP), which is subsequently incorporated into RNA(309). The modified uracil analog 4-thiouracil (4TU) can also be used as a substrate for UPRT, resulting in 4-thiol labelled UMP which can then be incorporated into nascent RNAs to label RNA in a similar way to the *in vitro* strategy described in Appendix Part 4.

To develop tissue specific expression of UPRT, mice expressing a Cre-inducible UPRT gene were obtained(310). These mice express the β-actin/CMV (CA) promoter driving a loxP-GFP-3xstop-loxP cassette followed by the UPRT gene containing an epitope-tagged hemaglutinin (HA) (subsequently called UPRT+) (Figure A-2A)(310). These mice were crossed with mice expressing the Cre recombinase driven by the Ins1 promoter (subsequently called MIP+), allowing for tissue specific expression of Cre in beta cells (Figure A-2B)(311). Expression of Cre in beta cells results in recombination of the loxP sites flanking the GFP-3xstop, and expression of the UPRT transgene in beta cells only. This animal model provides tissue specificity and injection of 4TU provides temporal specificity, allowing for control of 4SU labelling of nascent RNAs to occur only in beta cells (cells expressing UPRT) and during a given window of time (between injection of 4TU and tissue collection). Importantly, expression of UPRT in cell culture, Drosophila and mice appears to have negligible effects on gene expression(308-310), making this an attractive model in which to label and trace miRNA intercellular communication *in vivo*. Therefore, the goal of this study was to test whether the UPRT mouse model could be used to label miRNAs in beta cells with 4TU and trace their delivery to hepatocytes using Trans-PAR-CLIP.

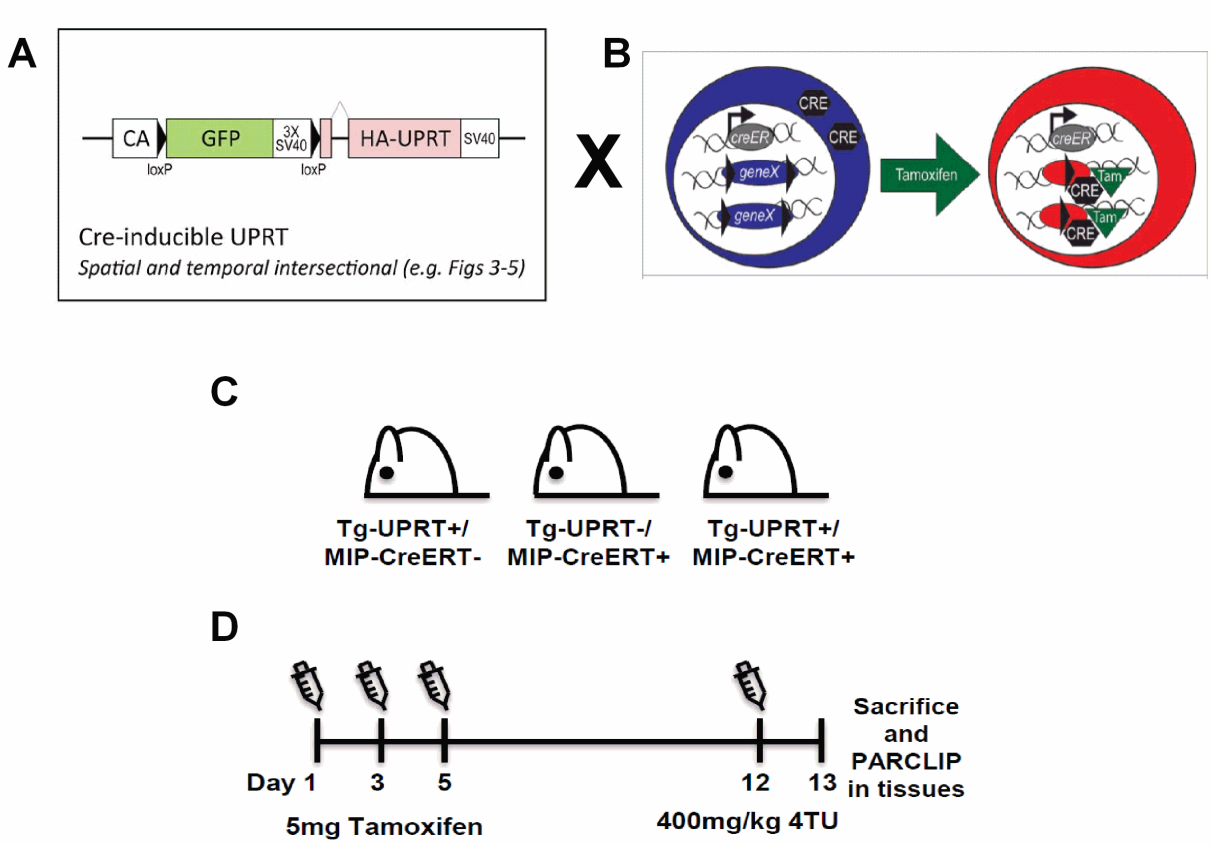

Figure A-2. Generation of beta cell specific UPRT transgenic mice. (A) From: Gay et. al., Mouse TU tagging: a chemical/genetic intersectional method for purifying cell type-specific nascent RNA. Genes Dev. 2013 Jan 1; 27(1): 98–115. Cre-inducible UPRT (Tg-UPRT) mice were crossed to mice expressing (B) tamoxifen-inducible Cre under the control of the mouse insulin promoter (MIP-CreERT+), to produce mice that will specifically express the uracil phosphoribosyltransferase (UPRT) in beta-cells. From: Johnson, et. al., A practical guide to genetic engineering of pancreatic ß-cells in vivo: Getting a grip on RIP and MIP, Islets, 2014; 6:3, e944439 (C) Mice expressing Tg-UPRT only or MIP-CreERT only were used as controls. Mice expressing both transgenes, Tg-UPRT and MIP-CreERT were the experimental mice. (D) Three doses of tamoxifen were administered by oral gavage one week after the last tamoxifen dose, 4-thiouracil (4TU) was injected 24 prior to sacrifice.

Materials and Methods

Animals

All animal experimentation was approved by and carried out in accordance to the Vanderbilt Institutional Animal Care and Use Committee. The mice were maintained in a 12-h/12-h light/dark cycle with unlimited access to chow and water. B6;D2-Tg(CAG-GFP,-Uprt)985Cdoe/J (also known as Tg-UPRT, here labelled UPRT+) were a kind gift from Dr. Guoqiang Gu, Ph.D. at Vanderbilt University(310). B6.Cg-Tg(Ins1-cre/ERT)1Lphi/J (also known as MIP-CreERT, here labelled MIP+) were a kind gift from Dr. Maureen Gannon, Ph.D. at Vanderbilt University(311). MIP-CreERT mice were crossed with Tg-UPRT mice to obtain the following three groups: UPRT+ (control), MIP+ (control), and UPRT/MIP+ (experimental) (Figure A-2C). The primers used for genotyping are listed in Table A-13.

To induce Cre expression, 8-20 week old mice were given three 5mg doses of tamoxifen (Sigma-Aldrich) by oral gavage; one injection per day on days 1, 3 and 5 (Figure A-2D). Tamoxifen was made freshly the week of the injection and dissolved in filtered corn oil (Sigma-Aldrich) by sonication at a concentration of 25mg/ml. On day 12 mice were administered 400mg/kg 4TU (Sigma-Aldrich) in one part dimethyl sulfoxide (DMSO, Sigma) and three parts corn oil (Sigma-Aldrich) (Figure A-2D). Animals were sacrificed after 24h and tissues were analyzed as described next.

Islet isolation, flow cytometry and immunofluorescence

Primary mouse islets were isolated from the transgenic mice by the Vanderbilt Islet and Procurement Core as previously described(179). Briefly, pancreata were injected with 0.6 mg/mL collagenase P (Roche, Cat # 11213865001) into the pancreatic bile duct. Dissociated tissue was fractionated using Histopaque-1077 (Sigma-Aldrich, Cat # 10771), followed by hand-picking of islets to obtain >99% purity. Experiments were performed in 17 week old female mice: UPRT+ (n=1), MIP+ (n=1), and UPRT/MIP+ (n=3).

For flow cytometry: Islets were collected in Hank's Balanced Salt Solution (HBSS, Invitrogen, Cat # 14025092) supplemented with 10% FBS (Invitrogen), and centrifuged to obtain cell pellet. Islets were digested to single-cell suspension with Accumax (Sigma-Aldrich, Cat# A7089) supplemented with 10 units/mL DNase (Invitrogen, AM2222) for 10-15 min at 37°C. Cells were then filtrated (35-µm strainer), centrifuged and fixed in 4% paraformaldehyde (Sigma-Aldrich, Cat # P6148) for 20 min on ice. Cells were then permeabilized in Flow Cytometry Permeabilization/Wash Buffer I (R&D Systems, FC005) for 10 minutes on ice, and stained with antibodies in Table A-14. Cells were then washed in Flow Cytometry Permeabilization/Wash Buffer I (R&D Systems, FC005) three times, and in Flow Cytometry Buffer (R&D Systems, FC001) twice. Fluorescence was imaged on the BD 5-laser LSRII Instrument at the Vanderbilt University Flow Cytometry Shared Resource Core.

For immunofluorescence: After isolation, islets were dispersed by cytospin as previously described(312). Briefly, islets were washed with 2mM EDTA in PBS and dispersed in 0.025% Trypsin -2mM EDTA (Invitrogen, Cat # 25200056) by pipetting for 10-15 minutes at 37°C. Cells were resuspended in RPMI medium containing 5.6mM glucose, 10% FBS, and 1% Penicillin/Streptomycin. Cells were centrifuged onto a glass slide using a cytospin (Thermo Scientific) centrifuge for 3 mins. Slides were dried and immediately fixed in 4% paraformaldehyde (Sigma-Aldrich, Cat # P6148) for 12 mins and washed three times. Cells were permeabilized in 0.2% Triton-X (Sigma-Aldrich, Cat# T8787) for 10 mins and washed three times. Cells were blocked in 1% normal donkey serum (NDS, Abcam, Cat# ab7475), 0.1% Triton-X (Sigma-Aldrich, Cat# T8787) for 90 mins at room temperature. Cells were incubated with primary antibodies (Table A-14) in 0.1% Triton-X (Sigma-Aldrich, Cat# T8787) overnight at 4°C, washed three times with 0.1% Triton-X (Sigma-Aldrich, Cat# T8787), incubated with secondary antibodies (Table A-14) in 0.1% Triton-X (Sigma-Aldrich, Cat# T8787) for 1 hr at room temperature and washed with 0.1% Triton-X (Sigma-Aldrich, Cat# T8787). Cells were incubated with DAPI (4',6-Diamidino-2-Phenylindole, Dihydrochloride, 1:10,000, Invitrogen, Cat# D1306), and washed with 1x PBS three

Table A-13: Genotyping Primers

Allele	Forward Primer	Reverse Primer
MIP-CreERT	TGCCACGACCAAGTGACAGC	CCAGGTTACGGATATAGTTCATG
Tg-UPRT	ATTCCAAGATCTGTGGCGTC	CTTCTCGTAGATCAGCTTAGGC
UPRT internal control	CACGTGGGCTCCAGCATT	TCACCAGTCATTTCTGCCTTTG

Table A-14: Antibodies

Antibody	Flourophore	Company	Dilution
Hemagglutinin (HA)	Phycoerythrin (PE), excitation: 480, 565 emission: 575	Miltenyl Biotech (Cat # 130-098-806)	1:33
Insulin	Allophycocyanin (APC), excitation: 594nm, emission: 660nm	R&D Systems (Cat # IC1417A)	1:33
Guinea pig anti-insulin	-	Dako (Cat #A0564)	1:100
Chicken anti-HA	-	Abcam (Cat #ab9111)	1:100

times. Slides were mounted with Aqua-Poly/Mount (Warrington, PA). Slides with islets were imaged using a Leica Microsystems Epifluorescent Microscope DM1 6000B.

Isolation of Primary Hepatocytes

Mouse primary hepatocytes were isolated from UPRT+ (Experiment 1: n=4; Experiment 2: n=4), MIP+ (Experiment 1: n=1; Experiment 2: n=3), and UPRT/MIP+ (Experiment 1: n=3; Experiment 2: n=4) using perfusion buffer (Invitrogen, Cat# 17701-038) and digestion buffer (Invitrogen, Cat# 17703-034) as previously described(313). Cells were washed with hepatocyte wash buffer (Invitrogen, Cat# 17704-024) and live cells were separated from dead cells using Percoll (Sigma, Cat# P1644) density gradient separation, and washed twice with hepatocyte wash buffer (Invitrogen, Cat# 17704-024) prior to lysis for Trans-PAR-CLIP.

Trans-PAR-CLIP of primary hepatocytes ex vivo

This protocol was adapted from our protocol for in vitro trans-PAR-CLIP, described in Appendix 4 and from the original study describing PAR-CLIP(266, 300). Primary hepatocytes in 1x PBS were dispersed in a monolayer in a petri dish and crosslinked with 365nm UV light (0.15J/cm^2). Cells were then pelleted by centrifugation and lysed with 1x NP lysis buffer (5x NP lysis buffer: 50mM HEPES, pH 7.5, 150mM KCl, 2mM EDTA, 1mM NaF, 0.5% (v/v) NP40, 0.5mM DTT, complete EDTA-free protease inhibitory cocktail (Roche)) on ice for 10 minutes. Cell lysates were cleared by centrifugation and incubated with 1U/ul RNAse T1 (ThermoFisher) at 22 °C for 15 min and then on ice for 5 min. PureProteome NHS FlexiBind Magnetic Beads (Millipore) were complexed to 50ug Ago2 (Monoclonal Anti-Ago2, clone 11A9, Batch 023M4810V, Sigma) antibodies according to manufacturer's recommendations. Anti-Ago2-bound magnetic beads were then incubated with partial RNase T1-treated cell lysate at 4°C overnight. Beads were washed with 1x NP lysis buffer 4 times and were then incubated with 100U/µl RNAse T1 at 22 °C for 15 min and then on ice for 5 min. Beads were then washed in high salt wash buffer (50mM

HEPES–KOH, pH 7.5, 500mM KCl, 0.05% (v/v) NP40, 0.5mM DTT, complete EDTA-free protease inhibitor cocktail (Roche)) three times. Samples were then boiled in 1x PBS at 95°C for 5 mins. Proteins were digested in 1x proteinase K digestion buffer (2x proteinase K buffer: 100 mM Tris–HCl, pH 7.5 150 mM NaCl, 12.5 mM EDTA, 2 % (w/v) SDS) containing 1.2mg/ml of proteinase K (stock 20mg/ml, Macherey-Nagel) at 55°C for 30 minutes followed by incubation on ice. RNA was isolated using the miRNeasy Mini RNA isolation Kit (Qiagen, Cat# 217004).

Library preparation and Sequencing

RNA was prepared for small-RNA sequencing with NEXTflex Small RNA Sequencing Kit v3 for Illumina Platforms (Perkin Elmer, Cat# NOVA-5132-05). Library preparation was performed according to manufacturer's protocol, except that adapters were diluted 1:4 to decrease adapter dimers. Prior to sequencing samples were size-selected by Pippin-Prep (Sage Science) to collect cDNA 135-200 nts in length. Libraries were cleaned and concentrated (DNA Clean and Concentrator 5 kit, Zymo), tested for quality (High-Sensitivity DNA chips, 2100 Bioanalyzer, Agilent), and quantified (High-Sensitivity DNA assays, Qubit, Life Technologies). Equal concentrations samples were pooled for multiplex sequencing and concentrated (DNA Clean and Concentrator 5 kit, Zymo). Single-end sequencing of multiplexed libraries was performed on an Illumina HiSeq2500 sequencer SE50 at the Vanderbilt Technologies for Advanced Genomics (VANTAGE) core. miRNA sequencing data were analyzed by an in-house sRNA-seq data analysis pipeline (TIGER) (170). Cutadapt(302) was used to trim 3' adapters for raw reads. Quality control on both raw reads and adaptor-trimmed reads was performed using FastQC (www.bioinformatics.babraham.ac.uk/projects/fastqc). All reads with lengths less than 16nts in length were discarded. The adaptor-trimmed reads were formatted into a non-redundant FASTQ file, where the read sequence and copy number was recorded for each unique tag. The usable unique reads were mapped to the whole mouse genome by Bowtie1 (v1.1.2)(181) allowing only one mismatch. T->C mutations were analyzed using PARALYZER(303).

Results and Discussion

This mouse model requires numerous steps from expression of UPRT, to efficient labeling of RNA with 4TU to be useful to test whether miRNAs are transported via HDL to hepatocytes *in vivo*. Previous communications with Dr. Guoqiang Gu, Ph.D. (Vanderbilt University) suggested that expression of the UPRT transgene in the beta cell is chimeric, and that not all beta cells express UPRT. Therefore, prior to testing miRNA delivery, I first quantified the expression of UPRT in beta cells using flow cytometry and immunofluorescence. The percentage of insulin positive cells ranged from 41-53% (Figure A-3A,B). This is lower than previous reports that ~70-80% of mouse islet cells are composed of beta cells (insulin positive cells)(314). These low numbers may be due to a number of factors, including contamination of islets by acinar tissue during the isolation procedure, incomplete staining of beta cells by insulin antibody, or transdifferentiation of beta cells in this model and decrease in the number of insulin positive cells.

Tg-UPRT mouse should express GFP in every cell, driven by the ubiquitous promoter, CA (β-actin promoter). In UPRT/MIP+ mice, administration of tamoxifen induces the activity of Cre recombinase in beta cells, and the sequence containing GFP flanked by two loxP sites is recombined, allowing for expression of HA-tagged UPRT. Expression of UPRT occurs only in mice containing both transgenes, UPRT and MIP Cre (UPRT/MIP+) after treatment with tamoxifen. Mice expressing either of the transgenes individually (UPRT+ and MIP+) were also administered tamoxifen and served as controls (Figure A-2C,D). The percentage of beta cells with active transcription from the UPRT loci can be measured by quantifying the number of GFP and HA positive beta cells. As expected, < 1% of cells from the MIP+ mouse expressed GFP or HA (Figure A-3A,C). The UPRT+ mouse had the greatest expression of HA or GFP at 31%, whereas the double transgenic mice UPRT/MIP+ had variable levels of expression of GFP and HA ranging from <1% in one mouse to 20-25% in the other two animals studied (Figure A-3A,C). Furthermore, HA is tagged to UPRT protein and can be used as a surrogate for measuring UPRT expression.

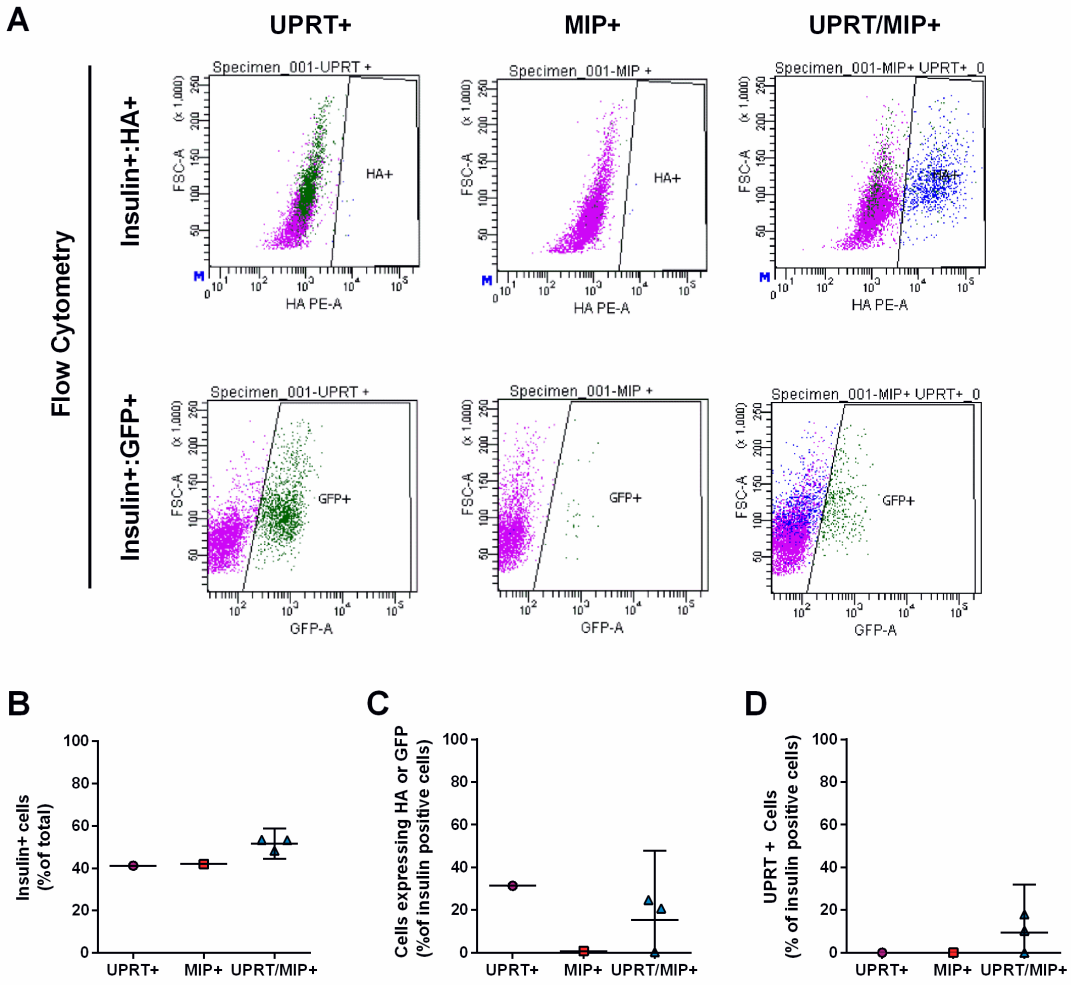

Figure A-3. Quantification of UPRT expression by flow cytometry (A) HA+ and GFP+ beta cells from one Tg-UPRT+ mouse, one MIP-CreERT+ mouse and a representative Tg-UPRT+/MIP-CreERT+ mouse. (B) Quantification of insulin positive cells, (C) cells expressing HA or GFP, and (D) cells expressing UPRT from Tg-UPRT+ (n=1), MIP-CreERT+ (n=1) and Tg-UPRT+/MIP-CreERT+ (n=3).

Control MIP+ and UPRT+ mice had <1% UPRT positive cells, whereas the expression of UPRT positive cells in UPRT/MIP+ mice ranged from <1% to 18% (Figure A-3A,C). Specifically, one mouse in this group did not express either GFP or HA, whereas in the two mice that did express either GFP or HA in insulin positive cells, about 50% of the cells had Cre recombination, resulting in 10% and 18% UPRT positive beta cells (Figure A-3A-C).

To complement the flow cytometry approach used above, islets were also dispersed onto slides and immunofluorescence was performed to visualize GFP expression in insulin positive and non-insulin positive cells from the islet. As expected, cells from a MIP+ mouse did not have any GFP positive cells (Figure A-4A), whereas the UPRT+ mouse had the highest number of GFP positive cells (Figure A-4B), indicating that expression occurred from the UPRT loci, but no recombination occurred. Although this approach is not quantitative, the double positive UPRT/MIP+ mouse had fewer GFP positive cells than the UPRT+ mouse (Figure A-4B,C), suggesting that recombination occurred in some of these cells to remove GFP and allow for expression of the UPRT transcript. Future studies should also include immunostaining for HA in these cells to assess how many beta cells express this transgene, and to measure whether any cells have dual expression of HA and GFP, which would likely indicate that Cre recombination occurred, but the residual GFP has not yet been turned over.

Although the number of beta cells that expressed UPRT were quite low in these mice, I sought to investigate whether I could trace any miRNAs labelled in beta cells and delivered to hepatocytes using the Trans-PAR-CLIP approach and detection of T->C mutation as a readout. Mice from all three genotypes were given a bolus of 4TU i.p. (Figure A-2D), and primary hepatocytes were isolated 24h later. PAR-CLIP was then performed on hepatocyte cell lysates and T->C mutations were quantified by smRNA sequencing. The first experiment was performed with MIP+ (n=1), UPRT+ (n=4), and UPRT/MIP+ (n=3). In all the mice, except for one Tg-UPRT+/MIP-CreERT+ mouse, 1-2% of miRNA encoded Ts were mutated to Cs as detected by small-RNA sequencing compared to the reference mouse genome (Figure A-5A). One

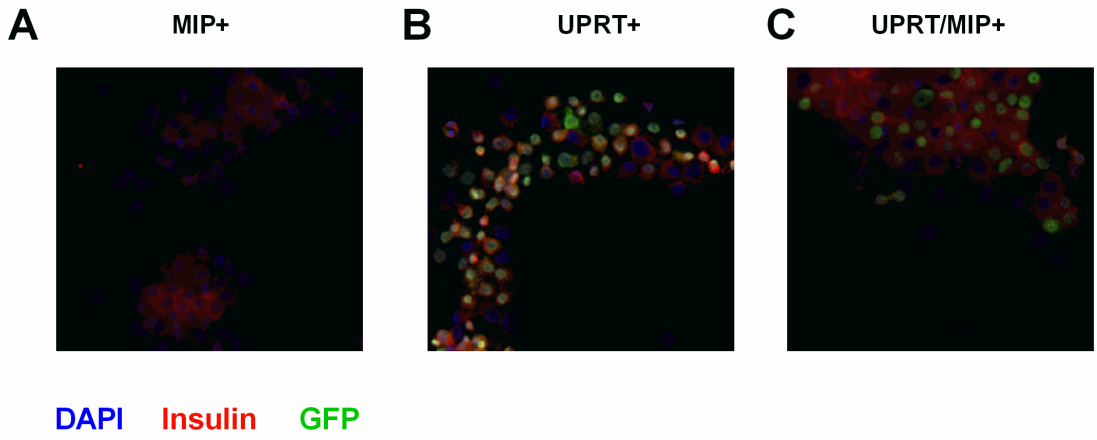

Figure A-4. Visualization of beta cells and GFP expression by immunofluorescence. Immunofluorescence of islet cells from (A) Tg-UPRT+, (B) MIP-CreERT+ and (C) Tg-UPRT+/MIP-CreERT+ mice. DAPI stain for nuclei is shown in blue, Insulin stain for beta cells is shown in red and GFP is shown in green

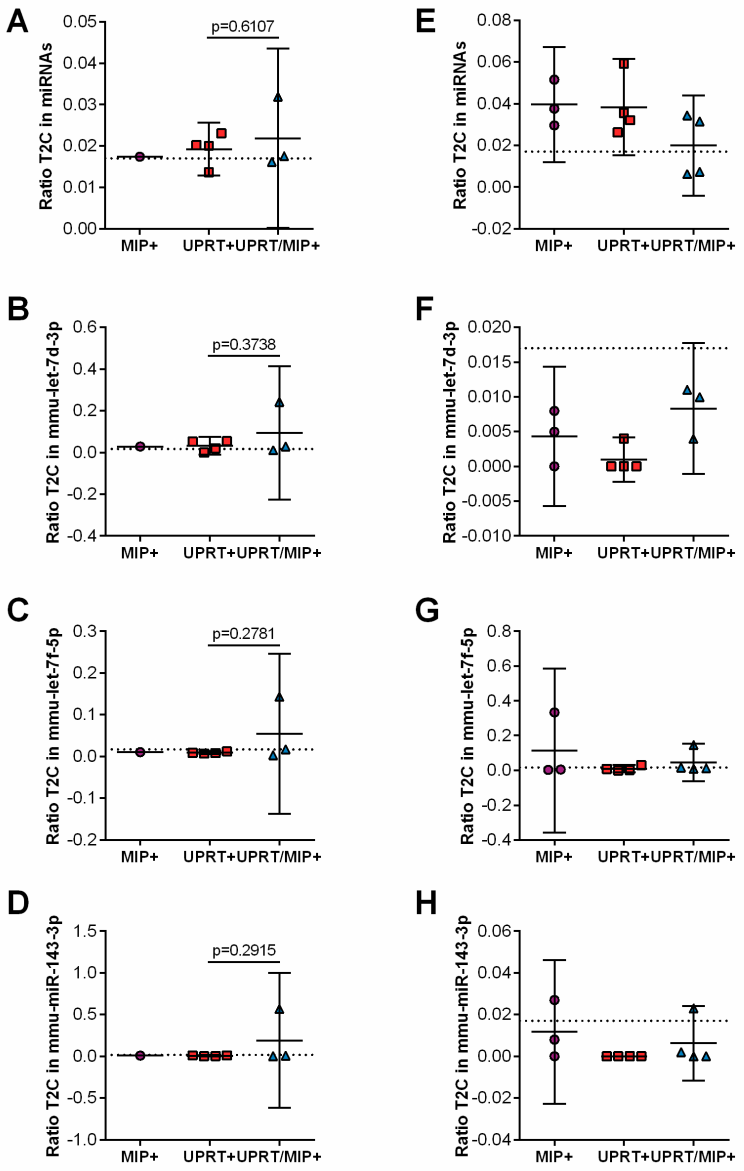

Figure A-5. Quantification of T->C mutations in miRNAs. Ratio of T->C mutations in (A, E) all miRNAs, (B, F) mmu-let-7d-3p, (C, G) mmu-let-7f-5p and (D, H) miR-143-3p immunoprecipitated in Ago2 from hepatocytes of Tg-UPRT+, MIP-CreERT+ and Tg-UPRT+/MIP-CreERT+ mice. For A-D, Student's t-test between UPRT+ and UPRT/MIP+; For E-H one-way ANOVA with Bonferroni post-test, alpha = 0.05.

UPRT/MIP+ mouse had a much higher T->C mutation rate, at ~3.5% (Figure A-5A). Importantly, there was not a significant enrichment in T->C rate in the UPRT/MIP+ mice, compared to the control genotypes. Although there was no enrichment in T->C rates in all miRNAs, it is possible that a few miRNAs may be labelled and transferred to hepatocytes, but that the effect is diluted by analyzing all miRNAs. In fact, three miRNAs, let-7d-3p, let-7f-5p, and miR-143-3p had T->C mutation rates above the background 1.3% in UPRT+/MIP+, however, this average was driven by a 3-15% T->C rate in one sample and lower than 2% in the other two samples (Figure A-5B-D). T->C mutation rates for all the miRNAs detected by sequencing can be found in Table A-15. Together these results suggest that while this strategy can be used to detect T->C mutations, there is dramatic variability across samples, and it is hard to realizably assess whether the T->C mutations are indicative of beta-cell originating RNAs or caused by to other factors.

Although the data from the first experiment were inconclusive, we performed this experiment with a second cohort of animals to test whether the T->C mutations identified in the first experiment were reproducible. This second cohort was composed of MIP+ (n=3), UPRT+ (n=4), and UPRT/MIP+ (n=3). In these animals, the T->C mutation rate of Ago2 immunoprecipitated miRNAs in hepatocytes was ~4% in MIP+ and UPRT+ mice, and slightly lower at ~2% in UPRT/MIP+ mice (Figure A-5E). Furthermore, the three miRNA we identified in the first cohort as potentially having enrichments in T->C rates in the UPRT/MIP+ mice compared to controls, did not exhibit higher rates of T->C rates in this second cohort (Figure A-5F-H). Only one miRNA, miR-30c-5p, was found to have significantly enriched T->C rate in UPRT/MIP+ (1.4% T->C) samples compared to UPRT+ (0.7% T->C); however, the one MIP+ mouse in this cohort had a rate of 1.3% T->C (Table A-16). In fact, in the first cohort only 8 miRNAs detected at >10 reads had T->C rates that were higher in the UPRT/MIP+ mice, compared to the two control genotypes (Table A-15). Of these, none were significantly different. Using the same criteria of >10 reads and T->C rates higher in UPRT/MIP+ compared to controls, 20 miRNAs were found to contain enrichment in T->C rates, albeit not significantly. Despite these findings, there was no

overlap between the miRNAs containing enrichment in T->C rates in the first and second cohorts. This suggests that either the miRNAs that are labelled in beta cells and transferred to hepatocytes vary across experiments, or that the T->C mutations detected do no originate from 4SU labelling.

To optimize the signal-to-noise ratio to confidently use this model to trace miRNAs, a number of steps will need to be optimized. First, the levels of UPRT expression and recombination are rather low in my hands. Previously, Gay *et al*. reported that near 100% of cells in the brain and heart expressed UPRT(310), however, they did not examine expression in the beta cell. The chimeric expression of UPRT in beta cells is likely due this transgene having been inserted in a genomic area that is contained in the heterochromatin in beta cells, but in euchromatin in the heart and brain. Alternatively, the poor expression may be due stochastic activity of the CA promoter in adult beta cells, which is used to drive the expression of UPRT in this model. Although unlikely, it may be possible to achieve greater expression of UPRT using different age or sex of mice, or by breeding these mice onto a different background. However, to ensure improvements in UPRT expression in beta cells, new transgenic mice will need to be developed using a highly active beta cell promoter, such as the insulin promoter, and using a targeted insertion strategy to ensure expression in this cell type. Therefore, the main optimization that can be done is to improve the expression of Cre and hence the recombination efficiency. This study estimated the recombination rate to be ~50%, and changing the dose, frequency, or route of administration of tamoxifen may improve expression of Cre in beta cells. Furthermore, additional work will be needed to evaluate the efficiency of labelling of RNAs in beta cells with 4TU, and to optimize this step. 4TU labelled RNA can be purified from total RNA using a sulfhydryl-reactive biotinylation reagent that conjugates biotin to thiol-RNA via a cleavable (reversible) disulfide bond and biotin-conjugated RNA can then be isolated using streptavidin beads(315). Moreover, it will be necessary to determine how efficient miRNA labelling is, as all the studies using *in vivo* and *in vitro* TU-tagging have measured labelling of mRNAs, which are substantially larger than miRNAs, and therefore the probability that a 4TU is incorporated is much greater(308-310).

Once these critical issues described above are overcome, future studies could look at additional tissues besides just hepatocytes to measure biodistribution of beta cell transferred RNAs. Additionally, this technique measures RNAs that are labelled in the beta cell and transferred to other tissues, but does not distinguish RNAs that are transferred via HDL or other extracellular vesicles, such as exosome or MVs. Future studies crossing UPRT expressing mice to HDL-deficient Apo-AI knockout mice will be required to distinguish which miRNAs are transferred by HDL and which are transferred by exosomes or MVs.

In summary, this study aimed to develop a mouse model in which to trace beta cell originating miRNAs and their delivery to hepatocytes. Taken together, the data presented here show that this model may have potential, but future work will be required to optimize a number of steps to improve the signal-to-noise ratio and confidently distinguish 4TU labelled miRNAs from other factors that cause a T->C mutation to be detected in Ago2 complexes.

Table A-15: T->C Mutation Rates in hepatic Ago2-IP miRNAs from first cohort

T->C mutation Rate Mean ± St.Dev	MIP+ (n=1)	UPRT+ (n=4)	URPT/MIP+ (n=3)	Mean reads
mmu-let-7a-5p	0.01	0.008 ± 0.003	0.018 ± 0.015	257.5
mmu-let-7b-3p	0.012	0.142 ± 0.239	0.026 ± 0.014	7.8
mmu-let-7b-5p	0.013	0.015 ± 0.006	0.033 ± 0.034	70.5
mmu-let-7c-5p	0.281	0.272 ± 0.232	0.165 ± 0.034	1113.8
mmu-let-7d-3p	0.029	0.032 ± 0.027	0.095 ± 0.129	149.9
mmu-let-7d-5p	0.006	0.009 ± 0.006	0.003 ± 0.006	4.1
mmu-let-7e-5p	0.005	0.005 ± 0.007	0.005 ± 0.007	2.2
mmu-let-7f-5p	0.01	0.009 ± 0.022	0.054 ± 0.077	63.9
mmu-let-7g-5p	0.01	0.008 ± 0.007	0.006 ± 0.003	39.1
mmu-let-7i-5p	0.006	0.197 ± 0.272	0.003 ± 0.006	7.6
mmu-miR-100-5p	0.5	0.013 ± 0.004	1 ± 0	1.0
mmu-miR-101a-3p	0.011	0.005 ± 0.01	0.003 ± 0.005	0.8
mmu-miR-101b-3p	0.007	0.007 ± 0.009	0.008 ± 0.001	3.0
mmu-miR-103-3p	0.006	0 ± 0	0.005 ± 0.009	1.3
mmu-miR-10a-5p	0	0 ± 0	0 ± 0	0.0
mmu-miR-122-3p	0.013	0.031 ± 0.035	0.011 ± 0.002	3931.1
mmu-miR-122-5p	0.012	0.011 ± 0.002	0.008 ± 0.002	139.4
mmu-miR-1247-5p	0.007	0 ± 0	0.003 ± 0.004	2.8
mmu-miR-1249-3p	0.004	0.001 ± 0.001	0.02 ± 0.031	26.8
mmu-miR-1258-5p	0	0.005 ± 0.007	0.003 ± 0.005	8.0
mmu-miR-125b-5p	0.006	0.006 ± 0.01	0.009 ± 0.012	4.4
mmu-miR-126a-3p	0.014	0 ± 0	0.002 ± 0.002	2.7
mmu-miR-128-3p	0.014	0 ± 0	0.019 ± 0	0.6
mmu-miR-132-3p	0	0 ± 0	0 ± 0	0.0
mmu-miR-133a-3p	0	0 ± 0	0.005 ± 0.005	0.6
mmu-miR-140-3p	0.009	0.013 ± 0.007	0.01 ± 0.002	3.7
mmu-miR-143-3p	0.009	0.007 ± 0.006	0.192 ± 0.325	18.5
mmu-miR-146a-5p	0	0.083 ± 0.167	0.061 ± 0.092	0.6
mmu-miR-146b-5p	0	0 ± 0	0 ± 0	0.0
mmu-miR-148a-3p	0.006	0.007 ± 0.005	0.006 ± 0.002	11.7
mmu-miR-148b-3p	0.015	0 ± 0	0.029 ± 0.001*	1.6
mmu-miR-149-5p	0.008	0.005 ± 0.009	0.002 ± 0.004	4.3
mmu-miR-151-3p	0.013	0 ± 0	0.014 ± 0	2.0
mmu-miR-151-5p	0.009	0 ± 0	0 ± 0	0.7
mmu-miR-16-5p	0.016	0.001 ± 0.002	0.004 ± 0.004	3.1
mmu-miR-181a-5p	0.006	0 ± 0	0.016 ± 0	1.6
mmu-miR-182-5p	0	0 ± 0	0.019 ± 0.021	1.0
mmu-miR-183-5p	0	0 ± 0	0.006 ± 0.006	0.6
mmu-miR-1843a-3p	0.01	0.006 ± 0.006	0.011 ± 0.011	9.4

mmu-miR-186-5p	0.005	0.025 ± 0.035	0.002 ± 0.004	0.7
mmu-miR-191-5p	0.022	0.02 ± 0.038	0.024 ± 0.02	1.8
mmu-miR-192-5p	0.011	0.004 ± 0.005	0.004 ± 0.006	2.1
mmu-miR-194-5p	0.008	0 ± 0	0.003 ± 0.004	4.8
mmu-miR-1a-3p	0.314	0.023 ± 0.025	0.273 ± 0.465	19.4
mmu-miR-200a-3p	0	0 ± 0	0 ± 0	0.0
mmu-miR-200b-3p	0	0 ± 0	0.012 ± 0.006	1.5
mmu-miR-203-3p	0.031	0.004 ± 0.005	0.002 ± 0.004	9.9
mmu-miR-20a-5p	0	0 ± 0	0 ± 0	0.0
mmu-miR-21a-5p	0.011	0.022 ± 0.004	0.022 ± 0.018	15.1
mmu-miR-221-3p	0.01	0.005 ± 0.006	0.019 ± 0.025	5.0
mmu-miR-222-3p	0.004	0 ± 0	0.003 ± 0.005	2.3
mmu-miR-223-3p	0.004	0.008 ± 0.014	0.003 ± 0.005	0.9
mmu-miR-22-3p	0.005	0.005 ± 0.007	0.039 ± 0.05	3.4
mmu-miR-23a-3p	0.006	0.03 ± 0.054	0.057 ± 0.075	20.8
mmu-miR-23b-3p	0.009	0.006 ± 0.005	0.009 ± 0.003	30.6
mmu-miR-24-3p	0	0.004 ± 0.008	0.111 ± 0.192	0.3
mmu-miR-25-3p	0.01	0.01 ± 0.013	0.014 ± 0.014	1.4
mmu-miR-26a-5p	0.008	0.004 ± 0.003	0.005 ± 0.001	10.0
mmu-miR-26b-5p	0.012	0.004 ± 0.005	0.015 ± 0.007	13.1
mmu-miR-27b-3p	0.012	0.014 ± 0.011	0.01 ± 0.003	8.1
mmu-miR-29a-3p	0.004	0.039 ± 0.059	0.004 ± 0.006	0.9
mmu-miR-30a-5p	0.011	0.006 ± 0.005	0.002 ± 0.003	3.3
mmu-miR-30b-5p	0.018	0.005 ± 0.006	0.006 ± 0.008	3.4
mmu-miR-30c-5p	0.013	0.007 ± 0.003	0.014 ± 0.003*	278.4
mmu-miR-30d-5p	0.005	0.006 ± 0.004	0.006 ± 0.005	2.8
mmu-miR-30e-5p	0.01	0.109 ± 0.152	0.006 ± 0.011	1.5
mmu-miR-320-3p	0.006	0.012 ± 0.008	0.111 ± 0.19	55.5
mmu-miR-328-3p	0.004	0.005 ± 0.006	0.012 ± 0	10.3
mmu-miR-340-5p	0	0.083 ± 0.167	0.01 ± 0.014	0.4
mmu-miR-350-3p	0.003	0.022 ± 0.024	0.004 ± 0.006	3.0
mmu-miR-361-3p	0	0 ± 0	0.009 ± 0	1.0
mmu-miR-361-5p	0.193	0 ± 0	0.003 ± 0.004	55.0
mmu-miR-362-5p	0	0 ± 0	0 ± 0	0.0
mmu-miR-365-3p	0.016	0.009 ± 0.011	0.011 ± 0.007	136.9
mmu-miR-375-3p	0	0 ± 0	0.013 ± 0	9.0
mmu-miR-378a-3p	0.013	0.095 ± 0.127	0.036 ± 0.063	25.4
mmu-miR-378c	0.004	0.043 ± 0.074	0.01 ± 0.013	8.3
mmu-miR-423-3p	0.009	0.008 ± 0.006	0.003 ± 0	4.7
mmu-miR-423-5p	0.006	0.013 ± 0.007	0.009 ± 0.015	2.3
mmu-miR-425-5p	0.002	0.337 ± 0.574	0.006 ± 0.01	0.9
mmu-miR-451a	0.893	0.021 ± 0.024	0.169 ± 0.287	9.0
mmu-miR-455-3p	0.084	0.037 ± 0.046	0.067 ± 0.024	1260.4

mmu-miR-484	0.006	0 ± 0	0.004 ± 0.003	4.4
mmu-miR-485-3p	0.031	0.024 ± 0.017	0.011 ± 0.019	76.3
mmu-miR-486a-5p	0.033	0.052 ± 0.07	0.012 ± 0.016	1.9
mmu-miR-5106	0.224	0.5 ± 0.707	1 ± 0	7.5
mmu-miR-574-3p	0.008	0.005 ± 0.003	0.006 ± 0.001	156.3
mmu-miR-664-3p	0.006	0.004 ± 0.007	0.01 ± 0.011	1.7
mmu-miR-671-3p	0.007	0.002 ± 0.002	0.001 ± 0.001	2.8
mmu-miR-7219-3p	0.01	0.007 ± 0.007	0.004 ± 0.005	5.8
mmu-miR-744-5p	0.05	0.012 ± 0.004	0.001 ± 0.001*	14.2
mmu-miR-7a-5p	0	0 ± 0	0.004 ± 0	0.4
mmu-miR-877-3p	0	0 ± 0	0 ± 0	0.0
mmu-miR-92a-3p	0.019	0.009 ± 0.001	0.006 ± 0*	36.1
mmu-miR-93-5p	0.019	0.002 ± 0.004	0.004 ± 0.006	1.1
mmu-miR-98-3p	0.008	0 ± 0	0.031 ± 0.035	33.6
mmu-miR-98-5p	0.881	0.258 ± 0.495	0.807 ± 0.209	88.9
mmu-miR-99a-5p	0.008	0.006 ± 0.005	0.004 ± 0.002	22.4
mmu-miR-99b-3p	0.007	0.001 ± 0.003	0.009 ± 0.01	1.5

*p<0.05 between UPRT+ vs UPRT/MIP+

Table A-16: T->C Mutation Rates in hepatic Ago2-IP miRNAs of second cohort

T->C mutation Rate Mean ± St.Dev	MIP+ (n=3)	UPRT+ (n=4)	URPT/MIP+ (n=4)	Mean reads
mmu-let-7a-5p	0.001 ± 0.002	0.027 ± 0.036	0.002 ± 0.002	3091.5
mmu-let-7b-3p	0 ± 0	0.01 ± 0.013	0 ± 0	30.3
mmu-let-7b-5p	0.005 ± 0.007	0.011 ± 0.014	0.002 ± 0.002	1308.6
mmu-let-7c-5p	0.17 ± 0.231	0.073 ± 0.115	0.127 ± 0.157	1876.7
mmu-let-7d-3p	0.003 ± 0.004	0.002 ± 0.002	0.003 ± 0.004*	312.4
mmu-let-7d-5p	0.005 ± 0.007	0.005 ± 0.007	0.003 ± 0.004	229.6
mmu-let-7e-5p	0.5 ± 0.707	0.006 ± 0.008	0.15 ± 0.2	13.7
mmu-let-7f-5p	0.146 ± 0.19	0.01 ± 0.013	0.05 ± 0.067	1440.3
mmu-let-7g-5p	0.002 ± 0.003	0.002 ± 0.002	0.04 ± 0.053	971.0
mmu-let-7i-5p	0.147 ± 0.191	0.003 ± 0.004	0.002 ± 0.002	97.6
mmu-miR-101b-3p	0 ± 0	0.001 ± 0.002	0 ± 0	155.3
mmu-miR-103-3p	0 ± 0	0 ± 0	0.007 ± 0.009	146.4
mmu-miR-10a-5p	0 ± 0	0 ± 0	0.001 ± 0.001	86.3
mmu-miR-1198-5p	0 ± 0	0.004 ± 0.005	0 ± 0	36.3
mmu-miR-122-3p	0.006 ± 0.008	0.03 ± 0.041	0.006 ± 0.008	10097.0
mmu-miR-122-5p	0.002 ± 0.003	0.003 ± 0.003	0.002 ± 0.003	7639.5
mmu-miR-1249-3p	0.003 ± 0.004	0.003 ± 0.003	0.001 ± 0.001	1112.8
mmu-miR-125a-5p	0.114 ± 0.148	0 ± 0	0.017 ± 0.023	127.6
mmu-miR-125b-5p	0 ± 0	0.004 ± 0.005	0.002 ± 0.002	120.3
mmu-miR-126a-3p	0 ± 0	0.375 ± 0.5	0 ± 0	1.8
mmu-miR-133a-3p	0 ± 0	0 ± 0	0 ± 0	15.9
mmu-miR-140-3p	0.005 ± 0.007	0.003 ± 0.004	0.438 ± 0.569	83.6
mmu-miR-142a-3p	0 ± 0	0 ± 0	0 ± 0	1.3
mmu-miR-143-3p	0.01 ± 0.014	0 ± 0	0.008 ± 0.011	154.3
mmu-miR-146a-5p	0.004 ± 0.005	0 ± 0	0.003 ± 0.004	163.2
mmu-miR-146b-5p	0 ± 0	0 ± 0	0 ± 0	2.0
mmu-miR-148a-3p	0.02 ± 0.028	0.003 ± 0.003	0.004 ± 0.005	109.3
mmu-miR-151-3p	0 ± 0	0.002 ± 0.003	0.005 ± 0.007	44.4
mmu-miR-15b-5p	0 ± 0	0 ± 0	0 ± 0	1.5
mmu-miR-16-5p	0.111 ± 0.144	0 ± 0	0.125 ± 0.167	69.9
mmu-miR-182-5p	0 ± 0	0 ± 0	0 ± 0	118.0
mmu-miR-183-5p	0 ± 0	0.002 ± 0.002	0.005 ± 0.006	104.5
mmu-miR-191-5p	0 ± 0	0.003 ± 0.004	0 ± 0	53.3
mmu-miR-1a-3p	0.125 ± 0.177	0.082 ± 0.109	0.159 ± 0.195	268.3
mmu-miR-203-3p	0.001 ± 0.001	0.002 ± 0.002	0.007 ± 0.01	236.4
mmu-miR-21a-5p	0.009 ± 0.012	0.006 ± 0.009	0.004 ± 0.005	1340.4
mmu-miR-221-3p	0.003 ± 0.003	0.006 ± 0.007	0.052 ± 0.07	219.0
mmu-miR-222-3p	0.001 ± 0.001	0.063 ± 0.084	0.008 ± 0.011	126.6

mmu-miR-223-3p	0 ± 0	0 ± 0	0 ± 0	5.1
mmu-miR-22-3p	0.318 ± 0.413	0.0364 ± 0.486	0 ± 0	72.5
mmu-miR-23a-3p	0.023 ± 0.03	0.038 ± 0.051	0.004 ± 0.005	165.5
mmu-miR-23b-3p	0.007 ± 0.01	0.02 ± 0.027	0.005 ± 0.006	586.5
mmu-miR-24-3p	0 ± 0	0 ± 0	0.041 ± 0.055	72.8
mmu-miR-25-3p	0.003 ± 0.004	0 ± 0	0 ± 0	36.1
mmu-miR-26a-5p	0.002 ± 0.003	0.028 ± 0.038	0.004 ± 0.006	347.3
mmu-miR-26b-5p	0.003 ± 0.004	0.008 ± 0.01	0.072 ± 0.096	542.1
mmu-miR-27a-3p	0 ± 0	0 ± 0	0 ± 0	17.7
mmu-miR-27b-3p	0 ± 0	0.029 ± 0.039	0 ± 0	71.6
mmu-miR-29a-3p	0.003 ± 0.003	0 ± 0	0.024 ± 0.034	86.9
mmu-miR-30a-5p	0.004 ± 0.005	0.001 ± 0.001	0.006 ± 0.008	182.8
mmu-miR-30c-5p	0.004 ± 0.005	0.007 ± 0.009	0.003 ± 0.004	952.8
mmu-miR-30d-5p	0.002 ± 0.003	0.002 ± 0.003	0.003 ± 0.003	368.3
mmu-miR-30e-5p	0.22 ± 0.286	0.002 ± 0.003	0.094 ± 0.125	39.5
mmu-miR-320-3p	0.009 ± 0.013	0.003 ± 0.004	0.089 ± 0.119	220.0
mmu-miR-328-3p	0.002 ± 0.003	0.005 ± 0.007	0.006 ± 0.008	394.4
mmu-miR-340-5p	0 ± 0	0 ± 0	0 ± 0	26.5
mmu-miR-342-3p	0 ± 0	0.375 ± 0.5	0.125 ± 0.167	16.2
mmu-miR-365-3p	0.002 ± 0.002	0.181 ± 0.241	0.004 ± 0.006	304.9
mmu-miR-375-3p	0 ± 0	0 ± 0	0 ± 0	1.0
mmu-miR-376b-3p	0.002 ± 0.003	0.016 ± 0.023	0.028 ± 0.037	291.0
mmu-miR-378a-3p	0.005 ± 0.006	0.338 ± 0.455	0.011 ± 0.015	136.6
mmu-miR-423-5p	0.002 ± 0.004	0 ± 0	0.013 ± 0.017	86.8
mmu-miR-425-5p	0 ± 0	0 ± 0	0 ± 0	1.4
mmu-miR-451a	0.019 ± 0.027	0.042 ± 0.059	0.02 ± 0.028*	83.1
mmu-miR-455-3p	0.075 ± 0.105	0.087 ± 0.121	0.04 ± 0.048$^{\#}$	1243.2
mmu-miR-484	0 ± 0	0.042 ± 0.056	0.006 ± 0.008	60.1
mmu-miR-485-3p	0.008 ± 0.011	0.348 ± 0.488	0.008 ± 0.011	209.3
mmu-miR-486a-5p	0.002 ± 0.002	0.005 ± 0.006	0.002 ± 0.003	668.1
mmu-miR-574-3p	0.001 ± 0.001	0.004 ± 0.005	0.004 ± 0.004	1287.5
mmu-miR-7a-5p	0.004 ± 0.005	0 ± 0	0.023 ± 0.029	100.5
mmu-miR-92a-3p	0.002 ± 0.003	0.026 ± 0.034	0.003 ± 0.005	545.5
mmu-miR-93-5p	0 ± 0	0 ± 0	0.124 ± 0.165	62.4
mmu-miR-98-5p	0 ± 0	0.003 ± 0.005	0.278 ± 0.382	59.8
mmu-miR-99a-5p	0.004 ± 0.005	0.002 ± 0.002	0.005 ± 0.006	148.1
mmu-miR-99b-3p	0.003 ± 0.003	0.003 ± 0.004	0.016 ± 0.023	88.9

$^{\#}p<0.05$ between MIP+ vs UPRT/MIP+

*p<0.05 between UPRT+ vs UPRT/MIP+

REFERENCES

1. Reusch JE, Manson JE. Management of Type 2 Diabetes in 2017: Getting to Goal. JAMA : the journal of the American Medical Association. 2017;317(10):1015-6. doi: 10.1001/jama.2017.0241. PubMed PMID: 28249081.

2. Katsarou A, Gudbjornsdottir S, Rawshani A, Dabelea D, Bonifacio E, Anderson BJ, Jacobsen LM, Schatz DA, Lernmark A. Type 1 diabetes mellitus. Nat Rev Dis Primers. 2017;3:17016. doi: 10.1038/nrdp.2017.16. PubMed PMID: 28358037.

3. Copenhaver M, Hoffman RP. Type 1 diabetes: where are we in 2017? Transl Pediatr. 2017;6(4):359-64. doi: 10.21037/tp.2017.09.09. PubMed PMID: 29184816; PMCID: PMC5682377.

4. Paschou SA, Papadopoulou-Marketou N, Chrousos GP, Kanaka-Gantenbein C. On type 1 diabetes mellitus pathogenesis. Endocr Connect. 2018;7(1):R38-R46. doi: 10.1530/EC-17-0347. PubMed PMID: 29191919; PMCID: PMC5776665.

5. Klinke DJ, 2nd. Extent of beta cell destruction is important but insufficient to predict the onset of type 1 diabetes mellitus. PloS one. 2008;3(1):e1374. doi: 10.1371/journal.pone.0001374. PubMed PMID: 18167535; PMCID: PMC2147725.

6. Wu J, Yan LJ. Streptozotocin-induced type 1 diabetes in rodents as a model for studying mitochondrial mechanisms of diabetic beta cell glucotoxicity. Diabetes Metab Syndr Obes. 2015;8:181-8. doi: 10.2147/DMSO.S82272. PubMed PMID: 25897251; PMCID: PMC4396517.

7. Das SK, Elbein SC. The Genetic Basis of Type 2 Diabetes. Cellscience. 2006;2(4):100-31. doi: 10.1901/jaba.2006.2-100. PubMed PMID: 16892160; PMCID: PMC1526773.

8. Lin Y, Sun Z. Current views on type 2 diabetes. The Journal of endocrinology. 2010;204(1):1-11. doi: 10.1677/JOE-09-0260. PubMed PMID: 19770178; PMCID: PMC2814170.

9. Sales V, Patti ME. The Ups and Downs of Insulin Resistance and Type 2 Diabetes: Lessons from Genomic Analyses in Humans. Curr Cardiovasc Risk Rep. 2013;7(1):46-59. doi: 10.1007/s12170-012-0283-8. PubMed PMID: 23459395; PMCID: PMC3583548.

10. Grundy SM, Brewer HB, Jr., Cleeman JI, Smith SC, Jr., Lenfant C, National Heart L, Blood I, American Heart A. Definition of metabolic syndrome: report of the National Heart, Lung, and Blood Institute/American Heart Association conference on scientific issues related to definition. Arteriosclerosis, thrombosis, and vascular biology. 2004;24(2):e13-8. doi: 10.1161/01.ATV.0000111245.75752.C6. PubMed PMID: 14766739.

11. Uusitupa M. Lifestyles matter in the prevention of type 2 diabetes. Diabetes care. 2002;25(9):1650-1. PubMed PMID: 12196442.

12. Maddatu J, Anderson-Baucum E, Evans-Molina C. Smoking and the risk of type 2 diabetes. Transl Res. 2017;184:101-7. doi: 10.1016/j.trsl.2017.02.004. PubMed PMID: 28336465; PMCID: PMC5429867.

13. Joiner KL, Nam S, Whittemore R. Lifestyle interventions based on the diabetes prevention program delivered via eHealth: A systematic review and meta-analysis. Preventive medicine. 2017;100:194-207. doi: 10.1016/j.ypmed.2017.04.033. PubMed PMID: 28456513; PMCID: PMC5699208.

14. Shu Y, Sheardown SA, Brown C, Owen RP, Zhang S, Castro RA, Ianculescu AG, Yue L, Lo JC, Burchard EG, Brett CM, Giacomini KM. Effect of genetic variation in the organic cation transporter 1 (OCT1) on metformin action. The Journal of clinical investigation. 2007;117(5):1422-31. doi: 10.1172/JCI30558. PubMed PMID: 17476361; PMCID: PMC1857259.

15. Viollet B, Guigas B, Sanz Garcia N, Leclerc J, Foretz M, Andreelli F. Cellular and molecular mechanisms of metformin: an overview. Clinical science. 2012;122(6):253-70. doi: 10.1042/CS20110386. PubMed PMID: 22117616; PMCID: PMC3398862.

16. Hunter RW, Hughey CC, Lantier L, Sundelin EI, Peggie M, Zeqiraj E, Sicheri F, Jessen N, Wasserman DH, Sakamoto K. Metformin reduces liver glucose production by inhibition of fructose-1-6-bisphosphatase. Nature medicine. 2018;24(9):1395-406. doi: 10.1038/s41591-018-0159-7. PubMed PMID: 30150719.

17. Maida A, Lamont BJ, Cao X, Drucker DJ. Metformin regulates the incretin receptor axis via a pathway dependent on peroxisome proliferator-activated receptor-alpha in mice. Diabetologia. 2011;54(2):339-49. doi: 10.1007/s00125-010-1937-z. PubMed PMID: 20972533.

18. Meloni AR, DeYoung MB, Lowe C, Parkes DG. GLP-1 receptor activated insulin secretion from pancreatic beta-cells: mechanism and glucose dependence. Diabetes, obesity & metabolism. 2013;15(1):15-27. doi: 10.1111/j.1463-1326.2012.01663.x. PubMed PMID: 22776039; PMCID: PMC3556522.

19. White JR, Jr. A Brief History of the Development of Diabetes Medications. Diabetes Spectr. 2014;27(2):82-6. doi: 10.2337/diaspect.27.2.82. PubMed PMID: 26246763; PMCID: PMC4522877.

20. Sola D, Rossi L, Schianca GP, Maffioli P, Bigliocca M, Mella R, Corliano F, Fra GP, Bartoli E, Derosa G. Sulfonylureas and their use in clinical practice. Arch Med Sci. 2015;11(4):840-8. doi: 10.5114/aoms.2015.53304. PubMed PMID: 26322096; PMCID: PMC4548036.

21. Proks P, Reimann F, Green N, Gribble F, Ashcroft F. Sulfonylurea stimulation of insulin secretion. Diabetes. 2002;51 Suppl 3:S368-76. PubMed PMID: 12475777.

22. Aguilar-Bryan L, Nichols CG, Wechsler SW, Clement JPt, Boyd AE, 3rd, Gonzalez G, Herrera-Sosa H, Nguy K, Bryan J, Nelson DA. Cloning of the beta cell high-affinity sulfonylurea receptor: a regulator of insulin secretion. Science. 1995;268(5209):423-6. PubMed PMID: 7716547.

23. Uhde I, Toman A, Gross I, Schwanstecher C, Schwanstecher M. Identification of the potassium channel opener site on sulfonylurea receptors. The Journal of biological chemistry. 1999;274(40):28079-82. PubMed PMID: 10497157.

24. Vilsboll T. The effects of glucagon-like peptide-1 on the beta cell. Diabetes, obesity & metabolism. 2009;11 Suppl 3:11-8. doi: 10.1111/j.1463-1326.2009.01073.x. PubMed PMID: 19878257.

25. Buteau J. GLP-1 receptor signaling: effects on pancreatic beta-cell proliferation and survival. Diabetes Metab. 2008;34 Suppl 2:S73-7. doi: 10.1016/S1262-3636(08)73398-6. PubMed PMID: 18640589.

26. Hui H, Farilla L, Merkel P, Perfetti R. The short half-life of glucagon-like peptide-1 in plasma does not reflect its long-lasting beneficial effects. European journal of endocrinology / European Federation of Endocrine Societies. 2002;146(6):863-9. PubMed PMID: 12039708.

27. Agerso H, Jensen LB, Elbrond B, Rolan P, Zdravkovic M. The pharmacokinetics, pharmacodynamics, safety and tolerability of NN2211, a new long-acting GLP-1 derivative, in healthy men. Diabetologia. 2002;45(2):195-202. doi: 10.1007/s00125-001-0719-z. PubMed PMID: 11935150.

28. Lyu X, Zhu X, Zhao B, Du L, Chen D, Wang C, Liu G, Ran X. Effects of dipeptidyl peptidase-4 inhibitors on beta-cell function and insulin resistance in type 2 diabetes: meta-analysis of randomized controlled trials. Scientific reports. 2017;7:44865. doi: 10.1038/srep44865. PubMed PMID: 28322294; PMCID: PMC5359588.

29. Chiang JY. Bile acid metabolism and signaling. Compr Physiol. 2013;3(3):1191-212. doi: 10.1002/cphy.c120023. PubMed PMID: 23897684; PMCID: PMC4422175.

30. Herrema H, Meissner M, van Dijk TH, Brufau G, Boverhof R, Oosterveer MH, Reijngoud DJ, Muller M, Stellaard F, Groen AK, Kuipers F. Bile salt sequestration induces hepatic de novo lipogenesis through farnesoid X receptor- and liver X receptor alpha-controlled metabolic

pathways in mice. Hepatology. 2010;51(3):806-16. doi: 10.1002/hep.23408. PubMed PMID: 19998408.

31. Sonne DP, Hansen M, Knop FK. Bile acid sequestrants in type 2 diabetes: potential effects on GLP1 secretion. European journal of endocrinology / European Federation of Endocrine Societies. 2014;171(2):R47-65. doi: 10.1530/EJE-14-0154. PubMed PMID: 24760535.

32. Corsini A, Windler E, Farnier M. Colesevelam hydrochloride: usefulness of a specifically engineered bile acid sequestrant for lowering LDL-cholesterol. Eur J Cardiovasc Prev Rehabil. 2009;16(1):1-9. doi: 10.1097/HJR.0b013e32831215db. PubMed PMID: 19237992.

33. Bays HE, Goldberg RB, Truitt KE, Jones MR. Colesevelam hydrochloride therapy in patients with type 2 diabetes mellitus treated with metformin: glucose and lipid effects. Archives of internal medicine. 2008;168(18):1975-83. doi: 10.1001/archinte.168.18.1975. PubMed PMID: 18852398.

34. Goldberg RB, Fonseca VA, Truitt KE, Jones MR. Efficacy and safety of colesevelam in patients with type 2 diabetes mellitus and inadequate glycemic control receiving insulin-based therapy. Archives of internal medicine. 2008;168(14):1531-40. doi: 10.1001/archinte.168.14.1531. PubMed PMID: 18663165.

35. Fonseca VA, Rosenstock J, Wang AC, Truitt KE, Jones MR. Colesevelam HCl improves glycemic control and reduces LDL cholesterol in patients with inadequately controlled type 2 diabetes on sulfonylurea-based therapy. Diabetes care. 2008;31(8):1479-84. doi: 10.2337/dc08-0283. PubMed PMID: 18458145; PMCID: PMC2494667.

36. Takebayashi K, Aso Y, Inukai T. Role of bile acid sequestrants in the treatment of type 2 diabetes. World J Diabetes. 2010;1(5):146-52. doi: 10.4239/wjd.v1.i5.146. PubMed PMID: 21537442; PMCID: PMC3083899.

37. Potthoff MJ, Potts A, He T, Duarte JA, Taussig R, Mangelsdorf DJ, Kliewer SA, Burgess SC. Colesevelam suppresses hepatic glycogenolysis by TGR5-mediated induction of GLP-1

action in DIO mice. American journal of physiology Gastrointestinal and liver physiology. 2013;304(4):G371-80. doi: 10.1152/ajpgi.00400.2012. PubMed PMID: 23257920; PMCID: 3566618.

38. Hansen M, Scheltema MJ, Sonne DP, Hansen JS, Sperling M, Rehfeld JF, Holst JJ, Vilsboll T, Knop FK. Effect of chenodeoxycholic acid and the bile acid sequestrant colesevelam on glucagon-like peptide-1 secretion. Diabetes, obesity & metabolism. 2016;18(6):571-80. doi: 10.1111/dom.12648. PubMed PMID: 26888164.

39. Beysen C, Murphy EJ, Deines K, Chan M, Tsang E, Glass A, Turner SM, Protasio J, Riiff T, Hellerstein MK. Effect of bile acid sequestrants on glucose metabolism, hepatic de novo lipogenesis, and cholesterol and bile acid kinetics in type 2 diabetes: a randomised controlled study. Diabetologia. 2012;55(2):432-42. doi: 10.1007/s00125-011-2382-3. PubMed PMID: 22134839.

40. Shang Q, Saumoy M, Holst JJ, Salen G, Xu G. Colesevelam improves insulin resistance in a diet-induced obesity (F-DIO) rat model by increasing the release of GLP-1. American journal of physiology Gastrointestinal and liver physiology. 2010;298(3):G419-24. doi: 10.1152/ajpgi.00362.2009. PubMed PMID: 20044510.

41. Nwose OM, Jones MR. Atypical mechanism of glucose modulation by colesevelam in patients with type 2 diabetes. Clinical medicine insights Endocrinology and diabetes. 2013;6:75-9. doi: 10.4137/CMED.S12590. PubMed PMID: 24348081; PMCID: 3864737.

42. Wang CY, Liao JK. A mouse model of diet-induced obesity and insulin resistance. Methods in molecular biology. 2012;821:421-33. doi: 10.1007/978-1-61779-430-8_27. PubMed PMID: 22125082; PMCID: PMC3807094.

43. Wang B, Chandrasekera PC, Pippin JJ. Leptin- and leptin receptor-deficient rodent models: relevance for human type 2 diabetes. Curr Diabetes Rev. 2014;10(2):131-45. PubMed PMID: 24809394; PMCID: PMC4082168.

44. Zhang Y, Proenca R, Maffei M, Barone M, Leopold L, Friedman JM. Positional cloning of the mouse obese gene and its human homologue. Nature. 1994;372(6505):425-32. doi: 10.1038/372425a0. PubMed PMID: 7984236.

45. Kennedy AJ, Ellacott KL, King VL, Hasty AH. Mouse models of the metabolic syndrome. Dis Model Mech. 2010;3(3-4):156-66. doi: 10.1242/dmm.003467. PubMed PMID: 20212084; PMCID: PMC2869491.

46. Chen H, Charlat O, Tartaglia LA, Woolf EA, Weng X, Ellis SJ, Lakey ND, Culpepper J, Moore KJ, Breitbart RE, Duyk GM, Tepper RI, Morgenstern JP. Evidence that the diabetes gene encodes the leptin receptor: identification of a mutation in the leptin receptor gene in db/db mice. Cell. 1996;84(3):491-5. PubMed PMID: 8608603.

47. Lee GH, Proenca R, Montez JM, Carroll KM, Darvishzadeh JG, Lee JI, Friedman JM. Abnormal splicing of the leptin receptor in diabetic mice. Nature. 1996;379(6566):632-5. doi: 10.1038/379632a0. PubMed PMID: 8628397.

48. Dalboge LS, Almholt DL, Neerup TS, Vassiliadis E, Vrang N, Pedersen L, Fosgerau K, Jelsing J. Characterisation of age-dependent beta cell dynamics in the male db/db mice. PloS one. 2013;8(12):e82813. doi: 10.1371/journal.pone.0082813. PubMed PMID: 24324833; PMCID: PMC3855780.

49. Shafrir E, Ziv E. A useful list of spontaneously arising animal models of obesity and diabetes. American journal of physiology Endocrinology and metabolism. 2009;296(6):E1450-2. doi: 10.1152/ajpendo.00113.2009. PubMed PMID: 19468077.

50. Delic D, Eisele C, Schmid R, Luippold G, Mayoux E, Grempler R. Characterization of Micro-RNA Changes during the Progression of Type 2 Diabetes in Zucker Diabetic Fatty Rats. International journal of molecular sciences. 2016;17(5). doi: 10.3390/ijms17050665. PubMed PMID: 27153060; PMCID: PMC4881491.

51. Da Silva Xavier G. The Cells of the Islets of Langerhans. J Clin Med. 2018;7(3). doi: 10.3390/jcm7030054. PubMed PMID: 29534517; PMCID: PMC5867580.

52. In't Veld P, Marichal M. Microscopic anatomy of the human islet of Langerhans. Advances in experimental medicine and biology. 2010;654:1-19. doi: 10.1007/978-90-481-3271-3_1. PubMed PMID: 20217491.

53. Matthews DR, Rudenski AS, Burnett MA, Darling P, Turner RC. The half-life of endogenous insulin and C-peptide in man assessed by somatostatin suppression. Clinical endocrinology. 1985;23(1):71-9. PubMed PMID: 2863015.

54. Rorsman P, Ashcroft FM. Pancreatic beta-Cell Electrical Activity and Insulin Secretion: Of Mice and Men. Physiol Rev. 2018;98(1):117-214. doi: 10.1152/physrev.00008.2017. PubMed PMID: 29212789; PMCID: PMC5866358.

55. Komatsu M, Takei M, Ishii H, Sato Y. Glucose-stimulated insulin secretion: A newer perspective. J Diabetes Investig. 2013;4(6):511-6. doi: 10.1111/jdi.12094. PubMed PMID: 24843702; PMCID: PMC4020243.

56. Wang Z, Thurmond DC. Mechanisms of biphasic insulin-granule exocytosis - roles of the cytoskeleton, small GTPases and SNARE proteins. Journal of cell science. 2009;122(Pt 7):893-903. doi: 10.1242/jcs.034355. PubMed PMID: 19295123; PMCID: PMC2720925.

57. Rorsman P, Eliasson L, Renstrom E, Gromada J, Barg S, Gopel S. The Cell Physiology of Biphasic Insulin Secretion. News Physiol Sci. 2000;15:72-7. PubMed PMID: 11390882.

58. Newsholme P, Brennan L, Rubi B, Maechler P. New insights into amino acid metabolism, beta-cell function and diabetes. Clinical science. 2005;108(3):185-94. doi: 10.1042/CS20040290. PubMed PMID: 15544573.

59. Furman B, Ong WK, Pyne NJ. Cyclic AMP signaling in pancreatic islets. Advances in experimental medicine and biology. 2010;654:281-304. doi: 10.1007/978-90-481-3271-3_13. PubMed PMID: 20217503.

60. Xu G, Kaneto H, Laybutt DR, Duvivier-Kali VF, Trivedi N, Suzuma K, King GL, Weir GC, Bonner-Weir S. Downregulation of GLP-1 and GIP receptor expression by hyperglycemia:

possible contribution to impaired incretin effects in diabetes. Diabetes. 2007;56(6):1551-8. doi: 10.2337/db06-1033. PubMed PMID: 17360984.

61. Nauck MA, Heimesaat MM, Orskov C, Holst JJ, Ebert R, Creutzfeldt W. Preserved incretin activity of glucagon-like peptide 1 [7-36 amide] but not of synthetic human gastric inhibitory polypeptide in patients with type-2 diabetes mellitus. The Journal of clinical investigation. 1993;91(1):301-7. doi: 10.1172/JCI116186. PubMed PMID: 8423228; PMCID: PMC330027.

62. Vaillant CR, Lund PK. Distribution of glucagon-like peptide I in canine and feline pancreas and gastrointestinal tract. J Histochem Cytochem. 1986;34(9):1117-21. doi: 10.1177/34.9.3755450. PubMed PMID: 3755450.

63. Bell GI, Santerre RF, Mullenbach GT. Hamster preproglucagon contains the sequence of glucagon and two related peptides. Nature. 1983;302(5910):716-8. PubMed PMID: 6835407.

64. Unger RH, Orci L. The essential role of glucagon in the pathogenesis of diabetes mellitus. Lancet. 1975;1(7897):14-6. PubMed PMID: 46337.

65. Cryer PE. Minireview: Glucagon in the pathogenesis of hypoglycemia and hyperglycemia in diabetes. Endocrinology. 2012;153(3):1039-48. doi: 10.1210/en.2011-1499. PubMed PMID: 22166985; PMCID: PMC3281526.

66. Ben-Othman N, Vieira A, Courtney M, Record F, Gjernes E, Avolio F, Hadzic B, Druelle N, Napolitano T, Navarro-Sanz S, Silvano S, Al-Hasani K, Pfeifer A, Lacas-Gervais S, Leuckx G, Marroqui L, Thevenet J, Madsen OD, Eizirik DL, Heimberg H, Kerr-Conte J, Pattou F, Mansouri A, Collombat P. Long-Term GABA Administration Induces Alpha Cell-Mediated Beta-like Cell Neogenesis. Cell. 2017;168(1-2):73-85 e11. doi: 10.1016/j.cell.2016.11.002. PubMed PMID: 27916274.

67. Bonner-Weir S, Sullivan BA, Weir GC. Human Islet Morphology Revisited: Human and Rodent Islets Are Not So Different After All. J Histochem Cytochem. 2015;63(8):604-12. doi: 10.1369/0022155415570969. PubMed PMID: 25604813; PMCID: PMC4530393.

68. Cabrera O, Berman DM, Kenyon NS, Ricordi C, Berggren PO, Caicedo A. The unique cytoarchitecture of human pancreatic islets has implications for islet cell function. Proceedings of the National Academy of Sciences of the United States of America. 2006;103(7):2334-9. doi: 10.1073/pnas.0510790103. PubMed PMID: 16461897; PMCID: PMC1413730.

69. Brissova M, Fowler MJ, Nicholson WE, Chu A, Hirshberg B, Harlan DM, Powers AC. Assessment of human pancreatic islet architecture and composition by laser scanning confocal microscopy. J Histochem Cytochem. 2005;53(9):1087-97. doi: 10.1369/jhc.5C6684.2005. PubMed PMID: 15923354.

70. Bosco D, Armanet M, Morel P, Niclauss N, Sgroi A, Muller YD, Giovannoni L, Parnaud G, Berney T. Unique arrangement of alpha- and beta-cells in human islets of Langerhans. Diabetes. 2010;59(5):1202-10. doi: 10.2337/db09-1177. PubMed PMID: 20185817; PMCID: PMC2857900.

71. Kilimnik G, Jo J, Periwal V, Zielinski MC, Hara M. Quantification of islet size and architecture. Islets. 2012;4(2):167-72. doi: 10.4161/isl.19256. PubMed PMID: 22653677; PMCID: PMC3396703.

72. Wang X, Misawa R, Zielinski MC, Cowen P, Jo J, Periwal V, Ricordi C, Khan A, Szust J, Shen J, Millis JM, Witkowski P, Hara M. Regional differences in islet distribution in the human pancreas--preferential beta-cell loss in the head region in patients with type 2 diabetes. PloS one. 2013;8(6):e67454. doi: 10.1371/journal.pone.0067454. PubMed PMID: 23826303; PMCID: PMC3691162.

73. Orci L, Unger RH. Functional subdivision of islets of Langerhans and possible role of D cells. Lancet. 1975;2(7947):1243-4. PubMed PMID: 53729.

74. Gannon M, Ray MK, Van Zee K, Rausa F, Costa RH, Wright CV. Persistent expression of HNF6 in islet endocrine cells causes disrupted islet architecture and loss of beta cell function. Development. 2000;127(13):2883-95. PubMed PMID: 10851133.

75. Rorsman P, Braun M. Regulation of insulin secretion in human pancreatic islets. Annu Rev Physiol. 2013;75:155-79. doi: 10.1146/annurev-physiol-030212-183754. PubMed PMID: 22974438.

76. Rui L. Energy metabolism in the liver. Compr Physiol. 2014;4(1):177-97. doi: 10.1002/cphy.c130024. PubMed PMID: 24692138; PMCID: PMC4050641.

77. Han HS, Kang G, Kim JS, Choi BH, Koo SH. Regulation of glucose metabolism from a liver-centric perspective. Exp Mol Med. 2016;48:e218. doi: 10.1038/emm.2015.122. PubMed PMID: 26964834; PMCID: PMC4892876.

78. Ramnanan CJ, Edgerton DS, Kraft G, Cherrington AD. Physiologic action of glucagon on liver glucose metabolism. Diabetes, obesity & metabolism. 2011;13 Suppl 1:118-25. doi: 10.1111/j.1463-1326.2011.01454.x. PubMed PMID: 21824265; PMCID: PMC5371022.

79. Petersen MC, Vatner DF, Shulman GI. Regulation of hepatic glucose metabolism in health and disease. Nat Rev Endocrinol. 2017;13(10):572-87. doi: 10.1038/nrendo.2017.80. PubMed PMID: 28731034; PMCID: PMC5777172.

80. Hatting M, Tavares CDJ, Sharabi K, Rines AK, Puigserver P. Insulin regulation of gluconeogenesis. Annals of the New York Academy of Sciences. 2018;1411(1):21-35. doi: 10.1111/nyas.13435. PubMed PMID: 28868790; PMCID: PMC5927596.

81. Chang L, Chiang SH, Saltiel AR. Insulin signaling and the regulation of glucose transport. Mol Med. 2004;10(7-12):65-71. doi: 10.2119/2005-00029.Saltiel. PubMed PMID: 16307172; PMCID: PMC1431367.

82. Cooperberg BA, Cryer PE. Insulin reciprocally regulates glucagon secretion in humans. Diabetes. 2010;59(11):2936-40. doi: 10.2337/db10-0728. PubMed PMID: 20811038; PMCID: PMC2963553.

83. Hardy OT, Czech MP, Corvera S. What causes the insulin resistance underlying obesity? Current opinion in endocrinology, diabetes, and obesity. 2012;19(2):81-7. doi: 10.1097/MED.0b013e3283514e13. PubMed PMID: 22327367; PMCID: PMC4038351.

84. Smushkin G, Sathananthan M, Piccinini F, Dalla Man C, Law JH, Cobelli C, Zinsmeister AR, Rizza RA, Vella A. The effect of a bile acid sequestrant on glucose metabolism in subjects with type 2 diabetes. Diabetes. 2013;62(4):1094-101. doi: 10.2337/db12-0923. PubMed PMID: 23250357; PMCID: PMC3609563.

85. Meissner M, Herrema H, van Dijk TH, Gerding A, Havinga R, Boer T, Muller M, Reijngoud DJ, Groen AK, Kuipers F. Bile acid sequestration reduces plasma glucose levels in db/db mice by increasing its metabolic clearance rate. PloS one. 2011;6(11):e24564. doi: 10.1371/journal.pone.0024564. PubMed PMID: 22087215; PMCID: 3210115.

86. Rigby SP, Handelsman Y, Lai YL, Abby SL, Tao B, Jones MR. Effects of colesevelam, rosiglitazone, or sitagliptin on glycemic control and lipid profile in patients with type 2 diabetes mellitus inadequately controlled by metformin monotherapy. Endocr Pract. 2010;16(1):53-63. doi: 10.4158/EP09146.OR. PubMed PMID: 19789153.

87. Schwartz SL, Lai YL, Xu J, Abby SL, Misir S, Jones MR, Nagendran S. The effect of colesevelam hydrochloride on insulin sensitivity and secretion in patients with type 2 diabetes: a pilot study. Metab Syndr Relat Disord. 2010;8(2):179-88. doi: 10.1089/met.2009.0049. PubMed PMID: 20059361.

88. Henry RR, Aroda VR, Mudaliar S, Garvey WT, Chou HS, Jones MR. Effects of colesevelam on glucose absorption and hepatic/peripheral insulin sensitivity in patients with type 2 diabetes mellitus. Diabetes, obesity & metabolism. 2012;14(1):40-6. doi: 10.1111/j.1463-1326.2011.01486.x. PubMed PMID: 21831167; PMCID: PMC4955577.

89. Sedgeman LR, Beysen C, Allen RM, Ramirez Solano MA, Turner SM, Vickers KC. Intestinal bile acid sequestration improves glucose control by stimulating hepatic miR-182-5p in type 2 diabetes. American journal of physiology Gastrointestinal and liver physiology. 2018. doi: 10.1152/ajpgi.00238.2018. PubMed PMID: 30160993.

90. Feingold KR, Grunfeld C. Introduction to Lipids and Lipoproteins. In: De Groot LJ, Chrousos G, Dungan K, Feingold KR, Grossman A, Hershman JM, Koch C, Korbonits M,

McLachlan R, New M, Purnell J, Rebar R, Singer F, Vinik A, editors. Endotext. South Dartmouth (MA)2000.

91. Favari E, Chroni A, Tietge UJ, Zanotti I, Escola-Gil JC, Bernini F. Cholesterol efflux and reverse cholesterol transport. Handbook of experimental pharmacology. 2015;224:181-206. doi: 10.1007/978-3-319-09665-0_4. PubMed PMID: 25522988.

92. Kaur N, Pandey A, Negi H, Shafiq N, Reddy S, Kaur H, Chadha N, Malhotra S. Effect of HDL-raising drugs on cardiovascular outcomes: a systematic review and meta-regression. PloS one. 2014;9(4):e94585. doi: 10.1371/journal.pone.0094585. PubMed PMID: 24728455; PMCID: PMC3984171.

93. Vickers KC, Remaley AT. HDL and cholesterol: life after the divorce? J Lipid Res. 2014;55(1):4-12. doi: 10.1194/jlr.R035964. PubMed PMID: 23515282; PMCID: 3927467.

94. Vickers KC, Palmisano BT, Shoucri BM, Shamburek RD, Remaley AT. MicroRNAs are transported in plasma and delivered to recipient cells by high-density lipoproteins. Nature cell biology. 2011;13(4):423-33. doi: 10.1038/ncb2210. PubMed PMID: 21423178; PMCID: 3074610.

95. Tabet F, Vickers KC, Cuesta Torres LF, Wiese CB, Shoucri BM, Lambert G, Catherinet C, Prado-Lourenco L, Levin MG, Thacker S, Sethupathy P, Barter PJ, Remaley AT, Rye KA. HDL-transferred microRNA-223 regulates ICAM-1 expression in endothelial cells. Nature communications. 2014;5:3292. doi: 10.1038/ncomms4292. PubMed PMID: 24576947.

96. Bartel DP. MicroRNAs: genomics, biogenesis, mechanism, and function. Cell. 2004;116(2):281-97. PubMed PMID: 14744438.

97. Bushati N, Cohen SM. microRNA functions. Annu Rev Cell Dev Biol. 2007;23:175-205. doi: 10.1146/annurev.cellbio.23.090506.123406. PubMed PMID: 17506695.

98. Ha M, Kim VN. Regulation of microRNA biogenesis. Nat Rev Mol Cell Biol. 2014;15(8):509-24. doi: 10.1038/nrm3838. PubMed PMID: 25027649.

99. Gebert LFR, MacRae IJ. Regulation of microRNA function in animals. Nat Rev Mol Cell Biol. 2018. doi: 10.1038/s41580-018-0045-7. PubMed PMID: 30108335.

100. Klein M, Chandradoss SD, Depken M, Joo C. Why Argonaute is needed to make microRNA target search fast and reliable. Seminars in cell & developmental biology. 2017;65:20-8. doi: 10.1016/j.semcdb.2016.05.017. PubMed PMID: 27235676.

101. !!! INVALID CITATION !!! {}.

102. Xu S, Witmer PD, Lumayag S, Kovacs B, Valle D. MicroRNA (miRNA) transcriptome of mouse retina and identification of a sensory organ-specific miRNA cluster. The Journal of biological chemistry. 2007;282(34):25053-66. doi: 10.1074/jbc.M700501200. PubMed PMID: 17597072.

103. Jeon TI, Esquejo RM, Roqueta-Rivera M, Phelan PE, Moon YA, Govindarajan SS, Esau CC, Osborne TF. An SREBP-responsive microRNA operon contributes to a regulatory loop for intracellular lipid homeostasis. Cell metabolism. 2013;18(1):51-61. doi: 10.1016/j.cmet.2013.06.010. PubMed PMID: 23823476; PMCID: PMC3740797.

104. Jeon TI, Osborne TF. miRNA and cholesterol homeostasis. Biochimica et biophysica acta. 2016;1861(12 Pt B):2041-6. doi: 10.1016/j.bbalip.2016.01.005. PubMed PMID: 26778752; PMCID: PMC4980302.

105. Horton JD, Goldstein JL, Brown MS. SREBPs: activators of the complete program of cholesterol and fatty acid synthesis in the liver. The Journal of clinical investigation. 2002;109(9):1125-31. doi: 10.1172/JCI15593. PubMed PMID: 11994399; PMCID: PMC150968.

106. Marquart TJ, Allen RM, Ory DS, Baldan A. miR-33 links SREBP-2 induction to repression of sterol transporters. Proceedings of the National Academy of Sciences of the United States of America. 2010;107(27):12228-32. doi: 10.1073/pnas.1005191107. PubMed PMID: 20566875; PMCID: 2901433.

107. Rayner KJ, Suarez Y, Davalos A, Parathath S, Fitzgerald ML, Tamehiro N, Fisher EA, Moore KJ, Fernandez-Hernando C. MiR-33 contributes to the regulation of cholesterol

homeostasis. Science. 2010;328(5985):1570-3. doi: 10.1126/science.1189862. PubMed PMID: 20466885; PMCID: 3114628.

108. Najafi-Shoushtari SH, Kristo F, Li Y, Shioda T, Cohen DE, Gerszten RE, Naar AM. MicroRNA-33 and the SREBP host genes cooperate to control cholesterol homeostasis. Science. 2010;328(5985):1566-9. doi: 10.1126/science.1189123. PubMed PMID: 20466882; PMCID: 3840500.

109. Zhou J, Meng Y, Tian S, Chen J, Liu M, Zhuo M, Zhang Y, Du H, Wang X. Comparative MicroRNA Expression Profiles of Cynomolgus Monkeys, Rat, and Human Reveal that miR-182 Is Involved in T2D Pathogenic Processes. Journal of diabetes research. 2014;2014:760397. doi: 10.1155/2014/760397. PubMed PMID: 25530976; PMCID: 4235598.

110. Kim KM, Park SJ, Jung SH, Kim EJ, Jogeswar G, Ajita J, Rhee Y, Kim CH, Lim SK. miR-182 is a negative regulator of osteoblast proliferation, differentiation, and skeletogenesis through targeting FoxO1. J Bone Miner Res. 2012;27(8):1669-79. doi: 10.1002/jbmr.1604. PubMed PMID: 22431396.

111. Tang T, Wong HK, Gu W, Yu MY, To KF, Wang CC, Wong YF, Cheung TH, Chung TK, Choy KW. MicroRNA-182 plays an onco-miRNA role in cervical cancer. Gynecologic oncology. 2013;129(1):199-208. doi: 10.1016/j.ygyno.2012.12.043. PubMed PMID: 23313739.

112. Del Guerra S, Lupi R, Marselli L, Masini M, Bugliani M, Sbrana S, Torri S, Pollera M, Boggi U, Mosca F, Del Prato S, Marchetti P. Functional and molecular defects of pancreatic islets in human type 2 diabetes. Diabetes. 2005;54(3):727-35. PubMed PMID: 15734849.

113. Barthel A, Schmoll D. Novel concepts in insulin regulation of hepatic gluconeogenesis. American journal of physiology Endocrinology and metabolism. 2003;285(4):E685-92. doi: 10.1152/ajpendo.00253.2003. PubMed PMID: 12959935.

114. Hudson MB, Rahnert JA, Zheng B, Woodworth-Hobbs ME, Franch HA, Price SR. miR-182 attenuates atrophy-related gene expression by targeting FoxO3 in skeletal muscle. Am J

Physiol Cell Physiol. 2014;307(4):C314-9. doi: 10.1152/ajpcell.00395.2013. PubMed PMID: 24871856; PMCID: PMC4137139.

115. Sanchez AM, Candau RB, Bernardi H. FoxO transcription factors: their roles in the maintenance of skeletal muscle homeostasis. Cell Mol Life Sci. 2014;71(9):1657-71. doi: 10.1007/s00018-013-1513-z. PubMed PMID: 24232446.

116. Zhang D, Li Y, Yao X, Wang H, Zhao L, Jiang H, Yao X, Zhang S, Ye C, Liu W, Cao H, Yu S, Wang YC, Li Q, Jiang J, Liu Y, Zhang L, Liu Y, Iwai N, Wang H, Li J, Li J, Li X, Jin ZB, Ying H. miR-182 Regulates Metabolic Homeostasis by Modulating Glucose Utilization in Muscle. Cell Rep. 2016;16(3):757-68. doi: 10.1016/j.celrep.2016.06.040. PubMed PMID: 27396327.

117. Yang WM, Min KH, Lee W. Induction of miR-96 by Dietary Saturated Fatty Acids Exacerbates Hepatic Insulin Resistance through the Suppression of INSR and IRS-1. PloS one. 2016;11(12):e0169039. doi: 10.1371/journal.pone.0169039. PubMed PMID: 28036389; PMCID: PMC5201257.

118. Guo Y, Liu H, Zhang H, Shang C, Song Y. miR-96 regulates FOXO1-mediated cell apoptosis in bladder cancer. Oncol Lett. 2012;4(3):561-5. doi: 10.3892/ol.2012.775. PubMed PMID: 23741253; PMCID: PMC3673640.

119. Guttilla IK, White BA. Coordinate regulation of FOXO1 by miR-27a, miR-96, and miR-182 in breast cancer cells. J Biol Chem. 2009;284(35):23204-16. doi: 10.1074/jbc.M109.031427. PubMed PMID: 19574223; PMCID: PMC2749094.

120. Song HM, Luo Y, Li DF, Wei CK, Hua KY, Song JL, Xu H, Maskey N, Fang L. MicroRNA-96 plays an oncogenic role by targeting FOXO1 and regulating AKT/FOXO1/Bim pathway in papillary thyroid carcinoma cells. Int J Clin Exp Pathol. 2015;8(9):9889-900. PubMed PMID: 26617698; PMCID: PMC4637783.

121. Eliasson L. The small RNA miR-375 - a pancreatic islet abundant miRNA with multiple roles in endocrine beta cell function. Molecular and cellular endocrinology. 2017;456:95-101. doi: 10.1016/j.mce.2017.02.043. PubMed PMID: 28254488.

122. Baroukh NN, Van Obberghen E. Function of microRNA-375 and microRNA-124a in pancreas and brain. FEBS J. 2009;276(22):6509-21. doi: 10.1111/j.1742-4658.2009.07353.x. PubMed PMID: 20102393.

123. Bravo-Egana V, Rosero S, Molano RD, Pileggi A, Ricordi C, Dominguez-Bendala J, Pastori RL. Quantitative differential expression analysis reveals miR-7 as major islet microRNA. Biochem Biophys Res Commun. 2008;366(4):922-6. doi: 10.1016/j.bbrc.2007.12.052. PubMed PMID: 18086561; PMCID: PMC4104201.

124. van de Bunt M, Gaulton KJ, Parts L, Moran I, Johnson PR, Lindgren CM, Ferrer J, Gloyn AL, McCarthy MI. The miRNA profile of human pancreatic islets and beta-cells and relationship to type 2 diabetes pathogenesis. PloS one. 2013;8(1):e55272. doi: 10.1371/journal.pone.0055272. PubMed PMID: 23372846; PMCID: 3555946.

125. Latreille M, Herrmanns K, Renwick N, Tuschl T, Malecki MT, McCarthy MI, Owen KR, Rulicke T, Stoffel M. miR-375 gene dosage in pancreatic beta-cells: implications for regulation of beta-cell mass and biomarker development. Journal of molecular medicine. 2015;93(10):1159-69. doi: 10.1007/s00109-015-1296-9. PubMed PMID: 26013143; PMCID: PMC4589563.

126. Erener S, Mojibian M, Fox JK, Denroche HC, Kieffer TJ. Circulating miR-375 as a biomarker of beta-cell death and diabetes in mice. Endocrinology. 2013;154(2):603-8. doi: 10.1210/en.2012-1744. PubMed PMID: 23321698.

127. Poy MN, Eliasson L, Krutzfeldt J, Kuwajima S, Ma X, Macdonald PE, Pfeffer S, Tuschl T, Rajewsky N, Rorsman P, Stoffel M. A pancreatic islet-specific microRNA regulates insulin secretion. Nature. 2004;432(7014):226-30. doi: 10.1038/nature03076. PubMed PMID: 15538371.

128. Poy MN, Hausser J, Trajkovski M, Braun M, Collins S, Rorsman P, Zavolan M, Stoffel M. miR-375 maintains normal pancreatic alpha- and beta-cell mass. Proceedings of the National Academy of Sciences of the United States of America. 2009;106(14):5813-8. doi: 10.1073/pnas.0810550106. PubMed PMID: 19289822; PMCID: 2656556.

129. Avnit-Sagi T, Kantorovich L, Kredo-Russo S, Hornstein E, Walker MD. The promoter of the pri-miR-375 gene directs expression selectively to the endocrine pancreas. PloS one. 2009;4(4):e5033. doi: 10.1371/journal.pone.0005033. PubMed PMID: 19343226; PMCID: PMC2660411.

130. El Ouaamari A, Baroukh N, Martens GA, Lebrun P, Pipeleers D, van Obberghen E. miR-375 targets 3'-phosphoinositide-dependent protein kinase-1 and regulates glucose-induced biological responses in pancreatic beta-cells. Diabetes. 2008;57(10):2708-17. doi: 10.2337/db07-1614. PubMed PMID: 18591395; PMCID: 2551681.

131. Keller DM, Clark EA, Goodman RH. Regulation of microRNA-375 by cAMP in pancreatic beta-cells. Molecular endocrinology. 2012;26(6):989-99. doi: 10.1210/me.2011-1205. PubMed PMID: 22539037; PMCID: PMC3355542.

132. Esguerra JL, Bolmeson C, Cilio CM, Eliasson L. Differential glucose-regulation of microRNAs in pancreatic islets of non-obese type 2 diabetes model Goto-Kakizaki rat. PloS one. 2011;6(4):e18613. doi: 10.1371/journal.pone.0018613. PubMed PMID: 21490936; PMCID: PMC3072418.

133. Sebastiani G, Po A, Miele E, Ventriglia G, Ceccarelli E, Bugliani M, Marselli L, Marchetti P, Gulino A, Ferretti E, Dotta F. MicroRNA-124a is hyperexpressed in type 2 diabetic human pancreatic islets and negatively regulates insulin secretion. Acta Diabetol. 2015;52(3):523-30. doi: 10.1007/s00592-014-0675-y. PubMed PMID: 25408296.

134. Michell DL, Vickers KC. Lipoprotein carriers of microRNAs. Biochimica et biophysica acta. 2016;1861(12 Pt B):2069-74. doi: 10.1016/j.bbalip.2016.01.011. PubMed PMID: 26825691; PMCID: PMC4959968.

135. Sohel MH. Extracellular/Circulating MicroRNAs: Release Mechanisms, Functions and Challenges. Achievements in the Life Sciences. 2016;10(2):175-86. Epub 186.

136. Hunter MP, Ismail N, Zhang X, Aguda BD, Lee EJ, Yu L, Xiao T, Schafer J, Lee ML, Schmittgen TD, Nana-Sinkam SP, Jarjoura D, Marsh CB. Detection of microRNA expression in human peripheral blood microvesicles. PloS one. 2008;3(11):e3694. doi: 10.1371/journal.pone.0003694. PubMed PMID: 19002258; PMCID: PMC2577891.

137. Valadi H, Ekstrom K, Bossios A, Sjostrand M, Lee JJ, Lotvall JO. Exosome-mediated transfer of mRNAs and microRNAs is a novel mechanism of genetic exchange between cells. Nature cell biology. 2007;9(6):654-9. doi: 10.1038/ncb1596. PubMed PMID: 17486113.

138. Chen X, Ba Y, Ma L, Cai X, Yin Y, Wang K, Guo J, Zhang Y, Chen J, Guo X, Li Q, Li X, Wang W, Zhang Y, Wang J, Jiang X, Xiang Y, Xu C, Zheng P, Zhang J, Li R, Zhang H, Shang X, Gong T, Ning G, Wang J, Zen K, Zhang J, Zhang CY. Characterization of microRNAs in serum: a novel class of biomarkers for diagnosis of cancer and other diseases. Cell research. 2008;18(10):997-1006. doi: 10.1038/cr.2008.282. PubMed PMID: 18766170.

139. Arroyo JD, Chevillet JR, Kroh EM, Ruf IK, Pritchard CC, Gibson DF, Mitchell PS, Bennett CF, Pogosova-Agadjanyan EL, Stirewalt DL, Tait JF, Tewari M. Argonaute2 complexes carry a population of circulating microRNAs independent of vesicles in human plasma. Proceedings of the National Academy of Sciences of the United States of America. 2011;108(12):5003-8. doi: 10.1073/pnas.1019055108. PubMed PMID: 21383194; PMCID: 3064324.

140. da Silva EB, Soares MG, Mariane B, Vallim MA, Pascon RC, Sartorelli P, Lago JH. The seasonal variation of the chemical composition of essential oils from Porcelia macrocarpa R.E. Fries (Annonaceae) and their antimicrobial activity. Molecules. 2013;18(11):13574-87. doi: 10.3390/molecules181113574. PubMed PMID: 24189296.

141. Sohel MM, Hoelker M, Noferesti SS, Salilew-Wondim D, Tholen E, Looft C, Rings F, Uddin MJ, Spencer TE, Schellander K, Tesfaye D. Exosomal and Non-Exosomal Transport of

Extra-Cellular microRNAs in Follicular Fluid: Implications for Bovine Oocyte Developmental Competence. PloS one. 2013;8(11):e78505. doi: 10.1371/journal.pone.0078505. PubMed PMID: 24223816; PMCID: PMC3817212.

142. Rubio M, Bustamante M, Hernandez-Ferrer C, Fernandez-Orth D, Pantano L, Sarria Y, Pique-Borras M, Vellve K, Agramunt S, Carreras R, Estivill X, Gonzalez JR, Mayor A. Circulating miRNAs, isomiRs and small RNA clusters in human plasma and breast milk. PloS one. 2018;13(3):e0193527. doi: 10.1371/journal.pone.0193527. PubMed PMID: 29505615; PMCID: PMC5837101.

143. Kamm RC, Smith AG. Ribonuclease activity in human plasma. Clinical biochemistry. 1972;5(4):198-200. PubMed PMID: 4674387.

144. Kamm RC, Smith AG. Nucleic acid concentrations in normal human plasma. Clinical chemistry. 1972;18(6):519-22. PubMed PMID: 5026765.

145. El-Hefnawy T, Raja S, Kelly L, Bigbee WL, Kirkwood JM, Luketich JD, Godfrey TE. Characterization of amplifiable, circulating RNA in plasma and its potential as a tool for cancer diagnostics. Clinical chemistry. 2004;50(3):564-73. doi: 10.1373/clinchem.2003.028506. PubMed PMID: 14718398.

146. Hessvik NP, Llorente A. Current knowledge on exosome biogenesis and release. Cell Mol Life Sci. 2018;75(2):193-208. doi: 10.1007/s00018-017-2595-9. PubMed PMID: 28733901; PMCID: PMC5756260.

147. Chevillet JR, Kang Q, Ruf IK, Briggs HA, Vojtech LN, Hughes SM, Cheng HH, Arroyo JD, Meredith EK, Gallichotte EN, Pogosova-Agadjanyan EL, Morrissey C, Stirewalt DL, Hladik F, Yu EY, Higano CS, Tewari M. Quantitative and stoichiometric analysis of the microRNA content of exosomes. Proceedings of the National Academy of Sciences of the United States of America. 2014;111(41):14888-93. doi: 10.1073/pnas.1408301111. PubMed PMID: 25267620; PMCID: PMC4205618.

148. Ying W, Riopel M, Bandyopadhyay G, Dong Y, Birmingham A, Seo JB, Ofrecio JM, Wollam J, Hernandez-Carretero A, Fu W, Li P, Olefsky JM. Adipose Tissue Macrophage-Derived Exosomal miRNAs Can Modulate In Vivo and In Vitro Insulin Sensitivity. Cell. 2017;171(2):372-84 e12. doi: 10.1016/j.cell.2017.08.035. PubMed PMID: 28942920.

149. Bala S, Csak T, Momen-Heravi F, Lippai D, Kodys K, Catalano D, Satishchandran A, Ambros V, Szabo G. Biodistribution and function of extracellular miRNA-155 in mice. Scientific reports. 2015;5:10721. doi: 10.1038/srep10721. PubMed PMID: 26024046; PMCID: PMC4448655.

150. Thomou T, Mori MA, Dreyfuss JM, Konishi M, Sakaguchi M, Wolfrum C, Rao TN, Winnay JN, Garcia-Martin R, Grinspoon SK, Gorden P, Kahn CR. Adipose-derived circulating miRNAs regulate gene expression in other tissues. Nature. 2017;542(7642):450-5. doi: 10.1038/nature21365. PubMed PMID: 28199304; PMCID: PMC5330251.

151. Endzelins E, Berger A, Melne V, Bajo-Santos C, Sobolevska K, Abols A, Rodriguez M, Santare D, Rudnickiha A, Lietuvietis V, Llorente A, Line A. Detection of circulating miRNAs: comparative analysis of extracellular vesicle-incorporated miRNAs and cell-free miRNAs in whole plasma of prostate cancer patients. BMC cancer. 2017;17(1):730. doi: 10.1186/s12885-017-3737-z. PubMed PMID: 29121858; PMCID: PMC5679326.

152. Tang LL, Wu YB, Fang CQ, Qu P, Gao ZL. NDRG2 promoted secreted miR-375 in microvesicles shed from M1 microglia, which induced neuron damage. Biochem Biophys Res Commun. 2016;469(3):392-8. doi: 10.1016/j.bbrc.2015.11.098. PubMed PMID: 26631961.

153. Shefler I, Salamon P, Reshef T, Mor A, Mekori YA. T cell-induced mast cell activation: a role for microparticles released from activated T cells. Journal of immunology. 2010;185(7):4206-12. doi: 10.4049/jimmunol.1000409. PubMed PMID: 20810987.

154. Jaiswal R, Gong J, Sambasivam S, Combes V, Mathys JM, Davey R, Grau GE, Bebawy M. Microparticle-associated nucleic acids mediate trait dominance in cancer. FASEB journal :

official publication of the Federation of American Societies for Experimental Biology. 2012;26(1):420-9. doi: 10.1096/fj.11-186817. PubMed PMID: 21965597.

155. Yuan A, Farber EL, Rapoport AL, Tejada D, Deniskin R, Akhmedov NB, Farber DB. Transfer of microRNAs by embryonic stem cell microvesicles. PloS one. 2009;4(3):e4722. doi: 10.1371/journal.pone.0004722. PubMed PMID: 19266099; PMCID: PMC2648987.

156. Zernecke A, Bidzhekov K, Noels H, Shagdarsuren E, Gan L, Denecke B, Hristov M, Koppel T, Jahantigh MN, Lutgens E, Wang S, Olson EN, Schober A, Weber C. Delivery of microRNA-126 by apoptotic bodies induces CXCL12-dependent vascular protection. Science signaling. 2009;2(100):ra81. doi: 10.1126/scisignal.2000610. PubMed PMID: 19996457.

157. Turchinovich A, Weiz L, Langheinz A, Burwinkel B. Characterization of extracellular circulating microRNA. Nucleic acids research. 2011;39(16):7223-33. doi: 10.1093/nar/gkr254. PubMed PMID: 21609964; PMCID: 3167594.

158. Turchinovich A, Burwinkel B. Distinct AGO1 and AGO2 associated miRNA profiles in human cells and blood plasma. RNA biology. 2012;9(8):1066-75. doi: 10.4161/rna.21083. PubMed PMID: 22858679; PMCID: PMC3551861.

159. Assmann G, Gotto AM, Jr. HDL cholesterol and protective factors in atherosclerosis. Circulation. 2004;109(23 Suppl 1):III8-14. doi: 10.1161/01.CIR.0000131512.50667.46. PubMed PMID: 15198960.

160. Zhou L, Li C, Gao L, Wang A. High-density lipoprotein synthesis and metabolism (Review). Mol Med Rep. 2015;12(3):4015-21. doi: 10.3892/mmr.2015.3930. PubMed PMID: 26082200.

161. Hill SA, McQueen MJ. Reverse cholesterol transport--a review of the process and its clinical implications. Clinical biochemistry. 1997;30(7):517-25. PubMed PMID: 9399019.

162. Lee H, Kim SI, Shin D, Yoon Y, Choi TH, Cheon GJ, Kim M. Hepatic siRNA delivery using recombinant human apolipoprotein A-I in mice. Biochem Biophys Res Commun. 2009;378(2):192-6. doi: 10.1016/j.bbrc.2008.11.029. PubMed PMID: 19017527.

163. Wagner J, Riwanto M, Besler C, Knau A, Fichtlscherer S, Roxe T, Zeiher AM, Landmesser U, Dimmeler S. Characterization of levels and cellular transfer of circulating lipoprotein-bound microRNAs. Arteriosclerosis, thrombosis, and vascular biology. 2013;33(6):1392-400. doi: 10.1161/ATVBAHA.112.300741. PubMed PMID: 23559634.

164. Menck K, Sonmezer C, Worst TS, Schulz M, Dihazi GH, Streit F, Erdmann G, Kling S, Boutros M, Binder C, Gross JC. Neutral sphingomyelinases control extracellular vesicles budding from the plasma membrane. J Extracell Vesicles. 2017;6(1):1378056. doi: 10.1080/20013078.2017.1378056. PubMed PMID: 29184623; PMCID: PMC5699186.

165. Figliolini F, Cantaluppi V, De Lena M, Beltramo S, Romagnoli R, Salizzoni M, Melzi R, Nano R, Piemonti L, Tetta C, Biancone L, Camussi G. Isolation, characterization and potential role in beta cell-endothelium cross-talk of extracellular vesicles released from human pancreatic islets. PloS one. 2014;9(7):e102521. doi: 10.1371/journal.pone.0102521. PubMed PMID: 25028931; PMCID: PMC4100900.

166. Guay C, Menoud V, Rome S, Regazzi R. Horizontal transfer of exosomal microRNAs transduce apoptotic signals between pancreatic beta-cells. Cell Commun Signal. 2015;13:17. doi: 10.1186/s12964-015-0097-7. PubMed PMID: 25880779; PMCID: PMC4371845.

167. Song I, Roels S, Martens GA, Bouwens L. Circulating microRNA-375 as biomarker of pancreatic beta cell death and protection of beta cell mass by cytoprotective compounds. PloS one. 2017;12(10):e0186480. doi: 10.1371/journal.pone.0186480. PubMed PMID: 29040320; PMCID: PMC5645134.

168. Zhang A, Li D, Liu Y, Li J, Zhang Y, Zhang CY. Islet beta cell: An endocrine cell secreting miRNAs. Biochem Biophys Res Commun. 2018;495(2):1648-54. doi: 10.1016/j.bbrc.2017.12.028. PubMed PMID: 29223394.

169. Gumurdu A, Yildiz R, Eren E, Karakulah G, Unver T, Genc S, Park Y. MicroRNA exocytosis by large dense-core vesicle fusion. Scientific reports. 2017;7:45661. doi: 10.1038/srep45661. PubMed PMID: 28358390; PMCID: PMC5372467.

170. Allen RM, Zhao S, Ramirez-Solano MA, Michell DL, Wang Y, Shyr Y, Sethupathy P, Linton MF, Graf GA, Sheng Q, Vickers KC. Bioinformatic analysis of endogenous and exogenous small RNAs on lipoproteins. bioRxiv. 2018.

171. Roat R, Hossain MM, Christopherson J, Free C, Jain S, Guay C, Regazzi R, Guo Z. Identification and Characterization of microRNAs Associated With Human beta-Cell Loss in a Mouse Model. Am J Transplant. 2017;17(4):992-1007. doi: 10.1111/ajt.14073. PubMed PMID: 27700000.

172. Marchand L, Jalabert A, Meugnier E, Van den Hende K, Fabien N, Nicolino M, Madec AM, Thivolet C, Rome S. miRNA-375 a Sensor of Glucotoxicity Is Altered in the Serum of Children with Newly Diagnosed Type 1 Diabetes. Journal of diabetes research. 2016;2016:1869082. doi: 10.1155/2016/1869082. PubMed PMID: 27314045; PMCID: PMC4895032.

173. Samandari N, Mirza AH, Nielsen LB, Kaur S, Hougaard P, Fredheim S, Mortensen HB, Pociot F. Circulating microRNA levels predict residual beta cell function and glycaemic control in children with type 1 diabetes mellitus. Diabetologia. 2017;60(2):354-63. doi: 10.1007/s00125-016-4156-4. PubMed PMID: 27866223.

174. Zhu H, Leung SW. Identification of microRNA biomarkers in type 2 diabetes: a meta-analysis of controlled profiling studies. Diabetologia. 2015;58(5):900-11. doi: 10.1007/s00125-015-3510-2. PubMed PMID: 25677225.

175. Higuchi C, Nakatsuka A, Eguchi J, Teshigawara S, Kanzaki M, Katayama A, Yamaguchi S, Takahashi N, Murakami K, Ogawa D, Sasaki S, Makino H, Wada J. Identification of circulating miR-101, miR-375 and miR-802 as biomarkers for type 2 diabetes. Metabolism: clinical and experimental. 2015;64(4):489-97. doi: 10.1016/j.metabol.2014.12.003. PubMed PMID: 25726255.

176. Al-Muhtaresh HA, Al-Kafaji G. Evaluation of Two-Diabetes Related microRNAs Suitability as Earlier Blood Biomarkers for Detecting Prediabetes and type 2 Diabetes Mellitus. J

Clin Med. 2018;7(2). doi: 10.3390/jcm7020012. PubMed PMID: 29373500; PMCID: PMC5852428.

177. Stancill JS, Cartailler JP, Clayton HW, O'Connor JT, Dickerson MT, Dadi PK, Osipovich AB, Jacobson DA, Magnuson MA. Chronic beta-Cell Depolarization Impairs beta-Cell Identity by Disrupting a Network of Ca2+-Regulated Genes. Diabetes. 2017;66(8):2175-87. doi: 10.2337/db16-1355. PubMed PMID: 28550109; PMCID: PMC5521870.

178. Miki T, Nagashima K, Tashiro F, Kotake K, Yoshitomi H, Tamamoto A, Gonoi T, Iwanaga T, Miyazaki J, Seino S. Defective insulin secretion and enhanced insulin action in KATP channel-deficient mice. Proceedings of the National Academy of Sciences of the United States of America. 1998;95(18):10402-6. PubMed PMID: 9724715; PMCID: PMC27906.

179. Brissova M, Fowler M, Wiebe P, Shostak A, Shiota M, Radhika A, Lin PC, Gannon M, Powers AC. Intraislet endothelial cells contribute to revascularization of transplanted pancreatic islets. Diabetes. 2004;53(5):1318-25. PubMed PMID: 15111502.

180. Montemurro C, Vadrevu S, Gurlo T, Butler AE, Vongbunyong KE, Petcherski A, Shirihai OS, Satin LS, Braas D, Butler PC, Tudzarova S. Cell cycle-related metabolism and mitochondrial dynamics in a replication-competent pancreatic beta-cell line. Cell Cycle. 2017;16(21):2086-99. doi: 10.1080/15384101.2017.1361069. PubMed PMID: 28820316; PMCID: PMC5731404.

181. Langmead B, Trapnell C, Pop M, Salzberg SL. Ultrafast and memory-efficient alignment of short DNA sequences to the human genome. Genome Biol. 2009;10(3):R25. doi: 10.1186/gb-2009-10-3-r25. PubMed PMID: 19261174; PMCID: 2690996.

182. Love MI, Huber W, Anders S. Moderated estimation of fold change and dispersion for RNA-seq data with DESeq2. Genome Biol. 2014;15(12):550. doi: 10.1186/s13059-014-0550-8. PubMed PMID: 25516281; PMCID: 4302049.

183. Chen S, Turner S, Tsang E, Stark J, Turner H, Mahsut A, Keifer K, Goldfinger M, Hellerstein MK. Measurement of pancreatic islet cell proliferation by heavy water labeling.

American journal of physiology Endocrinology and metabolism. 2007;293(5):E1459-64. doi: 10.1152/ajpendo.00375.2007. PubMed PMID: 17726142.

184. Lee WN, Bassilian S, Guo Z, Schoeller D, Edmond J, Bergner EA, Byerley LO. Measurement of fractional lipid synthesis using deuterated water (2H2O) and mass isotopomer analysis. Am J Physiol. 1994;266(3 Pt 1):E372-83. doi: 10.1152/ajpendo.1994.266.3.E372. PubMed PMID: 8166257.

185. Foretz M, Hebrard S, Leclerc J, Zarrinpashneh E, Soty M, Mithieux G, Sakamoto K, Andreelli F, Viollet B. Metformin inhibits hepatic gluconeogenesis in mice independently of the LKB1/AMPK pathway via a decrease in hepatic energy state. The Journal of clinical investigation. 2010;120(7):2355-69. doi: 10.1172/JCI40671. PubMed PMID: 20577053; PMCID: PMC2898585.

186. Robertson RP, Harmon J, Tran PO, Tanaka Y, Takahashi H. Glucose toxicity in beta-cells: type 2 diabetes, good radicals gone bad, and the glutathione connection. Diabetes. 2003;52(3):581-7. PubMed PMID: 12606496.

187. LeRoith D. Beta-cell dysfunction and insulin resistance in type 2 diabetes: role of metabolic and genetic abnormalities. Am J Med. 2002;113 Suppl 6A:3S-11S. PubMed PMID: 12431757.

188. von Eckardstein A, Widmann C. High-density lipoprotein, beta cells, and diabetes. Cardiovasc Res. 2014;103(3):384-94. doi: 10.1093/cvr/cvu143. PubMed PMID: 24903496.

189. Fryirs MA, Barter PJ, Appavoo M, Tuch BE, Tabet F, Heather AK, Rye KA. Effects of high-density lipoproteins on pancreatic beta-cell insulin secretion. Arteriosclerosis, thrombosis, and vascular biology. 2010;30(8):1642-8. doi: 10.1161/ATVBAHA.110.207373. PubMed PMID: 20466975.

190. Kruit JK, Brunham LR, Verchere CB, Hayden MR. HDL and LDL cholesterol significantly influence beta-cell function in type 2 diabetes mellitus. Current opinion in lipidology. 2010;21(3):178-85. doi: 10.1097/MOL.0b013e328339387b. PubMed PMID: 20463468.

191. Plaisance V, Waeber G, Regazzi R, Abderrahmani A. Role of microRNAs in islet beta-cell compensation and failure during diabetes. Journal of diabetes research. 2014;2014:618652. doi: 10.1155/2014/618652. PubMed PMID: 24734255; PMCID: PMC3964735.

192. Dalgaard LT, Eliasson L. An 'alpha-beta' of pancreatic islet microribonucleotides. Int J Biochem Cell Biol. 2017;88:208-19. doi: 10.1016/j.biocel.2017.01.009. PubMed PMID: 28122254.

193. Tattikota SG, Rathjen T, McAnulty SJ, Wessels HH, Akerman I, van de Bunt M, Hausser J, Esguerra JL, Musahl A, Pandey AK, You X, Chen W, Herrera PL, Johnson PR, O'Carroll D, Eliasson L, Zavolan M, Gloyn AL, Ferrer J, Shalom-Feuerstein R, Aberdam D, Poy MN. Argonaute2 mediates compensatory expansion of the pancreatic beta cell. Cell metabolism. 2014;19(1):122-34. doi: 10.1016/j.cmet.2013.11.015. PubMed PMID: 24361012; PMCID: PMC3945818.

194. Eliasson L. The small RNA miR-375- a pancreatic islet abundant miRNA with multiple roles in endocrine beta cell function. Molecular and cellular endocrinology. 2017. doi: 10.1016/j.mce.2017.02.043. PubMed PMID: 28254488.

195. Li N, Wu JX, Ding D, Cheng J, Gao N, Chen L. Structure of a Pancreatic ATP-Sensitive Potassium Channel. Cell. 2017;168(1-2):101-10 e10. doi: 10.1016/j.cell.2016.12.028. PubMed PMID: 28086082.

196. Seino S, Shibasaki T. PKA-dependent and PKA-independent pathways for cAMP-regulated exocytosis. Physiol Rev. 2005;85(4):1303-42. doi: 10.1152/physrev.00001.2005. PubMed PMID: 16183914.

197. Seino S, Takahashi H, Fujimoto W, Shibasaki T. Roles of cAMP signalling in insulin granule exocytosis. Diabetes, obesity & metabolism. 2009;11 Suppl 4:180-8. doi: 10.1111/j.1463-1326.2009.01108.x. PubMed PMID: 19817800.

198. Susini S, Van Haasteren G, Li S, Prentki M, Schlegel W. Essentiality of intron control in the induction of c-fos by glucose and glucoincretin peptides in INS-1 beta-cells. FASEB journal :

official publication of the Federation of American Societies for Experimental Biology. 2000;14(1):128-36. PubMed PMID: 10627287.

199. Jo S, Chen J, Xu G, Grayson TB, Thielen LA, Shalev A. miR-204 Controls Glucagon-Like Peptide 1 Receptor Expression and Agonist Function. Diabetes. 2018;67(2):256-64. doi: 10.2337/db17-0506. PubMed PMID: 29101219; PMCID: PMC5780066.

200. Ji Y, Jian B, Wang N, Sun Y, Moya ML, Phillips MC, Rothblat GH, Swaney JB, Tall AR. Scavenger receptor BI promotes high density lipoprotein-mediated cellular cholesterol efflux. J Biol Chem. 1997;272(34):20982-5. Epub 1997/08/22. PubMed PMID: 9261096.

201. Assanasen C, Mineo C, Seetharam D, Yuhanna IS, Marcel YL, Connelly MA, Williams DL, de la Llera-Moya M, Shaul PW, Silver DL. Cholesterol binding, efflux, and a PDZ-interacting domain of scavenger receptor-BI mediate HDL-initiated signaling. J Clin Invest. 2005;115(4):969-77. doi: 10.1172/JCI23858. PubMed PMID: 15841181; PMCID: 1069105.

202. Oram JF, Vaughan AM. ATP-Binding cassette cholesterol transporters and cardiovascular disease. Circ Res. 2006;99(10):1031-43. doi: 10.1161/01.RES.0000250171.54048.5c. PubMed PMID: 17095732.

203. Assmann TS, Recamonde-Mendoza M, De Souza BM, Crispim D. MicroRNA expression profiles and type 1 diabetes mellitus: systematic review and bioinformatic analysis. Endocr Connect. 2017;6(8):773-90. doi: 10.1530/EC-17-0248. PubMed PMID: 28986402.

204. Ashcroft FM. Mechanisms of the glycaemic effects of sulfonylureas. Hormone and metabolic research = Hormon- und Stoffwechselforschung = Hormones et metabolisme. 1996;28(9):456-63. doi: 10.1055/s-2007-979837. PubMed PMID: 8911983.

205. Kamalden TA, Macgregor-Das AM, Kannan SM, Dunkerly-Eyring B, Khaliddin N, Xu Z, Fusco AP, Yazib SA, Chow RC, Duh EJ, Halushka MK, Steenbergen C, Das S. Exo-miR-15a Transfer from the Pancreas Augments Diabetic Complications by Inducing Oxidative Stress. Antioxidants & redox signaling. 2017. doi: 10.1089/ars.2016.6844. PubMed PMID: 28173719.

206. Cianciaruso C, Phelps EA, Pasquier M, Hamelin R, Demurtas D, Alibashe Ahmed M, Piemonti L, Hirosue S, Swartz MA, De Palma M, Hubbell JA, Baekkeskov S. Primary Human and Rat beta-Cells Release the Intracellular Autoantigens GAD65, IA-2, and Proinsulin in Exosomes Together With Cytokine-Induced Enhancers of Immunity. Diabetes. 2017;66(2):460-73. doi: 10.2337/db16-0671. PubMed PMID: 27872147.

207. Sun T, Li CT, Xiong L, Ning Z, Leung F, Peng S, Lu WW. miR-375-3p negatively regulates osteogenesis by targeting and decreasing the expression levels of LRP5 and beta-catenin. PloS one. 2017;12(2):e0171281. doi: 10.1371/journal.pone.0171281. PubMed PMID: 28158288; PMCID: PMC5291413.

208. Wang Y, Huang C, Reddy Chintagari N, Bhaskaran M, Weng T, Guo Y, Xiao X, Liu L. miR-375 regulates rat alveolar epithelial cell trans-differentiation by inhibiting Wnt/beta-catenin pathway. Nucleic acids research. 2013;41(6):3833-44. doi: 10.1093/nar/gks1460. PubMed PMID: 23396279; PMCID: PMC3616718.

209. Miao CG, Shi WJ, Xiong YY, Yu H, Zhang XL, Qin MS, Du CL, Song TW, Li J. miR-375 regulates the canonical Wnt pathway through FZD8 silencing in arthritis synovial fibroblasts. Immunol Lett. 2015;164(1):1-10. doi: 10.1016/j.imlet.2015.01.003. PubMed PMID: 25619565.

210. Wang Y, Dong X, Li Z, Wang W, Tian J, Chen J. Downregulated RASD1 and upregulated miR-375 are involved in protective effects of calycosin on cerebral ischemia/reperfusion rats. Journal of the neurological sciences. 2014;339(1-2):144-8. doi: 10.1016/j.jns.2014.02.002. PubMed PMID: 24548484.

211. Joglekar MV, Joglekar VM, Hardikar AA. Expression of islet-specific microRNAs during human pancreatic development. Gene Expr Patterns. 2009;9(2):109-13. doi: 10.1016/j.gep.2008.10.001. PubMed PMID: 18977315.

212. Cheng J, Wang L, Xu L, Wang H, Liu P, Bu S, Ye M, Zhang L, Wang Q, Duan S. Gender-dependent miR-375 promoter methylation and the risk of type 2 diabetes. Experimental

and therapeutic medicine. 2013;5(6):1687-92. doi: 10.3892/etm.2013.1069. PubMed PMID: 23837055; PMCID: PMC3702700.

213. Goto Y, Kakizaki M, Masaki N. Production of spontaneous diabetic rats by repetition of selective breeding. Tohoku J Exp Med. 1976;119(1):85-90. PubMed PMID: 951706.

214. Do OH, Gunton JE, Gaisano HY, Thorn P. Changes in beta cell function occur in prediabetes and early disease in the Lepr (db) mouse model of diabetes. Diabetologia. 2016;59(6):1222-30. doi: 10.1007/s00125-016-3942-3. PubMed PMID: 27048248; PMCID: PMC4869737.

215. Zampetaki A, Kiechl S, Drozdov I, Willeit P, Mayr U, Prokopi M, Mayr A, Weger S, Oberhollenzer F, Bonora E, Shah A, Willeit J, Mayr M. Plasma microRNA profiling reveals loss of endothelial miR-126 and other microRNAs in type 2 diabetes. Circ Res. 2010;107(6):810-7. doi: 10.1161/CIRCRESAHA.110.226357. PubMed PMID: 20651284.

216. Kong L, Zhu J, Han W, Jiang X, Xu M, Zhao Y, Dong Q, Pang Z, Guan Q, Gao L, Zhao J, Zhao L. Significance of serum microRNAs in pre-diabetes and newly diagnosed type 2 diabetes: a clinical study. Acta diabetologica. 2011;48(1):61-9. doi: 10.1007/s00592-010-0226-0. PubMed PMID: 20857148.

217. Sun K, Chang X, Yin L, Li J, Zhou T, Zhang C, Chen X. Expression and DNA methylation status of microRNA-375 in patients with type 2 diabetes mellitus. Mol Med Rep. 2014;9(3):967-72. doi: 10.3892/mmr.2013.1872. PubMed PMID: 24366165.

218. Seyhan AA, Nunez Lopez YO, Xie H, Yi F, Mathews C, Pasarica M, Pratley RE. Pancreas-enriched miRNAs are altered in the circulation of subjects with diabetes: a pilot cross-sectional study. Scientific reports. 2016;6:31479. doi: 10.1038/srep31479. PubMed PMID: 27558530; PMCID: PMC4997329.

219. Ortega FJ, Mercader JM, Moreno-Navarrete JM, Rovira O, Guerra E, Esteve E, Xifra G, Martinez C, Ricart W, Rieusset J, Rome S, Karczewska-Kupczewska M, Straczkowski M, Fernandez-Real JM. Profiling of Circulating MicroRNAs Reveals Common MicroRNAs Linked to

Type 2 Diabetes That Change With Insulin Sensitization. Diabetes care. 2014;37(5):1375-83. doi: 10.2337/dc13-1847. PubMed PMID: 24478399.

220. Yan S, Wang T, Huang S, Di Y, Huang Y, Liu X, Luo Z, Han W, An B. Differential expression of microRNAs in plasma of patients with prediabetes and newly diagnosed type 2 diabetes. Acta Diabetol. 2016;53(5):693-702. doi: 10.1007/s00592-016-0837-1. PubMed PMID: 27039347.

221. Flowers E, Aouizerat BE, Abbasi F, Lamendola C, Grove KM, Fukuoka Y, Reaven GM. Circulating microRNA-320a and microRNA-486 predict thiazolidinedione response: Moving towards precision health for diabetes prevention. Metabolism: clinical and experimental. 2015;64(9):1051-9. doi: 10.1016/j.metabol.2015.05.013. PubMed PMID: 26031505; PMCID: PMC4546550.

222. Karolina DS, Tavintharan S, Armugam A, Sepramaniam S, Pek SL, Wong MT, Lim SC, Sum CF, Jeyaseelan K. Circulating miRNA profiles in patients with metabolic syndrome. The Journal of clinical endocrinology and metabolism. 2012;97(12):E2271-6. doi: 10.1210/jc.2012-1996. PubMed PMID: 23032062.

223. Flowers E, Gadgil M, Aouizerat BE, Kanaya AM. Circulating micrornas associated with glycemic impairment and progression in Asian Indians. Biomark Res. 2015;3:22. doi: 10.1186/s40364-015-0047-y. PubMed PMID: 26966540; PMCID: PMC4785747.

224. Yang Z, Chen H, Si H, Li X, Ding X, Sheng Q, Chen P, Zhang H. Serum miR-23a, a potential biomarker for diagnosis of pre-diabetes and type 2 diabetes. Acta Diabetol. 2014;51(5):823-31. doi: 10.1007/s00592-014-0617-8. PubMed PMID: 24981880.

225. Prabu P, Rome S, Sathishkumar C, Aravind S, Mahalingam B, Shanthirani CS, Gastebois C, Villard A, Mohan V, Balasubramanyam M. Circulating MiRNAs of 'Asian Indian Phenotype' Identified in Subjects with Impaired Glucose Tolerance and Patients with Type 2 Diabetes. PloS one. 2015;10(5):e0128372. doi: 10.1371/journal.pone.0128372. PubMed PMID: 26020947; PMCID: PMC4447457.

226. Santovito D, De Nardis V, Marcantonio P, Mandolini C, Paganelli C, Vitale E, Buttitta F, Bucci M, Mezzetti A, Consoli A, Cipollone F. Plasma exosome microRNA profiling unravels a new potential modulator of adiponectin pathway in diabetes: effect of glycemic control. The Journal of clinical endocrinology and metabolism. 2014;99(9):E1681-5. doi: 10.1210/jc.2013-3843. PubMed PMID: 24937531.

227. Yan X, Wang Z, Westberg-Rasmussen S, Tarbier M, Rathjen T, Tattikota SG, Peck BCE, Kanke M, Oxvig C, Frystyk J, Starup-Linde J, Sethupathy P, Friedlander MR, Gregersen S, Poy MN. Differential Impact of Glucose Administered Intravenously and Orally on Circulating miR-375 Levels in Human Subjects. The Journal of clinical endocrinology and metabolism. 2017;102(10):3749-55. doi: 10.1210/jc.2017-01365. PubMed PMID: 28973164.

228. Mittelbrunn M, Gutierrez-Vazquez C, Villarroya-Beltri C, Gonzalez S, Sanchez-Cabo F, Gonzalez MA, Bernad A, Sanchez-Madrid F. Unidirectional transfer of microRNA-loaded exosomes from T cells to antigen-presenting cells. Nature communications. 2011;2:282. doi: 10.1038/ncomms1285. PubMed PMID: 21505438; PMCID: PMC3104548.

229. Kahn SE, Hull RL, Utzschneider KM. Mechanisms linking obesity to insulin resistance and type 2 diabetes. Nature. 2006;444(7121):840-6. doi: 10.1038/nature05482. PubMed PMID: 17167471.

230. Nwose OM, Jones MR. Atypical Mechanism of Glucose Modulation by Colesevelam in Patients with Type 2 Diabetes. Clinical medicine insights Endocrinology and diabetes. 2013;6:75-9. doi: 10.4137/CMED.S12590. PubMed PMID: 24348081; PMCID: 3864737.

231. Tu H, Okamoto AY, Shan B. FXR, a bile acid receptor and biological sensor. Trends in cardiovascular medicine. 2000;10(1):30-5. PubMed PMID: 11150726.

232. Fernandez-Hernando C, Moore KJ. MicroRNA modulation of cholesterol homeostasis. Arteriosclerosis, thrombosis, and vascular biology. 2011;31(11):2378-82. doi: 10.1161/ATVBAHA.111.226688. PubMed PMID: 22011750; PMCID: 3298754.

233. Bartel DP. MicroRNAs: target recognition and regulatory functions. Cell. 2009;136(2):215-33. doi: 10.1016/j.cell.2009.01.002. PubMed PMID: 19167326; PMCID: PMC3794896.

234. Farh KK, Grimson A, Jan C, Lewis BP, Johnston WK, Lim LP, Burge CB, Bartel DP. The widespread impact of mammalian MicroRNAs on mRNA repression and evolution. Science. 2005;310(5755):1817-21. doi: 10.1126/science.1121158. PubMed PMID: 16308420.

235. Deiuliis JA. MicroRNAs as regulators of metabolic disease: pathophysiologic significance and emerging role as biomarkers and therapeutics. Int J Obes (Lond). 2016;40(1):88-101. doi: 10.1038/ijo.2015.170. PubMed PMID: 26311337; PMCID: PMC4722234.

236. Mirra P, Nigro C, Prevenzano I, Leone A, Raciti GA, Formisano P, Beguinot F, Miele C. The Destiny of Glucose from a MicroRNA Perspective. Front Endocrinol (Lausanne). 2018;9:46. doi: 10.3389/fendo.2018.00046. PubMed PMID: 29535681; PMCID: PMC5834423.

237. Willeit P, Skroblin P, Kiechl S, Fernandez-Hernando C, Mayr M. Liver microRNAs: potential mediators and biomarkers for metabolic and cardiovascular disease? European heart journal. 2016;37(43):3260-6. doi: 10.1093/eurheartj/ehw146. PubMed PMID: 27099265; PMCID: PMC5146692.

238. Kaur K, Bhatia H, Datta M. MicroRNAs in hepatic pathophysiology in diabetes. World J Diabetes. 2011;2(10):158-63. doi: 10.4239/wjd.v2.i10.158. PubMed PMID: 22013501; PMCID: PMC3196616.

239. Sud N, Taher J, Su Q. MicroRNAs and Noncoding RNAs in Hepatic Lipid and Lipoprotein Metabolism: Potential Therapeutic Targets of Metabolic Disorders. Drug Dev Res. 2015;76(6):318-27. doi: 10.1002/ddr.21269. PubMed PMID: 26286650; PMCID: PMC4760898.

240. Yang Z, Wang L. Regulation of microRNA expression and function by nuclear receptor signaling. Cell Biosci. 2011;1(1):31. doi: 10.1186/2045-3701-1-31. PubMed PMID: 21936947; PMCID: PMC3192659.

241. de Aguiar Vallim TQ, Tarling EJ, Kim T, Civelek M, Baldan A, Esau C, Edwards PA. MicroRNA-144 regulates hepatic ATP binding cassette transporter A1 and plasma high-density lipoprotein after activation of the nuclear receptor farnesoid X receptor. Circulation research. 2013;112(12):1602-12. doi: 10.1161/CIRCRESAHA.112.300648. PubMed PMID: 23519696; PMCID: PMC3995747.

242. Shao S, Fang Z, Yu X, Zhang M. Transcription factors involved in glucose-stimulated insulin secretion of pancreatic beta cells. Biochem Biophys Res Commun. 2009;384(4):401-4. doi: 10.1016/j.bbrc.2009.04.135. PubMed PMID: 19410555.

243. Tsuchiya K, Ogawa Y. Forkhead box class O family member proteins: The biology and pathophysiological roles in diabetes. J Diabetes Investig. 2017;8(6):726-34. doi: 10.1111/jdi.12651. PubMed PMID: 28267275; PMCID: PMC5668485.

244. Chen W, Roeder RG. Mediator-dependent nuclear receptor function. Seminars in cell & developmental biology. 2011;22(7):749-58. doi: 10.1016/j.semcdb.2011.07.026. PubMed PMID: 21854863; PMCID: PMC3207035.

245. Dambal S, Shah M, Mihelich B, Nonn L. The microRNA-183 cluster: the family that plays together stays together. Nucleic Acids Res. 2015;43(15):7173-88. doi: 10.1093/nar/gkv703. PubMed PMID: 26170234; PMCID: PMC4551935.

246. Lynn FC. Meta-regulation: microRNA regulation of glucose and lipid metabolism. Trends in endocrinology and metabolism: TEM. 2009;20(9):452-9. doi: 10.1016/j.tem.2009.05.007. PubMed PMID: 19800254.

247. Fonseca VA, Handelsman Y, Staels B. Colesevelam lowers glucose and lipid levels in type 2 diabetes: the clinical evidence. Diabetes, obesity & metabolism. 2010;12(5):384-92. doi: 10.1111/j.1463-1326.2009.01181.x. PubMed PMID: 20415686; PMCID: PMC2871173.

248. Le TA, Chen J, Changchien C, Peterson MR, Kono Y, Patton H, Cohen BL, Brenner D, Sirlin C, Loomba R, San Diego Integrated NRC. Effect of colesevelam on liver fat quantified by

magnetic resonance in nonalcoholic steatohepatitis: a randomized controlled trial. Hepatology. 2012;56(3):922-32. doi: 10.1002/hep.25731. PubMed PMID: 22431131; PMCID: PMC3400720.

249. Yamakawa T, Ogihara K, Utsunomiya H, Muraoka T, Kadonosono K, Terauchi Y. Colestimide improves glycemic control via hepatic glucose production in db/db mice. Endocr J. 2014;61(5):425-36. PubMed PMID: 24553582.

250. Bai L, Jia Y, Viswakarma N, Huang J, Vluggens A, Wolins NE, Jafari N, Rao MS, Borensztajn J, Yang G, Reddy JK. Transcription coactivator mediator subunit MED1 is required for the development of fatty liver in the mouse. Hepatology. 2011;53(4):1164-74. doi: 10.1002/hep.24155. PubMed PMID: 21480322; PMCID: PMC3076129.

251. Watanabe M, Morimoto K, Houten SM, Kaneko-Iwasaki N, Sugizaki T, Horai Y, Mataki C, Sato H, Murahashi K, Arita E, Schoonjans K, Suzuki T, Itoh H, Auwerx J. Bile acid binding resin improves metabolic control through the induction of energy expenditure. PloS one. 2012;7(8):e38286. doi: 10.1371/journal.pone.0038286. PubMed PMID: 22952571; PMCID: PMC3430641.

252. Aiman U, Najmi A, Khan RA. Statin induced diabetes and its clinical implications. J Pharmacol Pharmacother. 2014;5(3):181-5. doi: 10.4103/0976-500X.136097. PubMed PMID: 25210397; PMCID: PMC4156828.

253. de Aguiar Vallim TQ, Tarling EJ, Edwards PA. Pleiotropic roles of bile acids in metabolism. Cell metabolism. 2013;17(5):657-69. doi: 10.1016/j.cmet.2013.03.013. PubMed PMID: 23602448; PMCID: PMC3654004.

254. Li T, Francl JM, Boehme S, Chiang JY. Regulation of cholesterol and bile acid homeostasis by the cholesterol 7alpha-hydroxylase/steroid response element-binding protein 2/microRNA-33a axis in mice. Hepatology. 2013;58(3):1111-21. doi: 10.1002/hep.26427. PubMed PMID: 23536474; PMCID: PMC3735649.

255. Zhu Y, Qi C, Jain S, Rao MS, Reddy JK. Isolation and characterization of PBP, a protein that interacts with peroxisome proliferator-activated receptor. The Journal of biological chemistry. 1997;272(41):25500-6. PubMed PMID: 9325263.

256. Yuan CX, Ito M, Fondell JD, Fu ZY, Roeder RG. The TRAP220 component of a thyroid hormone receptor- associated protein (TRAP) coactivator complex interacts directly with nuclear receptors in a ligand-dependent fashion. Proceedings of the National Academy of Sciences of the United States of America. 1998;95(14):7939-44. PubMed PMID: 9653119; PMCID: PMC20908.

257. Jia Y, Guo GL, Surapureddi S, Sarkar J, Qi C, Guo D, Xia J, Kashireddi P, Yu S, Cho YW, Rao MS, Kemper B, Ge K, Gonzalez FJ, Reddy JK. Transcription coactivator peroxisome proliferator-activated receptor-binding protein/mediator 1 deficiency abrogates acetaminophen hepatotoxicity. Proceedings of the National Academy of Sciences of the United States of America. 2005;102(35):12531-6. doi: 10.1073/pnas.0506000102. PubMed PMID: 16109766; PMCID: PMC1187948.

258. Jiang P, Hu Q, Ito M, Meyer S, Waltz S, Khan S, Roeder RG, Zhang X. Key roles for MED1 LxxLL motifs in pubertal mammary gland development and luminal-cell differentiation. Proceedings of the National Academy of Sciences of the United States of America. 2010;107(15):6765-70. doi: 10.1073/pnas.1001814107. PubMed PMID: 20351249; PMCID: PMC2872411.

259. Zhu Y, Qi C, Jia Y, Nye JS, Rao MS, Reddy JK. Deletion of PBP/PPARBP, the gene for nuclear receptor coactivator peroxisome proliferator-activated receptor-binding protein, results in embryonic lethality. J Biol Chem. 2000;275(20):14779-82. doi: 10.1074/jbc.C000121200. PubMed PMID: 10747854.

260. Chen W, Zhang X, Birsoy K, Roeder RG. A muscle-specific knockout implicates nuclear receptor coactivator MED1 in the regulation of glucose and energy metabolism. Proceedings of

the National Academy of Sciences of the United States of America. 2010;107(22):10196-201. doi: 10.1073/pnas.1005626107. PubMed PMID: 20479251; PMCID: PMC2890439.

261. Matsumoto K, Yu S, Jia Y, Ahmed MR, Viswakarma N, Sarkar J, Kashireddy PV, Rao MS, Karpus W, Gonzalez FJ, Reddy JK. Critical role for transcription coactivator peroxisome proliferator-activated receptor (PPAR)-binding protein/TRAP220 in liver regeneration and PPARalpha ligand-induced liver tumor development. The Journal of biological chemistry. 2007;282(23):17053-60. doi: 10.1074/jbc.M701956200. PubMed PMID: 17438330.

262. Viswakarma N, Jia Y, Bai L, Gao Q, Lin B, Zhang X, Misra P, Rana A, Jain S, Gonzalez FJ, Zhu YJ, Thimmapaya B, Reddy JK. The Med1 subunit of the mediator complex induces liver cell proliferation and is phosphorylated by AMP kinase. The Journal of biological chemistry. 2013;288(39):27898-911. doi: 10.1074/jbc.M113.486696. PubMed PMID: 23943624; PMCID: PMC3784705.

263. Ge K, Guermah M, Yuan CX, Ito M, Wallberg AE, Spiegelman BM, Roeder RG. Transcription coactivator TRAP220 is required for PPAR gamma 2-stimulated adipogenesis. Nature. 2002;417(6888):563-7. doi: 10.1038/417563a. PubMed PMID: 12037571.

264. Sturek JM, Castle JD, Trace AP, Page LC, Castle AM, Evans-Molina C, Parks JS, Mirmira RG, Hedrick CC. An intracellular role for ABCG1-mediated cholesterol transport in the regulated secretory pathway of mouse pancreatic beta cells. The Journal of clinical investigation. 2010;120(7):2575-89. doi: 10.1172/JCI41280. PubMed PMID: 20530872; PMCID: 2898593.

265. Kruit JK, Wijesekara N, Fox JE, Dai XQ, Brunham LR, Searle GJ, Morgan GP, Costin AJ, Tang R, Bhattacharjee A, Johnson JD, Light PE, Marsh BJ, Macdonald PE, Verchere CB, Hayden MR. Islet cholesterol accumulation due to loss of ABCA1 leads to impaired exocytosis of insulin granules. Diabetes. 2011;60(12):3186-96. doi: 10.2337/db11-0081. PubMed PMID: 21998401; PMCID: 3219942.

266. Hafner M, Landthaler M, Burger L, Khorshid M, Hausser J, Berninger P, Rothballer A, Ascano M, Jr., Jungkamp AC, Munschauer M, Ulrich A, Wardle GS, Dewell S, Zavolan M, Tuschl T. Transcriptome-wide identification of RNA-binding protein and microRNA target sites by PAR-CLIP. Cell. 2010;141(1):129-41. doi: 10.1016/j.cell.2010.03.009. PubMed PMID: 20371350; PMCID: 2861495.

267. Meissner M, Wolters H, de Boer RA, Havinga R, Boverhof R, Bloks VW, Kuipers F, Groen AK. Bile acid sequestration normalizes plasma cholesterol and reduces atherosclerosis in hypercholesterolemic mice. No additional effect of physical activity. Atherosclerosis. 2013;228(1):117-23. doi: 10.1016/j.atherosclerosis.2013.02.021. PubMed PMID: 23497783.

268. Li W, Koutmou KS, Leahy DJ, Li M. Systemic RNA Interference Deficiency-1 (SID-1) Extracellular Domain Selectively Binds Long Double-stranded RNA and Is Required for RNA Transport by SID-1. The Journal of biological chemistry. 2015;290(31):18904-13. doi: 10.1074/jbc.M115.658864. PubMed PMID: 26067272; PMCID: PMC4521010.

269. Duxbury MS, Ashley SW, Whang EE. RNA interference: a mammalian SID-1 homologue enhances siRNA uptake and gene silencing efficacy in human cells. Biochem Biophys Res Commun. 2005;331(2):459-63. doi: 10.1016/j.bbrc.2005.03.199. PubMed PMID: 15850781.

270. Elhassan MO, Christie J, Duxbury MS. Homo sapiens systemic RNA interference-defective-1 transmembrane family member 1 (SIDT1) protein mediates contact-dependent small RNA transfer and microRNA-21-driven chemoresistance. The Journal of biological chemistry. 2012;287(8):5267-77. doi: 10.1074/jbc.M111.318865. PubMed PMID: 22174421; PMCID: PMC3285307.

271. Aizawa S, Fujiwara Y, Contu VR, Hase K, Takahashi M, Kikuchi H, Kabuta C, Wada K, Kabuta T. Lysosomal putative RNA transporter SIDT2 mediates direct uptake of RNA by lysosomes. Autophagy. 2016;12(3):565-78. doi: 10.1080/15548627.2016.1145325. PubMed PMID: 27046251; PMCID: PMC4836006.

272. Gao J, Gu X, Mahuran DJ, Wang Z, Zhang H. Impaired glucose tolerance in a mouse model of sidt2 deficiency. PloS one. 2013;8(6):e66139. doi: 10.1371/journal.pone.0066139. PubMed PMID: 23776622; PMCID: PMC3679015.

273. Mendez-Acevedo KM, Valdes VJ, Asanov A, Vaca L. A novel family of mammalian transmembrane proteins involved in cholesterol transport. Scientific reports. 2017;7(1):7450. doi: 10.1038/s41598-017-07077-z. PubMed PMID: 28785058; PMCID: PMC5547113.

274. Geng X, Li L, Watkins S, Robbins PD, Drain P. The insulin secretory granule is the major site of K(ATP) channels of the endocrine pancreas. Diabetes. 2003;52(3):767-76. PubMed PMID: 12606519.

275. Xia F, Gao X, Kwan E, Lam PP, Chan L, Sy K, Sheu L, Wheeler MB, Gaisano HY, Tsushima RG. Disruption of pancreatic beta-cell lipid rafts modifies Kv2.1 channel gating and insulin exocytosis. The Journal of biological chemistry. 2004;279(23):24685-91. doi: 10.1074/jbc.M314314200. PubMed PMID: 15073181.

276. Panten U, Zielmann S, Schrader MT, Lenzen S. The dihydropyridine derivative, Bay K 8644, enhances insulin secretion by isolated pancreatic islets. Naunyn Schmiedebergs Arch Pharmacol. 1985;328(3):351-3. PubMed PMID: 2580242.

277. Vasseur M, Debuyser A, Joffre M. Sensitivity of pancreatic beta cell to calcium channel blockers. An electrophysiologic study of verapamil and nifedipine. Fundam Clin Pharmacol. 1987;1(2):95-113. PubMed PMID: 3315915.

278. Farbstein D, Levy AP. HDL dysfunction in diabetes: causes and possible treatments. Expert Rev Cardiovasc Ther. 2012;10(3):353-61. doi: 10.1586/erc.11.182. PubMed PMID: 22390807; PMCID: PMC3332215.

279. Cerf ME. Beta cell dysfunction and insulin resistance. Front Endocrinol (Lausanne). 2013;4:37. doi: 10.3389/fendo.2013.00037. PubMed PMID: 23542897; PMCID: PMC3608918.

280. Porte D, Jr., Kahn SE. beta-cell dysfunction and failure in type 2 diabetes: potential mechanisms. Diabetes. 2001;50 Suppl 1:S160-3. PubMed PMID: 11272181.

281. Klein D, Misawa R, Bravo-Egana V, Vargas N, Rosero S, Piroso J, Ichii H, Umland O, Zhijie J, Tsinoremas N, Ricordi C, Inverardi L, Dominguez-Bendala J, Pastori RL. MicroRNA expression in alpha and beta cells of human pancreatic islets. PloS one. 2013;8(1):e55064. doi: 10.1371/journal.pone.0055064. PubMed PMID: 23383059; PMCID: 3558471.

282. Mandelbaum AD, Melkman-Zehavi T, Oren R, Kredo-Russo S, Nir T, Dor Y, Hornstein E. Dysregulation of Dicer1 in beta cells impairs islet architecture and glucose metabolism. Exp Diabetes Res. 2012;2012:470302. doi: 10.1155/2012/470302. PubMed PMID: 22991506; PMCID: PMC3443614.

283. Lynn FC, Skewes-Cox P, Kosaka Y, McManus MT, Harfe BD, German MS. MicroRNA expression is required for pancreatic islet cell genesis in the mouse. Diabetes. 2007;56(12):2938-45. doi: 10.2337/db07-0175. PubMed PMID: 17804764.

284. Kalis M, Bolmeson C, Esguerra JL, Gupta S, Edlund A, Tormo-Badia N, Speidel D, Holmberg D, Mayans S, Khoo NK, Wendt A, Eliasson L, Cilio CM. Beta-cell specific deletion of Dicer1 leads to defective insulin secretion and diabetes mellitus. PloS one. 2011;6(12):e29166. doi: 10.1371/journal.pone.0029166. PubMed PMID: 22216196; PMCID: PMC3246465.

285. Goodwin B, Jones SA, Price RR, Watson MA, McKee DD, Moore LB, Galardi C, Wilson JG, Lewis MC, Roth ME, Maloney PR, Willson TM, Kliewer SA. A regulatory cascade of the nuclear receptors FXR, SHP-1, and LRH-1 represses bile acid biosynthesis. Molecular cell. 2000;6(3):517-26. PubMed PMID: 11030332.

286. Lee J, Padhye A, Sharma A, Song G, Miao J, Mo YY, Wang L, Kemper JK. A pathway involving farnesoid X receptor and small heterodimer partner positively regulates hepatic sirtuin 1 levels via microRNA-34a inhibition. The Journal of biological chemistry. 2010;285(17):12604-11. doi: 10.1074/jbc.M109.094524. PubMed PMID: 20185821; PMCID: PMC2857134.

287. Karolina DS, Armugam A, Tavintharan S, Wong MT, Lim SC, Sum CF, Jeyaseelan K. MicroRNA 144 impairs insulin signaling by inhibiting the expression of insulin receptor substrate

1 in type 2 diabetes mellitus. PloS one. 2011;6(8):e22839. doi: 10.1371/journal.pone.0022839. PubMed PMID: 21829658; PMCID: PMC3148231.

288. Zhang T, Kim DH, Xiao X, Lee S, Gong Z, Muzumdar R, Calabuig-Navarro V, Yamauchi J, Harashima H, Wang R, Bottino R, Alvarez-Perez JC, Garcia-Ocana A, Gittes G, Dong HH. FoxO1 Plays an Important Role in Regulating beta-Cell Compensation for Insulin Resistance in Male Mice. Endocrinology. 2016;157(3):1055-70. doi: 10.1210/en.2015-1852. PubMed PMID: 26727107; PMCID: PMC4769368.

289. Oh KJ, Han HS, Kim MJ, Koo SH. CREB and FoxO1: two transcription factors for the regulation of hepatic gluconeogenesis. BMB Rep. 2013;46(12):567-74. PubMed PMID: 24238363; PMCID: PMC4133859.

290. Horton JD, Bashmakov Y, Shimomura I, Shimano H. Regulation of sterol regulatory element binding proteins in livers of fasted and refed mice. Proceedings of the National Academy of Sciences of the United States of America. 1998;95(11):5987-92. PubMed PMID: 9600904; PMCID: PMC27572.

291. Zhang N, Lin JK, Chen J, Liu XF, Liu JL, Luo HS, Li YQ, Cui S. MicroRNA 375 mediates the signaling pathway of corticotropin-releasing factor (CRF) regulating pro-opiomelanocortin (POMC) expression by targeting mitogen-activated protein kinase 8. The Journal of biological chemistry. 2013;288(15):10361-73. doi: 10.1074/jbc.M112.425504. PubMed PMID: 23430746; PMCID: PMC3624419.

292. Chang Y, Lin J, Tsung A. Manipulation of autophagy by MIR375 generates antitumor effects in liver cancer. Autophagy. 2012;8(12):1833-4. PubMed PMID: 22929050; PMCID: PMC3541295.

293. Jin Y, Liu Y, Zhang J, Huang W, Jiang H, Hou Y, Xu C, Zhai C, Gao X, Wang S, Wu Y, Zhu H, Lu S. The Expression of miR-375 Is Associated with Carcinogenesis in Three Subtypes of Lung Cancer. PloS one. 2015;10(12):e0144187. doi: 10.1371/journal.pone.0144187. PubMed PMID: 26642205; PMCID: PMC4671676.

294. Alam KJ, Mo JS, Han SH, Park WC, Kim HS, Yun KJ, Chae SC. MicroRNA 375 regulates proliferation and migration of colon cancer cells by suppressing the CTGF-EGFR signaling pathway. International journal of cancer Journal international du cancer. 2017;141(8):1614-29. doi: 10.1002/ijc.30861. PubMed PMID: 28670764.

295. Zhou J, Song S, He S, Zhu X, Zhang Y, Yi B, Zhang B, Qin G, Li D. MicroRNA-375 targets PDK1 in pancreatic carcinoma and suppresses cell growth through the Akt signaling pathway. Int J Mol Med. 2014;33(4):950-6. doi: 10.3892/ijmm.2014.1638. PubMed PMID: 24481267.

296. Wei R, Yang Q, Han B, Li Y, Yao K, Yang X, Chen Z, Yang S, Zhou J, Li M, Yu H, Yu M, Cui Q. microRNA-375 inhibits colorectal cancer cells proliferation by downregulating JAK2/STAT3 and MAP3K8/ERK signaling pathways. Oncotarget. 2017;8(10):16633-41. doi: 10.18632/oncotarget.15114. PubMed PMID: 28186962; PMCID: PMC5369990.

297. Chen X, Liang H, Zhang J, Zen K, Zhang CY. microRNAs are ligands of Toll-like receptors. Rna. 2013;19(6):737-9. doi: 10.1261/rna.036319.112. PubMed PMID: 23554231; PMCID: PMC3683908.

298. Park CK, Xu ZZ, Berta T, Han Q, Chen G, Liu XJ, Ji RR. Extracellular microRNAs activate nociceptor neurons to elicit pain via TLR7 and TRPA1. Neuron. 2014;82(1):47-54. doi: 10.1016/j.neuron.2014.02.011. PubMed PMID: 24698267; PMCID: PMC3982230.

299. Bernard MA, Zhao H, Yue SC, Anandaiah A, Koziel H, Tachado SD. Novel HIV-1 miRNAs stimulate TNFalpha release in human macrophages via TLR8 signaling pathway. PloS one. 2014;9(9):e106006. doi: 10.1371/journal.pone.0106006. PubMed PMID: 25191859; PMCID: PMC4156304.

300. Hafner M, Landthaler M, Burger L, Khorshid M, Hausser J, Berninger P, Rothballer A, Ascano M, Jungkamp AC, Munschauer M, Ulrich A, Wardle GS, Dewell S, Zavolan M, Tuschl T. PAR-CliP--a method to identify transcriptome-wide the binding sites of RNA binding proteins.

Journal of visualized experiments : JoVE. 2010(41). doi: 10.3791/2034. PubMed PMID: 20644507; PMCID: 3156069.

301. Danan C, Manickavel S, Hafner M. PAR-CLIP: A Method for Transcriptome-Wide Identification of RNA Binding Protein Interaction Sites. Methods in molecular biology. 2016;1358:153-73. doi: 10.1007/978-1-4939-3067-8_10. PubMed PMID: 26463383; PMCID: PMC5142217.

302. Martin M. Cutadapt removes adapter sequences from high-throughput sequencing reads. EMBnetjournal. 2011;17:10-2. doi: http://dx.doi.org/10.14806/ej.17.1.200.

303. Corcoran DL, Georgiev S, Mukherjee N, Gottwein E, Skalsky RL, Keene JD, Ohler U. PARalyzer: definition of RNA binding sites from PAR-CLIP short-read sequence data. Genome biology. 2011;12(8):R79. doi: 10.1186/gb-2011-12-8-r79. PubMed PMID: 21851591; PMCID: PMC3302668.

304. Ascano M, Hafner M, Cekan P, Gerstberger S, Tuschl T. Identification of RNA-protein interaction networks using PAR-CLIP. Wiley interdisciplinary reviews RNA. 2012;3(2):159-77. doi: 10.1002/wrna.1103. PubMed PMID: 22213601; PMCID: PMC3711140.

305. Chak LL, Okamura K. Argonaute-dependent small RNAs derived from single-stranded, non-structured precursors. Frontiers in genetics. 2014;5:172. doi: 10.3389/fgene.2014.00172. PubMed PMID: 24959173; PMCID: PMC4050365.

306. Matsui M, Prakash TP, Corey DR. Argonaute 2-dependent Regulation of Gene Expression by Single-stranded miRNA Mimics. Molecular therapy : the journal of the American Society of Gene Therapy. 2016;24(5):946-55. doi: 10.1038/mt.2016.39. PubMed PMID: 26903376; PMCID: PMC4881773.

307. Ridder K, Sevko A, Heide J, Dams M, Rupp AK, Macas J, Starmann J, Tjwa M, Plate KH, Sultmann H, Altevogt P, Umansky V, Momma S. Extracellular vesicle-mediated transfer of functional RNA in the tumor microenvironment. Oncoimmunology. 2015;4(6):e1008371. doi: 10.1080/2162402X.2015.1008371. PubMed PMID: 26155418; PMCID: PMC4485784.

308. Cleary MD, Meiering CD, Jan E, Guymon R, Boothroyd JC. Biosynthetic labeling of RNA with uracil phosphoribosyltransferase allows cell-specific microarray analysis of mRNA synthesis and decay. Nature biotechnology. 2005;23(2):232-7. doi: 10.1038/nbt1061. PubMed PMID: 15685165.

309. Miller MR, Robinson KJ, Cleary MD, Doe CQ. TU-tagging: cell type-specific RNA isolation from intact complex tissues. Nature methods. 2009;6(6):439-41. doi: 10.1038/nmeth.1329. PubMed PMID: 19430475; PMCID: PMC2783170.

310. Gay L, Miller MR, Ventura PB, Devasthali V, Vue Z, Thompson HL, Temple S, Zong H, Cleary MD, Stankunas K, Doe CQ. Mouse TU tagging: a chemical/genetic intersectional method for purifying cell type-specific nascent RNA. Genes & development. 2013;27(1):98-115. doi: 10.1101/gad.205278.112. PubMed PMID: 23307870; PMCID: 3553287.

311. Johnson JD. A practical guide to genetic engineering of pancreatic beta-cells in vivo: getting a grip on RIP and MIP. Islets. 2014;6(3):e944439. doi: 10.4161/19382014.2014.944439. PubMed PMID: 25322827; PMCID: PMC4376052.

312. Dean ED, Li M, Prasad N, Wisniewski SN, Von Deylen A, Spaeth J, Maddison L, Botros A, Sedgeman LR, Bozadjieva N, Ilkayeva O, Coldren A, Poffenberger G, Shostak A, Semich MC, Aamodt KI, Phillips N, Yan H, Bernal-Mizrachi E, Corbin JD, Vickers KC, Levy SE, Dai C, Newgard C, Gu W, Stein R, Chen W, Powers AC. Interrupted Glucagon Signaling Reveals Hepatic alpha Cell Axis and Role for L-Glutamine in alpha Cell Proliferation. Cell metabolism. 2017;25(6):1362-73 e5. doi: 10.1016/j.cmet.2017.05.011. PubMed PMID: 28591638; PMCID: PMC5572896.

313. Langhi C, Baldan A. CIDEC/FSP27 is regulated by peroxisome proliferator-activated receptor alpha and plays a critical role in fasting- and diet-induced hepatosteatosis. Hepatology. 2015;61(4):1227-38. doi: 10.1002/hep.27607. PubMed PMID: 25418138; PMCID: PMC4376564.

314. Jo J, Choi MY, Koh DS. Size distribution of mouse Langerhans islets. Biophysical journal. 2007;93(8):2655-66. doi: 10.1529/biophysj.107.104125. PubMed PMID: 17586568; PMCID: PMC1989722.

315. Radle B, Rutkowski AJ, Ruzsics Z, Friedel CC, Koszinowski UH, Dolken L. Metabolic labeling of newly transcribed RNA for high resolution gene expression profiling of RNA synthesis, processing and decay in cell culture. Journal of visualized experiments : JoVE. 2013(78). doi: 10.3791/50195. PubMed PMID: 23963265; PMCID: PMC3854562.